THE UNIVERSITY
of LIVERPOOL

Magnetic studies of tephra in late Holocene peats and loessic soils from SE Iceland

Thesis submitted in accordance with the requirement of the University of Liverpool for the degree of Doctor in Philosophy

By Dunsheng Xia

March 2003

Magnetic studies of tephra in late Holocene peats and loessic soils from Iceland

By Dunsheng Xia

Abstract

Magnetic and geochemical properties of five late Holocene peat and loessial soil sections in SE Iceland have been studied. The aims were (i) to establish a reliable tephrochronology for the sections, using geochemical analysis of tephra shards; (ii) to establish high resolution bulk sample records of mineral magnetic and geochemical properties; (iii) to test the ability of magnetic properties to correlate distal tephra layers; (iv) to assess the possible environmental significance of mineral magnetic time series and (v) to use records of loessial accumulation rates to assess human impact on the environment in SE Iceland.

The work has been successful in establishing a reliable tephrostratigraphy for the studied sections. This was achieved using electron microprobe analyses (EMPA) of the geochemistry of tephra shards concentrated using a density separation technique. The results of detailed mineral magnetic measurements suggest that the main magnetic minerals in the tephras are probably ferrimagnetic minerals (e.g. magnetite) and canted antiferromagnetic minerals (e.g. haematite), with abundant paramagnetic material also present. Cross plots of M_{rs}/M_s vs. $(B_0)_{cr}/(B_0)_c$ and $\chi_{fd\%}$ vs. χ_{ARM}/SIRM indicate the main magnetic grain size in the tephras are pseudo-single domain (PSD) and multi domain (MD). The results indicate that the 'fingerprint' of both hysteresis and Curie temperature properties are insufficiently consistent within the tephra layers to provide an obviously sound basis for correlating tephra layers from one profile to the next. However, initial correlation of tephra layers was achieved, using all the measured magnetic parameters, by the use of the multivariate statistical measures of Similarity Coefficient (SC) and Euclidean Distance (ED). Tephra layer correlation was performed first time here using magnetic measurements. This demonstrates that magnetic techniques can potentially assist in the identification and correlation of distal tephra.

Iceland offers a unique opportunity to study the role of humans in land degradation processes because of the late and well documented literature of settlements 1100 years ago. In this context, higher sedimentation rates in the upper part of two soils and one peat profile are interpreted as reflecting the effect of Landnam on deforestation and soil degradation.

I declare that the content of this thesis is my own work and that it has not been submitted for examination at any other university.

Dunsheng Xia
April 2003

ACKNOWLEDGEMENTS

This research has been financially supported by an Overseas Research Scholarship (ORS) from Universities UK and a studentship from the Faculty of Science, University of Liverpool.

First and foremost, I would like to thank my supervisors: Jan Bloemendal, John Dearing and Richard Chiverrell in the University of Liverpool. The initial idea for the project was theirs, they recruited me despite my absolute lack of magnetic knowledge and, without their patient guidance, this thesis would never have seen the light of day.

I would like to thank Drs. Richard Chiverrell and Jan Bloemendal for organizing the University of Liverpool Iceland Expedition during 1999 and 2000 at Iceland, and providing all the samples and the photographs included in this study.

I would like to thank Professor John Shaw for the discussion of the results of magnetic experiments; Dr. Andrew J. Plater for comments on a previous version of the manuscript; Dr. John F. Boyle for help with the X-Ray Fluorescence (XRF) analysis; and Drs. Gez Foster, Jack Hannam for their useful comments and kind encouragement. I am grateful to Mr. Bob Jude, Mr. Alan Henderson, Mrs. Hilda Hull, and Mrs. Irene Cooper for their assistance in my laboratory work. I am also indebted to everyone in the Department of Geography who has helped me out. Thanks must go to Dr. Mimi Hill for her kind assistance in VFTB work carried out in the Geomagnetism Laboratory, Department of Earth Science. Thanks must go to Mr. Paul Hands, Department of Geography, Earth & Environmental Sciences, the University of Birmingham and Mr. Dave Plant, Department of Earth Sciences, the University of Manchester for help with the EMPA analysis.

Lastly, I am very grateful to my wife Ye Yu, to whose infinite patience and support I am indebted. I dedicate this thesis to my son Fangzhou.

Contents

List of Figures

List of Tables

List of Appendices

Chapter 1 Introduction

1.1 Introduction

In Iceland, tephrochronology has been applied to studies of the eruption history of the most active volcanoes. It has also been utilized in archaeological research and palynology, studies of fluvial erosion, wind erosion, and in cryopedological and glaciological research.

Sigurdur Thorarinsson, 1980

The word tephra, from the Greek, meaning 'ash', as defined by Thorarisson (1944, 1981) applies to all of the clastic volcanic material, which during an eruption is transported from the crater through the air (Fig. 1.1). It is a collective term for all airborne pyroclasts including both air-fall and pyroclastic fall material (Gonzalez *et al.*, 1999; Hafildason *et al.*, 2000), but not deposits resulting from flowage events.

Tehpra is classified chiefly by clast size, shape, vesicularity and composition (Table 1.1 and Fig. 1.2). Particles whose intermediate axes measure 2 mm or less are described as ash. Fine and coarse ash particles are smaller and larger than 1/16 mm across, respectively. Lapilli have intermediate axes from 2 to 64 mm in length, and blocks and

bombs are more than 64 mm wide. Bombs have shapes or textures such as vesicularity that indicate they were liquid or plastic when erupted. Blocks generally are more angular and were solid when erupted (Fig. 1.2).

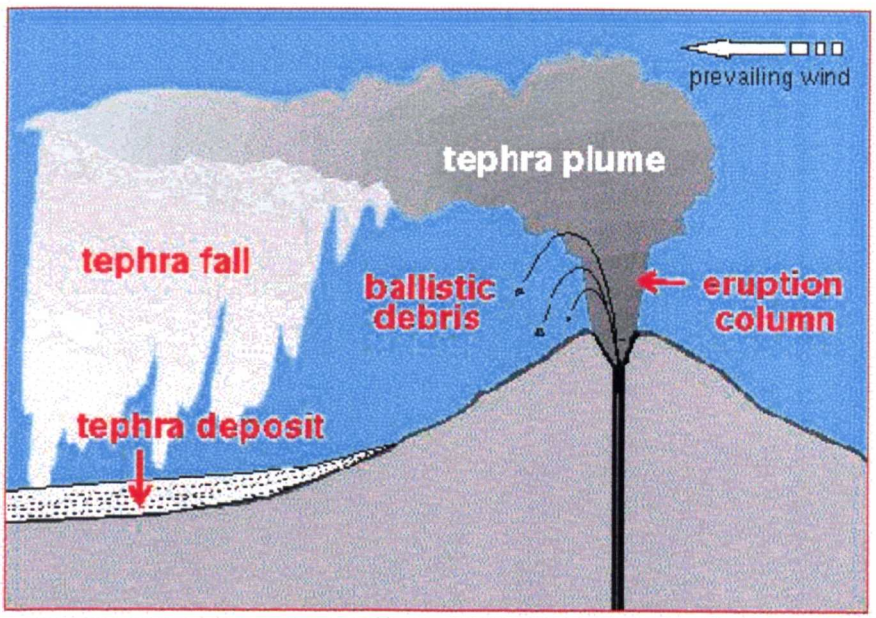

Figure 1-1 Volcanic eruption and the process of producing tephra
(Based on US Geological survey volcanic hazards, http://volcanoes.usgs.gov/)

In general, identification of tephra (i.e. volcanic ash) is an important method for two reasons: firstly, there is interest in the volcanic impact on climate and the environment (e.g. Rampino, 1991; Grattan and Sadler, 1999); and secondly, because of its potential as a chronological tool in different depositional environments, e.g. terrestrial, marine, lacustrine, and ice sheets (e.g. Thorarinsson, 1944, 1981; Kvamme *et al.*, 1989; Haflidason, 1992; Dugmore, *et al.*, 1995; 1998; Larsen, 1999; Haflidason *et al.*, 2000).

Table 1-1 Tephra terminology and particle size limits as originally defined by Fisher (1961)

(US Geological survey volcanic hazards, http://volcanoes.usgs.gov/)

Grain Size (mm)	Weathered fragments		Pyroclastic fragments
256	Boulders (and blocks)	Coarse and Fine	**Blocks**
64	Cobble		**Bombs**
2	Pebble		**Lapilli**
1/16	Sand	Coarse	
1/256	Silt	Fine	**Ash**
	Clay		

Figure 1-2 Photographic glossary of tephra

(Based on US Geological survey volcanic hazards, http://volcanoes.usgs.gov/)

Geological records show possible connections between volcanism and climate change on various spatial and temporal scales, from documented seasonal and regional climatic effects of historic eruptions to the long-term impact of episodes of increased global volcanism on atmospheric composition, climate and life (e.g. Rampino, 1991; Grattan and Sadler, 1999; Giles *et al.*, 1999). Widespread tephra layers can provide information on the size, frequency, and location of past eruptions, and the composition of erupted magma.

The use of tephra layers as a chronological tool (i.e. tephrochronology) was originally developed in Iceland (Thorarinsson, 1944, 1980) and has since been applied to other volcanically active areas such as Japan (e.g. Momose, 1968), the Mediterranean (Thunell *et al.*, 1979), New Zealand (e.g. Walker, 1980; Shane, 2000) and North America (e.g. Rose *et al.*, 1980). This technique allows isochronous marker horizons formed by tephra layers to be mapped across inter-continental scale distances. These can form a dating framework against which other techniques can be checked and validated. Certain tephra layers have played an important role in dating and correlating sequences as they can be relatively easily identified and isolated in different depositional media, and therefore can link these archives over large distances (Thorarinsson, 1981; Dugmore, *et al.*, 1995; Larsen, 1999; Haflidason *et al.*, 2000). The use of tephra layers as chronostratigraphical event markers has been especially important for the Holocene (Thorarinsson, 1944, Dugmore, *et al.*, 1995; Larsen, 1999; Haflidason *et al.*, 2000), where the application of the radiocarbon dating method is hampered by low organic carbon content of sediments and by radiocarbon plateaux (Haflidason *et al.*, 2000).

Pioneering work in tephra studies, using their physical properties (e.g. colour, grain-size, lithic content), was completed by Thorarinsson (1944, 1981) in Iceland. Usually, these provide a reliable means of identification and correlation of tephra in regions near source vents, and to some extent for distal tephra horizons, especially deposited in historical time (Haflidason *et al.*, 2000). The identification of the tephra layers in the field is achieved in many ways, such as by their stratigraphic relation, their colour, which is an indicator of their chemical composition, their thickness and grain sizes, which are, within certain limits, an exponential function of distance from their source (Thorarinsson; 1944, 1981; Haflidason *et al.*, 2000). In the laboratory the tephra layers are identified by determination of their mineralogical, chemical, and physical characteristics; microprobe analyses of their glasses are the most useful method. In addition, various granulometric parameters reveal the type of explosive activity (Dugmore *et al.*, 1995; Haflidason *et al.*, 2000). The identification of distal tephra layers of Icelandic origin, often very thin and discontinuous, in peat (Larsen, 1999), lake sediments (Bradshaw and Thompson, 1985) and soil of the late Quaternary (Gonalez *et al.*, 1999) and especially the Holocene (Bogaard *et al.*, 1994; Eiriksson *et al.*, 2000) age in North Europe, has marked an important development in geochronological research (Haflidason *et al.*, 2000).

There are many ways of characterising tephras, for example, by geochemical (Kvamme *et al.*, 1989; Haflidason, 1992; Dugmore *et al.*, 1989, 1992, 1995; Haflidason *et al.*, 2000) and X-ray fluorescence (Sigvaldason, 1974; Cormie *et al.*, 1980; Pawes *et al.*, 1998) analyses. At present, geochemical characteristics have been used more systematically as

a tool for the definition of individual tephra layers (Kvamme *et al.*, 1989; Haflidason, 1992; Dugmore, *et al.*, 1992, 1995; Pouclet *et al.*, 1999; Haflidason *et al.*, 2000). On the wider topic of the application of geochemical techniques in tephra studies, Haflidason *et al.* (2000) and Larsen *et al.* (2001) give comprehensive literature reviews. Bulk sample analyses are not always useful because mineralogical and compositional fractionation often occurs during transport (Haflidason *et al.*, 2000). The chemical composition of tephra shards has been shown to be the most appropriate method for identifying particular volcanic events (e.g. Dugmore *et al.*, 1992; Haflidason *et al.*, 2000).

This technique for the identification and correlation of tephra, at present, is accomplished by comparison of geochemistry with reference data from a suspected source. Dugmore *et al.* (1992) reported tephra shards could retain their overall chemical integrity whether collected from peat or loess, whether treated with acid or left untreated, at least on a four millennial time scale in contrasting depositional environments. The distinct petrographic character of tephra glass shards, combined with unique geochemical fingerprints characterizing most of these widespread tephra layers, has made it possible to isolate and identify single volcanic glass shards with high precision and to link them to their respective tephra horizons (Haflidason *et al.*, 2000). However, disadvantages of this technique are apparent; for example, only a few selected oxides can be compared at once and even if multiple plots are used it is not easy to assess differences in the geochemical composition (Charman and Grattan, 1999). In time, any sequence of magma development may be replicated sufficiently closely to produce tephra with indistinguishable major element content. Larsen *et al.* (1999) gave an

important caveat with the examples of Hekla 1510 and Hekla 1947 tephras, which despite intervening eruptions are very similar in composition.

In comparison with certain geochemical methods, an important aspect of environmental magnetism is that its techniques are relatively rapid, simple, non-destructive, and inexpensive (e.g. Bloemendal *et al.*, 1979; Thompson *et al.*, 1980; Thompson and Oldfield, 1986; Oldfield, 1991; Verosub *et al.*, 1995; Frederichs *et al*; 1999; Walden *et al.*, 1999 and, Maher and Thompson, 1999). Characterization of tephra using magnetic properties is attractive and has met with some success. Momose et al. (1968) showed that a number of different tephra horizons in Japan could be distinguished by their Curie temperature. McDougall *et al.* (1983) observed that tephra sources in the Mediterranean area could be identified from a simple combination of natural remanent magnetization (NRM) intensity, saturation magnetization (Ms) and low field magnetic susceptibility (χ). Magnetic measurements of lake and marine sediments in volcanic areas show that tephra layers are often marked by peaks in magnetic susceptibility (Oldfield et al., 1980, 1983; Thompson and Oldfield, 1986).

Robertson (1993) attempted to evaluate the discriminating potential of magnetic parameters (magnetic susceptibility, hysteresis parameters, thermomagnetic curves and IRM acquisition) for tephra identification and correlation. His results indicate that magnetic measurements may potentially help identify and correlate distal tephras. However, he found that the fingerprint of the measured hysteresis properties is insufficiently consistent within layers to provide any sound basis for correlating layers

from one profile to the next due to many reasons (Robertson, 1993). Van den Bogaard *et. al.* (1994) reported that SIRM measurements could provide an excellent means of detecting volcanic ash in peat cores that is too dispersed or faint to show up macroscopically.

Recently, several attempts (Pawes et al., 1998; Gonzalez et al., 1999) have been made to 'invert' the hysteresis properties numerically to obtain concentration and grain size information. Pawes *et al.* (1998) used magnetic hysteresis properties to identify tephra with the aid of electron spin resonance spectroscopy (ESR), and suggested that hysteresis measurements and ESR have the potential to be used as tools to identify distal tephra when used in conjunction with geochemical or mineralogical data. Gonzalez et al. (1999) combined empirical studies with multivariate statistical analysis to identify the magnetic signature of individual tephras, and concluded that it is possible to discriminate between different types of material in sections, and even to correlate some tephras between sections.

1.2 Objectives and thesis structure

In this project, using Icelandic tephra, high-resolution measurements of magnetic properties and element concentrations were undertaken on five loessic soil and peat sections from SE Iceland. The primary objective was to investigate the application potential of magnetic techniques to characterize Icelandic tephra. The main aims of the research can be summarized as follows:

(1) To produce a tephrochronology for the studied sections, using the established method of geochemical analysis of individual tephra shards.

(2) To determine the mineral magnetic and geochemical characteristics of closely-spaced bulk samples from the studied sections, as well as of individual tephra layers within the sections.

(3) To test the possibility of distinguishing tephras on the basis of their magnetic properties

(4) To test the application of bulk sample XRF geochemistry to distinguish the tephras.

(5) To use the established tephrochronology to date the profiles, thereby enabling sedimentation rates to be calculated and thus to help assess human impact on the environment in SE Iceland.

This thesis is subdivided into ten chapters. This introductory chapter is followed by a general description of the literature relevant to studies of environmental magnetism (Chapter 2). Chapter 3 contains a description of the environmental background of the study area — Iceland, including the location, geology, climate, volcanic system, tephrochronology and human history. Chapter 4 presents the methods and techniques used in the field and laboratory to collect data sets concerned with tephra layers in five profiles from two study areas. Data preparation techniques, prior to the application of analytical methods, are also outlined. Chapter 5 describes the results of elemental analysis of individual tephra shards from selected samples, and uses the results to establish a tephrochronology for the study sections. Chapter 6 presents the

mineral magnetic and geochemical stratigraphies of the two peat profiles. Chapter 7 presents the mineral magnetic and geochemical stratigraphies of the three soil profiles Chapter 8 is divided into two parts: the first part summarizes the magnetic properties of the tephras in the studied sections and then uses those properties to infer the types of magnetic mineral assemblages present; and the second part uses the tephrochronology established in Chapter 5 to test the ability of the magnetic properties to characterise, or 'fingerprint', the tephras generated by individual volcanic eruptions. Chapter 9 develops a simple model to examine the contribution to dating of the soil profiles, and the calculation of soil sedimentation rates to help assess human impact on the Icelandic environment. Finally, Chapter 10 describes the conclusions of this study and gives some suggestions for future research.

1.3 Conventions and definitions

The following abbreviations are used :

ARM anhysteretic remanent magnetization.

$(B_0)_c$ coercivity, or coercive force.

$(B_0)_{cr}$ coercivity of remanence.

ED Euclidean distance.

IRM isothermal remanent magnetisation.

HIRM high field remanent magnetization.

MD multidomain.

M_{rs} or SIRM saturation isothermal remanent magnetisation.

PCA principal component analysis.

PSD	pseudo single domain.
SC	similarity coefficient.
SD	single domain.
SPSS	Statistical Package for the Social Sciences
SSD	stable single domain grain.
SP	superparamagnetism.
κ	volume susceptibility.
χ	mass-specific magnetic susceptibility.
χ_{fd}	frequency-dependent susceptibility.
χ_{low}	low field susceptibility.
χ_{high}	high field susceptibility.
χ_{para}	the mass-specific susceptibility of paramagnetic material.
$\chi_{para\%}$	the percentage paramagnetic susceptibility of the total susceptibility.
χ_{ferri}	the difference between χ low and χ high.
$\chi_{ferri\%}$	the percentage ferrimagnetic component of the total susceptibility, χ.
XRF	X-ray fluorescence

Chapter 2 Principles of Environmental magnetism

2.1 Introduction

Environmental magnetism is a versatile methodology applicable to a wide range of environmental studies and contexts.

Frank Oldfield, 1991

Rock and environmental magnetic measurements are the main technique used in this study. The physical principles and detailed studies of rock and environmental magnetism have been discussed in many books and publications, especially in Thompson and Oldfield (1986), Dunlop and Ozdemir (1997), and Maher and Thompson (1999). In the first part of this chapter, some of the magnetic properties, concepts and definitions involved in this study are described briefly; in the second part, examples of the application of the techniques to environmental studies are given.

2.2 Physical properties

2.2.1 Magnetic behaviour

The magnetic behaviour of all natural materials is the result of the orbital motion of electrons around the nucleus of the atom or the spin of the electron around its own axis. The main types of magnetic behaviour (Table 2.1) are: diamagnetism, paramagnetism, ferromagnetism and ferrimagnetism (Thompson and Oldfield, 1986).

Diamagnetism arises from the interaction of an applied magnetic field with the orbital motion of electrons and results in a very weak negative magnetization. It is lost when the

magnetic field is removed and is for all practical purposes independent of temperature. Many common natural minerals (e.g. quartz, feldspar, calcite and water, in Table 2.1) exhibit diamagnetic behaviour.

Table 2. 1 Magnetic minerals and their magnetic behaviour (based on Robinson, 1997).

Mineral	**Formula**	**Magnetic behaviour**
Iron	Fe	Ferromagnetic
Nickel	Ni	Ferromagnetic
Cobalt	Co	Ferromagnetic
Magnetite	Fe_3O_4	Ferrimagnetic
Titanomagnetite	Fe_3TiO_4	Ferrimagnetic
Ulvospinel	Fe_2TiO_4	Paramagnetic
Maghaemite	γ-Fe_2O_3	Ferrimagnetic
Haematite	α - Fe_2O_3	Canted-antif
Ilmenite	$FeTiO_3$	Paramagnetic
Pseudobrookite	Fe(1-2)Ti(2-1)O5	Paramagnetic
Wustite	FeO	Paramagnetic
Goethite	α-FeOOH	Canted-antif.
Lepidocrocite	γ-FeOOH	Paramagnetic
Pyrrhotite	Fe(1-0.87)S	Ferrimagnetic
Triolite	FeS	Antif.
Mackinagsitwe	FeS	Paramagnetic
Pyrite	FeS_2	Paramagnetic
Chalcopyrite	$CuFeS_2$	Paramagnetic
Siderite	$FeCO_3$	Paramagnetic
Chamosite	$(Fe/Mg/Al)_6[(Al/Si)_4O10](OOH)_{3-4}$	Paramagnetic
Glauoconite	$K(Fe/Al)_2(Si/Al)4O10(OH)_2$	Paramagnetic
Chromite	$FeCr_2O_4$	Ferrimagnetic
Jacobsite	$MnFe_2O_4$	Ferrimagnetic
Hercynite	$FeAl_2O_4$	Ferrimagnetic
Franklinite	$ZnFe_2O_4$	Ferrimagnetic
Magnesioferrite	$MgFe_2O_4$	Ferrimagnetic
Tervorite	$NiFe_2O_4$	Ferrimagnetic
Fe-Olivine	Fe_2SiO_4	Paramagnetic
Orthopyroxene	$FeSiO_3$ (24%FeO)	Paramagnetic
Biotite	$K(Mg/Fe)_3(Al/Si3)O10(OH,F)2$	Paramagnetic
Chlorite		Paramagnetic
Illite		Paramagnetic
Montmorillonite		Paramagnetic
Nontronite		Paramagnetic
Feldspar		Diamagnetic
Quartz	SiO_2	Diamagnetic
Carbonate Minerals	$CaCO_3$, $CaMgCO_3$ etc.	Diamagnetic
Pure Calcium Carbonate	$CaCO_3$	Diamagnetic
PVC Perspex etc.	P.V.C.	Diamagnetic

Paramagnetism is due to the electron spins of unpaired electrons, which tend to align themselves parallel with the direction of applied field and cause a weak positive magnetization. This paramagnetic moment is lost once the applied field is removed. Examples of paramagnetic materials are iron oxyhydroxides, biotite, pyroxene, garnet, and carbonates of iron and manganese (Table 2.1).

Ferrimagnetism is a weak form of ferromagnetism. The natural ferromagnetic minerals are commonly iron oxides (e.g. magnetite and maghemite, Table 2.1) with a spinel structure containing two types of magnetic sites, which have antiparallel magnetic moment of different magnitudes. Therefore the magnetic moment of the ferromagnetic minerals are ordered in an antiparallel sense, with the sum of the moments leading to a net magnetization.

Ferromagnetic minerals acquire a strong positive magnetization in an applied field and subsequently carry a remanent magnetization, which will be reduced to zero at the Curie temperature. When the spin atomic magnetic moments in the sublattices are defective (i.e. canted from their perfect antiparallel orientation), a weak net spontaneous magnetization results. This is described as *canted or imperfect antiferromagnetism* (AFM) and is displayed by haematite and goethite. These minerals acquire a positive magnetic moment much weaker than ferromagnetic ones in a magnetic field and retain part of the moment when the applied field is removed.

There are many types of magnetic minerals in different types of natural and anthropogenic materials, such as rocks, sediments, soils, peats, ice deposits, atmospheric particulate and waste products of human agricultural or industrial processes (Table 2.1). Magnetic minerals amount to only a very small fraction of natural sediments. There are no natural ferromagnetic minerals (e.g. native iron, nickel and cobalt). Natural magnetic minerals are classified as ferrimagnetic (e.g. magnetite, maghaemite, pyrrhotite, greigite) or canted antiferromagnetic (e.g. haematite, goethite). Ferrimagnets exhibit much higher but less stable magnetization compared to canted antiferromagnets. All other constituents are diamagnetic (e.g. organic matter, carbonate, quartz and water) or paramagnetic, which acquire a weak induced magnetization in a magnetic field. They can be discerned by their susceptibility, which is negative for diamagnetic and positive for paramagnetic minerals.

Empirical methods of characterizing natural materials on the basis of magnetic properties are open to criticism on two grounds. Firstly, the iron oxide minerals responsible for most of the magnetic properties are likely to undergo diagenesis, thus altering the magnetic 'fingerprint' (Robertson, 1993). Secondly, natural materials commonly contain several different phases of iron oxide minerals, all of which might contribute to the magnetic signature although not all need be diagnostic of the stratigraphic unit (Robertson, 1990). From past work (e.g. Haggerty, 1979), Fe-, Ca- and K-containing minerals are particularly useful for diagnostic purposes. Iron-titanium oxides are the most commonly used minerals in characterization studies. They are quite

sensitive to the environmental conditions of initial crystallization and bulk rock chemistry.

2.2.2 Magnetic grain size

Magnetism is associated with the existence of magnetic domains with uniformly oriented atomic moments (Table 2.2). As a function of grain-size, the number of domains within a magnetic particle increases from one to several hundred. *Single domain* (SD) and *multi domain* (MD) particles differ considerably in their magnetic characteristics. MD grains with a very few domains have similar properties to SD particles and are categorized as *pseudo-single domain* (PSD). The magnetization of ultra-fine particles belonging to a certain threshold size is unstable due to thermal activation (Maher *et al.*, 1999). Because of their high magnetic susceptibility and their inability to carry a remanence, they are called superparamagnetic (SP) particles, and contrast with stable single domain (SSD) grains (Thompson and Oldfield, 1986; Frederichs *et al.*, 1999).

The grain size thresholds between the four domain states (SP, SD, PSD and MD) primarily depend on mineralogy (Thompson and Oldfield, 1986). For magnetite, the SP/SD transition is at 0.03 μm (Dunlop, 1973), the SD/PSD boundary is at 0.1 μm and particles larger than 10 μm show MD behaviour (Bailey and Dunlop, 1983; Frederichs *et al.*, 1999).

Table 2. 2 Magnetic domains and their magnetic properties (Based on Yu, 1989; Lees, 1994).

Type	Grain Size (μm)					Characteristics	Magnetic Properties
	Dunlop (1973)	Dunlop (1981)	Thompson &Oldfield (1986)	Maher (1986)	Yu (1989)		
MD		>0.06	60-100	10-100		Large crystals	Show loss of magnetization Ms and SIRM. Low SIRM/ χ and ARM/ χ, high SIRM/ARM ratio.
PSD			1-10	1-10		Between MD and SSD	Intermediate characteristics.
SSD	>0.03	>0.03 <0.05	0.075-0.75	0.01-1	0.05	Grains of 0.05 μm. Each grain forms its own domain.	Higher remanence than MD. SIRM/ χ, ARM/ χ reach a maximum in SSD grains. SIRM/ARM is relatively low.
Viscous					0.02	Between SSD and SP, c. 0.02 μm in diameter	Response to changes in magnetic field is delayed. High χ -important in a narrow band of grains.
SP	<0.03	<0.025	0.075-0.01	0-0.01	0.001-0.01	Extremely small grains. 0.001-0.01 μm in diameter	Too small to retain remanence at a room temperature. Any magnetic moment induced in a strong field is immediately lost by thermal vibration. Zero SIRM and ARM. Disproportionately high susceptibility.

2.2.3 Magnetic hysteresis

Magnetic hysteresis is the variation of magnetization (M) with applied field (H) (Fig. 2.1).

Hysteresis reflects the fact that the magnetization of magnetic materials lags behind the external-inducing field. It is one of most important magnetic properties with which to characterize magnetic materials. Hysteresis measurements are used to characterize magnetic properties by hysteresis loop and derived magnetic parameters such as M_{rs}, M_s, χ_{low}, χ_{high}, χ_{ferri}, χ_{para} %, and their ratios (Table 2.3). The most important parameters which are derived from the hysteresis behaviour of natural materials are (1) magnetic susceptibility and frequency-dependent susceptibility; (2) isothermal remanent magnetization (IRM); (3) saturation magnetization (M_s) and saturation isothermal

remanence (SIRM) and (4) coercive force $(B_0)_c$ and coercivity of isothermal remanence $(B_0)_{cr}$. (Thompson and Oldfield, 1986; Robinson, 1997).

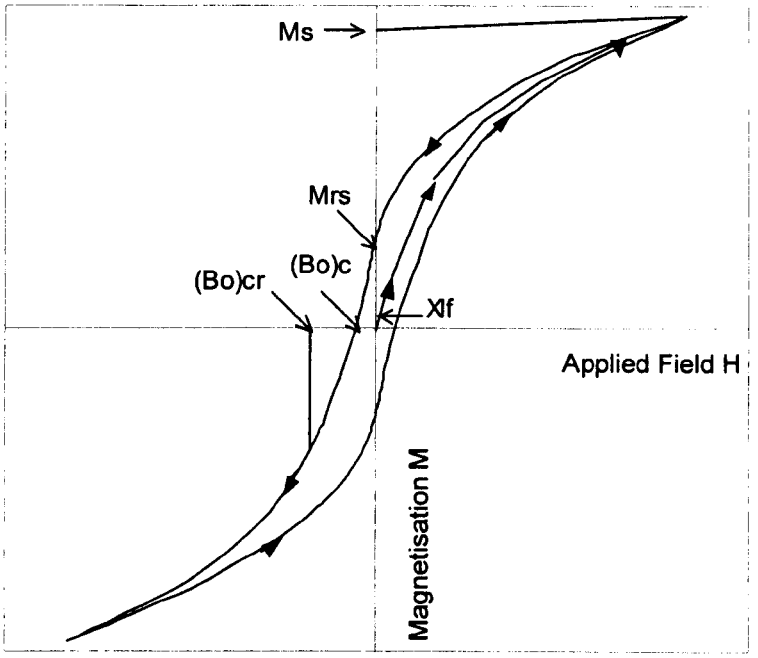

Figure 2.1 Schematic magnetic hysteresis loop, initial magnetization curve and associated magnetic parameters.

The hysteresis loop can be interpreted as a magnetic mineralogical signature by its shape. The heights of the loops are a function of the concentrations and types of magnetic minerals in natural samples. The width of the loops (expressed by $(B_0)_c$) is entirely controlled by the 'hardness' of minerals. The 'soft' minerals such as magnetite and pyrrhotite produce steep and narrow loops; greigite's behaviour is harder than that of magnetite and pyrrhotite, and so produces a flat and broader loop; haematite has an even broader loop. A reversible linear relationship, between magnetisation and applied field without any loop produced, is characteristic of paramagnetic or diamagnetic minerals; but the same property may be due to saturation at the maximum field (1T) available for

the VSM (Molyneux Vibrating Sample Magnetometer) measurements used in this work. Hence some samples do not exhibit significant hysteresis, and instead behave like paramagnets (Lees and Dearing, 1999).

Table 2.3 VSM hysteresis parameters (based on Lees, 1994).

Parameter	Units	Magnetic minerals	Grain size	Interpretation
χ_{low}	m^3kg^{-1}	Ferri, Canted-anti, Para Diamagnetic	MD, SD, SP	Low-field magnetic susceptibility. Like χ_{lf} indicates the ferrimagnetic, paramagnetic and canted-antiferromagnetic component of a material minus the diamagnetic component
χ_{high}	m^3kg^{-1}	Canted-anti, Para*m*, Dia*m*	MD, SD	High-field magnetic susceptibility. Indicates the paramagnetic and canted-antiferromagnetic component of a material minus the diamagnetic component.
χ_{ferri}	m^3kg^{-1}	Fine-grained ferri	SP	The mass specific susceptibility component of ferrimagnetic minerals calculated from the different between χlow and χhigh. Also calculated is the percentage ferrimagnetic component of the total susceptibility χ ferri%.
χ_{para}	m^3kg^{-1}			χ para is the mass specific susceptibility of the paramagnetic material, χpara% is the percentage paramagnetic susceptibility of the total susceptibility.
M_s	Am^2kg^{-1}	Ferrim, canted-anti	MD, SD, SP	The saturation magnetization of a ferrimagnetic component of material and is calculated by extrapolating the high field magnetisation.
M_{rs}	Am^2kg^{-1}	Ferrim, canted-anti	MD, SD	The saturation remanence of material is the remanence value at zero field following magnetization at 1 T.
M_{rs}/M_s				In the absence of paramagnetic minerals, this gives information about 'magnetite' type and grains sizes
$HIRM_{+100mT}$				The total concentration of remanence carrying haematites can be approximated.
'S'ratio				Indicates the proportions of soft magnetic minerals, such as magnetite, to total remanence carrying mineral content.

The shapes of hysteresis loops also reflect grain size variation. The saturation magnetisation is independent of grain size variation; grain sizes only affect the width of the loop. 'Hard' SD ferrimagnetic grains produce broader loops than 'soft' MD grains; and the 'softest' component, SP grains, do not display a hysteresis loop at all (Thompson & Oldfield, 1986; Yu, 1997). The most general use of hysteresis parameters is to determine bulk magnetic domain state. The ratios M_{rs}/M_s and $(B_0)_{cr}/(B_0)_c$ are plotted in a Day plot (Day *et al.*, 1977; Dunlop and Ozdemir, 1997; Thompson and Oldfield, 1986)

with different regions of the plot depicting MD, PSD and SD bulk domain states. For ideal MD grains $M_{rs}/M_s \leq 0.05$ (Dunlop and Ozdemir, 1997). $(B_0)_{cr}/(B_0)_c$ has less discriminating power than M_{rs}/M_s; however $(B_0)_{cr}/(B_0)_c \approx 1$ for SD grains and for ideal MD grains $(B_0)_{cr}/(B_0)_c \geq 4$ (Dunlop and Ozdemir, 1997). The majority of basaltic samples fall in PSD size range.

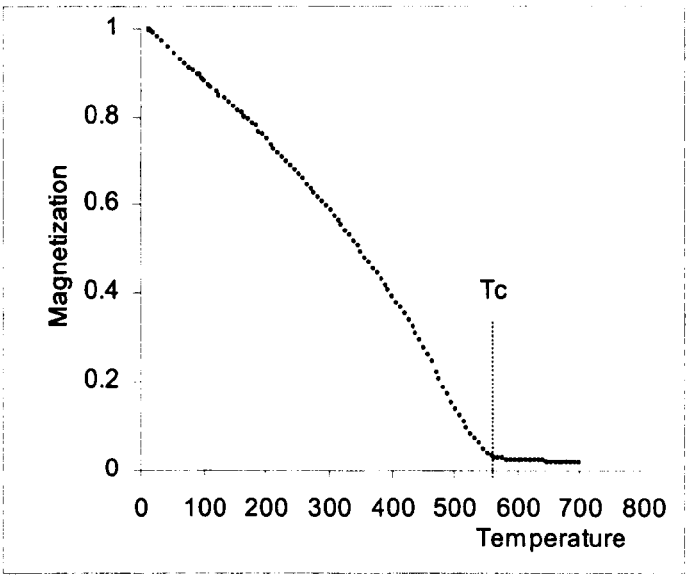

Figure 2.2 Schematic Curie, curve illustrating the graphical determination of Curie point.

2.2.4 Curie temperatures

The identification of magnetic minerals from Curie temperature measurements is based on the observation of thermal changes in spontaneous magnetization. It has been found that on heating beyond a critical temperature, ferrimagnetic or antiferromagnetic materials become paramagnetic, thus exhibiting magnetic proportional dependence on temperature. In the absence of an applied field there is no magnetisation above the Curie

temperature (Fig. 2.2). In an applied field, however, the paramagnetic component will acquire a magnetization. The temperature, T, dependence of the magnetization of paramagnetic minerals is governed by the Curie-Weiss law (e.g. Dunlop and Ozdemir, 1997)

$$\chi = \frac{M}{H} = \frac{C}{T}$$

where χ is the susceptibility, M the magnetization, H the magnetic field and C the Curie constant.

Table 2.4 Typical magnetic properties of natural minerals (After Maher *et al.*, 1999, page 31).

Mineral	Tc (°C)	M_s (Am^2kg^{-1})	χ ($\times10^{-6}m^3kg^{-1}$)	ARM (mAm^2kg^{-1})	SIRM (Am^2Kg^{-1})
Magnetite (Soft)	575	92	560	18	9
Magnetite (Hard)	575	92	400	110	22
Titanomagnetite (soft)	200	24	170	80	7
Titanomagnetite (hard)	200	24	200	480	12
Haematite	675	0.5	0.6	0.002	0.24
Ilmenohaematite	100	30	25	480	8
Greigite	300	20	120	110	11
Pyrrhotite	300	17	50	80	4.5
Goethite	150	0.5	0.7	0.005	0.05
Iron	770	220	2000	800	80
Paramagnet	1/T	--	~1	0	0
Diamagnet	const	--	-0.006	0	0

Curie point determination becomes complicated when thermomagnetic changes occur during heating. However, such processes can be used as a diagnostic signature (Table

2.4); generally, heating is associated with an oxidation process, and causes transformation of minerals from low oxidation states to high oxidation states, i.e. iron sulphides will be transformed into magnetite and hematite. However, an opposite process may be caused on heating when a sample contains sufficient organic matter to create a reducing environment on combustion. The formation of new minerals observed by the increase or decrease of magnetization in Ms-T curves could, therefore, be helpful in certain cases in distinguishing magnetic minerals. For example, a massive increase in magnetization on heating and a much higher cooling curve than the heating one is caused by mineral transformation from a very weak magnetic material to a strong one, i.e. from paramagnetic to ferrimagnetic minerals (Thompson & Oldfield, 1986).

2.3 Magnetic parameters

Magnetic parameters are widely used to characterise magnetic minerals because they are sensitive to magnetic mineralogy, as well to the grain size and shapes of magnetic grains (Tables 2.3 and 2.5). Several parameters (Tables 2.5 and 2.6), used in this study, are briefly described below.

Magnetic susceptibility (χ) is a measure of the ease with which a substance becomes magnetized in an external field. It is defined as the ratio of the magnetization to the applied field, M/H. It can be measured in high and low applied fields and at different frequencies. Using a Bartington MS2B dual frequency sensor (Dearing, 1994; 1999), the mass dependent susceptibility has been determined in low field at low (470Hz) and high (4700 Hz) frequency. At room temperature, it is roughly proportional to the

concentration of ferrimagnetic and paramagnetic minerals within the sample (Thompson and Oldfield, 1986; Robinson, 1997). Dearing *et al.*'s (1996, 1997) work indicates that ferrimagnetic minerals dominate magnetic mineral assemblages. Magnetic susceptibility is controlled by the following factors in order of decreasing importance: mineral concentration (χ_{lf} varies by a factor of $20000\text{-}30000\times10^{-6}m^3kg^{-1}$), mineral composition (χ_{lf} varies by a factor of $300\text{-}400\times10^{-6}m^3kg^{-1}$) and crystal size and shape (χ_{lf} varies by a factor of $<200\times10^{-6}m^3kg^{-1}$) (Dearing, 1999).

Mass-specific frequency dependent susceptibility (χ_{fd}), or percentage frequency dependent susceptibility (χ_{fd} %) is the variation of susceptibility between two frequencies (470 Hz and 4700 Hz), χ_{lf} and χ_{hf}.

$$\chi_{fd} = \chi_{lf} - \chi_{hf}$$

$$\chi_{fd}\% = \frac{\chi lf - \chi hf}{\chi lf} \times 100$$

High values of χ_{fd} % indicate the presence of ferrimagnetic grains lying at the SD/SP boundary (~0.02 μm), as a proportion of those grains become blocked in and will no longer contribute to χ_{hf} as SP but SD grains. If the χ_{fd} % values are medium (~2.0-10.0 %), this indicates there is an admixture of SP and coarse grains, or SP grains <0.005 μm (Bloemendal et al., 1985; Thompson & Oldfield, 1986; Verosub and Roberts, 1995; Dearing, 1997, 1999). Recently, Dearing et al. (1999) suggested that it may help to discriminate between grain-size and domain state if plots of χ_{fd} % versus χ lf and χ_{fd} are used (Dearing et al., 1996). Samples dominated by relatively coarse-grained non-SP ferrimagnets show relatively high χ lf but virtually zero χ_{fd}. Samples with a significant

proportion of SP grains have χ_{fd}% values >6 and occupy an envelop bounded by limits which may define grains <0.015μm and >0.015 μm. Values of χ_{fd}% <5 are typical for samples in which non-SP grains dominate the assemblage or where extremely fine grains (<0.005 μm) dominate the SP fraction. For samples with χ_{fd}% >10, SP grains dominate the assemblage and χ_{fd} can be used semi-quantitatively to estimate their total concentration (Dearing *et al.*, 1997).

ARM or χ_{ARM} is produced by exposure to a gradually decreasing alternating frequency (AF) field with a weak steady (DC) field superimposed. It is more sensitive than most other parameters to variations in magnetic grain size, both of ferrimagnetic and canted-antiferromagnetic grains. ARM is always most sensitive to the fine-grained ferrimagnetic components, if present; then to the PSD ferrimagnets; and lastly, to the MD canted antiferromagnets (Hu, 1998). The peak of χ_{ARM} occurs in the finest SD grains, somewhere near the boundary of SP and SD, from which it decreases towards to the coarse end and declines rapidly to zero towards to the finer end. Thus χ_{ARM} may be used to indicate the concentration of fine ferrimagnetic grains. χ_{ARM}/χ is particularly sensitive to variations in the proportion of the fine magnetic grain sizes and magnetic mineralogy (Banerjee *et al.*, 1981; King *et al.*, 1982; Bloemendal *et al.*, 1985; Thompson & Oldfield, 1986; Robinson 1997). χ_{ARM} /χ_{lf} indicates changes in magnetite grain size if the magnetic mineralogy is dominantly magnetite. It varies inversely with magnetite grain size, being particularly sensitive to magnetic grains within the 1-10 um size range (Stoner et al, 1996, Nolan, 1999). However interpretation of χ_{ARM} /χ_{lf} is complicated by SP and paramagnetic grains (Bloemendal *et al.*, 1992). The difference between the

response of χ_{ARM} /χ_{lf} and χ_{ARM} /SIRM, in the same sample may occur as a result of a large superparamagnetic component (Thompson & Oldfield, 1986; Robinson 1997).

Table 2.5 Properties of the measured magnetic parameters (after Thompson and Oldfield, 1986; Lees, 1994; Robinson, 1997).

Parameter	Interpretation
χ	Its value is roughly proportional to the concentration of ferrimagnetic and paramagnetic minerals within the sample. If the concentration of ferrimagnetic constituents in the sample is extremely low (e. g. <0.1), then the susceptibility of any canted-antiferromagnetic or paramagnetic material present may become important.
ARM or χ_{ARM}	The remanence produced in a sample by subjecting it to an increasing and decreasing (0mT--100 mT--0 mT) alternating magnetic field superimposed upon a steady dc magnetic field (0.04 mT). The remanence is proportional to the steady field. It can be measured on a constant volume or mass-specific basis. ARM is more sensitive than any other concentration-dependent parameter to variation in magnetic grain size, both of ferrimagnetic and canted-antiferromagnetic grains.
SIRM	The highest amount of magnetic remanence that can be produced in and retained by a sample at a given temperature (usually room temperature). It can be measured on a constant volume or mass-specific basis. SIRM is highest for SD ferrimagnetic grains (particularly uniaxial SSD ferrimagnetic particles) and decreases as magnetic grain size opposes that of χ_{lf}, but this parameter is much more sensitive to grain size in the SD-MD range.
IRM	The remanence produced in a sample by the application and subsequent removal of a known magnetic field (-20 mT, -40mT, -100mT, -200mT and -300 mT), the magnetization grows parallel to the applied field. IRM and SIRM are also very strongly dependent on ferrimagnetic concentration but, unlike χ, are much more sensitive to contributions made by canted-antiferromagnetic minerals in the sample.

IRM and SIRM are also very strongly dependent on the ferrimagnetic constituents in samples. SIRM is highest for SD ferrimagnetic grains and decreases as magnetic grain size rises logarithmically. Soft, the IRM acquired at -20mT, is often used as an indicator of the magnetically 'soft' component, i.e. mainly MD ferrimagnetic grain components in

samples. Hard isothermal remanence (HIRM), the difference between SIRM and IRM_{300mT}, is proportional to the concentration of canted antiferromagnetic material, because ferrimagnetic components are saturated in magnetic fields of 200-300 mT (Thompson & Oldfield, 1986; Robinson 1997).

Table 2.6 Typical magnetic ratios of natural magnetic minerals (based on Maher *et al.*, 1999).

Mineral	SIRM/χ (kAm^{-1})	S_{-40}	S_{-100}	ARM/SIRM	ARM/χ (kAm^{-1})
Magnetite (Soft)	1.6	0.83	0.97	0.02	0.03
Magnetite (Hard)	55	0.26	0.85	0.005	0.3
Titanomagnetite (soft)	10	0.5	0.82	0.004	0.
Titanomagnetite (hard)	60	0.08	0.34	0.04	2.4
Haematite	400	0.005	0.003	0.001	0.01
Ilmenohaematite	320	0.02	0.13	0.004	19.0
Greigite	92	0.03	0.38	0.01	0.9
Pyrrhotite	90	0.8	0.95	0.018	1.6
Goethite	70	0.005	0.02	0.01	1.0
Iron	40	0.4	0.8	0.01	0.4

SIRM/χ is made-up of two fundamental hysteresis parameters. It is a useful indicator of overall hysteresis behaviour of a sample, bearing a direct and predictable relationship to differences in their magnetic mineralogy and granulometry. SIRM/χ and χ_{ARM}/χ have high values in the range of SSD, and low values in SP grains and in large MD grains (Tauxe, 1993; Verosub and Roberts, 1995).

χ_{ARM} /SIRM is particularly useful for discriminating between ferrimagnetic grain size categories (Maher, 1988). Because both χ_{ARM} and SIRM are remanence parameters, they are unaffected by paramagnetic contributions and hence the ratio is more size-sensitive. At the same time, SIRM/ARM is sensitive to variations in coarser grained magnetic grains, particularly ferrimagnetic grains greater than 10 um. The ratio is relatively insensitive to varations in the finer magnetic grain size fractions, but is more sensitive to these variations than SIRM/χ (Robinson, 1997).

2.4 Application of magnetic techniques to environmental studies

Following the suggestion by Thompson *et al.* (1980), a relatively new expansion of geophysics is called environmental magnetism. It is also the title of a milestone textbook by Thompson and Oldfield (1986), which brought the field to the attention of a wider audience and was instrumental in the recent, rapid expansion in the use of mineral magnetic techniques to address a variety of environmental problems. In environmental magnetism studies, not only the materials studied but also the object of rock-magnetic characterization is different from those of conventional mineral magnetism. It is the use of magnetic measurements to identify the nature and concentration of Fe-containing minerals in environmental materials. Magnetic measurements are simple, rapid, sensitive and non-destructive and have been applied to a variety of environmental materials. Recent reviews of environmental magnetism, including those by Oldfield (1991) and King and Channell (1991), Verosub and Roberts (1995) and Frederichs *et al.* (1999), show that environmental magnetism is an ideal tool for environmental studies in a variety of environmental or palaeo-environmental investigations

Magnetic properties have been used to characterize soils, and it was found that the magnetic properties were different between topsoil and subsoil horizons (Le Borgne, 1955; Tite and Mullins, 1971; Vadyunina and Babanin, 1972; Smith *et al.*, 1990), due to a magnetic enhancement in the topsoil, as a result of the neoformation of magnetite or maghemite by burning (e.g. Mullins, 1977; Rummery *et al.*, 1979), pedogenic factors (e.g. Singer *et al.*, 1992; Fine *et al.*, 1989), or bacterial action (Fassbinder *et al.*, 1990). Subsoil has lower magnetic values and overall the use of mixing models for sources of colluvium was proposed (Smith *et al.*, 1990). Maher (1988) has proposed that the supply of Fe is less of a limiting factor for neoformation than the competitive interplay between the formation of secondary ferrimagnetic minerals and non-ferrimagnetic secondary minerals. Hanesch and Petersen (1999) used a combination of mineral magnetic measurements, TEM and experimental growth media to demonstrate the important of iron-reducing bacteria in the growth of extracellular bacterial magnetite in a parabrown soil. Dearing *et al.* (2001) demonstrated that the ferrimagnetic component of strongly enhanced surface soil is dominated by SP grains with minor proportions of larger SSD/PSD grains that may derive from magnetosomes and magnetic inclusions based on a combination of magnetic, geochemical and DNA analyses of a small set of bulk and fine fraction samples of highly magnetic English topsoils. Moreover, the contribution of *in situ* pedogenic magnetite to the magnetic properties in loess sections (Heller and Liu 1986; Kukla 1987; Kukla and An, 1989; Zhou *et al.*, 1990; Chen *et al.*, 1993; Chen *et al.*, 1997, 2000) might give a significance clue to this issue (Oldfield, 1991).

Lake sediments provided the initial impetus for the development of environmental magnetism (Oldfield, 1991). Thompson *et al.* (1975) found that magnetic susceptibility was positively correlated with the amount of inorganic material present in lake sediment cores. Magnetic measurements, e.g. magnetic susceptibility, could provide an empirical basis for calculation of sediment influxes within lake catchments (e.g. Bloemendal *et al.*, 1979). A wide variety of magnetic parameters can be measured and their stratigraphic variations assessed in terms of particle size, erosion intensity, soil-forming processes, redox potentials and bacterial activity, which are directly and indirectly controlled by climate change and human impact (Oldfield *et al.*, 1978, 1983, 1985, 2000; Thompson and Morton, 1979; Dearing *et al.*, 1981, 1983; Appleby *et al.*, 1986; Foster *et al.*, 1988, 1990). Kodama *et al.* (1997) showed a strong correlation between rainfall observations over the past 250 years and the concentration of detrital magnetic minerals in lake sediments. Zolitschka (1998) demonstrated a significant relationship between the accumulation rate of mineral sediment of detrital origin and the initial magnetic susceptibility of a 14 000 year lake sediment core. Recently, Snowball (1997, 1999) reported that paramagnetic susceptibility reflects the concentration of detrital minerogenic material, which is controlled to a large extent by the intensity of spring snow melt; and the concentration of ferrimagnetic magnetite is positively correlated to the concentration of organic carbon, which is most likely of an autochthonous origin (Snowball *et al.*, 2002).

Studies of marine sediments illustrate a wide range of fascinating possibilities (Bloemendal, 1980; Bloemendal *et al.*, 1988, 1989, 1992, 1993; Kent, 1982; Robinson, 1986, 1989, Sager and Hall, 1990; Stoner *et al.*, 1996, Frederichs *et al.*, 1999).

Bloemendal (1980), Kent (1982) and Robinson (1989) have demonstrated detailed linkages between climatic variations and the magnetic mineral and grain size assemblages preserved in sediments accumulating above the carbonate compensation depth. Mead *et al.* (1986) applied spectral analysis to magnetic susceptibility data to illustrate their relation to the orbitally driven periodicities. Bloemendal *et al.* (1988) used magnetic parameter core logs as a direct proxy for oxygen isotope records. Doh *et al.* (1988) identified the aeolian contribution to central North Pacific sediments. DeMenocal *et al.* (1988) found variations in bottom current activity in cores from the Bermuda Rise. Sager and Hall (1990) described the magnetic signature of turbidity currents. Bloemendal and DeMenocal (1989) showed the variations in the magnetic susceptibility signal were closely correlated with the variations in Earth's orbital parameters in Arabian Sea sediments. Subsequent work demonstrated a strong relationship between the concentration of terrigenous material and various mineral magnetic parameters, e.g. χ (DeMenocal *et al.*, 1991; Bloemendal *et al.*, 1993). However, Meynadier *et al.* (1991) showed that the ratio of magnetite to haematite had remained fairly constant despite the occurrence of major climatic changes in the Somali Basin. Bloemendal *et al.* (1992) related rock magnetic parameters to sediment source, lithology and diagenetic processes. Stoner et al. (1996) correlated the magnetic characteristics of detrital horizons from deep Labraor Sea to North Atlantic Heinrich layers.

The occurrence of atmospherically transported magnetic particles in sediments has been known for many years. Magnetic measurements are well suited to differentiating atmospheric dust and aerosols from different types of source (Hunt *et al.*, 1984; Oldfield

et al., 1985; Hunt, 1986; Hay *et al.*, 1997; Charlesworth and Lees, 1997; Xie *et al.*, 1999, 2000; Shu *et al.*, 2000, 2001). In these studies, the sediments were characterized and discriminated from other deposits using magnetic parameters. Magnetic measurements of recent peat and lake sediments with consistently low catchment-derived magnetic input appear to provide a good record of the deposition of particulate pollutants (Oldfield *et al.*, 1985; Battarbee *et al.*, 1988). Environmental magnetic studies of the aeolian components of deep-sea sediments have been widely used in paleoclimate studies (Robinson, 1986; Bloemendal and DeMenocal, 1989) in locations, where there is the large influence of terrigenous dust. The magnetic susceptibility record of the Chinese loess plateau (Kukla and An, 1988) was used to correlate the continental loess stratigraphy with a record from an Antarctic ice core (Li *et al.*, 1992) and with dust flux to the Northwest Pacific Ocean (Hovan *et al*, 1989). However, Maher and Thompson (1992) demonstrated that such a correlation is not ideal because the susceptibility variations in the Chinese loess appear to be pedogenically controlled (Zhou *et al*, 1990; Maher and Thompson, 1991).

One of the most urgent needs in environmental magnetism is to translate the magnetic measurement results into statistically defined, mathematically accessible and more easily communicable components (Oldfield, 1991, 1999; Xie *et al.*, 1999). There have been several complementary attempts to do this. The statistical procedure of discrimination analysis was used by Hunt (1986), and showed that this may well provide a relatively simple and objective basis for grouping samples into statistically definable assemblages on the basis of a wide range of environmentally diagnostic magnetic properties.

Thompson (1986) described two approaches to modeling magnetization data: the first by modeling the magnetic properties of natural materials in terms of mixtures of possible source materials, and the second by modeling the magnetic properties of natural materials in terms of mixtures of magnetite and haematite crystals of varying concentrations and grain sizes. Another attempt is represented by the development of empirical models to estimate the contributions of magnetically differentiated types of source material (Stott, 1986; Yu and Oldfield, 1989; Lees 1997). On the basis of the magnetic properties of some synthetic submicron magnetites, Maher (1988) proposed a method of magnetic granulometry using a sequence of measurements, such as the ratio χ_{ARM}/SIRM and χ_{fd} percentage, which has been further tested by Oldfield (1994) and Dearing et al., (1997). Robertson and France (1994) and Stockhausen (1998) tried to discriminate among magnetic phases using cumulative log Gaussian functions to model IRM acquisition curves. Recently the concept of partial susceptibility for quantitative analysis of carriers of magnetic susceptibility was introduced in marine sediments (Von Dobeneck 1998 and Frederichs *et al.,* 1999) and street dust (Xie *et al.*, 1999).

Environmental magnetism can be used to investigate the effects of diagenesis on the detrital paleomagnetic record, due to, the fact that magnetic minerals can provide insight into the processes active in the depositional and post-depositional environment (Verosub and Roberts, 1995). Dissolution of detrital magnetic minerals is vert common in sediments deposited under sulfate-reducing conditions (Canfield and Berner, 1987). Hydrogenous Fe-Mn hydroxides and oxides can form and these minerals often obscure any primary depositional remenence in slowly deposited oxic sediments with little

organic matter (Henshaw and Merrill, 1980). In more rapidly deposited sediments with higher organic contents, manganese oxides are precipitated, and biogenic magnetite can be formed in the sediments just above the iron reduction zone (Karlin *et al.*, 1987; Peterman and Bleil, 1993; Hesse, 1994). Deeper in the sediment column, in the iron reduction zone, many of these fine-grained magnetites and detrital magnetic phases are dissolved. If sulphide reduction occurs, the magnetic oxic inverts to iron sulphides, particularly pyrite. However, iron monosulphides such as mackinawite and greigite are sometimes preserved (Karlin and Levi, 1983, 1985; Canfield and Berner, 1987; Karlin, 1990, Leslie et al., 1990). In sulphate-limited environments (e.g. lakes, bogs, estuaries, and some rapidly deposited marine sediments), pyritization does not go to completion and ferrimagnetic greigite can be preserved (Tric et al., 1991; Williams, 1992; Roberts and Turner, 1993).

Chapter 3 Environmental Background of Iceland

The situation in Iceland for establishing a tephrochronological time scale is very good. This is due to the great number of volcanic eruptions in the post glacial time, a great range of variation in chemistry between tephra layers, a rapid thickening of the soil, separating layers with small age difference, and the existence of detailed accounts of many historical eruptions.

Sigurdur Thorarinsson, 1980

3.1 Introduction

Iceland, the second largest island in Europe, is located in the Atlantic Ocean (latitude 63° N to 67° N, and longitude 13° W to 25° W) northwest of Scotland (798 km), west of Norway (970 km) and southeast of Greenland (287 km) (Fig. 3.1). The main island, which stretches 500 km east to west and 300 km north to south, is distinguished by its Tertiary and Quaternary volcanic origin. Over half of the country is above 400 m, with the highest point, Hvannadalshnúkur in the Öræfajökull glacier in Southeast Iceland, rising to 2119 m. The greater part of Iceland's land mass consists of a central plateau, which is unsuitable for human habitation. Only 21 % of the land, all near the coast, is considered arable and habitable. The bulk of Iceland's population and agriculture is concentrated in the southwest near Reykjavik.

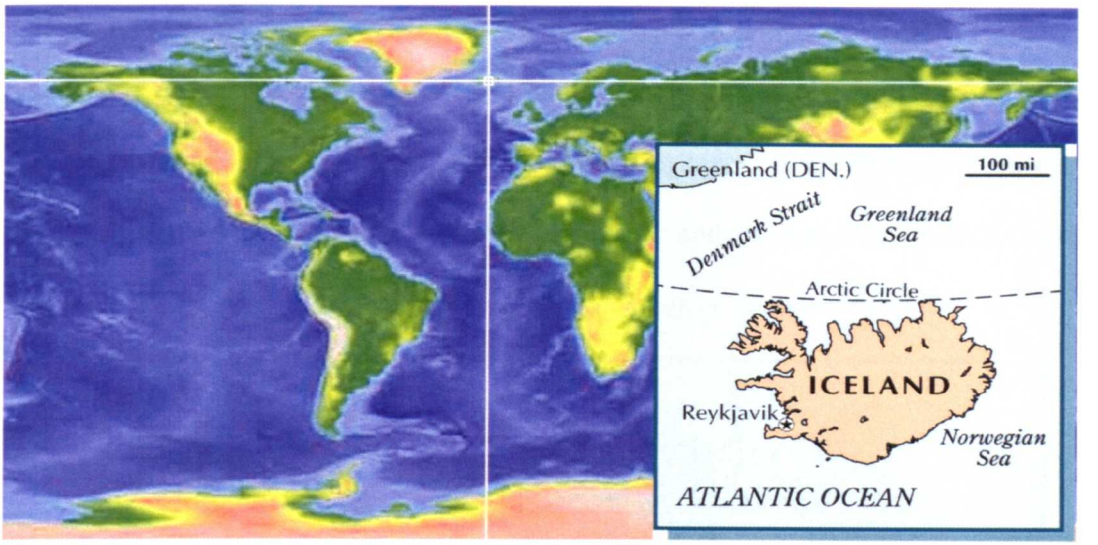

Figure 3.1 Location of Iceland.

(Based on: http://www.traveljournals.net/countries/mapzoom.asp?c=ic7517; http://www.bartleby.com/61/imagepages/A4icelan.html)

3.2 Geology

In terms of its geologic origin, Iceland is perhaps one of the most easily explained independent islands in the world. This is because it is almost entirely composed of extruded basaltic lava (Fig. 3.2; Wilcoxson, 1967). Although the era of mass flood eruption ended many millions of years ago, present-day activity is still considerable, showing on a smaller scale the uniform processes that have created and developed the island.

Iceland is situated in the North Atlantic where two large physiographic structures meet - the Mid-Atlantic Ridge and the Greenland-Faeroes Ridge. Because of the elevated topography, high heat flow and discharge of volcanic rocks, Iceland has been defined as

an anomaly of the spreading Mid-Atlantic Ridge (Jackobsson *et al.*, 1980). It is an abrupt and jagged landscape. Volcanic eruptions have been numerous and frequent, averaging 20 per century during historical time. Consequently, most of the island is geologically young, and is characterized by desert plateaus, sandy deltas, volcanoes, lava fields, and icecaps. In terms of vegetation cover and land-use much of the country consists of expanses of tundra, grassland, bog and barren desert.

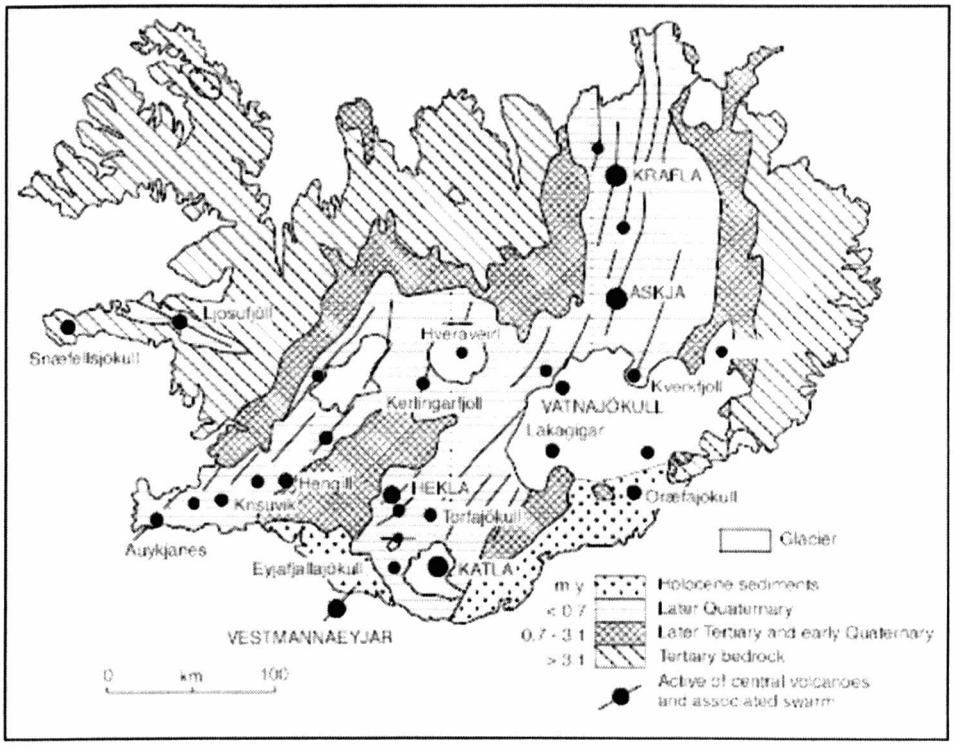

Figure 3.2 Geological map of Iceland

3.3 Climate

Iceland is situated at a meeting point for cold air from the polar region and warmer air from the Atlantic. The surrounding seas are driven by two principal contrasting ocean currents: the warm Irminger current and the cold East Greenland current. These factors

determine the variability of Icelandic climate. Another major feature of the climate of Iceland is its proximity to the Arctic sea ice. Ice generated in the cold polar region is carried southward to Icelandic shores by the East Greenland current. The northern, northwestern and eastern coasts are most commonly affected. The extent of the ice varies on all time scales. There have been relatively few 'ice years' in the twentieth century, but in the eighteenth and nineteenth centuries there was a high incidence of sea ice off the Icelandic coasts. Although the relationship between temperature and sea ice is complex, some research (e.g. Bergthorsson, 1969) has confirmed that it is valid to assume a colder climate in Iceland during periods of high sea ice incidence than in times of little or no ice off the coasts.

Table 3.1 Icelandic climate data for 1961-1990. All stations are shown in Figure 3.3. (Source: http://www.vedur.is/english/index_eng.html?)

Site	(°C, mm)	Jan.	Feb.	Mar.	Apr.	May	Jun.	Jul.	Aug.	Sept.	Oct.	Nov.	Dec.	Year
Reykjavik	Mean tem.	-0.5	0.4	0.5	2.9	6.3	9	10.6	10.3	7.4	4.4	1.1	-0.2	4.3
Station No. 1	Precipitation	75.6	71.8	81.8	58.3	43.8	50	51.8	61.8	66.5	85.6	72.5	78.7	799
Akureyri	Mean tem.	-2.2	-1.5	-1.3	1.6	5.5	9.1	10.5	10	6.3	3	-0.4	-1.9	3.2
Station No. 422	Precipitation	55.2	42.5	43.3	29.2	19.3	28.2	33	34.1	39.1	58	54.2	52.8	490
Teigarhorn	Mean tem.	-0.3	0.2	0.4	2.2	4.5	7.3	8.8	8.8	6.9	4.4	1.3	-0.1	3.7
Station No. 675	Precipitation	129	109	107	70.4	76.8	71.9	83.8	109.8	110.1	152	97.8	111	1229
Hornafirthi	Mean tem.	0.1	0.7	1	3.1	6	8.6	10.2	9.8	7.5	4.8	1.5	0	4.4
Station No. 710	Precipitation	164	130	121	94.8	95.7	86	84.4	110.7	119	183	116.8	145.9	1453
Fagurholsmyr	Mean tem.	0.3	0.9	1.3	3.4	6.2	8.7	10.5	10	7.5	4.8	1.6	0.1	4.6
Station No. 745	Precipitation	170	152	143	128	129	133	115	152.9	156	213	153	157.4	1802
Kirkjubaejarklaustu	Mean tem.	-0.4	0.2	0.7	3.2	6.5	9.4	11.2	10.4	7.5	4.5	1.1	-0.4	4.5
Station No. 772	Precipitation	145	130	131	115	118	131	121	158.7	141	185	137	133.1	1645

Considering the northerly location of Iceland, its climate is much milder than might be expected, especially in winter. Summers tend to be cool - the mean temperature was 10.6

°C for July in Reykjavik during 1961-1990 (Table 3.1). Winter is generally not very cold, and the corresponding figure for January, often the coldest month, is -0.5 °C (Table 3.1). Rain falls frequently, and the mean annual rainfall for Reykjavik for 1961 to 1990 was 799 mm. The annual precipitation (Fig. 3.3) on the south coast is about 3,000 mm, whereas in the highlands north of Vatnajökull it drops to 400 mm or less (Thorarinsson, 1961).

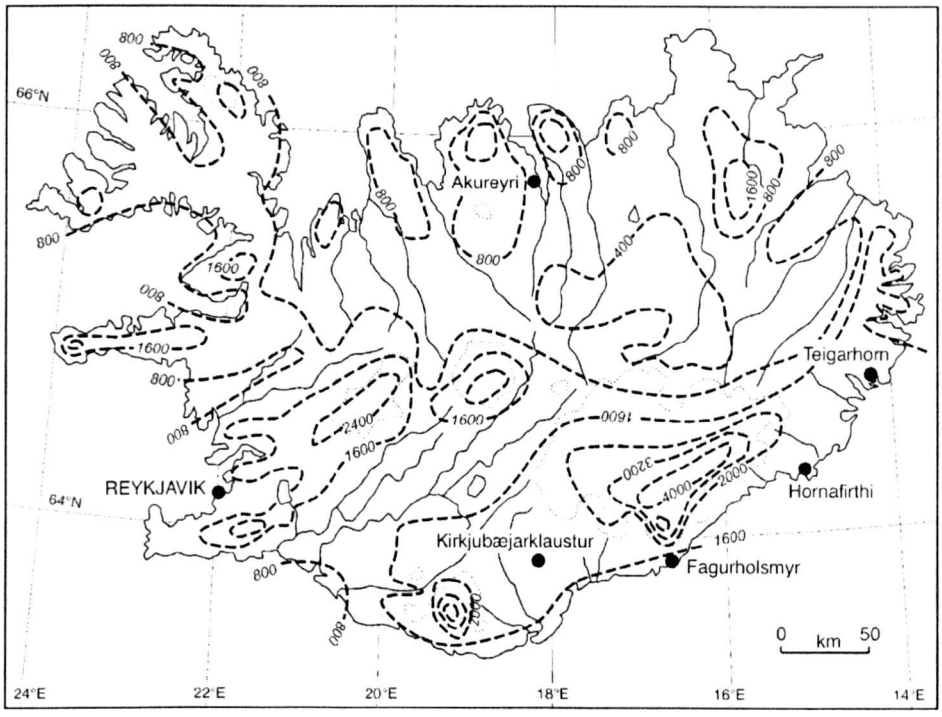

Figure 3. 3 The mean annual precipitation map of Iceland. (Based on Thorarinsson, 1961).

3.4 The Icelandic volcanic system

Jakobsson (1979) defines a volcanic system as a "spatial grouping of eruption sites in a certain period of time, with particular characteristics of tectonics, petrography and geochemistry". Volcanic systems usually start off as fissure swarms producing basaltic

rocks. In time, more evolved rocks are produced and activity often becomes concentrated in one area; a caldera, central volcano and high temperature thermal field eventually follow. Volcanic systems generally have a life of between 300,000 and 500,000 years, but central volcanoes may reach an age of over 2 million years.

From a petrogenetic viewpoint, two main types of volcano have been active: purely basaltic ones, and central volcanoes producing intermediate and acid rocks besides basalt (Larsen *et al.*, 1999). Nearly every type of volcano found globally is represented in Iceland (Jakobsson, 1979). Hekla, Orafajokull, Eyjafjallajokull, Torfajokull and Askja, transect the island from southeast to northwest (Larsen *et al.*, 1999).

The volcanically active areas of Iceland can be divided into 5 volcanic zones (Fig. 3.4). These are the Snæfellsness Zone, the West (or Reykjanes-Langjokull) Zone, the Northern Zone, the Eastern Zone (quoted in http://www.geo.ed.ac.uk/tephra/tephrochron.html; Jakobsson, 1979), and Southeast (or Öræfajökull) Zone. Within these zones are found volcanic systems (Fig. 3.3). The Eastern Volcanic Zone (EVZ) has produced the most tephra in the Holocene and it might be for this reason that a lot of attention has been paid to it (Jakobsson, 1979; Larsen, 1981; 1982; 1999). The sections below provide some details of several important volcanic systems mainly from the Eastern Volcanic Zone and Southeast (or Öræfajökull) Zone, which occur around the study area (see section 4.2).

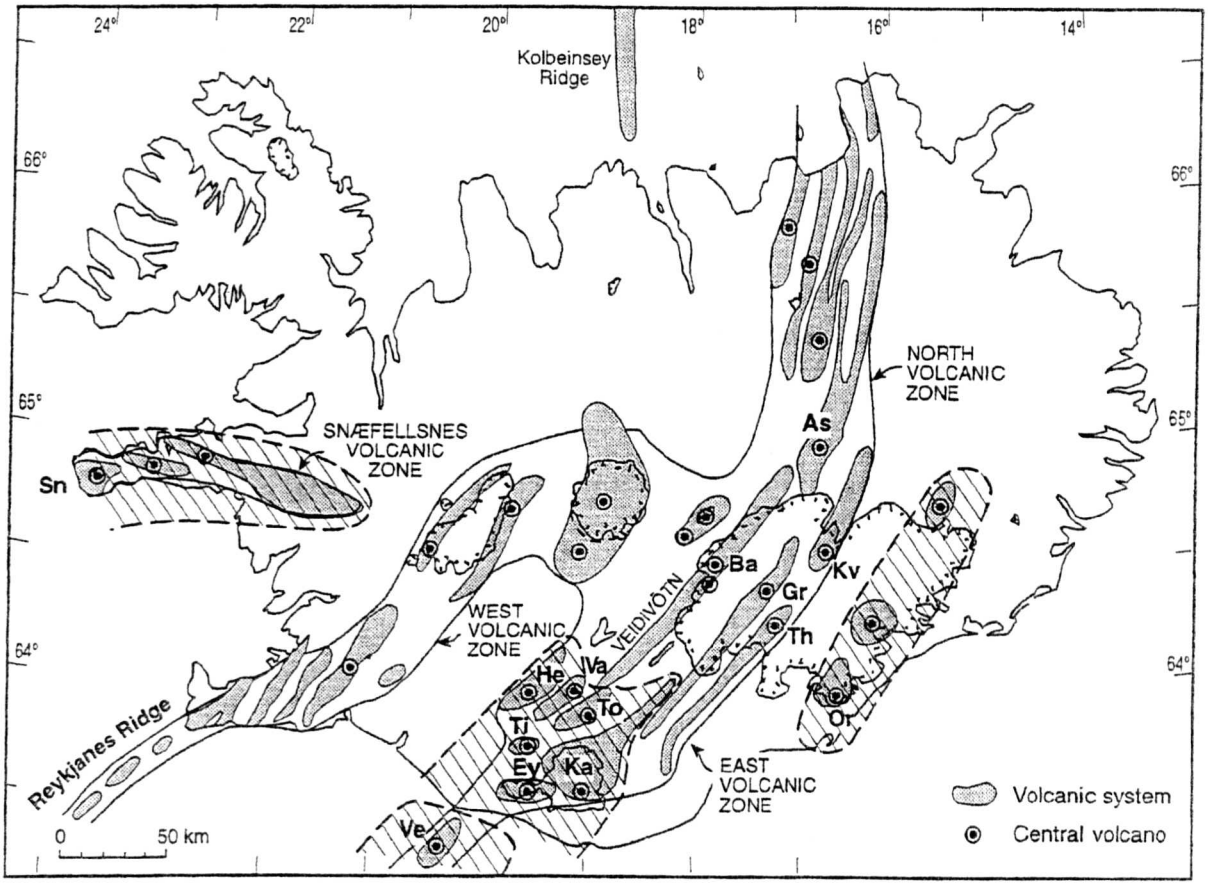

Figure 3.4 Volcanic zones and systems in Iceland. The volcanic systems named in the text are abbreviated as follows: As, Askja; Sn, Snaefellsjokull; Ba, Bardarbunga; Kv, Kverkfjoll; Gr, Grimsvötn; Th, Thordarhyrna; He, Hekla; Va, Vatnafjoll; To, Torfadalsvatn; Or, Öraefajökull; Ti, Tindafjallajokull; Ey, EyjafjLLjokull; Ve, Vestmannaeyjar. (Based on Jakobsson, 1979 and Hafldason *et al.*, 2000).

The Hekla (63.98 N, 19.70 W) volcanic system, about 40 km long and 7 km wide (Fig. 3.4), is the central volcanic system within the transitional-alkalic province of the EVZ. Since the eruption of Hekla 5 about 6000 years BP, Hekla has produced about 6.7 km^3 of acid rocks and 12 km^3 of intermediate rocks, but no basalts (Jakobsson, 1979). During historical time there have been 16 eruptions (i.e. 1158, 1206, 1222, 1300, 1341, 1510,

1597, 1636, 1693, 1766, 1845, 1947, 1970, 1980, 1991 and 2000; Mulligan, 2001). Besides these, many smaller eruptions have occurred on the flanks of Hekla. For each eruption the initial chemical composition is a roughly linear function of the length of the preceeding quiet period (Thorarinsson, 1967). This relationship is also apparent in the volume of extruded material, which indicates large magma chambers (Jakobsson, 1979). Electron Probe Micro-Analysis (EPMA) data show that the glass composition in a single large tephra layer can range from ~ 74- 57 % (e.g. Thorarinsson, 1967; Dugmore *et al.* 1992 and Laresen *et al.*, 1999).

The Torfajökull volcanic system, situating in the center of the EVZ (Fig. 3.4), is the largest area of acid and intermediate rocks in Iceland (Larsen *et al.*, 1999). Although this swarm is a separate volcanic system, it seems to be a direct continuation of the Veidivötn fissure swarm. Both volcanic systems are clearly separated petrologically (Blake, 1984; Larsen, 1984; Larsen *et al.*, 1999). During post-glacial time, approximately 12-18 lavas have been erupted in the Torfajökull volcanic system. In historical time, 2 volcanic episodes may have occurred in the area, around AD 1477 and around AD 870 (Gronvold *et al.*, 1995 and Larsen *et al.*, 1999). In the 9th century, or just at the time of the settlement in Iceland, a large tholeiitic eruption occurred in the 18 km long Vatnaoldur fissure within the Veidivötn system. The Holocene tephras from Torfajokull caldera, including the silicic tephras, are characterized by high K_2O content, exceeding 4% in all known instances where SiO_2 >70% (Larsen *et al.*, 1999).

The volcanic system of Eyjafjoll is situated on the Eastern Volcanic Zone near the south coast of Iceland (Fig. 3.4). During the last glacial period considerable amounts of intermediate and acid lavas were erupted. Four eruption centres are covered by ice at the present time. Two eruptions have occurred during the historical time in Eyjafjoll, AD 1613 and AD 1821-23 (Larsen *et al.*, 1999). The later eruption in the main crater (caldera) produced light-to-dark acid tephra that formed a series of small lobes towards the north, west and south. The total volume of extruded post-glacial lava in the Eyjafjoll system is small, only about 0.26 km^3 (Jakobsson, 1979). The tephra is estimated to be ~0.004 km^3 in volume, and a distinctive feature is the high Na_2O and FeO content (Larsen et al., 1999).

The partly ice-covered Katla volcanic system (Fig. 3.4) has been among the most active volcanic systems in Iceland (Jakobsson, 1979; Larsen, 1999). Located in the southern part of the EVZ and covered by the Myrdalsjokull ice cap, it is about 30 km wide at its southwest part, narrows gradually to the northeast and reaches a length of 78 km. In the ice-free areas of the volcanic system, there has been only moderate volcanic activity, altogether 34 individual eruptions units having been identified, which are all basaltic. Under Myrdalsjokull, mainly in the Katla area, there has been intensive volcanic activity with 18 eruptions from the Katla area in historical times; volcanic eruptions have occurred at an average frequency of two per century (Larsen, 1999). The number of pre-historical eruptions is not known but may approach 100 (Jakobsson, 1979). A major pre-Holocene eruption of the Katla system produced both basaltic high-Ti and the silicic component of North Atlantic Ash Zone one (Jakobsson, 1979; Larsen *et al.*, 2001).

The major part of the Grimsvötn system is covered by the Vatnajökull ice cap (Fig. 3.4). The sub-glacial Grimsvötn central volcano has been highly active, at least in historical times, with 19 probable eruptions listed since 1598. Only 8 individual eruption units have been identified in the region outside Vatnajökull. Of the 19 eruptions believed to have occurred in the Grimsvötn area since about 1598, four of these have probably occurred southwest of Grimsvötn: in 1783, 1867, 1887 and 1903. Knowledge about volcanism during historical time before 1598 is very fragmentary and there is no information on pre-historic sub-glacial activity in the area. Most of the sub-aerial lava has been dated with tephrochronology to between 2000-6000 years BP. The eruption sites are dominantly cinder-spatter cone rows. The trend of the four major sub-aerial eruption fissures is about northeast, which coincides with the trend of the system. In the SW part of the system, however, the fissures trend about north-northeast (Jakobsson, 1979).

The Veidivotn volcanic system differs from other systems in the EVZ, because there is no acid central volcano associated with it (Fig. 3.4). Altogether 75 individual eruption units have tentatively been identified in the volcanic system, all of them basaltic. At least two eruptions within the system have occurred in historical time. The Veidivotn lava and the Svartkrokur tephra were produced after the Norse settlement and even as late as in the 16th century. There are indications of two distinct eruption periods in the southern part of the system, one from approximately 11000-6500 (?) BP and another 4000-0 BP. The Veidivotn system is characterised by long eruption fissures, which in

many cases extend tens of kilometres. The most common eruption site is the spatter cones row (9 cases) while cinder spatter cone rows were found in 11 cases and cinder cone rows in 9 cases (Jakobsson, 1979).

The Dyngjufjoll Volcanic System is located on one of the 5 major fissure systems in the Northern Volcanic Zone. The system is approximately 100 km long and 20 km wide. Intense activity in the southern part of the system has built up the Dyngjufjoll volcanic centre represented by Askja. The area also has several shield volcanoes. The first activity was the large plinian eruption of Askja in 1875 (Jakobsson, 1979).

Öræfajökull (64.00° N, 16.65° W), the largest active post-glacial volcano in Iceland, is situated east of the EVZ in an intra-plate setting (Fig. 3.4). Öræfajökull has erupted only twice in historical times, once in AD 1362 and then again in AD 1727. The 1362 event was explosive and in regard to the amount of tephra produced, was the largest in Icelandic historical time, most likely the third largest in post-glacial history, and devastated the adjacent settlement. By the 1400s a new settlement had sprung up again in this area under the name of Öræfajökull, meaning 'wasteland' in Icelandic. In 1727 Öræfajökull erupted again explosively with similar effects, but the eruption was smaller than the one in 1362. EPMA data of the Öræfajökull 1362 tephra, from the lowermost units of the air-fall tephra, show it is characterized by high Na_2O and very low MgO, and Öræfajökull 1727 has prominent higher FeO (>13.26%) and lower MgO content (Larsen *et al.*, 1999).

3.5 Icelandic tephrochrochronology

Tephrochronology is a chronology that involves the dating of tephra layers, together with the use of these dated layers for various geological, geomorphological and also archaeological purposes. Every wholly or partly explosive volcanic eruption leaves on the ground more or less extensive layers of tephra. Where the tephra layers have not been stripped off by wind or water, but covered by subsequent soil formation, they appear in more or less distinct horizons in the soil profiles. Owing to their, geologically speaking, instantaneous formation and very wide dispersal, coupled with usually narrow thickness and characteristic appearance, these layers are very useful geological guide horizons.

In Iceland, extensive tephra layers are more numerous than one would expect in a mainly basalt-producing area. This is due to the fact that some of the most active volcanoes (Fig. 3.5), such as Katla and Hekla, are blanketed by ice and their eruptions are phreatomagmatic and wholly explosive, or almost so (Thorarinsson, 1980). Black basaltic tephra layers alternate in soil sections with brownish intermediate and light acidic layers. The acidic layers stand out most clearly in soil sections and are easiest to follow from one place to another. There are 24 widespread acidic tephra layers in the post-glacial soils (Larsen *et al.*, 1999).

The establishment of tephrochronology in Iceland by field studies is helped by the country being one of the few highly active volcanic areas in the world where peat formation and loessial soil formation are very rapid (Thorarinsson, 1980). This means

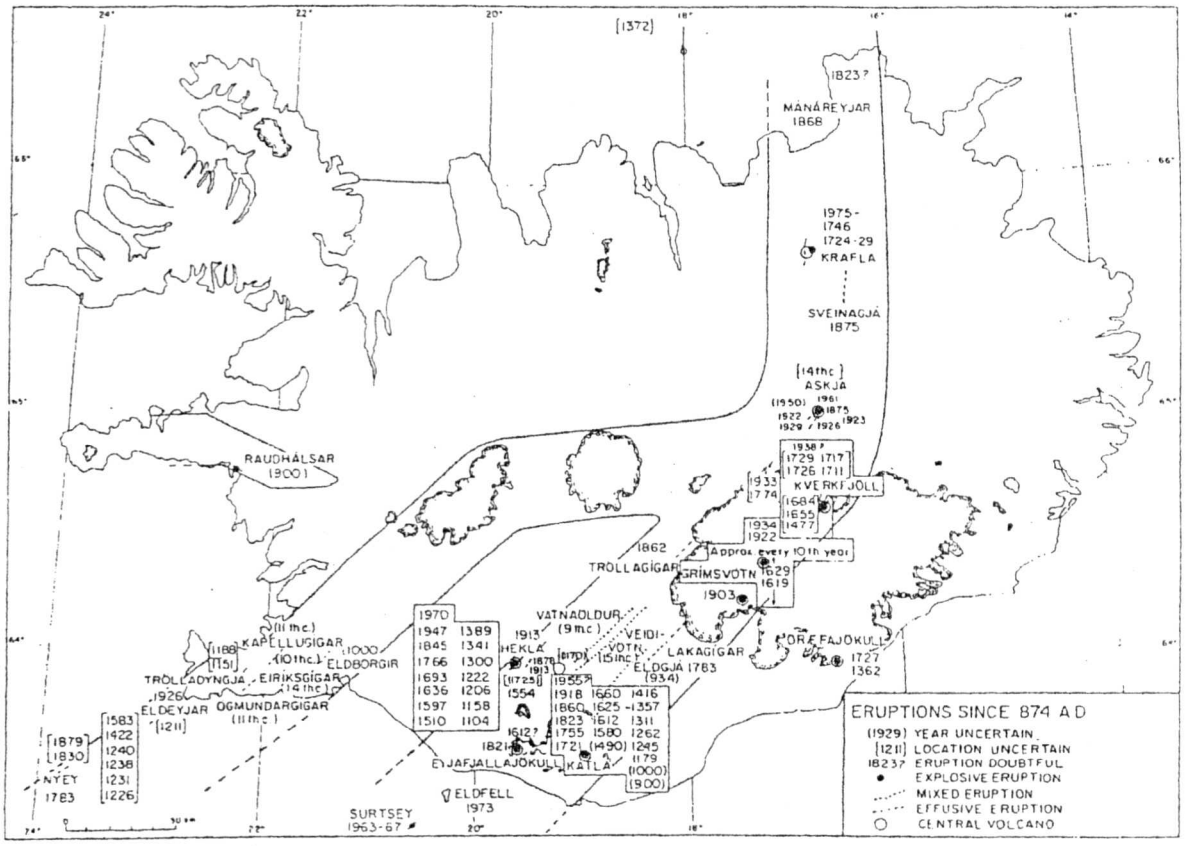

Figure 3.5 Volcanic activity in Iceland in historical time. (After Thorarinsson, 1980).

that the soil cover increases in thickness so quickly that tephra layers of small difference in age are separated in the soil sections. In the harsh climate, the disintegration of organic material is slow and wind erosion has greatly increased the rate of the thickening, especially since the arrival of man (Larsen *et al.*, 1992). As a consequence, the tephra layers of only a few years difference in age can be clearly separated in soil sections. It has proven possible to define in the field between 150 tephra layers in a single post-glacial loessial soil section (Thorarinsson, 1980). Furthermore, Iceland is a country where reliable accounts of volcanic eruptions and tephra falls are more plentiful and go farther back in time than in most other volcanic areas (Thorarinsson, 1980). Recently, the tephrochronology of Iceland and the North Atlantic region was reviewed by

Haflidason *et al.* (2000), who provided an overview of present knowledge regarding the geochemical signatures and age of the tephra layers identified in the/around Iceland for the last 400 kyr BP.

In Iceland, tephra (mainly tephrochronology) has been applied in studies of: 1) eruption-history and eruption-mechanism of the volcanoes; 2) fluvial erosion and wind erosion; 3) dating of glacier oscillations, using ice cores from glaciers; and periglacial phenomena especially frost crack polygons; 4) pollen-analytical studies of vegetation changes; 5) archaeological studies, especially dating of farm ruins; 6) establishing a tephrochronological connection between Iceland and other countries (referenced in Thorarinsson, 1980).

3.6 Human history of Iceland

Since one of the aims of this study is to use tephrochronology to reconstruct soil accumulation rates, which are probably related to deforestation, the human history of Iceland is briefly reviewed. The Icelanders are the only European nation whose birth and infancy in the Dark Ages are still remembered. The first people known to have inhabitated Iceland were Irish monks who came in the eighth century. But they left with the arrival of the pagan Norsemen, who systematically settled Iceland in AD 870 and made their home at Reykjavik (Thorarinsson, 1961; Harstup, 1990; Palsson, 1999) (Fig. 3.6). Over the next six decades, hundreds of other settlers followed the Norsemen and occupied most of the inhabitable parts of Iceland. Immigration stopped about AD 930,

after which the Icelanders organized themselves into a distinctive society, with the creation of the Althing, or parliament, in AD 930 (Harstup, 1990; Palsson, 1999).

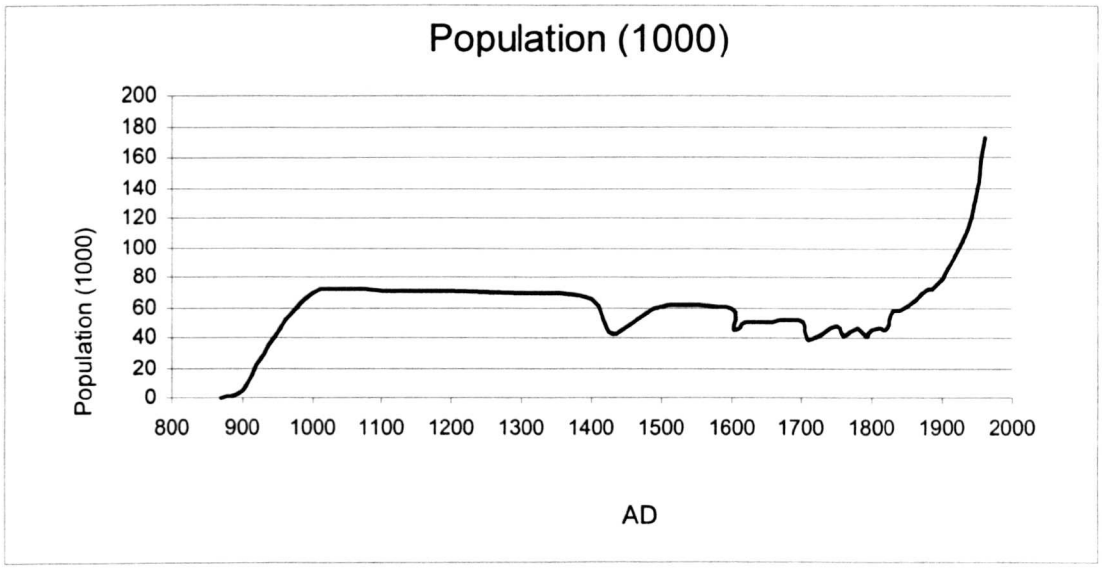

Figure 3.6 The population history of Iceland. (Based on Thorarinsson, 1961).

The period from AD 870 to AD 930, when the Iceland nation was still in the making, is called the Age of Settlements. The next phase in Icelandic history is the so-called Saga Age (AD 930-AD1050; Palsson, 1999). The original settlement of Iceland is regarded as having come to an end by AD 930. The most likely estimate of the size of the population at this time is about 30,000, but this is uncertain (Thorarinsson, 1961). Other estimates are provided by calculations based on the census that Bishop Gizur Isleifsson had taken in ~1905 of all farmers in the country, except those who did not pay tax. According to this census the number of such farmers was about 4500, and from that figure scholars have arrived at estimates for the total population ranging from 50,000 to 105,000 (Thorarinsson, 1961).

Early Icelandic society was completely rural in character. There were no towns or villages; the entire population lived on farms and crofts, which were scattered about in coastal areas, inland valleys and other inhabitable low-lying regions. The principal occupation was animal husbandry: sheep, cattle, goats, pigs, and horses. Transhumance was widely practiced. In summer, milch ewes were moved to shielings on higher ground to save the pastures near home, and all the barren sheep were driven away in summer up to moors and mountains. In autumn they were rounded up, and then sorted out at the public folds. Some grain was grown in early Iceland, particularly in the south, mostly barley. Fishing was an important industry. Dried fish was part of the staple diet, and farmers would keep it in large quantities. Seals and whales were the only wild mammals yielding meat. There are no trees in Iceland at the early time (Paalsson, 1999).

Chapter 4 Field & Laboratory Methods

4.1 Introduction

This chapter describes the study sites and field methods (sections 4.2 and 4.3), the sedimentology of the sampled peats and soils (section 4.4), the laboratory techniques used for analysing samples (section 4.5) and finally the application of a procedure for multivariate data analysis (section 4.6).

4.2 The study sites

Two study areas, near the glacier Vatnajökull in southeast Iceland, were selected, in fairly close proximity to several volcanoes (Fig. 4.1). The main advantage of the chosen study area is that in general the tephra layers are more numerous and thicker east of the active volcanic zones than west of them, because the wind direction at higher levels of the troposphere is predominantly westerly.

The first study area is located in Skaftafell National Park (64.0° N, 17.12° W), which is near the western outlet of Öræfa glaciers (Fig. 4.1). The park and the surrounding area are a nature preserve: Skaftafell. It consists of hillslopes, surrounded by glaciers, moraine and sandur environments. There are loess-soils at higher elevations and peat bogs in the lower lying areas. Two sections, one peat section (Ska1) and one soil section (Ska2), were studied from Skaftfellsheidi, Iceland.

The second study area is Jokulla I Loni (Fig. 4.1). Here, the landscape is characterised by vegetation classified as tundra and there is the nearly complete vegetation cover with a significant proportion of shrubby plants. The coastal areas are characterised by grassland, bogs and marshlands, and at higher elevations the ground is covered with both hard and soft or boggy tundra (Mulligan, 20001). Three sections, including two soil sections (JL1 and JL2), and one peat section (Lax), were sampled in this area.

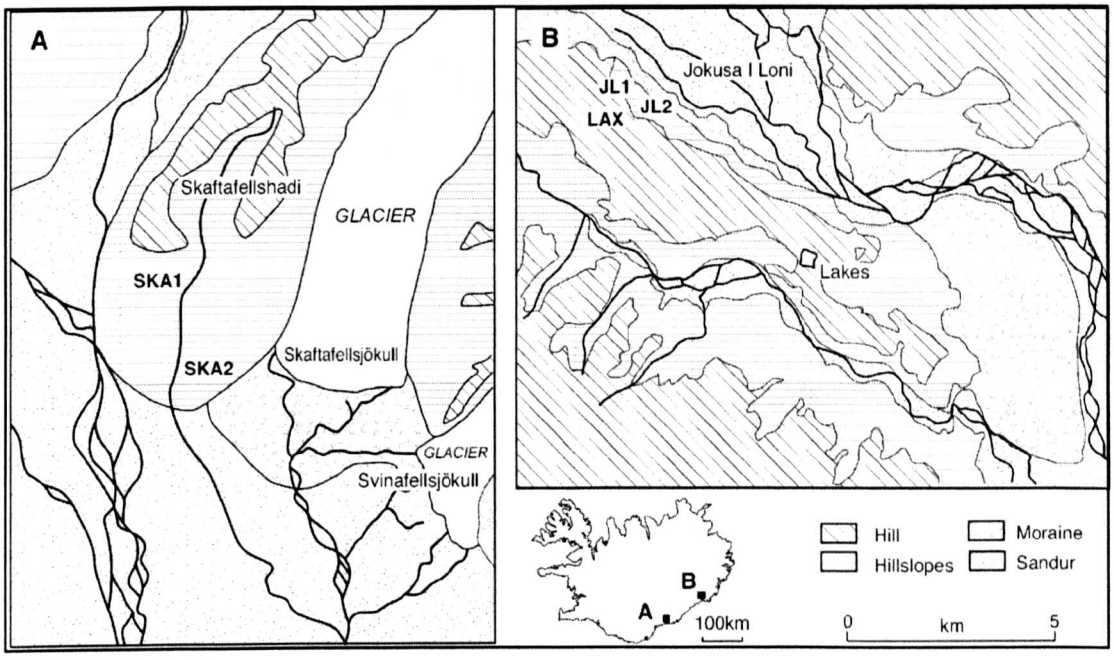

Figure 4.1 The study areas: Skaftafellshadi (Ska) and Jokulla I Loni (JL), in SE Iceland. The locations of the five study sites are shown: Ska1, Ska2, Lax, JL1 and JL2.

Therefore, five sections, Ska1 and Ska2 (Iceland: 64.0° N, 17.12° W), Lax (Iceland: 63.81° N, 15.08° W), and JL1 and JL2 (Iceland: 63.83° N, 15.08° W) (Figs. 4.1), were studied in this project.

4.3 Field methods

The samples were collected by Drs. Richard Chiverrell and Jan Bloemendal during two field seasons of the University of Liverpool Iceland Expedition, in 1999 and 2000. The peat samples of Lax and Ska1 were collected using 6.5 cm diameter, 50 cm - long drain pipes in the field during the summer of 1999. They were transported back to Liverpool as whole cores. The three soil sections (i.e. Ska2, JL1 and JL2) were logged, cleaned, described, sampled and bagged at 2 cm intervals in the field during summer, 2000.

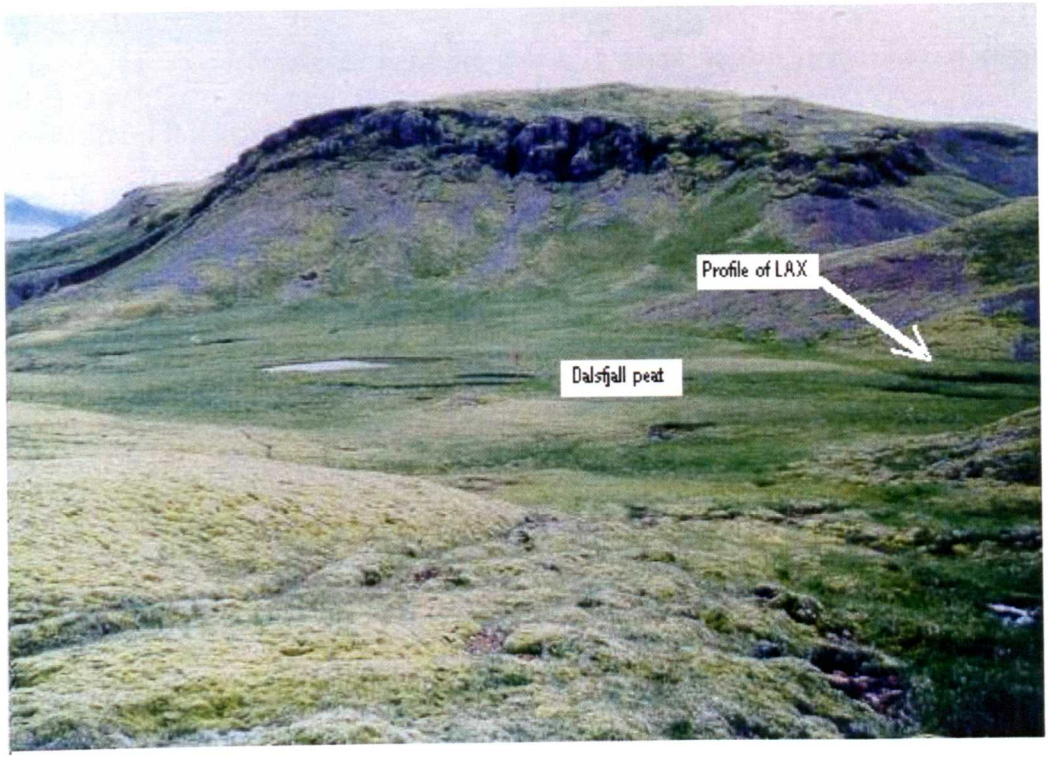

Figure 4.2 Photograph of Dalsfjall peat bog (Source: Richard Chiverrell).

4.4 Sedimentology

4.4.1 Lax

Lax, a 160 cm-long peat section, is located within Dalsfjall peat bog (63.81° N, 15.08° W), between Laxadalar and Jokula I Loni, SE Iceland (Figs. 4.1 and 4.2). The peat samples of Lax were described in detail before cutting in the laboratory. 22 tephra layers were found in the upper 160 cm of Lax (Fig. 4.3 and Table 4.1). The core can be divided into three parts in term of lithology. There are 13 different soil horizons with 13 intercalated tephra horizons (Fig. 4.3) in the uppermost 54 cm of the core. The tephra at the depth of 35-37.5 cm is light in colour ('white tephra') and has a rhyolitic composition. It is correlated with the AD 1362 Oraefa tephra (see Chapter 5), which is a key marker horizon in this study area. The second part of the core, 56-110 cm, is peat and can be subdivided on the basis of variations in colour (Table 4.1 and Fig. 4.3). The lowest part of the core (110-160 cm) consists of peat with 9 clearly defined tephra horizons (Table 4.1 and Fig. 4.3). All of the cores were cut into contiguous slices 1-0.5 cm thick in the laboratory, and 194 samples were obtained. During cutting, an attempt was made to prevent the incorporation of more than one tephra into a single sample; however, this was not always possible in the case of adjacent fine tephras. This also applies to Skal (below).

4.4.2 Skal

A 280 cm-long peat core was obtained at site Skal. The site is located in Skaftafell National Park (Iceland: 64.0° N, 17.12° W), near the Oraefa Glaciers (Fig. 4.1). The samples were described in detail before cutting in the laboratory. The lithology of this long core is quite complex, with at least 48 tephra layers present (Fig. 4.4 and Table 4.2).

Table 4.1 Peat profile Laxadalar, SE Iceland.

Depth (cm)		Description
0	-3	dark grey/brown fine sandy soil
3	-4	fine black tephra
4	-6	dark grey/brown fine sandy soil
6	-7	fine black tephra
7	-12	dark grey/brown fine sandy soil
12	-14	middle black tephra
14	-17	green brown fine silty sandy soil
17	-19	dark grey tephra
19	-23.5	grey brown clayey soil
23.5	-25	fine black tephra
25	-26	grey brown clayey soil
26	-29	fine dark brown tephra
29	-31	grey brown clayey soil
31	-32	fine black tephra
32	-33	grey brown clayey soil
33	-34	fine black tephra
34	-35	grey brown clayey soil
35	-37.5	fine white tephra—Öraefa 1362
37.5	-40	grey brown clayey soil
40	-42.5	fine black tephra
42.5	-46	green brown clayey silt
46	-47	fine black tephra
47	-52	grey green silty peat
52	-53	fine dark grey tephra
54.5	-54	fine black tephra
54	-60	grey green silty peat
60	-85	brown silty peat
85	-90	brown grey silty peat
90	-110	green brown silty clayey peat
110	-111.5	fine black tephra
111.5	114	green brown silty clayey peat
114	-115	fine grey tephra
115	-121	dark brown silty peat
121	-123	fine white tephra (needles)
123	-128	grey brown silty peat
128	-135	fine dark grey and white tephra
135	-139	dark brown peat
139	-140.5	fine dark brown tephra
140.5	-147.5	dark brown peat
147.5	-150	fine dark brown and white tephra
150	-153	grey brown peat
153	-154	fine/m dark grey & black tephra
155	-156	fine black tephra
156	-159.5	grey brown peat
159.5	-160	fine black tephra

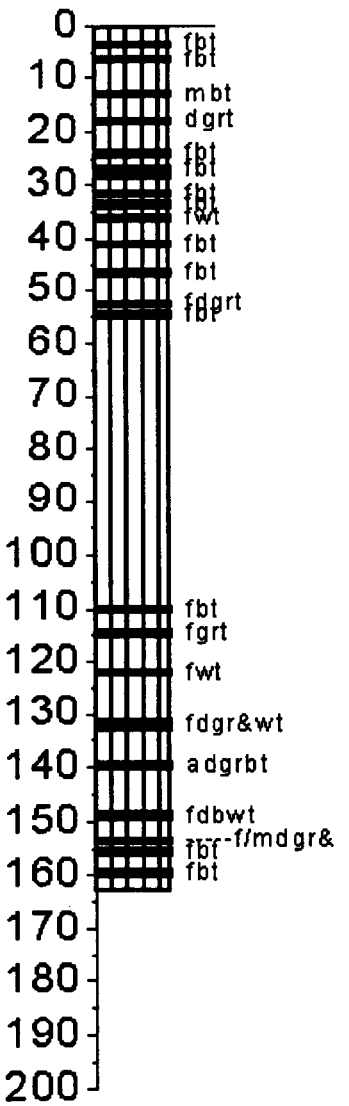

Figure 4.3 The stratigraphic field section of Laxadalar, peat, SE Iceland.

Most of the 36 tephra layers were black in colour, but white tephra layers were also found, at depths of 68.5-69 cm, 115.5-116 cm and 230.5-231 cm. Geochemistry results (Chapter 5) indicate that the top white tephra layer originates from Oraefa AD 1727, and the second white tephra is characteristic of the AD 1362 Oraefa eruption. The last 9 tephra layers in this core are olive green in colour, and in which there is a silicic component (Fig. 4.4 and Table 4.2). There are two gravelly soil layers at depths of 22-27.5 cm and 55-61 cm. All of the cores were cut into contiguous slices 1-0.5 cm thick in the laboratory, and 319 samples were obtained.

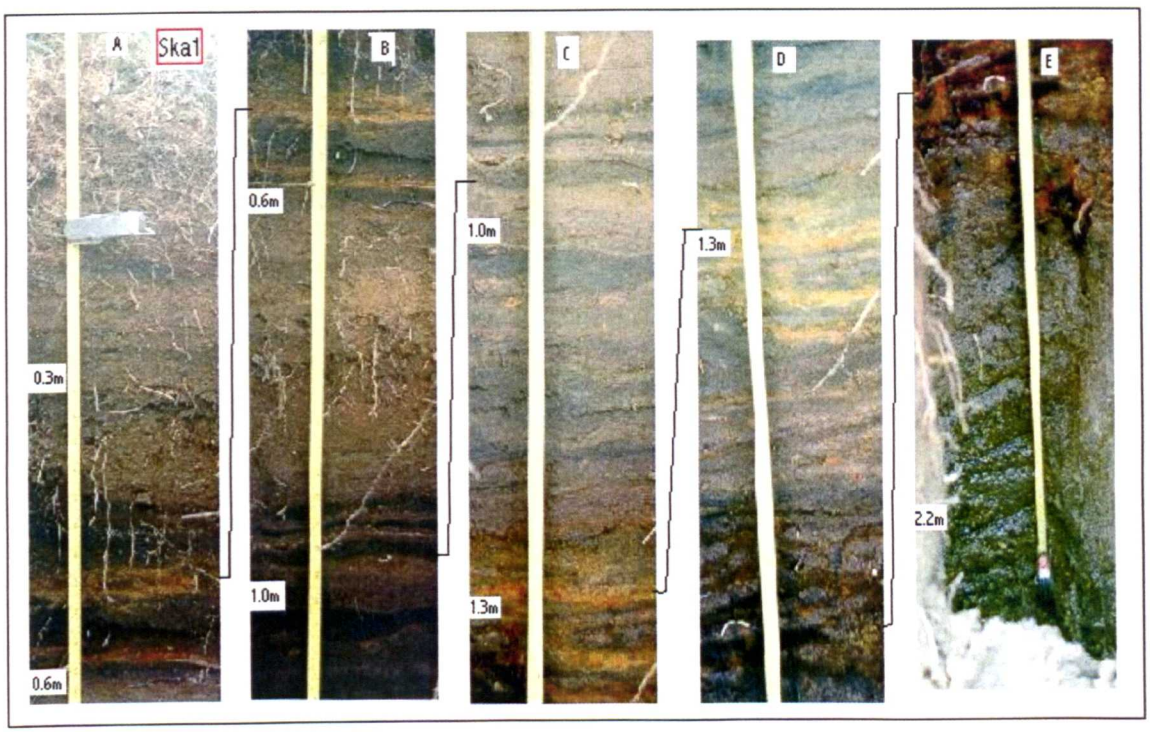

Figure 4. 4 Photograph of the Ska1 section, SE Iceland (Source: Richard Chiverrell).

Table 4. 2 Peat profile Ska1, SE Iceland.

Depth (cm)		Description
0	-8	equisetum peat
8	-12	black tephra
17	-18.5	black tephra
20	-22	black tephra
26	-27.5	gravelly soil
27.5	-28.5	black tephra
30.5	-32	black tephra
32	-32.5	black tephra
34	-34.5	black tephra
36.5	-36.75	black tephra
37.5	-38	black tephra
39	-40	olive green tephra
45	-45.5	black tephra
55	-61	gravelly soil
65	-65.5	black tephra
67	-67.5	black tephra
68.5	-69	white tephra
69	-70	black tephra
70	-70.5	olive green tephra
75	-78	black tephra
82	-82.5	dark grey green tephra
82.5	-83	black tephra
87	-92	black tephra
94	-94.5	dark grey green tephra
94.5	-95	black tephra
97	-98	black tephra
103	-112	black tephra
112	-114	iron stained peat
114	-115	black tephra
115	-115.5	white tephra
115.5	-116	olive green tephra
116	-117	black tephra
117	-118	black tephra
123	-123.5	black tephra
123.5	-124	iron stained peat
127.5	-128.5	black tephra
130.5	-131	black tephra
133	-134	white tephra
135	-135.5	black tephra
135.5	-139	charcoal layer
143	-145	black tephra
148	-148.5	olive green tephra
151	-152	black tephra
153	-155	olive green tephra
155.5	-162	olive green tephra
169	-171	black tephra
175.5	-178.5	olive green tephra
203	-208	black tephra
230.5	-231	white tephra
226	-232	black tephra
243	-248	white tephra
257	-259	olive green tephra
262	-263	very coarse brown tephra

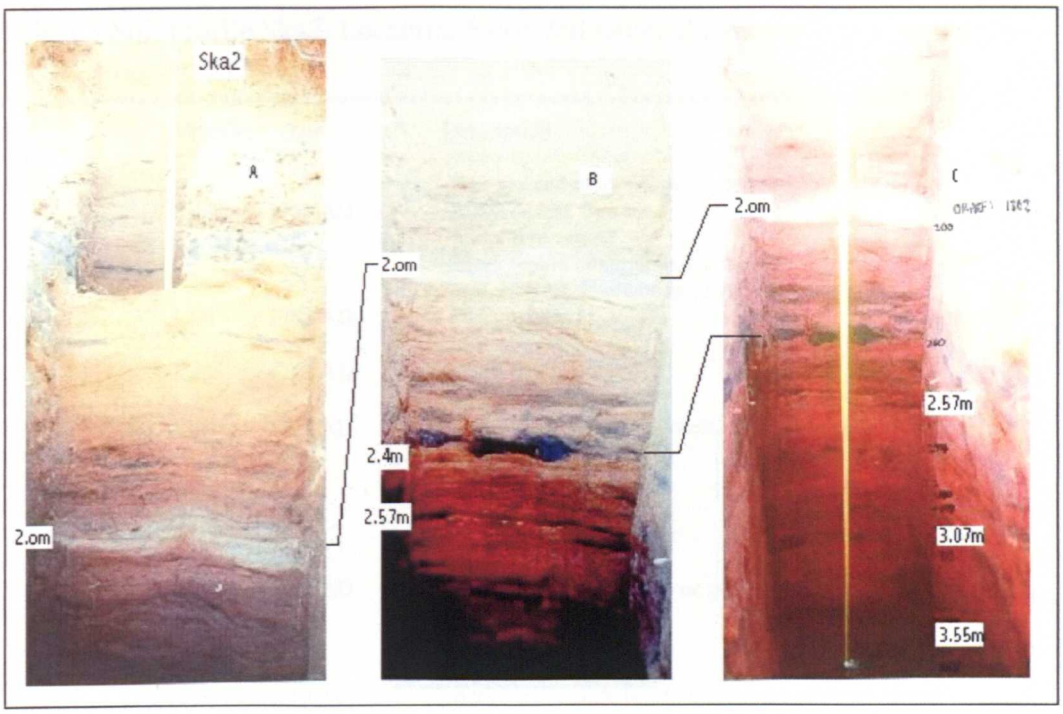

Figure 4.5 Photograph of the Ska2 section, SE Iceland. (Source: Richard Chiverrell).

4.4.3 Ska2

Ska2 is located close to Ska1 (64.0° N, 17.12° W) (Fig.4.1), a 380 cm loessic soil section was dug out and described in the field. 39 tephra layers were found (Fig. 4.5 and Table 4.3). The section was sampled and bagged at 2 cm intervals, yielding 173 samples. During sampling of the three loessial soil profiles, an attempt was made to avoid inclusion of more than one tephra in a single sample; however, this was not possible in the case of thin, adjacent tephras. This is the key section used for tephrochronological dating, using the regional framework established by Thorarinsson (1944, 1958, 1981), Haflidason *et al.* (2000) and Larsen *et al.* (1999, 2001), and supported by magnetic measurements and additional chemical analysis data (Chapters 5 and 7).

Table 4.3 Soil profile Ska2. Location: Skaftafell national park.

Depth (cm)	Volcano	Date	Description
0-27			fine grained sand, fibrous and woody, mostly willow.
27-28	Katla	1918 AD	black tephra, fine sand
28-36			soil, more coarse
36-36.3			black tephra continuous but wavy
36.3-66			soil, fibrous, 5%+woody roots
66-66.6	Laki	1783 AD	black tephra
66.6-73.5			soil
73.5-74.3	Katla	1755 AD	black tephra
74.3-84			soil
84-84.5	Öræfa	1727 AD	grey tephra, pumice, Öraefa, coarse grained
84.5-87			soil
87-87.3			very light grey band
87.3-101.5			soil
101.5-101.7			ghost black tephra layer
101.7-103			soil
103-105	Katla	1625 AD	dark black tephra, katla or grimsvotn
105-108			soil
108-108.3			black tephra
108.3-120			soil
120-121.5	Grimsvotn	1619 AD	dark black tephra layer, med/coarse sand, grimsvotn?
121.5-124			soil
124-130	Grimsvotn	1540's	thick black tephra, med/coarse grained
130-141			soil, soapy silt sand, granular soil
141-141.5	C?		laterally diffuse tephra
141.5-144			soil, mixture of silt/fine sands, granular soil, dry
144-145	B?		black tephra
145-149			soil, less silt, fine sand, not soapy at all, no structure, granular
149-150.5	Katla	1490	black tephra, fine sand, grained
150.5-160			soil, fine sand and silt, more sandy, brown, granular, <1% roots
160-160.5			diffuse black tephra, fine sand, wavy
160.5-167			soil, fine sand silt, granular, 1% roots
167-167.5			wavy diffuse black tephra, fine sand, wavy
167.5-168			same as soil above
168-169	Veidvotn?	1477	black tephra coarse/medium
169-170			same as soil above
170-171	Katla ?	1440	fine black tephra
171-172			same as soil as above
172-173			wavy, diffuse fine black tephra
173-176			same as soil as above
176-188	Hekla	1389 AD	banded black tephra's mixed with Öraefa pumice
188-200	Öræfa	1362 AD	Öraefa, coarse pumice rich white tephra
200-202			soil
20-202.3	Katla	1359 AD	diffuse black tephra
200-210			soil, more silt to fine sand, <1% roots, granular texture
210-212.5			soil, mostly silt, no roots, no sand
212.5-212.8	Hekla/Katla	1200's	diffuse wavy black tephra, fine sand
212.8-214.5			same as soil as above
214.5-214.8	Hekla/Katla	1200's	diffuse wavy black tephra, fine sand
218-218.5	Hekla/Katla	1200's	diffuse wavy black tephra, very fine sand
221-226	Hekla/Katla	1200's	black tephra, fine sand
266-228			soil, silt, no roots, fairly structureless, no peds, granular

Table 4.4 Continuation of soil profile Ska2, Iceland, Location: Skaftafell national park.

Depth	Volcano	Date	Description
228-230	Hekla 1	1104	med/fine sand, black tephra
230-234			soil, silt, no clay
234-240	Eldgja	934	black tephra, fine sand
240-241.5			soil, silt, dark brown, no roots, small blocky peds
241.5-242	Veidvotn	870 AD	diffuse grey/green tephra, fine sand
242-245			same as soil as above
245-248			band of black tephra, coarse sand
248-249			green tephra, fine sand
249-251			black tephra
251-255			same as soil as above
255-256.5			black tephra, course
256.5-257	Skaftafellsheidi	1540 ±50 BP	white tephra
257-274			soil, slightly sticky, silt clay, blocky and irregular peds
274-277			black tephra
277-290			soil, dark reddish brown, up to 10% dead rootlets, blocky peds under pressure, soapy but slightly thick, silt clay, slightly plastic
285-286	Svinafellsheidi	2100 BP?	white tephra
290-292			black tephra
292-298			same as soil as above
298-300			black tephra
300-307			same as soil as above
307-309			black tephra
309-313			same as soil as above, 10% roots
313-313.5			diffuse thin black tephra
313.5-337			same as soil as above
337-340	Hekla S (underlies BT)	2860 BP	black layers, not tephra, silt with tephra
340-355			same as soil as above
355-359	Hekla 4	3830 BP	white tephra
359-362			same as soil as above

4.4.4 JL1

Jökulsárlón is on the boundary between the settlements of Hrollaugur Rögnvaldsson and Þórður illugi (Figs 4.1 and 4.6). The 360 cm long loess-soil section of JL1 was dug out on the bank of the river Jokula I Loni (63.83° N, 15.08° W). The site is an exposed section in a stream gully (Fig. 4.7). The section was sampled at 2 cm intervals, yielding 177 samples. 16 tephra layers were found in this section (Fig. 4.8 and Table 4.4).

Figure 4.6 Photograph of the locality of Jokula I Loni at Jökulsárlón, SE Iceland. (Source: Richard Chiverrell).

There is only one white tephra layer at a depth of 189-190 cm, and it is characteristic of the AD 1362 Öræfa tephra. There are two mixtures of black and white tephra layers, at the depths of 90-92 cm and 94-94.5 cm (Table 4.4). The rest of the tephra layers in this profile are of more basic composition (grey or black in colour), which are associated with other volcanoes (Fig. 4.2 and Table 4.5).

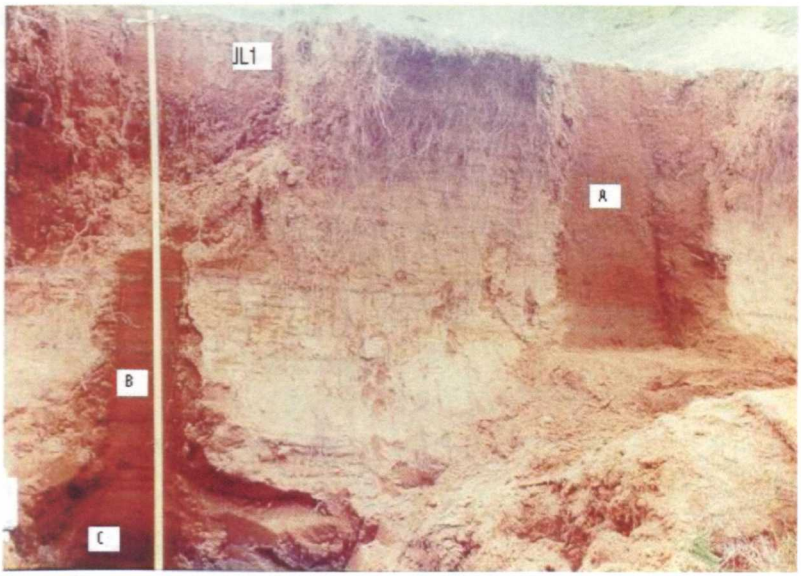

Figure 4.7 Photograph of the JL1 section, SE Iceland. (Source: Richard Chiverrell).

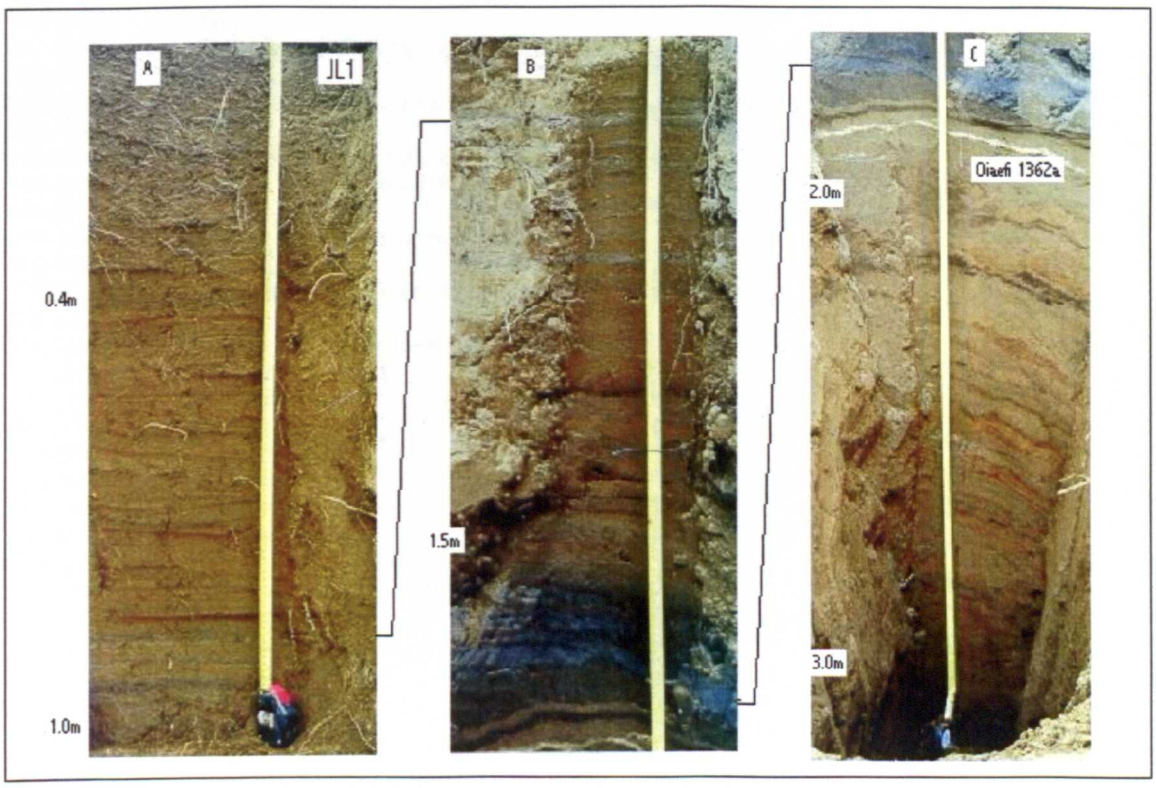

Figure 4.8 Photograph of the JL1 section, SE Iceland. (Source: Richard Chiverrell). The positions of A, B and C are shown in Figure 4.7.

Table 4.5 Peat profile JL1, SE Iceland. Location: Jokulsa I Loni, SE Iceland.

Depths	Description
0-3cm	Root litter
3-38cm	Brown root rich soil. Orange/brown in colour. Penetrated by grass rootlets.
38-40cm	Thin black tephra.
40-85cm	Brown banded soil with alternating orange soil and grey. Banding no more than 2cm thick.
85-85.5cm	Thin black tephra.
85.5-90cm	Banded soil.
90-92cm	Mixture of black and white tephra. c.f. Öræfa
92-94cm	Soil.
94-94.5cm	Mixture of black and white tephra.
94.5-97.5cm	Soil.
97.5-99cm	Fine course sand.
End of	smaller top profile. Base of previous located at 98cm on new.
98-110cm	Banded soil.
110-111cm	Grey grit layer (Quite rounded)
111-131cm	Soil.
131-132cm	Black tephra.
132-148cm	Soil.
148-149cm	Black tephra.
149-151cm	Soil.
151-151.5cm	Black tephra.
151.5-161cm	Soil.
161-179cm	Very coarse black tephra. c.f. Grimsvotn ?
179-181cm	Soil.
181-183cm	Diffuse wavy black tephra.
183-185cm	Soil.
185-186cm	Fine grained black tephra.
186-189cm	Soil.
189-190cm	Fairly coarse white tephra. c.f. Oraefi ?
190-190.25cm	Diffuse black tephra. c.f. Katla ?
190.25-212cm	Soil.
212- 216cm	Wavy brown diffuse layer. Probably tephra.
216-218.5cm	Soil.
218.5-218.6cm	1mm diffuse wavy green tephra. Possibly landnam.
218.6-224cm	Soil.
224-229cm	Diffuse fine grained thick layer of black tephra.
229-242cm	Grey/brown soil.
242-245cm	Iron stained soil.
245-257cm	Grey/brown soil.
257-259cm	Distinct grey band.
259-261cm	Iron stained soil.
261-268cm	Grey/brown soil.
268-269cm	Wavy black band.
269-274cm	Orange iron stained soil.
274-275cm	Thin black layer. Possibly tephra.
275-281cm	Grey/brown soil.
281-283cm	Iron stained soil.
283-285cm	Grey/brown soil.
285-286cm	Iron stained soil.
286-292cm	Grey/brown soil.
292-293cm	Iron stained soil.
293-298cm	Grey silty fine sand soil.
298-300cm	Iron stained sand.
300-303cm	Iron stain getting lighter.
303-318cm	Grey soil.
318-320cm	Black tephra.
320-360cm	Grey/brown soil to base.

4.4.5 JL2

The loess-soil section of JL2 is quite close to JL1 (Iceland: 63.83° N, 15.08° W) (Figs. 4.1 and 4.6), but much shorter in length (140 cm) than JL1. The section was cleaned, logged, sampled and bagged at 2 cm intervals. 72 samples were obtained and 8 tephra layers were recognised (Fig. 4.9 and Table 4.6). Due to the rhyolitic composition and light colour, the tephra at a depth of 86-88 cm is correlated with the AD 1362 Oraefa eruption. The rest of the tephras in the profile are black in colour (more basic composition).

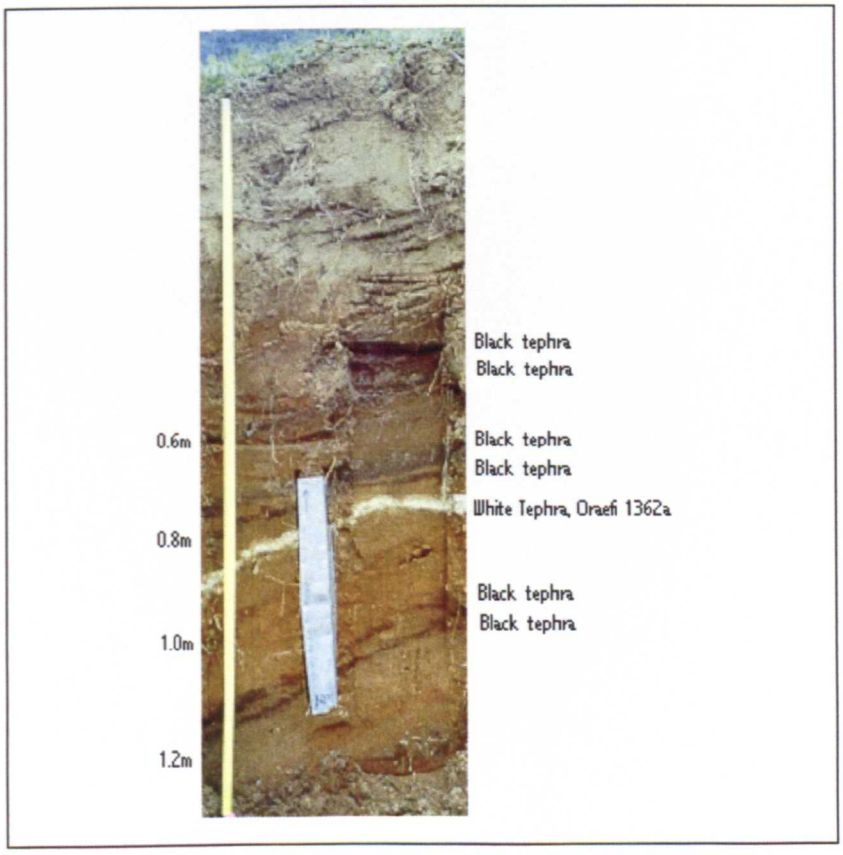

Figure 4.9 Photograph of the JL1 section, SE Iceland. (Source: Richard Chiverrell).

Table 4.6 Soil profile JL2, SE Iceland.

Location: Jokulsa I Loni

Depth (cm)	Description	Volcano Year
0-10	Root litter.	
10-50	Soil.	
50-51	Black tephra.	
51-61	Soil.	
61-61.5	Black tephra.	
61.5-73	Soil.	
73-77	Black tephra.	
77-78	Soil.	
78-79	Black tephra.	
79-86	Soil.	
86-88	White tephra.	Öræfa 1362 AD
88-88.5	Black tephra.	Katla 1359 AD
88.5-112	Soil.	
112-113	Black tephra.	
113-115	Soil.	
115-116	Black tephra.	
116-142	Soil to base.	

4.5 Laboratory techniques

4.5.1 Sample preparation

The two peat cores of Lax and Ska1 were described in detail before cutting in the laboratory. 48 tephra layers in Ska1, and 22 tephra layers in 160 cm upper part of Lax were found (Tables 4.1 and 4.2). Then all the cores were cut into contiguous slices 1-0.5 cm thick in the laboratory. The three sections Ska2, JL1 and JL2 were described and sampled in the field. 39 tephra layers in Ska2, 16 tephra layers in JL1, and 8 tephra layers in JL2 were found (Tables 4.4-4.6).

In summary, 935 samples, of which 319 samples in Ska1, 173 samples in Ska2, 194 samples in Lax, 177 samples in JL1, and 72 samples in JL2, were obtained from the five peat/soil sections. The sub-samples were then freeze-dried.

4.5.2 Magnetic measurements

All sample holders and packing materials were measured empty first, and unsuitable pots and packing were rejected. The 'blank' values were subtracted from the magnetic susceptibility measurements. Samples of known weight (with an accuracy of 0.001 g - thus facilitating accurate mass-specific computation of magnetic results) were packed into 10 cc plastic pots for magnetic measurements. The sub-samples were measured in the Environmental Magnetism Laboratory of the Department of Geography. The sequence of measurements was as follows (see also Chapter 2, Table 2.3):

Mass-specific magnetic susceptibility ($\chi \times 10^{-8} m^3 kg^{-1}$) was measured with a Kappa bridge meter (KLY-3), and then with a Bartington Instruments MS2 sensor on the 0.1 range, using a dual-frequency (470 and 4700 Hz) MS2B sensor. The difference between low- and high-frequency susceptibility ($\chi_{lf} - \chi_{hf}$) is expressed as a mass-specific term ($\chi_{fd} \times 10^{-8} m^3 kg^{-1}$) and as a percentage of low-frequency susceptibility (χ_{fd} %).

Anhysteretic Remanent Magnetisation (ARM) was imparted using a DTECH AF demagnetiser with a peak AF field of 100 mT and a DC bias field of 0.04 mT superimposed. Measurements are expressed as susceptibility of ARM ($\chi_{ARM} \times 10^{-8} m^3 kg^{-1}$) by dividing the strength of the steady field.

Stepwise demagnetisation of **Saturation Isothermal Remanent Magnetisation** (SIRM), imparted at 1 Tesla, was done using four reverse fields -20mT, -40mT, -100mT, and -300mT. An MMPM5 pulse magnetizer was used. SIRM, SIRM-IRM_{-20mT}, and

SIRM+IRM_{-300} are expressed on a mass-specific basis as SIRM, SOFT and HIRM, respectively. IRMs in the reverse fields (-20mT, -40mT, -100mT, and –300mT) are expressed as the percentage of SIRM and are designated 'S' ($S_{-20\ mT}$, $S_{-40\ mT}$, $S_{-100\ mT}$, and $S_{-300\ mT}$). The parameters were formally calculated as follows:

$$SOFT = ((SIRM - IRM_{-20\ mT})/2))\ /mass$$

$$HIRM = ((SIRM + IRM_{-300\ mT})/2\ )/\ mass$$

$$Sx = \left[\frac{(^{-IRM_{-x}}/_{SIRM})+1}{2}\right] \times 100$$

Where x is the reverse field of either -20mT, -40mT, -100mT, or –300mT

All remanence measurements were made using a Minispin magnetometer, with a noise level of $\times 10^{-7}$ Am^2.

127 samples were selected from individual tephra layers for further measurement as follows:

Magnetisation curves and **hysteresis loops** were obtained on a VSM (Molyneux Vibrating Sample Magnetometer) following the procedure of Lees and Dearing (1999). A fixed sample is vibrated within a variable magnetic field to obtain a numeric value corresponding to the distortion of that magnetic field. *Loop* (full hysteresis loop) applies and measures the characteristics of a hysteresis loop pattern. *Loop2* (useful for χ_{high}, χ_{low}, χ_{ferri}, *Mrs,* etc) applies and measures a field, followed by measuring a zero field remanence. Samples must not have been previously magnetised. *Loop2* was measured

before *loop*. The 127 selected samples were measured using typical fields of 0.1, 1, 5, 10, 20, 100, 300, 1000, -5, -10, -20 mT. Then they were measured for *loop*, with typical fields of 1000, 800, 500, 300, 200, 150,100, 80, 50, 30, 20, 10, 5 mT. The coercivity of SIRM ($(B_0)_{cr}$) was calculated as follows:

$$(B_0)_{cr} = \{(field2-field1)*(m1-m2)\}/M1+field1$$

where M1 field1 is the negative value to the left of zero and field2 is the positive value to the right of zero. M1 and M2 are the field values in mT.

The Curie temperature (Tc) was determined in the Geomagnetism Laboratory, Department of Earth Sciences, the University of Liverpool, using a VFTB (Variable Field Translation Balance). The VFTB is a one-dimensional harmonic oscillator with damping in the forced oscillation mode, which can be used to measure hysteresis loops, remanence coercivity and IRM acquisition curves. The heating/cooling (H/C) makes it possible to make measurements at temperatures between –174°C and +700 °C. Thermo-magnetic curves can be measured to obtain the Curie temperature of the material. The samples were measured using a thermomagnetic run to 700 °C, at a rate of 30 °C /min, then waiting for 10 seconds, in a field of 800 mT, followed by cooling to 100 °C with the same rate as heating.

4.5.3 Supplementary measurements

4.5.3.1 Loss on Ignition (LOI)

Samples from one peat core (Lax) and one soil profile (Ska2) and tephra layer samples from other cores and profiles were measured for LOI. Selected sub-samples were weighed, oven-dried at 105 °C overnight, re-weighed and then ignited in a muffle furnace at 450 °C for 4 hours. The value of LOI is then expressed as the percentage of weight lost after the 105 °C over night drying. % weight of LOI was calculated as:

$$\text{LOI} = (\text{weight loss in furnace})/(\text{oven dry weight}) \times 100$$

4.5.3.2 X-Ray Fluorescence (XRF)

Samples from one peat core (Lax) and one soil profile (Ska2) were measured for XRF, using a Metorex XMET920 system. This comprises software, two X-met PC system (XPCS) boards, and two analysis probes - a heavy element probe (HEPS, 3-20 keV) using a ^{109}Cd source and a light element probe (LEPS, 0.8-5.9 keV) using a ^{55}Fe source (Boyle, 2000). Major element analysis was carried out on selected samples for Si, Ti, Ca, K, Fe, Mn, Cl, S, Nb, Ni, Pb, Rb, Sr, Zn and Zr. Loss on ignition (LOI) was used as an approximate measure of organic matter concentration and is used in the calculation of metal concentrations from an in-house computer programme, DECONV (Boyle, 2000; Xie *et al.*, 2000).

4.5.3.3 Electron Probe Micro-analysis (EPMA)

The major element composition of individual tephra shards from tephra layers from the five profiles (Lax, Ska1, Ska2, JL1 and JL2) was measured by EPMA at the Universities of Edinburgh and Manchester.

Sample preparation procedure: Turney (1998) and Lowe and Turney (1996) made a very useful contribution to the problem of extracting rhyolitic microtephra from bulk samples by using a density-separation method based on heavy liquids. The procedure used here strictly followed Turney (1998) and was tested with different densities by the author. For the Iceland research, a heavy liquid separation range between 2.4 to 2.8 gcm^{-3} was used to concentrate the tephra shards.

In detail, the method used was as follows:

a) Sieving was used to retain particles between 74 and 25 μm in diameter, which is the typical size range of tephra.

b) Place 1 g sample into a 15 ml centrifuge tube and add sodium polytungstate of density 2.4 gcm^{-3} to the sample and stir thoroughly.

c) Centrifuge for 20 minutes at a speed of 2500 rpm with brake rate 0.

d) Decant the float (density <2.4 gcm^{-3}) into a 50 ml centrifuge tube. Add double distilled water and stir.

e) Centrifuge for 15 minutes at 2500 rpm with brake rate 9.

f) Decant supernatant (diluted sodium polytungstate) from the float into a beaker to be filtered and recycled.

g) Repeat steps b-f on the original sample pellet. The float in the 50 ml tube can be disposed of or retained depending on whether further analysis of this component is required.

h) Place the remaining liquid (>2.4 gcm^{-3}) into 15 ml centrifuge tubes. Add sodium polytungstate with a relative density of 2.8 gcm^{-3} and stir thoroughly.

i) Centrifuge for 20 minutes at a speed of 2500 rpm with brake rate 0.

j) Decant the float (including the tephra) into a fresh labelled 50 ml centrifuge tube. Add double distilled water and stir.

k) Repeat steps h-j using the same 50 ml tube for 'float'.

l) Centrifuge for 15 minutes at 2500 rpm, brake rate 9.

m) Decant the supernatant into a beaker to be filtered and recycled. The float was centrifuged in distilled water three times to remove sodium polytungstate. The residue, of density greater than 2.8 gcm^{-3}, was diluted in distilled water and centrifuged to recover the supernatant (2500 rpm, brake rate 9 for 15 minutes). The sediment (>2.8gcm^{-3}) was disposed of.

Electron Probe Micro Analyser (EPMA) measurements in Edinburgh: The chemical composition (i.e. SiO_2, TiO_2, Al_2O_3, FeO, MnO, MgO, CaO, Na_2O and K_2O) of tephra shards of 17 samples was determined by Richard Chiverrell at the Tephrochronology Unit, Department of Geography, the University of Edinburgh. Thin sections were prepared and polished using 6 μm and 1 μm diamond pastes. Electron probe analysis was conducted on a Cambridge Instruments Microscan V using standard WDS (wavelength dispersive) technique at an accelerating voltage of 20 kV and a beam

current of 15 nA, as measured across a Faraday cup. The beam was *c.* 5 μm in diameter and counting time of 10 seconds for each pair of major elements was employed in order to minimise sodium migration; nine major components were analysed. Total analysis time was 50 seconds. The standards used were mixtures of pure metals and simple silica compounds. Counter dead time, fluorescence and atomic number effects were compensated for with the ZAF correction programme (Swearman and Long, 1969). An andradite standard of known composition was analysed at regular periods throughout all analytical sessions in order to guard against unexpected variations in machine operating conditions, and to provide an additional measure of comparability with other data sets (Dugmore *et al.*, 1992; 1995; Larsen *et al.*, 1999; 2001).

EPMA analysis procedure at the Department of Earth Sciences, University of Manchester: Concentrated tephra shards were incorporated into a thickness of about 75 μm and polished with 6 μm and 1 μm diamond pastes. After carbon coating the samples were analysed using a Cameca SX100. The SX100 is equipped with 5 WDS spectrometers that contain a total of 14 diffracting crystals (2 LLIF, LIF, 2 LPET, 2 PET, 3 TAP, PC0, PC1, LPC2, PC3). The configuration of crystals and spectrometers affords exceptional versatility of application (http://www.earth.man.ac.uk/MEMF/sx100/sx100.html, 2002).

4.6 Multivariate statistical analysis

Multivariate statistical analysis can examine many variables simultaneously in a matrix. These methods are invaluable in many scientific fields in which patterns and trends in

complex systems must be studied. They simplify the data so that the major trends are emphasized and the minor variations ignored (Kovach, 1995). Here, several multivariate statistical methods were employed to display the main trends in the magnetic and geochemical datasets and, in particular, to correlate the tephra layers between the various sections.

4.6.1 Factor analysis (FA)

Factor analysis is a multivariate statistical technique of data reduction and is concerned with explaining correlations amongst the original variables (Kovach, 1995; Walden and Smith, 1995). It begins with a principal components analysis (PCA) of the original data matrix, in which the variables are combined into a smaller number of principal components, which account for decreasing amounts of the variance in the data set. To interpret the components and produce a distinctive cluster of variables associated with each component, the solution is rotated. The varimax rotation is a widely used method; it emphasises column simplification in the component loading (correlation) matrix (Ebdon, 1985). Gonzalez *et al.* (1999) and Xie (2000) have used the method satisfactorily for source apportionment. Here the method is applied to investigate associations between magnetic properties, element concentrations and between the two groups, using the SPSS package.

4.6.2 Principal coordinates analysis (PCO)

Principal coordinates analysis (PCO) was applied to the unprocessed data to get the distance or similarities between the measurement results directly, and the eigenvectors

represent the scores for the samples (Kovach, 1995). This procedure calculates a wide variety of statistics measuring either similarities or distances, either between pairs of variables or between pairs of items. These similarity or distance measures can then be used with other procedures (e.g. multidimensional scaling) to help analyze complex data sets.

Euclidean Distance (ED) between two items, X and Y, is the square root of the sum of the squared differences between the values for the items:

$$ED\ (X, Y) = \sqrt{\sum_i (X_i - Y_i)^2}$$

This is closest to what is measured when the distance between two points in the real world are considered, except that it is extended to work in a multidimensional space, rather than three dimensions. The susceptible of some large data values can be minimized by using the normalized Euclidean distance; this is done by placing raw data points at equal distance from the origin of the graph, and then measuring the distance between the two points.

Similarity Coefficient (SC) between two samples, X and Y, is the cosine theta (inclination) between the values of measured properties for the two samples. The SC analysis was derived using the follow equation:

$$r_{xy} = \cos\theta_{xy} = \sum_{k=1}^{n}(x_k y_k) \Big/ \left(\sqrt{\sum_{k=1}^{n} x_k^2}\sqrt{\sum_{k=1}^{n} y_k^2}\right)$$

Where: r_{xy} is the SC value between two sets of observations for samples x and y, and k is a magnetic parameter.

The similarity coefficient can be used to combine mixed data, in which some variables are measurements whereas others are binary or multivariate. It gives a measure that indicates how closely the variations in different species abundances are correlated across several samples.

In this study, these methods were used to 1) evaluate the ED and SC between tephra layers for samples from site Ska2 and known tephra layers based on nine geochemical properties (i.e. SiO_2, TiO_2, Al_2O_3, MgO, CaO, MnO, FeO, Na_2O and K_2O; and 2) to evaluate the ED and SC of tephra samples from the 2 peat sections and 3 soil sections, based on 15 magnetic properties (χ_{lf}, SOFT, χ_{fd}, $\chi_{fd\%}$, χ_{ARM}, SIRM, HIRM, SIRM/ARM, χ_{ARM}/SIRM, χ_{ARM}/χ_{lf}, SIRM/χ_{lf}, S_{-20}, S_{-40}, S_{-100}, and S_{-300}). Version 10.1 of The Statistical Package for the Social Sciences (SPSS) was used for all analyses.

Chapter 5 Tephrochronology of the study sections

5.1 Introduction

Measurement of the major element geochemistry of individual tephra shards is the routinely applied method of determining the source eruptions of both distal and proximal tephra (Dugmore, 1989; Hunt and Hill, 1993). This chapter presents the results of EPMA (Electron Probe Micro-analysis) employed to determine the geochemical signature of tephra layers from soil and peat profiles at Laxadalar (Lax), Skaftafellsheidi (Ska1 and Ska2) and Jokulsa I Loni (JL1 and JL2). EPMA was undertaken on discrete tephra layers from the five profiles. 17 samples from 17 layers were analysed at the Tephrochrology Unit at the Department of Geophysics, the University of Edinburgh. 20 additional samples from 18 layers were analysed at the EPMA unit at the Department of Earth Sciences, University of Manchester.

5.2 Major element geochemistry of Icelandic volcanic systems

In Iceland, volcanism occurs within geographically distinct volcanic fissure swarms and associated central volcanoes, each collectively termed a volcanic system (Jacobsson, 1979; Larsen *et al.*, 1999). The details of Icelandic volcanic systems were reviewed in Chapter 3. The geochemical signatures of several events are summarised here.

Tephra shards can be subdivided into 3 categories based on their general geochemical composition. *Basic* shards consist of 41-52 % SiO_2; *intermediate* shards

consist of 52-63 % SiO_2 and *silicic* shards consist of >63 % SiO_2 (Dugmore *et al.*, 1995). Magma-generated silicic and intermediate materials are confined to the central volcanoes of each system, whereas basaltic lava and tephra have erupted both from the associated fissure swarms and from the central volcanoes. The tephras associated with each of these volcanic centres can generally be distinguished by the major element chemistry of their glass, as determined by EPMA, and such differences may be shown using simple bivariate or ternary plots of oxides selected (Fig. 5.1; Larsen *et al.*, 1999).

In general, the chemical composition of volcanic glasses has been shown to be the most appropriate method for identifying particular tephras (Larsen, 1981; Haflidason, *et al.*, 2000). In many cases, geochemical characteristics can be used to identify the products of particular systems. The most useful oxides for discrimination of tephra are FeO, TiO_2, CaO, K_2O and MgO (Larsen *et al.*, 1999). Fig. 5.1 shows the geochemical fields for variations in a) iron and titanium, b) iron and calcium, c) titanium and potassium, and d) iron and magnesium based upon Icelandic tephras identified in Iceland and even across northwest Europe.

Hekla is one of the large central volcanoes of the volcanic system in Iceland (Chapter 3, Fig. 3.4). Hekla tephras are some of the most widely identified volcanic chronological markers in Holocene sequences in NW Europe. Hekla tephras are often distinctive because of their high silica content. The silica content is highest during the initial phase of an eruption, and the quantity of SiO_2 increases proportionally with the length of the preceding repose time. During major eruptions, the silica content of the products decreases through time. For example, the silica

content of the Hekla 4 (3834 BP) tephra ranges from ca. 74-57 % towards the end of the eruption. In addition to their relatively high content of SiO_2, the Hekla tephras are distinctive in term of their low FeO content (average 6.5 %), low TiO_2 content (average 1.7 %), low MgO (with a mean of 1 %) content and high K_2O content (average 2.2 %).

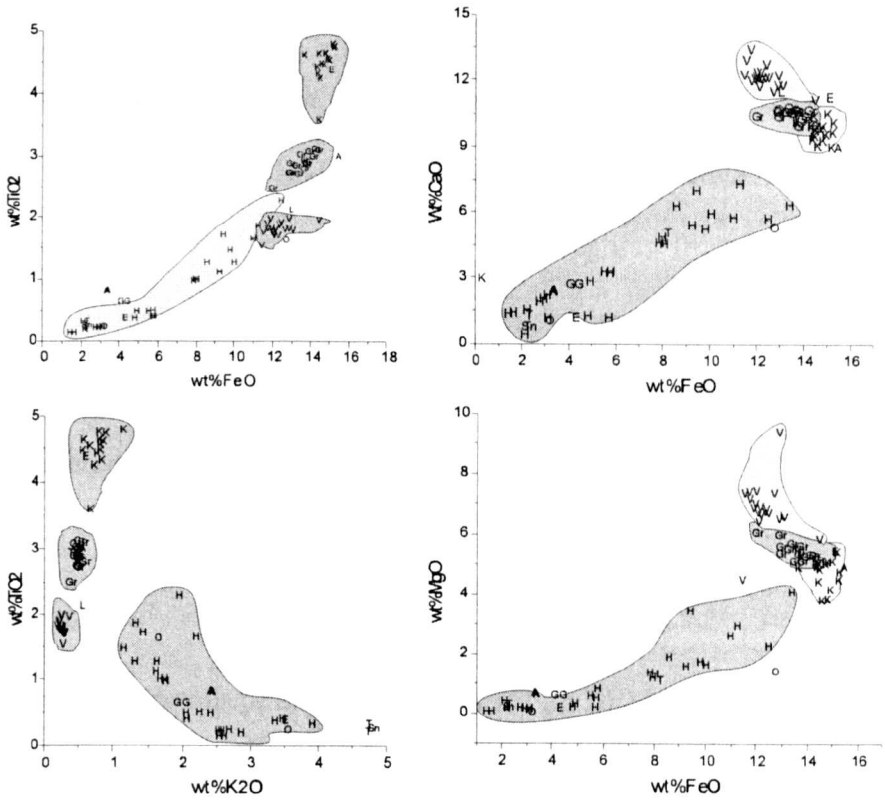

Figure 5.1 Binary plot of geochemical data for the known tephra-generating eruptions in Iceland. The volcanic system names are abbreviated as follows: Gr, Grimsvötn; H, Hekla; A, Askja; K, Katla; Th, Thordarhrna; V, Veidivötn, E, Eyjafjallajökull; O, Öraefajökull.

The group of tephras from the Katla system are characterised by high TiO_2 (>4 %) and FeO content (>13.5 %, with one exception), moderate MgO (4-9 %) and low

K_2O (<1 %, with one exception). The geochemistry of products from the Katla system has not varied significantly during the Holocene and individual eruptions remain difficult to distinguish. Identification of Katla tephra layers in Iceland depends on establishing accurate stratigraphical relations with known tephras (Boygle, 1999).

The signature of the Veidivötn tephra is high CaO content (11-13 %), high FeO content (11.4-14.4 %), high MgO content (4.5-9.3 %), moderate TiO_2 content (1.5-1.9 %), and low K_2O content (0.16-0.33 %). Tephras from the Grimsvötn are characterised by high iron content (12.3-13.4 %), moderate TiO_2 content (2.7-3.2 %), moderate calcium content (9.9-10.7 %), moderate magnesium (5.1-6 %), and low potassium content (4-5.2 %).

5.3 Results

Table 5.1 gives the details of the 37 samples used for EPMA analysis, together with the inferred source eruption, while Tables 5.2-5.22 give the results. The samples comprise 4 tephra layers from Lax, 4 tephra layers from Ska1, 15 tephra layers from Ska2, 4 tephra layers from JL1 and, 2 tephra layers from JL2. All results for the 5 profiles are also presented in Appendix 4.

Table. 5.1 The Icelandic tephra samples for analysis by EPMA, and summarise the results of tephrochronology analysis in this study.

Section	Depth(cm)	Density(g/ml)	Name[d]	Age[e]	ED[f]	SC[g]	Measurement	No.a	No.b
Ska2	26-28	2.4-2.6					Manchester	1	1
Ska2	26-28	2.6-2.8	G1892	AD 1892	0.025	0.999	Manchester	2	2
Ska2	84-86	2.4-2.6	O1727	AD1727	0.03	0.999	Manchester	3	3
Ska2	104-106	2.6-2.8	G1659	AD1659	0.01	1	Manchester	4	5
Ska2	122-124	2.4-2.6	G1619	AD1619	0.007	1	Manchester	5	7
Ska2	126-128	2.4-2.6					Manchester	6	8
Ska2	148-150	2.6-2.8					Manchester	7	11
Ska2	168-170	2.6-2.8	V1477	AD1477	0.006	1	Manchester	8	14
Ska2	194-196	2.4-2.8	G1354	AD1354	0.007	1	Manchester	13	33
Ska2	222-224	2.4-2.6	V1340	AD 1340	0.025	0.999	Manchester	9	12
Ska2	228-230	2.4-2.8	G1159	AD1159	0.01	1	Manchester	10	18
Ska2	256-258	2.4-2.8	Settlement	AD 870	0.011	1	Manchester	11	19
Ska2	274-276	2.4-2.8	G150	AD150	0.012	1	Manchester	12	20
Ska2	292-294	2.4-2.8	O1940 BP	1940BP			Manchester	14	34
Ska2	298-300	2.4-2.8	SvV BP	2500BP	0.012	1	Manchester	15	35
Ska2	354-356	2.4-2.8	H4	3830BP			Manchester	16	36
JL1	170-172	2.4-2.6	V1739	AD1739	0.017	1	Manchester	17	15
JL1	38-40	2.4-2.8	G1892	AD1892			Manchester	18	21
JL1	318-320	2.4-2.6	V150	AD150	0.01	1	Manchester	19	23
JL1	90-92	2.4-2.8	G1774	AD 1774	0.011	1	Manchester	20	30
Lax	17-19		K1918	AD1918	0.01	1	Edinburgh	21	Lax(18)
Lax	36-38		O1362	AD1362	0.007	1	Edinburgh	22	Lax(38)
Lax	121-123		T-c AD 550	AD550	0.018	1	Edinburgh	23	Lax(121)
Lax	153-154		G150	AD150	0.009	1	Edinburgh	24	Lax(154)
Ska1	75-78		K1721	AD1721	0.009	1	Edinburgh	25	Ska1(75)
Ska1	133-134		H1158	AD1158	0.017	1	Edinburgh	26	Ska1(136)
Ska1	175-176		G650	AD150?	0.017	1	Edinburgh	27	Ska1(175)
Ska1	230-231		HS	3500BP	0.004	1	Edinburgh	28	Ska1(237)
Ska2	84-86		K1721	AD1721	0.009	1	Edinburgh	29	Ska2(89)
Ska2	256-258		V150?	AD150?	0.019	1	Edinburgh	30	Ska2(256)
Ska2	356-358		H4	3834BP	0.006	1	Edinburgh	31	Ska2 H4
Jl1	38-40		E1821?	AD1821	0.021	0.999	Edinburgh	32	JL1(38)
JL1	173-175		V1717	AD1717	0.01	1	Edinburgh	33	JL1(174)
JL1	185-186		G1619	AD1619	0.014	1	Edinburgh	34	JL1(186)
JL1	189-190		O1362	AD1362	0.008	1	Edinburgh	35	JL1 (190)
JL2	74-76		V1697	AD 1697	0.016	1	Edinburgh	36	JL2 (74)
JL2	86-88		O1362	AD1362	0.006	1	Edinburgh	37	JL2 (86)

Notes: d: the known eruption in Iceland (Haflidason, *et al.*, 2000); e: the age of the known eruptions in Iceland; f: the Euclidean Distance between the measurement result in this study and the known eruptions in Iceland; g: the Similarity Coefficient between the measurement results in this study and the known eruption on Iceland (See Chapter 4).

5.3.1 Test of the consistency of the density separation technique

The geochemical results of two sub-samples, obtained using two different heavy liquid densities (2.4-2.6 gcm^{-3} and 2.6-2.8 gcm^{-3}), from the same tephra layer are plotted in Figure 5.2. The results show that the tephra shards concentrated using the two different heavy liquid densities have almost the same geochemical signature. Therefore, in this study a heavy liquid separation range between 2.4 to 2.8 gcm^{-3} procedures was used to concentrate the tephra shards.

5.3.2 Comparison of the results from the two EMPA systems

Two EMPA systems were used in this study. The first set of 17 sub-samples were analysed at the University of Edinburgh, and the second set of 20 sub-samples was measured at the University of Manchester. In order to check the consistency of results between the two instruments, three pairs of sub-samples, from the same layer of profile Ska2 (A03 and A29, A11 and A30 and, A16 and A31 in Table 5.1), were measured by EPMA separately in Edinburgh and Manchester (Tables 5.11, 5.19, and 5.24; Figs. 5.11, 5.19 and 5.24). The results of the first two pairs of sub-samples (A03 and A29, A11 and A30) are very similar, thus demonstrating that the EPMA measurements are highly comparable between the two instruments. However, the geochemical signatures of the last pair of samples are quite different (Table 5.24, and Fig. 5.24). This could be due either to differences in the preparation methods (e.g. the density separation) or to some slight difference in stratigraphic level (Table 5.1) of the two sub-samples, which could have resulted in the presence of tephra shards from different eruptions in the same sub-sample.

5.3.3 Laxadakar

Laxadakar 17-18 cm (Lax 18) (Table 5.2; Figure 5.2)

The geochemical signature of eight shards indicates that this 2 cm-thick dark grey tephra layer contains shards from three separate eruptions. All shards are of basic composition, with SiO_2 content ranging from 47.1-49.5 %. Six shards form a group a, their geochemistry is suggestive of a Katla source, with SiO_2 content of ca. 47 %, high TiO_2 content (>4 %), moderate MgO content (ca. 5 %) and a high FeO (>14 %). One shard (b in Table 5.2) has a Grimsvötn signature with moderate TiO_2 (i.e. 2.6 %), high CaO content (10.7 %). The last shard (labelled c) has a geochemical

signature of the Veidivötn tephra, low TiO_2 content (1.45 %) and high CaO content (12.8 %). ED (with a value of 0.01) and SC (with a value of 1) confirm the Katla tephra may source from Katla 1918 (Appendix 6). The Veidivötn shard may origin from V1862-1864. The Grimsvötn shard is difficulty to define its source because there are many candidates (e.g. G1922, G1934, G1903, G1892 even G1883). In summary, the age of this dark grey tephra layer is around AD 1918.

Table 5.2 Glass geochemistry of tephra from Laxadakar 17-18 cm, SE Iceland.

SiO2	TiO2	Al2O3	FeO	MnO	MgO	CaO	Na2O	K2O	Total	Group
47.51	4.91	12.27	14.8	0.28	5.03	9.67	3.27	0.73	98.47	a
47.03	4.84	12.32	14.59	0.24	4.98	9.87	3.08	0.81	97.76	a
47.1	4.78	12.51	14.52	0.26	4.93	9.78	3.1	0.77	97.75	a
46.97	4.77	12.29	14.9	0.23	4.96	9.63	3.19	0.7	97.64	a
47.7	4.72	12.32	15.17	0.22	4.95	9.56	3.3	0.74	98.68	a
47.14	4.71	12.37	14.9	0.27	4.94	9.88	3.15	0.78	98.14	a
49.53	2.63	13.06	12.99	0.24	6.07	10.72	2.89	0.43	98.56	b
49.03	1.45	13.6	10.95	0.21	7.84	12.8	2.05	0.13	98.06	c

Laxadakar 35-38 cm (Lax 38) (Table 5.3; Figure 5.3)

The geochemical data from nine shards imply that this 3 cm thick fine white tephra layer contains shards derived from one eruption. This tephra is of silicic composition, with SiO_2 content ranging from 72.1 % to 73.3 %. The geochemical signature is suggestive of an Öræfajökull source, with high SiO_2 content (>72 %), high K_2O content (>3 %), low FeO content (ca. 3 %), low CaO content (ca. 1 %) and, low TiO_2 content (ca. 0.2 %). ED (with a value of 0.07) and SC (with a value of 1) confirm that the tephra shards are Öraefa 1362, and hence the age of this tephra layer is AD 1362.

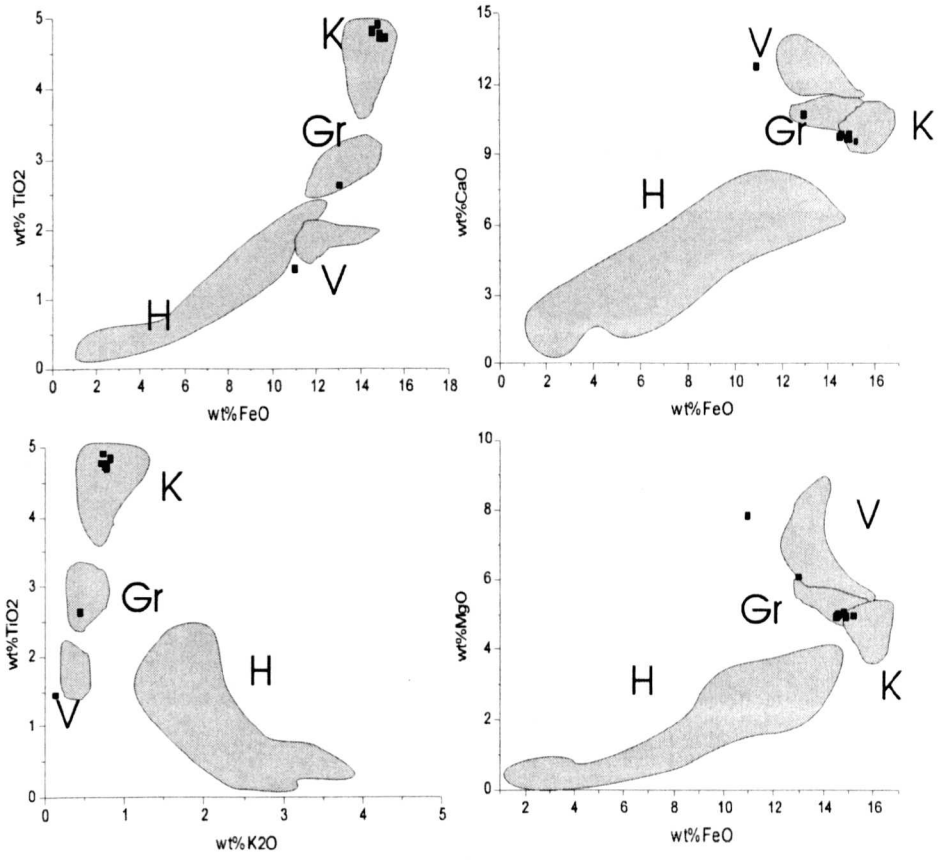

Figure 5.2 Binary plots of chemical data of Laxadakar 17-18 cm, SE Iceland, showing the tephra shards in this layer are mainly derived from a Katla eruption.

Table 5.3 Glass geochemistry of tephra from Laxadakar 35-38 cm, SE Iceland. Values expressed as wt % and total iron as FeO.

SiO2	TiO2	Al2O3	FeO	MnO	MgO	CaO	Na2O	K2O	Total
72.77	0.23	12.73	3.25	0.05	0.01	1.04	4.75	3.46	98.29
72.13	0.24	13.17	3.42	0.09	0	1.02	4.63	3.41	98.11
72.81	0.16	13.06	3.53	0.04	0	0.97	4.85	3.35	98.77
73.2	0.17	12.95	3.21	0.09	0.02	1.04	4.75	3.59	99.02
72.71	0.17	12.94	3.35	0.07	0.04	1.03	4.76	3.32	98.39
72.45	0.19	13.09	3.13	0.11	0.03	0.94	4.47	3.52	97.93
72.68	0.19	13.31	3.18	0.06	0.01	1	4.76	3.54	98.73
73.25	0.17	13.07	3.16	0.08	0.03	1.14	4.54	3.71	99.15
72.3	0.25	12.93	2.99	0.09	0.03	1.13	4.57	3.6	97.89

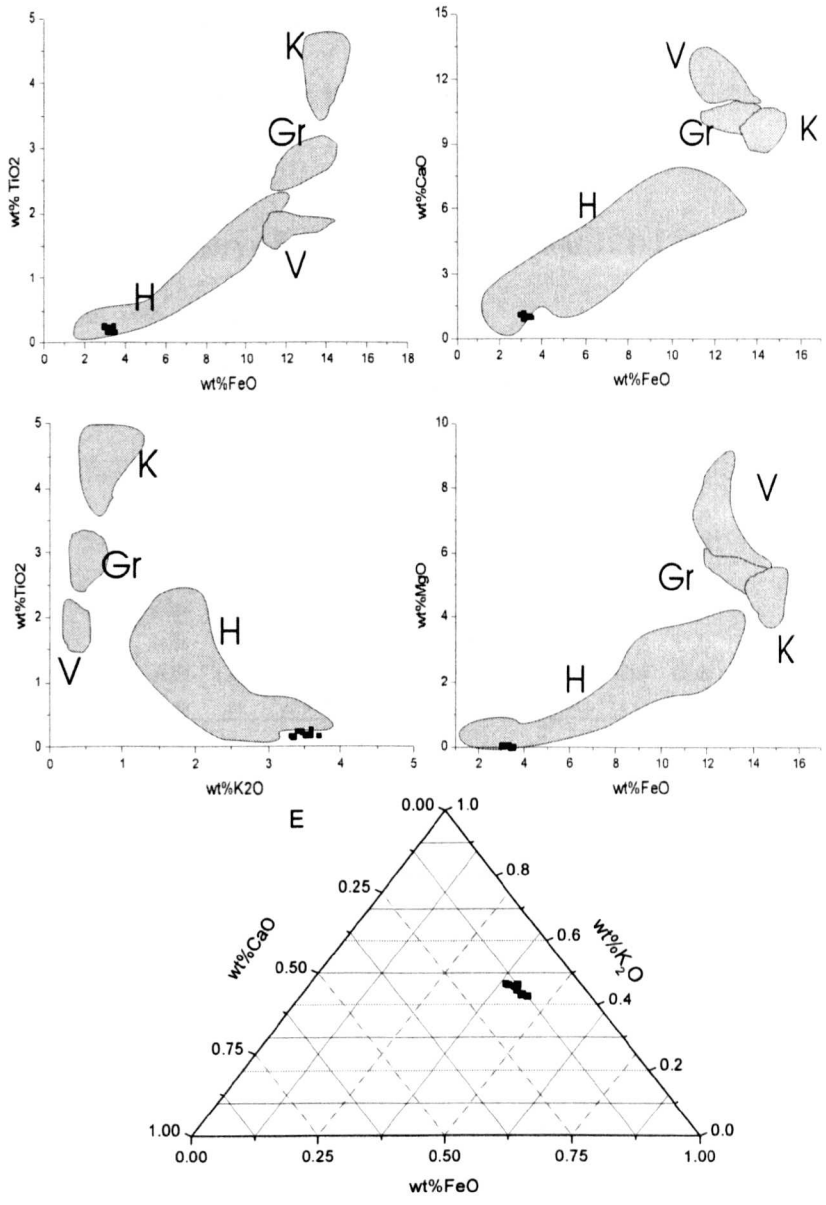

Figure 5.3 Binary and ternary plots of geochemical data for Laxadakar 35-38 cm, SE Iceland, showing the tephra shards in this layer are mainly derived from Öraefajökull 1362.

Laxadakar 121-122 cm (Lax 121) (Table 5.4; Figure 5.4)

The geochemical signature of nine shards suggests that this 2 cm-thick tephra layer contains shards derived from one eruption (Fig 5.4). The shards are of basic content, with SiO_2 content ca. 49%. The content of FeO (0.15-0.28%), TiO2 (1.27-2.14), CaO (ca.1%), K2O (0.04-0.25%) and MgO (<0.05%) indicate that these shards are

derived from a Veidivötn eruption. ED and SC indicate that the eruption is T-c AD 550, this confirming the age of this layer as ca. AD 550.

Table 5.4 Glass geochemistry of tephra from Laxadakar 121-122 cm, SE Iceland. Values expressed as wt% and total iron as FeO.

SiO2	TiO2	Al2O3	FeO	MnO	MgO	CaO	Na2O	K2O	Total
49.64	1.66	13.64	11.82	0.28	7	12.63	1.94	0.22	98.83
48.3	2.14	13.13	11.75	0.22	6.87	11.52	2.37	0.25	96.55
49.02	1.31	13.71	10.26	0.18	7.81	12.87	2.1	0.12	97.38
48.25	1.27	13.86	10.22	0.25	7.89	13.18	2.09	0.14	97.15
50.1	1.4	13.92	9.38	0.18	8.33	13.13	2.17	0.11	98.72
49.37	1.4	13.8	10.23	0.15	7.91	13.46	2.02	0.15	98.49
48.65	1.37	13.8	10.25	0.19	7.99	13.23	2.14	0.11	97.73
49.26	1.43	13.26	11.32	0.2	7.3	12.77	2.34	0.04	97.92
47.69	1.24	12.6	11.19	0.17	11.58	11.64	2.09	0.15	98.35

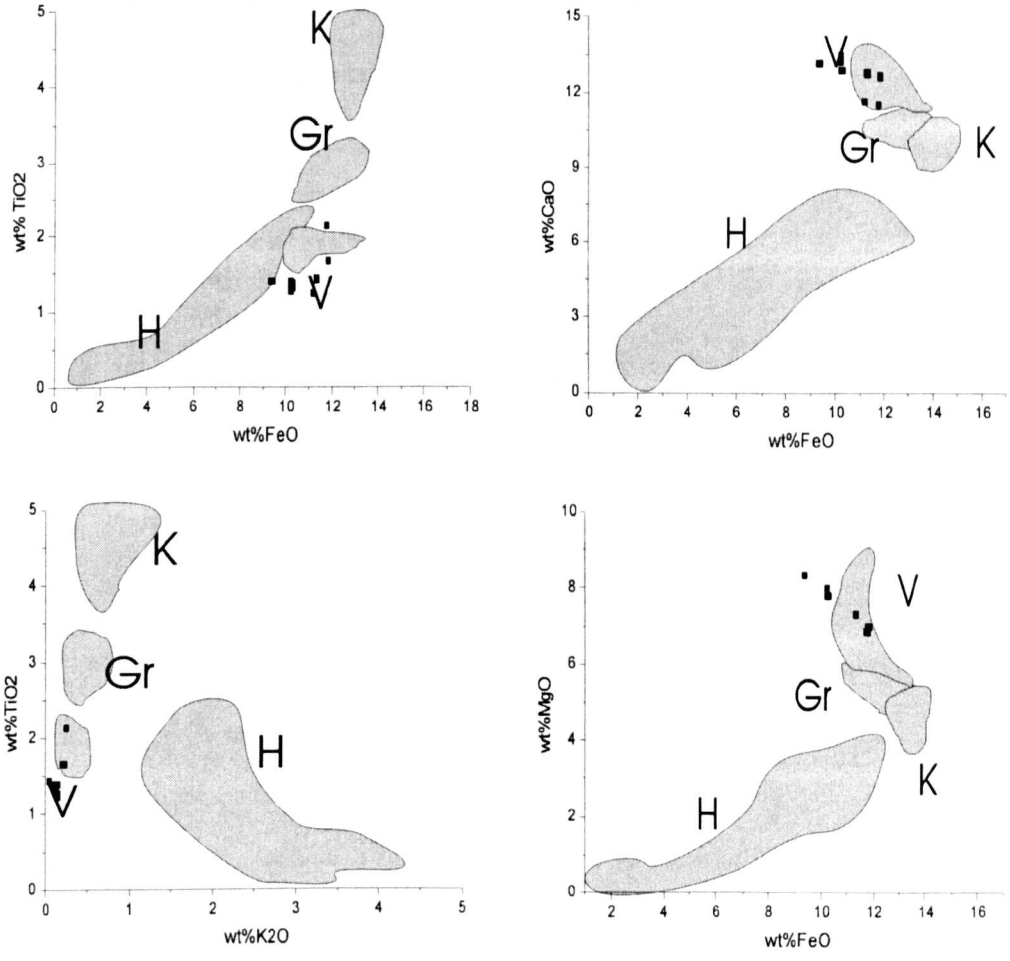

Figure 5.4 Binary plots of geochemical data for Laxadakar 121-122 cm, SE Iceland, showing the tephra shards in this layer are mainly derived from Veidivötn.

Laxadakar 153-154 cm (Lax 154) (Table 5.5; Figure 5.5)

The geochemical signature of nine shards indicates that this 1 cm-thick fine, dark grey/black tephra layer comprises shards derived from one eruption. All of the shards are of basic composition, with SiO_2 content ca. 49 %. The content of FeO (ca. 13 %), TiO_2 (2.53-2.74 %), CaO (ca. 11 %), K_2O (0.3-0.41 %) and, MgO (ca. 6 %) suggest that these shards have the Grimsvötn signature. The ED and SC indicate that the shards may originate from Grimsvötn AD 150 eruption (G150); hence the age is AD 150.

Table 5.5 Glass geochemistry of tephra from Laxadakar 153-154 cm, SE Iceland. Values expressed as wt % and total iron as FeO.

SiO2	TiO2	Al2O3	FeO	MnO	MgO	CaO	Na2O	K2O	Total
47.9	2.67	12.8	12.17	0.16	5.69	10.54	2.59	0.35	94.87
48.76	2.73	12.85	12.77	0.18	5.9	10.48	2.73	0.39	96.79
48.2	2.61	12.84	12.68	0.2	6.02	10.62	2.8	0.32	96.29
48.61	2.6	12.75	12.86	0.21	5.85	10.45	2.63	0.37	96.33
48.61	2.74	12.72	12.96	0.19	5.84	10.77	2.89	0.3	97.02
48.63	2.65	12.95	12.63	0.27	5.89	10.68	2.8	0.41	96.91
48.4	2.68	12.78	12.78	0.2	5.82	10.89	2.72	0.35	96.62
48.75	2.53	12.84	13.24	0.21	6.07	10.71	2.73	0.41	97.49
48.87	2.53	12.89	12.77	0.23	5.98	10.78	2.79	0.34	97.18

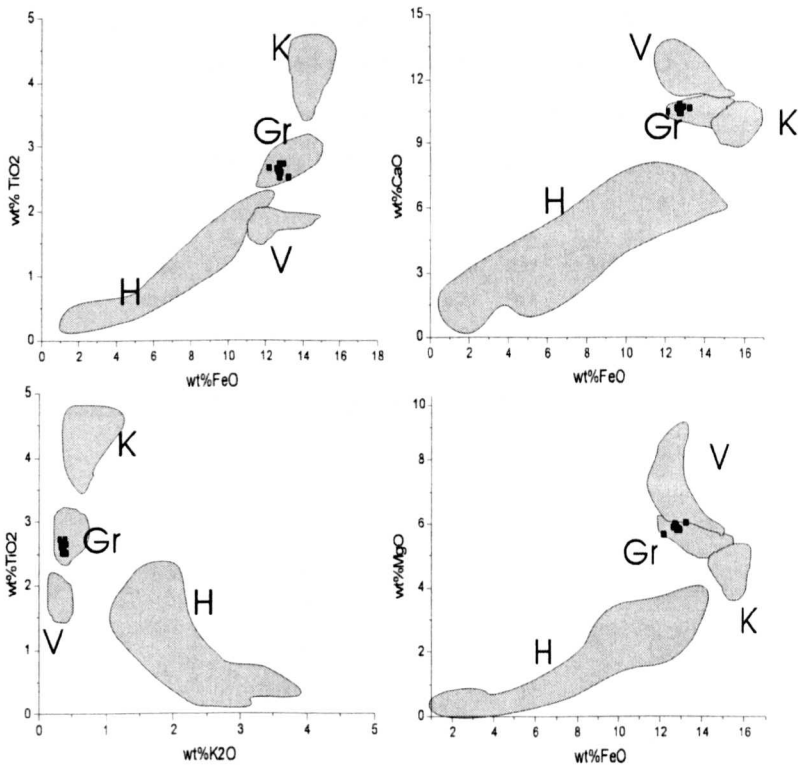

Figure 5.5 Binary plots of geochemical data for Laxadakar 153-154 cm, SE Iceland, showing the tephra shards in this layer are mainly derived from Grimsvötn.

.

5.3.4 Skaftfellsheidi Profile 1

Skaftfellsheidi Profile 1 75-78 cm (Ska1 75) (Table 5.6; Figure 5.6)

The geochemical signature of five shards suggests that this 3 cm-thick black tephra layer contains shards derived from one eruption. All shards are of basic composition, with SiO_2 content ranging from 45.9 % to 47.2 %. The geochemistry is suggestive of a Katla source, with high FeO content (>13.7 %), high TiO_2 content (>4 %), high CaO content (>9 %) and low K_2O content (<1 %). The stratigraphic level (Table 4.2) and ED and SC indicate these shards are from the Katla AD 1721 eruption (K1721). Hence the age of this layer is AD1721.

Table 5.6 Glass geochemistry of tephra from Skaftfellsheidi Profile 1 75-78 cm, SE Iceland. Values expressed as wt % and total iron as FeO.

Ska1(75)	SiO2	TiO2	Al2O3	FeO	MnO	MgO	CaO	Na2O	K2O	Total
	47.17	4.38	12.22	13.74	0.25	4.53	9.24	3.27	0.89	95.69
	45.09	4.74	11.84	15.03	0.26	4.89	9.57	3.06	0.79	95.27
	46.67	4.16	12.9	14.08	0.24	4.21	9.7	3.29	0.82	96.07
	46.18	4.6	12.41	13.96	0.29	4.84	9.86	3.04	0.68	95.86
	45.94	4.43	12.35	13.83	0.45	4.89	9.57	2.81	0.76	95.03
Mean	46.21	4.462	12.344	14.13	0.298	4.672	9.588	3.094	0.788	95.584

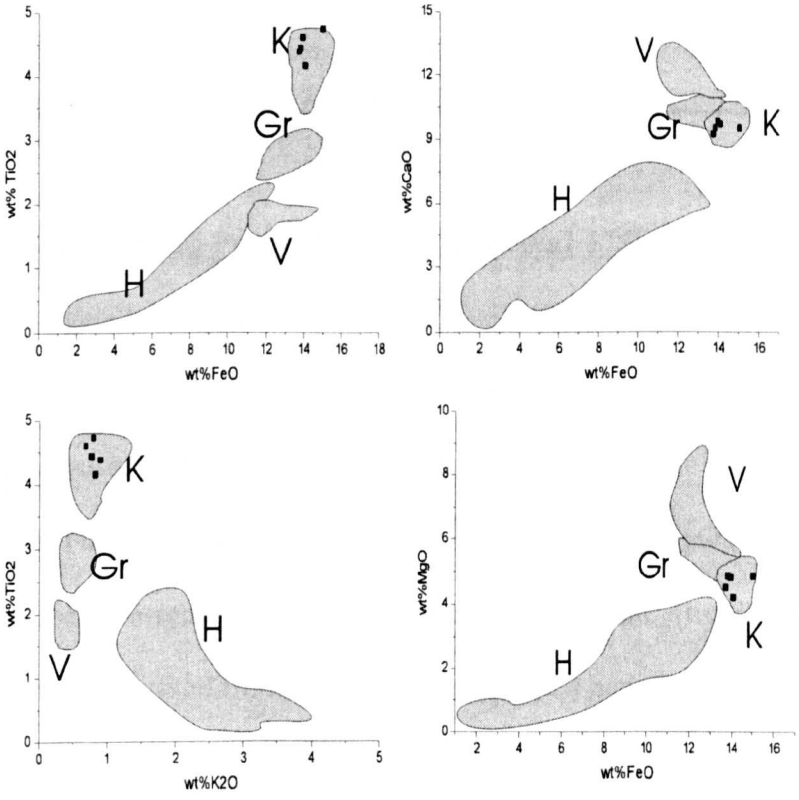

Figure 5.6 Binary plots of geochemical data from Skaftfellsheidi Profile 1 75-78 cm, SE Iceland, showing the tephra shards in this layer are mainly derived from Katla.

Skaftfellsheidi Profile 1 133-134cm (Ska1 136) (Table 5.8; Figure 5.8)

The geochemical data from four shards indicate that this 3 cm thick fine white tephra layer contains shards derived from one eruption. This tephra is of silicic composition, with SiO_2 content ranging from 72.1 % to 73.3 %. The geochemical signature is suggestive of a Hekla source, with high SiO_2 content (>72 %), high K_2O content (>3

%), low FeO content (ca. 3 %), low CaO content (ca. 1 %) and, low TiO_2 content (ca. 0.2 %). ED and SC confirm that the tephra shards are Hekla 1158, and hence the age of this tephra layer is AD 1158.

Table 5.7 Glass geochemistry of tephra from Skaftfellsheidi Profile 1 133-134 cm, SE Iceland. Values expressed as wt % and total iron as FeO.

Ska1(136)	SiO2	TiO2	Al2O3	FeO	MnO	MgO	CaO	Na2O	K2O	Total
	70.03	0.75	12.02	3.86	0.14	0.35	2.29	3.43	2.07	94.94
	72.27	0.46	12.24	3.66	0.12	0.37	2.24	3.45	2.09	96.9
	72.24	0.48	12.34	3.5	0.09	0.4	2.21	3.58	2.03	96.87
	72.89	0.55	12.46	3.69	0.33	0.43	2.32	3.54	2.11	98.32
Mean	71.8575	0.56	12.265	3.678	0.17	0.388	2.265	3.5	2.075	96.7575

Skaftfellsheidi Profile 1 175-176 cm (Ska1 175) (Table 5.8; Figure 5.8)

The geochemical characteristic of five shards indicates this 3 cm-thick olive-green tephra layer contains shards derived from one eruption. All the shards are of basic composition, with SiO_2 content less th+-an 51 %. The content of SiO_2 (mean 50.5 %), TiO_2 (3.1 %), CaO (5.4 %), K_2O (0.8 %) and, MgO (4.1 %) indicate that they probably originate from either Grimsvötn or Katla. The ED and SC results suggest they are derived from Twilling layer 'b', and hence their age is ca. AD 650.

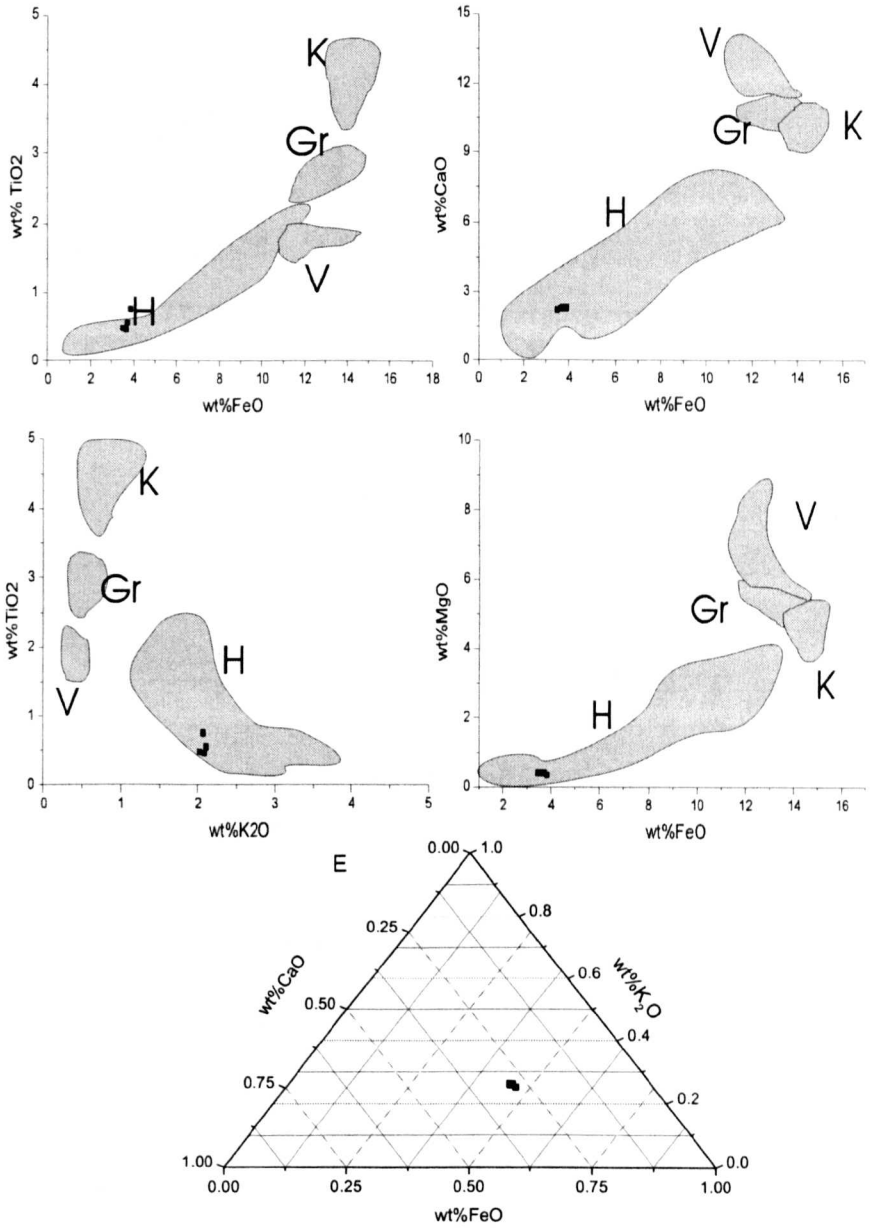

Figure 5.7 Binary and ternary plots of chemical data of Skaftfellsheidi Profile 1 133-134cm, SE Iceland, showing the tephra shards in this layer are mainly derived from Hekla 1158.

Table 5.8 Glass geochemistry of tephra from Skaftfellsheidi Profile 1 175-176 cm, SE Iceland. Values expressed as wt % and total iron as FeO.

Ska1(175)	SiO2	TiO2	Al2O3	FeO	MnO	MgO	CaO	Na2O	K2O	Total
	50.95	3.02	12.57	13.94	0.27	3.75	7.96	3.58	0.85	96.89
	51.12	3.05	12.06	12.78	0.27	4.7	9.19	3.22	0.82	97.21
	50.35	3.01	12.77	13.86	0.33	3.85	8.2	3.28	0.73	96.38
	50.22	3.29	12.72	14.04	0.31	4.09	8.23	3.16	0.76	96.82
	49.71	3.31	12.68	14.1	0.29	4.12	8.34	3.35	0.77	96.67
Mean	50.47	3.136	12.56	13.74	0.294	4.102	8.384	3.318	0.786	96.794

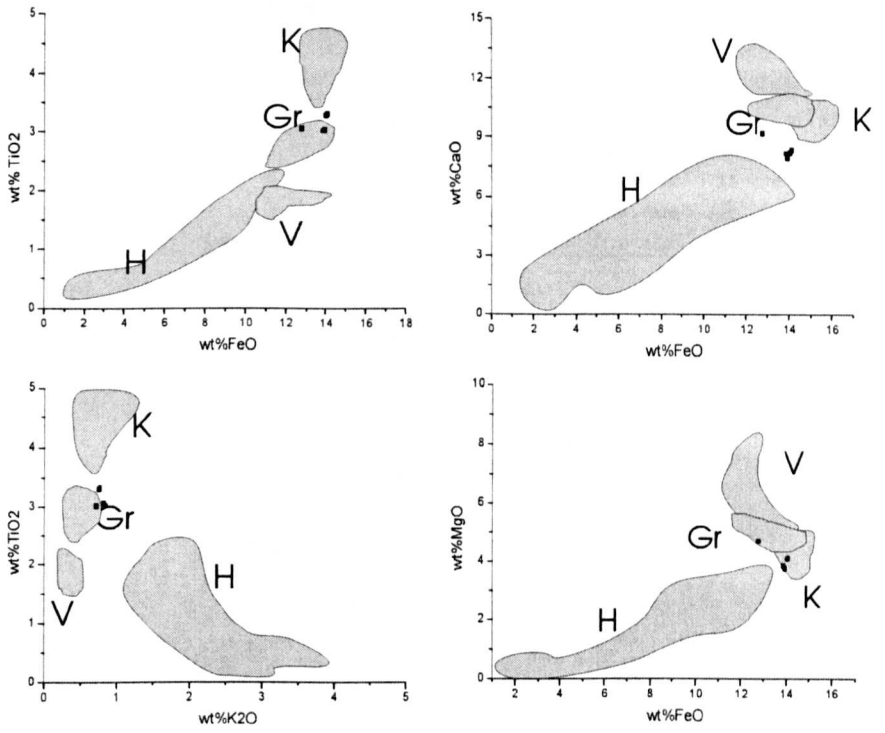

Figure 5.8 Binary plots of chemical data of Skaftfellsheidi Profile 1 175-176 cm, SE Iceland, showing the tephra shards in this layer are mainly derived from Grimsvötn or Katla.

Skaftfellsheidi Profile 1 230-231 cm (Ska1 237) (Table 5.9; Figure 5.9)

The geochemical signature of five shards indicates that this 1 cm-thick white tephra layer contains shards derived from one eruption. All the shards are of silicic composition, with SiO_2 content between 67-69 %. The chemical character is suggestive of a Hekla source, with high SiO_2 content (>67 %), moderate K_2O content (2-2.4 %), low TiO_2 content (<0.7 %), low FeO content (<6 %), low CaO content (< 4%) and, low MgO content (<0.7 %). ED and SC indicate it is HS, and thus the age is ca. 3500 BP.

Table 5.9 Glass geochemistry of tephra from Skaftfellsheidi Profile 1 230-231 cm, SE Iceland. Values expressed as wt% and total iron as FeO.

Ska1(237)	SiO2	TiO2	Al2O3	FeO	MnO	MgO	CaO	Na2O	K2O	Total
	68.12	0.67	14.92	6.11	0.18	0.61	3.72	4.41	2.02	100.76
	67.62	0.47	15.07	5.82	0.18	0.58	3.59	4.36	2.35	100.04
	68.24	0.56	14.97	6.05	0.2	0.57	3.57	4.48	2	100.64
	69.03	0.39	15.09	5.41	0.19	0.49	3.3	4.19	2.14	100.23
	67.74	0.44	15.32	5.52	0.14	0.56	3.57	4.29	2.12	99.7
Mean	68.15	0.506	15.074	5.782	0.178	0.562	3.55	4.346	2.126	100.274

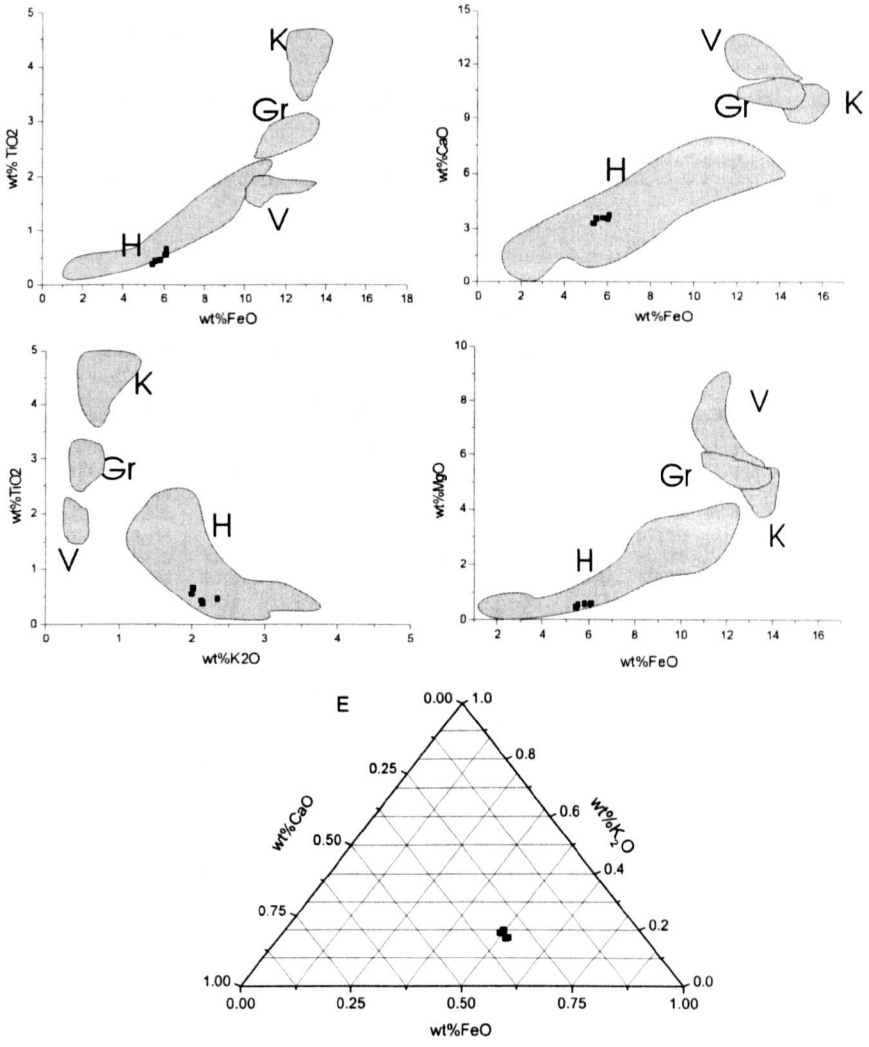

Figure 5.9 Binary and ternary plots of chemical data of Skaftfellsheidi Profile 1 230-231 cm, SE Iceland, showing the tephra shards in this layer are mainly derived from Hekla.

5.3.5 Shaftafellsheidi profile 2

Shaftafellsheidi profile 2 26-28 cm (Ska2 B01 and B02) (Table 5.10; Figure 5.10)

The geochemical signature of twenty shards indicates that this single black 1cm-thick tephra layer consists of shards derived from two separate eruptions. All shards are of basic composition, with SiO_2 content ranging from 47.7% to 49.7%. The

geochemical signature of group a (Table 5.10) is a low K_2O content (ca. 0.3 %), moderate TiO_2 content (<2 %), high CaO content (ca. 11 %), and high MgO content (ca. 6.5 %), which indicates that the source is Veidivötn (Figs. 5.1 and 5.10). On the other hand, the geochemical signature of group b (Table 5.10) matches Grimsvötn (TiO_2 content >2.6%). ED and SC (Appendix 6) indicate the Grimsvötn tephra shards originate from G1883, and the Veidivötn tephra is probably derived from V1864. In summary, the age of this tephra layer is ca. 1883.

Table 5.10 The geochemical composition of tephra shards from A01 and A02, 26-28 cm, Ska2 SE Iceland. Values expressed as wt % and total iron as FeO.

	SiO2	TiO2	Al2O3	MgO	CaO	MnO	FeO	Na2O	K2O	Total	densty
a	47.853	1.845	13.06	6.942	11.927	0.217	12.421	2.426	0.168	96.859	2
	47.955	1.889	12.911	6.428	11.313	0.213	12.946	2.368	0.215	96.238	2
	48.377	1.912	13.823	7.144	11.84	0.174	10.668	2.382	0.201	96.521	2
	48.56	1.98	13.504	7.186	11.882	0.175	11.245	2.347	0.289	97.168	1
	49.276	2.004	13.505	7.2	11.967	0.181	11.239	2.427	0.269	98.068	1
	48.691	2.085	12.829	5.73	10.181	0.221	13.354	2.771	0.324	96.186	2
	48.817	2.087	13.268	6.722	11.562	0.205	12.064	2.56	0.235	97.52	2
	48.727	2.144	13.266	6.775	11.478	0.2	11.78	2.779	0.327	97.476	1
	49.258	2.221	13.334	6.59	11.166	0.177	12.047	2.391	0.319	97.503	2
	49.465	2.235	13.443	6.49	11.257	0.221	12.243	2.526	0.32	98.2	1
	49.323	2.237	13.356	6.512	11.197	0.191	12.652	2.607	0.351	98.426	1
	48.066	2.243	13.24	6.588	11.158	0.211	12.014	2.585	0.319	96.424	2
	47.671	2.377	12.847	6.719	11.171	0.22	13.385	2.457	0.254	97.101	2
	48.895	2.379	13.206	6.28	10.878	0.189	12.439	2.742	0.317	97.325	2
b	48.621	2.61	12.81	6.053	10.416	0.223	12.967	2.804	0.365	96.869	2
	48.057	2.614	12.878	6.133	10.199	0.203	12.961	2.844	0.422	96.311	1
	49.701	2.619	13.322	6.069	10.952	0.226	12.366	2.958	0.321	98.534	1
	49.196	2.636	12.948	6.009	10.418	0.194	13.002	2.814	0.354	97.571	1
	48.833	2.643	12.724	6.092	10.485	0.196	12.832	2.754	0.361	96.92	1
	48.618	2.982	12.456	5.391	9.552	0.225	13.625	2.889	0.503	96.241	1

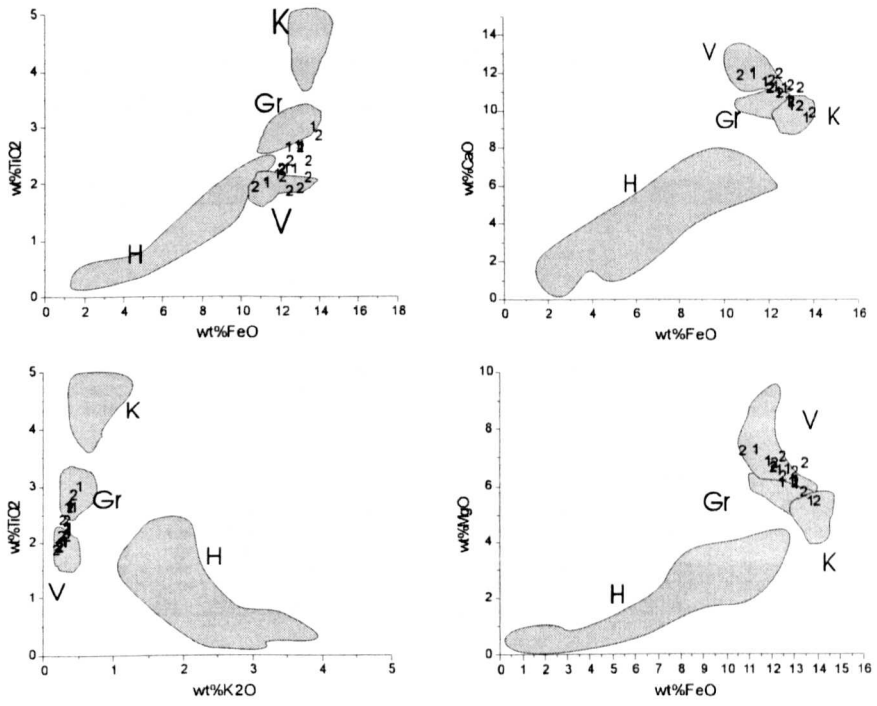

Figure 5.10 Binary plots of chemical data in Table 5.2 of A01 (1) and A02 (2), Ska2 (26-28 cm), which are from same tephra layer, but are of different density.

Skaftfellsheidi Profile 2 84-86 cm (Ska2, A03/B03) (Table 5.11; Figure 5.11)

The geochemical signatures of nineteen shards suggest that this single 2 cm-thick black tephra layer contains shards derived from three separate eruptions. The three groups are labelled A-C in Table 5.11. All three populations are of basic composition with relatively low SiO_2 content. Ten shards form cluster C and the geochemistry is suggestive of a Katla source, with SiO_2 content of ca. 46 %, high TiO_2 content (>5 %), moderate MgO content (6-5 %) and a high FeO (>14 %). Cluster A, consists of six shards, has a Veidivötn or Lakigigar signature with lower TiO_2 (< 3%) and higher MgO (>6 %) than cluster C. The final group, cluster B, consists of three shards that have a distinctive SiO_2 content with a different geochemistry. The shards have a higher SiO_2 content of 56 %. The ternary plot of CaO, K_2O and FeO for those shards is suggestive of an Öræfajökull source.

Table 5.11 Glass chemical data for tephra from A03, 84-86 cm, Ska2 SE Iceland. Sub-samples were measured in Edinburgh (e) and Manchester (m). Values expressed as wt % and total iron as FeO.

B03	SiO2	TiO2	Al2O3	MgO	CaO	MnO	FeO	Na2O	K2O	Total	Measurement
A	48.53	2.76	12.72	5.78	10.11	0.21	13.32	2.81	0.42	96.65	m
	48.65	2.71	12.78	5.51	9.88	0.23	13.34	3.03	0.41	96.54	m
	48.70	2.04	13.58	7.17	11.78	0.20	11.47	2.37	0.30	97.59	m
	48.78	2.70	12.69	5.52	9.99	0.22	13.38	2.86	0.42	96.56	m
	49.15	2.25	13.36	6.62	11.07	0.20	11.95	2.70	0.31	97.61	m
	49.53	1.78	13.20	6.86	11.49	0.21	12.48	2.52	0.20	98.26	m
	49.54	2.58	12.98	5.37	9.73	0.21	13.01	2.87	0.46	96.76	m
B	56.32	1.67	13.50	1.52	5.45	0.33	12.96	4.32	1.56	97.62	m
	56.51	1.58	13.37	1.35	5.33	0.33	12.90	4.63	1.68	97.69	m
	56.92	1.52	13.43	1.27	5.35	0.33	8.61	5.96	1.21	94.59	m
C	45.62	5.02	12.15	4.80	9.52	0.26	14.33	3.04	0.72	95.46	e
	45.74	4.63	12.39	5.09	9.46	0.32	14.41	2.77	0.74	95.55	e
	45.86	4.77	12.26	4.96	9.28	0.24	14.28	3.19	0.74	95.58	e
	46.17	4.67	12.37	4.99	9.80	0.23	14.41	3.21	0.79	96.64	e
	46.18	4.89	12.55	4.82	9.55	0.27	14.08	3.06	0.76	96.16	e
	46.35	4.55	12.34	4.95	9.74	0.28	14.62	3.13	0.70	96.66	e
	46.35	4.67	12.30	4.82	9.89	0.18	14.45	3.22	0.78	96.66	e
	46.38	4.56	12.33	4.94	9.67	0.27	14.20	3.14	0.74	96.23	e
	46.44	4.59	12.71	4.76	9.54	0.22	14.17	3.13	0.75	96.31	e
	46.55	4.69	12.54	5.20	7.85	0.24	16.53	3.67	0.91	98.19	e

Öræfajökull has only erupted twice in historical time (Larsen *et al.*, 1999). The AD 1362 Öræfajökull tephra is present in this profile at 188-192 cm and these shards are almost certainly from the AD 1727 eruption of Öræfajökull. The Katla shards (cluster C) closely match the AD 1721 eruption (Haflidason *et al.*, 2000). The third population of shards is more difficult to source, given that they match both Veidivotn and Lakigigar signatures. The known Lakigigar eruption is the AD 1783-1784 event, whereas successive Veidivotn eruptions between AD 1697 and AD 1979 are also possibilities. In summary the available data suggest a date of ca. AD 1721-1727 for the black layer at 86-84 cm, and highlights the problem of mixed populations of shards in aeolian soils in active volcanic regions.

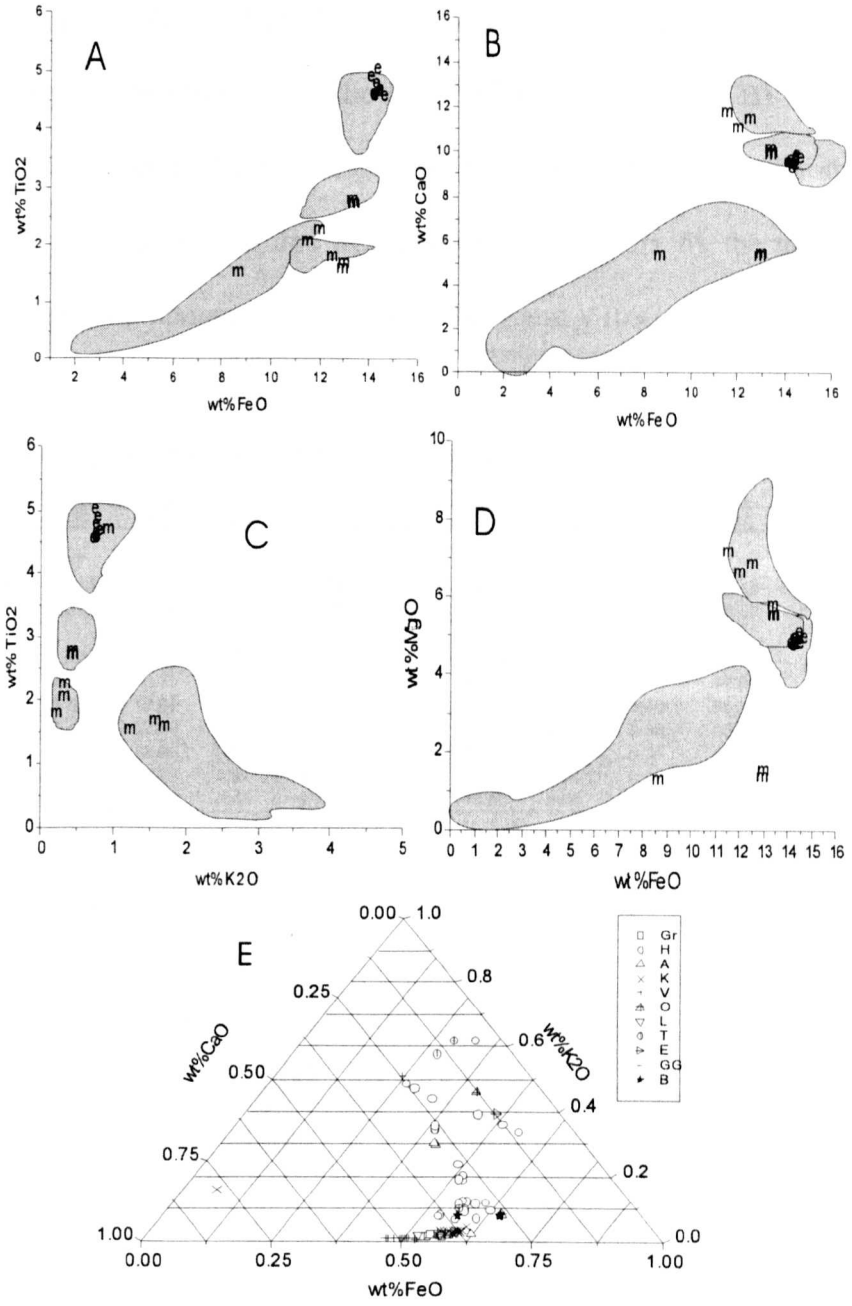

Figure 5.11 Binary plots (A, B, C and D) of data for A03, Ska2 (84-86 cm). Sub-samples were measured in Edinburgh (e) and Manchester (m). The ternary plot (E) matches A03 m2 to O1727. The volcanic system names are abbreviated as the follows: Gr, Grimsvötn; H, Hekla; A, Askja; K, Katla; Th, Thordarhrna; V, Veidivötn, E, Eyjafjallajpkull; O, Öræfajökull, and B, B03.

Skaftfellsheidi Profile 2 104-106 cm (Ska2, A04/B05) (Table 5.12; Figure 5.12)

The geochemical signatures of nine shards indicate that this tephra layer is composed of shards derived from two separate eruptions (A and B in Table 5.12, and Fig. 5.12). Both populations are of basic composition, with SiO_2 content ranging from 45.8 % to

49.5 %. Six shards (Group A) with FeO > 11%, TiO_2 >2.4 %, CaO <10 %, and MgO <6 %, closely match Grimsvötn. The other three shards (Group B) have low TiO_2 content (<2.4 %), and probably originate from Veidivötn. Using the stratigraphic level (Table 4.3) and the ED and SC values (see Appendix 6), the interpretation is that this tephra layer contains shards from G1659 and V1697.

Table 5.12 Glass geochemistry for tephra from A04, 104-106cm, Ska2 SE Iceland.

	SiO2	TiO2	Al2O3	MgO	CaO	MnO	FeO	Na2O	K2O	Total
A	49.37	1.87	13.19	6.50	11.29	0.20	12.85	2.46	0.22	97.95
	49.53	2.11	13.74	7.01	11.96	0.19	11.62	1.95	0.31	98.42
	48.10	2.21	13.19	6.70	11.15	0.19	11.97	2.58	0.34	96.42
	49.07	2.50	13.42	6.36	11.28	0.22	13.02	2.61	0.29	98.75
B	49.11	2.64	12.75	5.46	9.65	0.19	12.92	2.84	0.49	96.06
	48.22	2.78	12.64	5.46	9.75	0.22	13.89	3.00	0.40	96.35
	48.75	2.79	12.59	5.77	10.18	0.23	13.35	2.79	0.39	96.85
	49.29	3.21	12.65	5.67	10.08	0.22	13.84	2.95	0.34	98.25
	48.75	3.29	12.20	4.91	9.10	0.24	14.41	2.94	0.48	96.31
mean	*48.83*	*2.94*	*12.57*	*5.45*	*9.75*	*0.22*	*13.68*	*2.90*	*0.42*	*96.76*

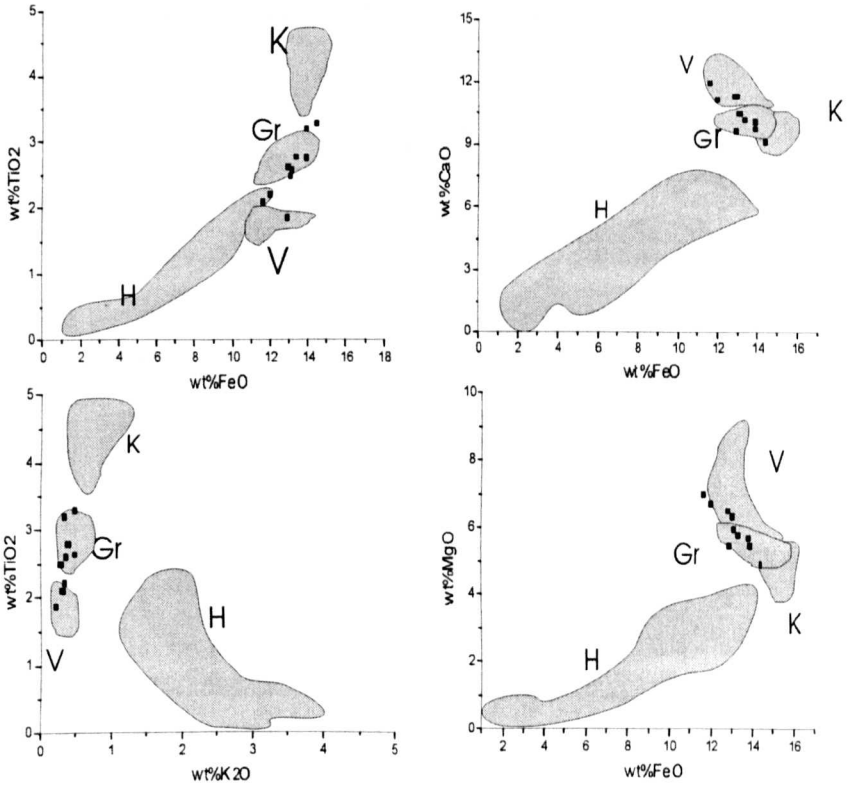

Figure 5.12 Binary plots of chemical data of A04, 104-106 cm, Ska2, SE Iceland, showing the tephra shards in this layer are mainly derived from two sources.

Skaftfellsheidi Profile 2 122-124 cm (Ska2, A05/B07) (Table 5.13; Figure 5.13)

The geochemical data for nine shards show that this dark black tephra layer contains shards derived from a single eruption. All shards are of basic composition, with the SiO_2 ca. 45.8 %. FeO (12.7-14.7 %), TiO_2 (1.9-3.3 %), CaO (9-11.3 %), K_2O (0.2-0.5 %), and MgO (4.8-6.6 %) oxides match quite closely those of Grimsvötn. The stratigraphic level (Table 4.3) and the ED and SC values (Appendix 6) indicate this tephra layer is probably from G1619, hence is dated ca. AD 1619.

Table 5.13 Glass chemical data for tephra from A05, 122-124 cm, Ska2 SE Iceland.

	SiO2	TiO2	Al2O3	MgO	CaO	MnO	FeO	Na2O	K2O	Total
b 07	48.096	2.585	12.96	5.976	10.297	0.211	12.653	2.732	0.361	95.871
	48.123	2.917	12.55	5.575	9.946	0.226	13.686	2.885	0.44	96.348
	48.66	1.923	13.018	6.558	11.224	0.198	12.773	2.655	0.227	97.236
	48.958	2.715	12.751	5.515	9.892	0.245	13.687	2.896	0.416	97.075
	48.991	2.606	12.838	6.101	10.575	0.22	12.906	2.613	0.392	97.242
	49.055	3.213	12.315	5.078	9.548	0.24	14.366	2.805	0.425	97.045
	49.149	2.966	12.508	5.432	9.808	0.217	13.889	2.844	0.406	97.219
	49.221	3.274	12.467	4.852	9.036	0.248	14.68	2.884	0.523	97.185
	49.339	1.878	13.09	6.486	11.31	0.191	12.886	2.635	0.235	98.05
mean	48.8436	2.67522	12.7219	5.73033	10.1818	0.22178	13.5029	2.77211	0.38056	97.0301

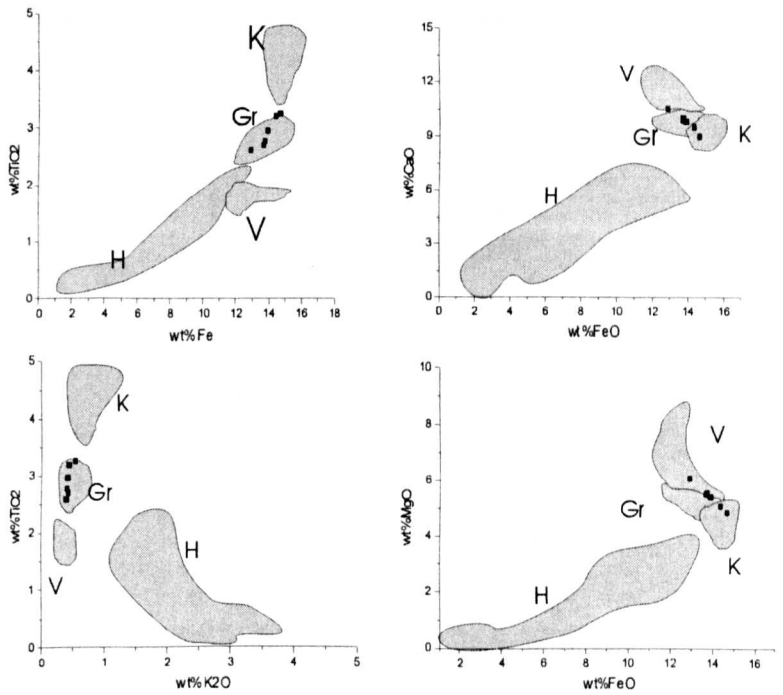

Figure 5.13 Binary plots of chemical data of A05, 122-124 cm, Ska2, SE Iceland, showing the tephra shards in this layer are mainly derived from Grimsvötn.

.Skaftfellsheidi Profile 2 126-128 cm (Ska2, A06/B08) (Table 5.14; Figure 5.14)

The geochemical signature of ten shards suggests this black 6cm thick tephra layer contains shards derived from one eruption. This tephra is of basic composition, with SiO_2 content ranging from 47.9 % to 49.1 %. The FeO, TiO_2, CaO, K_2O and MgO content suggest this tephra as Veidivötn (Fig. 5.14). ED and SC values indicate it originates from V1477; however, this layer is present at depth 168-170 cm in this profile. These shards are probably derived from an unknown Veidivötn eruption with age between AD 1500 and AD 1600, or are the result of reworking of the shards.

Table 5.14 Glass chemical data for tephra from A06, 126-128 cm, Ska2, SE Iceland

	SiO2	TiO2	Al2O3	MgO	CaO	MnO	FeO	Na2O	K2O	Total
b 08	47.938	1.9	12.911	6.597	11.078	0.226	12.806	2.562	0.264	96.282
	48.478	1.914	13.008	6.581	11.066	0.216	12.921	2.438	0.233	96.855
	48.655	1.894	13.107	6.581	11.184	0.22	12.727	2.532	0.226	97.126
	48.659	1.937	12.925	6.522	11.016	0.217	13.225	2.49	0.237	97.228
	48.716	1.827	13.019	6.602	11.368	0.227	12.45	2.572	0.204	96.985
	48.729	1.93	12.913	6.51	11.254	0.205	12.806	2.374	0.22	96.941
	48.887	1.882	13.139	6.561	11.253	0.196	12.729	2.655	0.216	97.518
	48.927	1.915	12.846	6.511	11.242	0.234	12.974	2.443	0.237	97.329
	49.026	1.937	12.962	6.503	11.104	0.233	12.818	2.39	0.199	97.172
	49.049	1.954	12.985	6.435	11.114	0.207	13.012	2.437	0.268	97.461
mean	48.7064	1.909	12.9815	6.5403	11.1679	0.2181	12.8468	2.4893	0.2304	97.0897

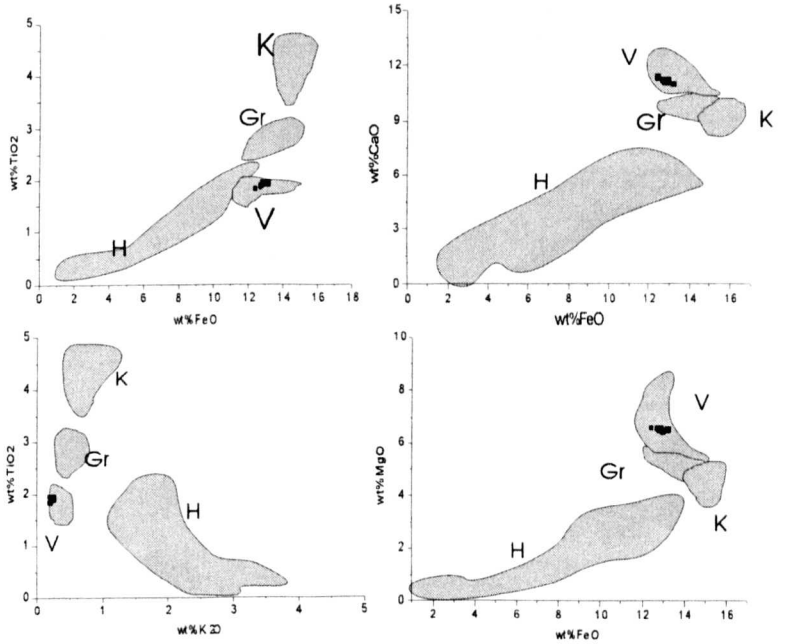

Figure 5.14 Binary plots of chemical data for A06, 126-128 cm, Ska2, SE Iceland, showing the tephra shards in this layer are mainly derived from Veidivötn.

Skaftfellsheidi Profile 2 148-150 cm (Ska2, A07/B11) (Table 5.14; Figure 5.14)

The geochemical data of ten shards indicate that this black 1.5 cm-thick tephra layer contains shards derived from one eruption (Fig. 5.15). The shards are of basic composition, with SiO_2 content ca. 45.5 %. The content of FeO (12.7-14.7 %), TiO_2 (1.9-3.3 %), CaO (9-11.3 %), potassium (0.2-0.5 %), and MgO (4.8-6.6 %) clearly show they are from Grimsvötn. ED and SC values indicate they are derived from G1619; however, the G1619 tephra is present at a depth of 122-124 cm in this profile. Therefore, this layer is probably an unknown Grimsvötn eruption, with an age between AD 1500-AD 1600, or may be the result of reworking of shards from Grimsvötn eruptions in the AD 1600s.

Table 5.15 Glass chemical data for tephra from A07, 148-150cm, Ska2, SE Iceland

	SiO2	TiO2	Al2O3	MgO	CaO	MnO	FeO	Na2O	K2O	Total
b 11	49.318	2.629	12.839	6.03	10.481	0.2	12.854	2.869	0.386	97.606
	48.719	2.661	12.854	5.934	10.485	0.214	13.124	2.813	0.362	97.166
	48.106	2.638	12.721	6.436	10.699	0.204	12.873	2.638	0.364	96.679
	48.655	2.616	12.958	5.945	10.527	0.2	13.116	2.699	0.37	97.086
	48.697	2.597	12.91	6.014	10.574	0.209	12.961	2.881	0.378	97.221
	48.701	2.632	12.885	5.66	10.421	0.19	13.452	2.739	0.389	97.069
	48.802	2.616	12.875	5.959	10.437	0.204	12.964	2.761	0.403	97.021
	48.3	2.614	12.738	6.023	10.605	0.198	13.013	2.725	0.399	96.615
	47.822	2.612	12.7	6.063	10.602	0.223	12.995	2.717	0.357	96.091
	48.367	2.827	12.75	5.699	10.258	0.219	13.548	2.814	0.397	96.879
mean	48.5487	2.6442	12.823	5.9763	10.5089	0.2061	13.09	2.7656	0.3805	96.9433

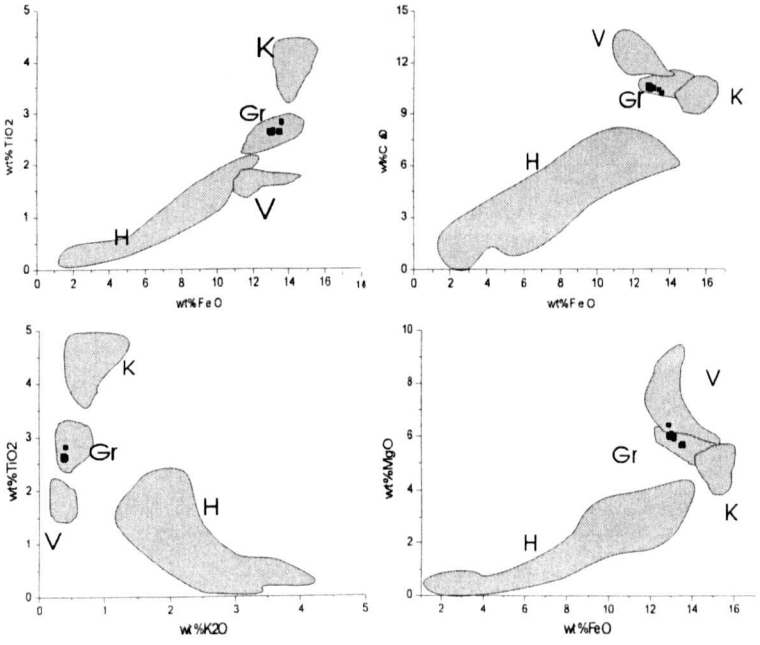

Figure 5.15 Binary plots of chemical data for A07, 148-150 cm, Ska2, SE Iceland, showing the tephra shards in this layer are mainly derived from Grimsvötn.

Skaftfellsheidi Profile 2 168-170 cm (Ska2, A08/B14) (Table 5.16; Figure 5.16)
The geochemical signature of ten shards suggests this 1 cm-thick black tephra layer contains shards derived from two separate eruptions. Both populations are of basic composition, with SiO_2 content ranging from 45.3 % to 49 %. Eight shards have FeO, TiO_2, CaO, K_2O and MgO content (population A) that closely matches a Veidivötn source, but three shards have a higher TiO_2 content of ca. 2.7 %, and are probably from Grimsvötn. ED and SC values (Appendix 6) indicate the Veidivötn shards are from V1477. In short, the age of this tephra layer is AD ca. 1477.

Table 5.16 Glass chemical data of tephra from A08, 168-170cm, Ska2 SE Iceland

b 14	SiO2	TiO2	Al2O3	MgO	CaO	MnO	FeO	Na2O	K2O	Total
	48.291	1.753	13.074	7.028	11.71	0.196	12.115	2.349	0.209	96.725
	48.475	1.992	13.548	7.191	12	0.186	11.177	2.316	0.261	97.146
	48.784	2.766	12.624	5.787	10.334	0.21	13.229	2.741	0.402	96.877
	48.848	2.726	12.713	5.548	9.974	0.211	13.603	2.857	0.415	96.895
	48.886	1.848	13.003	6.482	11.292	0.208	12.64	2.567	0.226	97.152
	49.037	1.98	12.945	6.238	11.17	0.212	13.013	2.481	0.242	97.318
	49.343	2.028	13.12	6.577	11.237	0.226	13.164	2.293	0.343	98.331
	49.358	1.759	13.153	6.848	11.626	0.213	12.373	2.43	0.21	97.97
	49.453	2.704	12.822	5.518	9.946	0.209	13.386	2.997	0.426	97.461
	49.538	1.968	13.429	6.426	11.349	0.206	13.082	2.701	0.153	98.852
mean	49.0013	2.1524	13.0431	6.3643	11.0638	0.2077	12.7782	2.5732	0.2887	97.4727

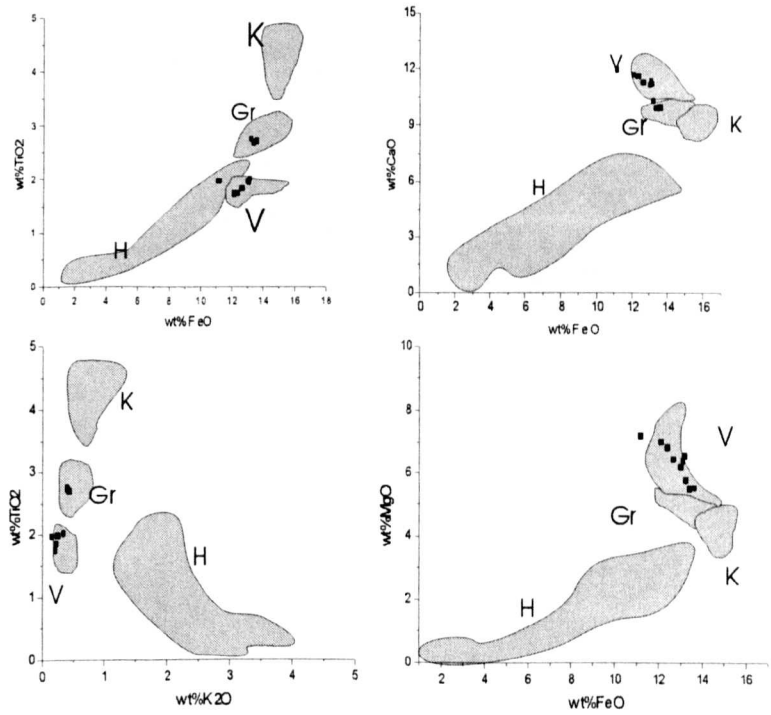

Figure 5.16 Binary plots of chemical data of A08, 168-170 cm, Ska2, SE Iceland, showing the tephra shards in this layer are mainly derived from Veidivötn.

Skaftfellsheidi Profile 2 222-224 cm (Ska2, A09/B12) (Table 5.17; Figure 5.17)

The geochemical signatures of 12 shards are very consistent, indicating a single eruption. This tephra is of basic, with the SiO_2 content ca. 48.0 %. The content of FeO (12.6-13.0 %), TiO_2 (1.8-1.9 %), CaO (11.1-11.3 %), K_2O (0.19-0.21 %), and MgO (6.3-6.6 %) closely match a Veidivötn signature. ED and SC values (Appendix 6) indicate that this tephra layer is probably from V1340; hence the age of this layer is ca. AD 1340.

Table 5.17 Glass chemical data for tephra from A09, 222-224 cm, Ska2 SE Iceland

	SiO2	TiO2	Al2O3	MgO	CaO	MnO	FeO	Na2O	K2O	Total
b12	47.343	1.883	12.927	6.442	11.238	0.214	12.812	2.529	0.21	95.598
	47.466	1.851	12.701	6.51	11.216	0.228	13.005	2.446	0.218	95.641
	47.603	1.877	12.834	6.495	11.318	0.206	12.832	2.422	0.216	95.803
	47.776	1.911	12.765	6.441	11.087	0.225	12.959	2.486	0.228	95.878
	47.845	1.898	12.902	6.362	11.177	0.194	13.043	2.574	0.198	96.193
	47.895	1.827	12.724	6.694	11.421	0.203	12.645	2.445	0.189	96.043
	47.898	1.86	12.8	6.457	11.304	0.212	12.93	2.465	0.207	96.133
	47.997	1.855	12.718	6.436	11.135	0.212	12.685	2.559	0.2	95.797
	48.179	1.884	12.748	6.417	11.171	0.214	12.954	2.524	0.22	96.311
	48.37	1.82	12.849	6.62	11.326	0.216	12.6	2.328	0.189	96.318
	48.449	1.892	12.746	6.436	11.189	0.205	13.027	2.384	0.195	96.523
	48.775	1.925	12.724	6.334	11.059	0.235	12.941	2.536	0.206	96.735
mean	47.9663	1.87358	12.7865	6.47033	11.2201	0.21367	12.8694	2.47483	0.20633	96.0811

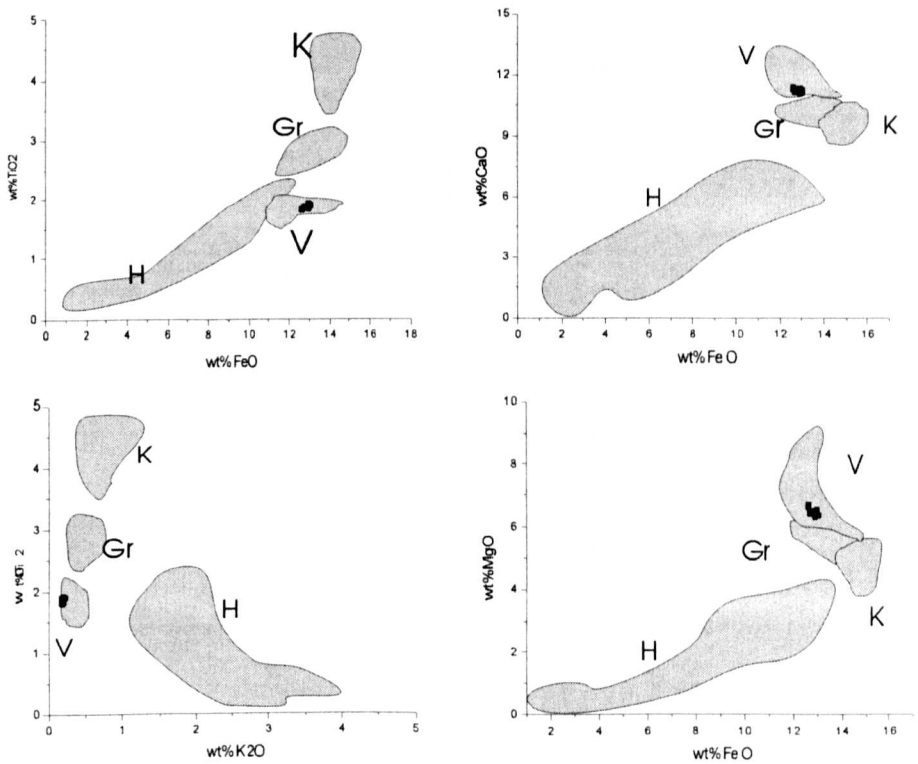

Figure 5.17 Binary plots of chemical data of A09, 222-224 cm, Ska2, SE Iceland, showing the tephra shards in this layer are mainly derived from Veidivötn.

Skaftfellsheidi Profile 2 228-230 cm (Ska2, A10/B18) (Table 5.18; Figure 5.18)

The geochemical data of ten shards from a 2cm-thick black tephra layer indicate they are derived from a single eruption. The tephra is of basic composition, with SiO_2 content of 47.2% to 49%. FeO (12.7-14.7%), TiO_2 (1.9-3.3%), CaO (9-11.3%), K_2O (0.2-0.5%), and MgO (4.8-6.6%); these characteristics indicate a Grimsvötn signature. ED and SC values (Appendix 6) indicate the tephra shards are probably from G1159. The age of this layer is thus ca. AD 1159.

Table 5.18 Glass chemical data for tephra from A10, 228-230 cm, Ska2 SE Iceland

	SiO2	TiO2	Al2O3	MgO	CaO	MnO	FeO	Na2O	K2O	Total
b 18	47.278	3.281	11.898	4.939	9.028	0.232	14.538	3.023	0.506	94.723
	47.446	3.287	12.093	4.938	9.079	0.241	14.623	2.978	0.554	95.239
	47.569	3.347	12.024	4.852	8.983	0.234	14.973	3.025	0.468	95.475
	47.756	3.102	12.215	5.216	9.512	0.227	14.022	2.77	0.445	95.265
	47.841	3.354	12.031	4.759	8.788	0.224	14.779	3.031	0.511	95.318
	48.196	3.332	12.019	4.877	9.022	0.233	14.909	3.061	0.513	96.162
	48.329	3.345	12.073	4.73	8.929	0.229	14.823	2.964	0.483	95.905
	48.421	3.372	11.982	4.726	8.868	0.221	14.86	3.025	0.51	95.985
	48.603	3.324	12.065	4.769	8.834	0.232	14.794	3.149	0.542	96.312
	49.048	3.316	11.974	4.66	8.867	0.223	14.607	2.839	0.544	96.078
mean	48.0487	3.306	12.0374	4.8466	8.991	0.2296	14.6928	2.9865	0.5076	95.6462

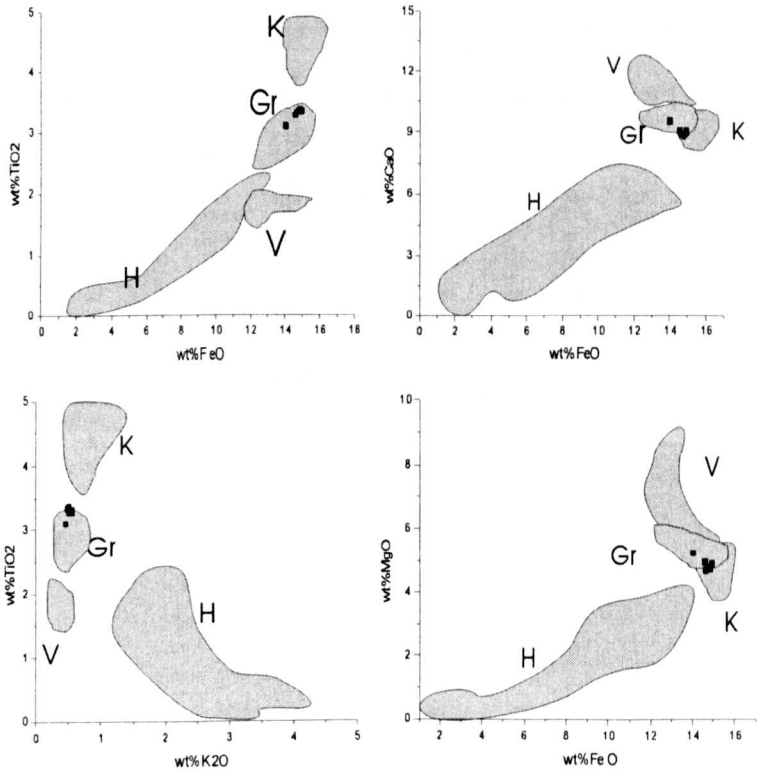

Figure 5.18 Binary plots of chemical data of A10, 228-230 cm, Ska2, SE Iceland, showing the tephra shards in this layer are mainly derived from Grimsvötn.

Skaftfellsheidi Profile 2 256-258 cm (Ska2, A11/B19) (Table 5.19; Figure 5.19)

Geochemical measurements of seventeen shards suggest that the tephra grains from a 2 cm-thick white tephra layer form two populations of glass shards, labelled A and B. Both populations are of basic composition with relatively low SiO_2 content. Thirteen shards closely match the Veidivötn signature with SiO_2 content (ca. 50 %), moderate TiO_2 content (ca. 2.0 %), and low K_2O content. ED and SC (Appendix 6) indicate that this layer is the 'Settlement' (Haflidason *et al.*, 2000) layer with the age of AD 870. The smaller population (with TiO_2 content >2.4 %) are of basic composition with SiO_2 content around 49% (Table 5.19). This tephra closely matches Grimsvötn; it is probably derived from an unknown Grimsvötn eruption. In short, the age of this layer is ca. AD 870.

Table 5.19 Glass chemical data for tephra from A11, 256-258 cm, Ska2 SE Iceland

b 19	SiO2	TiO2	Al2O3	MgO	CaO	MnO	FeO	Na2O	K2O	Total	measured
a	48.36	1.87	13.15	6.42	10.66	0.21	12	2.55	0.2	95.42	e
	49.65	1.896	13.162	6.569	11.223	0.217	12.556	2.558	0.223	98.054	m
	49.78	1.9	13	5.86	10.68	0.23	11.56	2.74	0.33	96.08	e
	49.574	1.927	13.129	6.552	11.102	0.226	12.907	2.495	0.227	98.139	m
	48.652	1.947	13.091	6.619	11.177	0.187	12.88	2.515	0.185	97.253	m
	48.66	1.96	13.23	6.36	10.98	0.19	12.15	2.56	0.22	96.31	e
	48.62	2.02	13.3	6.29	10.86	0.21	11.56	2.55	0.28	95.69	e
	50.048	2.05	13.04	5.932	10.392	0.228	13.269	2.711	0.332	98.002	m
	48.23	2.07	12.94	6.34	10.89	0.23	11.5	2.52	0.29	95.01	e
	51.547	2.188	13.026	5.106	9.255	0.196	13.123	2.762	0.437	97.64	m
	47.98	2.22	12.78	5.79	10.07	0.24	11.18	2.52	0.26	93.04	e
	49.151	2.239	13.271	6.694	11.243	0.196	12.239	2.609	0.317	97.959	m
	49.686	2.308	13.319	6.307	10.914	0.198	12.501	2.593	0.361	98.187	m
b	49.271	2.508	13.043	5.843	10.256	0.195	12.929	2.808	0.381	97.234	m
	49.774	2.529	13.074	5.856	10.361	0.194	12.961	2.871	0.372	97.992	m
	49.19	2.57	13.24	5.82	10.21	0.21	12.48	2.89	0.4	97.01	e
	49.342	2.647	12.737	5.579	9.907	0.206	13.42	2.937	0.378	97.153	m

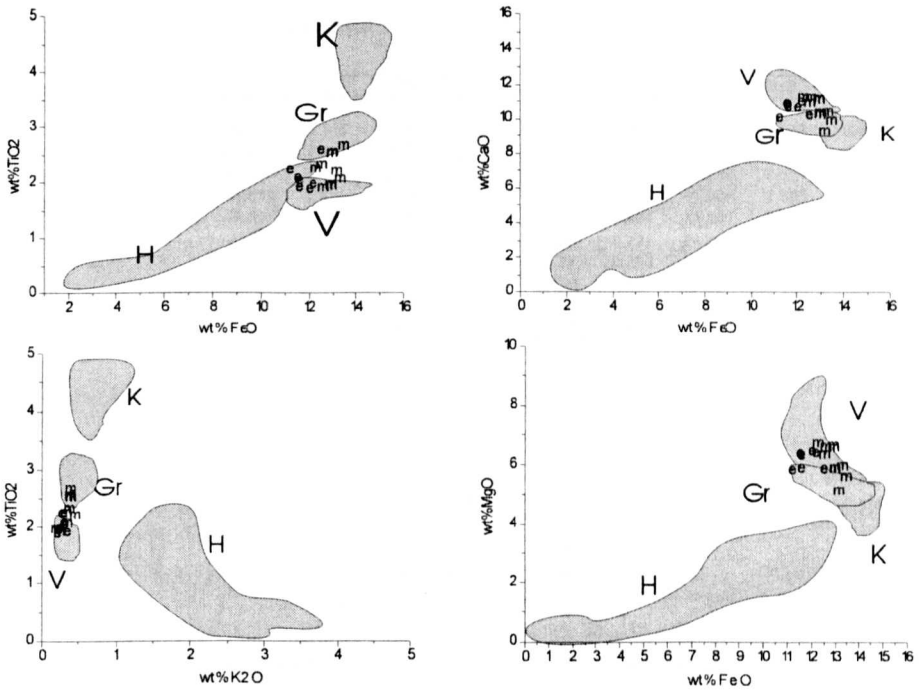

Figure 5.19 Binary plots of chemical data of A11, 256-258 cm, Ska2, SE Iceland, showing the tephra shards in this layer are mainly derived from two sources.

Skaftfellsheidi Profile 2 274-276 cm (Ska2, A12/B20) (Table 5.20; Figure 5.20)

The geochemical signature of nine shards indicates that this 3cm-thick black tephra layer contains shards derived from two eruptions. Both populations are of basic composition with SiO_2 content ranging from 47.1% to 49.7%. The FeO, TiO_2, CaO, K_2O and MgO content of the dominant population closely matches a Grimsvötn signature; the subordinate population (with TiO_2 content >3.4%) is probably from Katla. ED and SC values (Appendix 6) indicate that this tephra layer may be G150, and the Katla tephra closely match 'Twilling b' (Haflidason *et al.*, 2000). The age of this layer is ca. AD 150.

Table 5.20 Glass chemical data for tephra from A12, 274-276 cm, Ska2 SE Iceland

b 20	SiO2	TiO2	Al2O3	MgO	CaO	MnO	FeO	Na2O	K2O	Total
	47.141	3.148	12.239	5.177	9.372	0.207	14.667	2.966	0.412	95.329
	47.458	2.567	12.708	6.181	10.626	0.193	12.949	2.746	0.337	95.765
	47.921	3.183	12.032	5.308	9.395	0.24	14.692	2.854	0.412	96.037
	48.619	2.529	12.686	6.197	10.713	0.214	12.907	2.666	0.39	96.921
	48.626	3.201	12.092	4.993	9.16	0.244	14.801	2.996	0.485	96.598
	48.64	3.033	12.266	5.406	9.698	0.228	14.227	2.945	0.367	96.81
	48.641	3.327	12.114	4.933	9.3	0.223	14.743	2.935	0.468	96.684
	49.477	2.503	12.811	5.437	9.896	0.2	12.786	3.036	0.418	96.564
	49.733	3.665	11.92	3.941	7.839	0.272	14.885	3.386	0.58	96.221
mean	48.4729	3.01733	12.3187	5.28589	9.55544	0.22456	14.073	2.94778	0.42989	96.3254

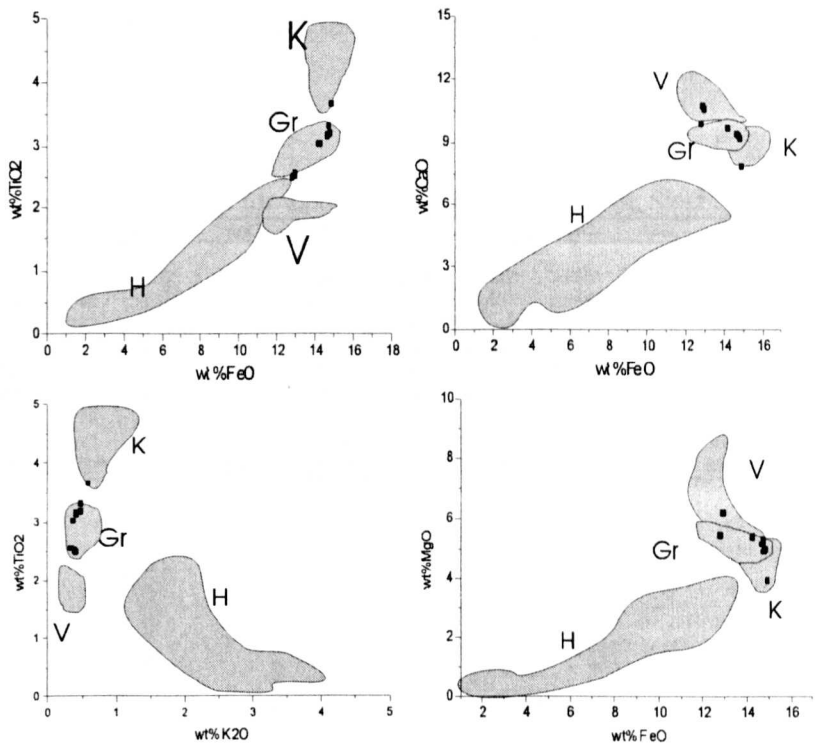

Figure 5.20 Binary plots of chemical data of A12, 274-276 cm, Ska2, SE Iceland, showing the tephra shards in this layer are mainly derived from Grimsvötn.

Skaftfellsheidi Profile 2 194-196 cm (Ska2, A13/B33) (Table 5.21; Figure 5.21)

The geochemical data of eight shards from this 2 cm-thick black tephra layer indicate a basic composition, with the SiO_2 content ca. 49.2%. The content of FeO (13.5-14.0 %), TiO_2 (2.7-3.0 %), CaO (9.7 -11.1 %), K_2O (0.35-0.44 %), and MgO (5.1-6.6 %) match quite closely to Grimsvötn. ED and SC values (Appendix 6) indicates this tephra layer may be G1534. Hence the age of this layer is ca. AD 1534.

Table 5.21 Glass chemical data for tephra from A13, 194-196 cm, Ska2 SE Iceland

b 33	SiO2	TiO2	Al2O3	MgO	CaO	MnO	FeO	Na2O	K2O	Total
	48.699	2.73	12.56	5.568	9.888	0.249	13.542	2.935	0.365	96.536
	48.872	2.752	12.752	5.566	10.073	0.226	13.497	2.941	0.392	97.071
	48.992	2.297	13.181	6.594	11.123	0.196	12.546	2.541	0.346	97.816
	49.089	2.755	12.711	5.726	10.019	0.217	13.458	2.725	0.397	97.097
	49.38	3.028	12.568	5.262	9.635	0.289	14.004	2.958	0.454	97.578
	49.382	2.872	12.503	5.124	9.474	0.208	13.857	3.026	0.422	96.868
	49.52	2.879	12.44	5.228	9.646	0.217	13.758	2.866	0.425	96.979
	49.529	2.921	12.624	5.447	9.945	0.21	13.993	2.822	0.441	97.932
mean	49.1829	2.77925	12.6674	5.56438	9.97538	0.2265	13.5819	2.85175	0.40525	97.2346

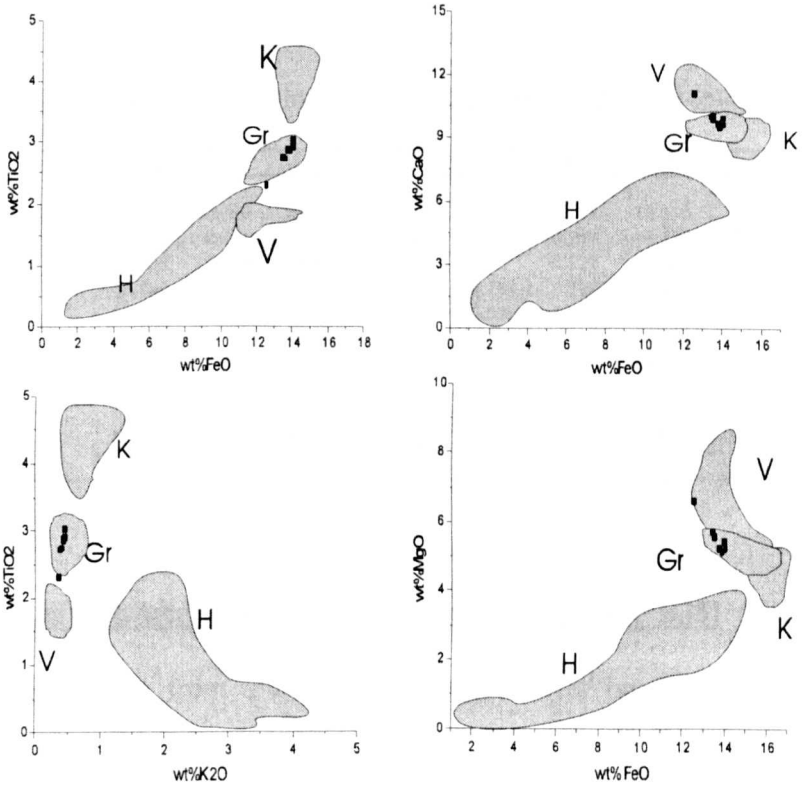

Figure 5.21 Binary plots of chemical data of A13, 194-196 cm, Ska2, SE Iceland, showing the tephra shards in this layer are mainly derived from Grimsvötn.

Skaftfellsheidi Profile 2 292-294 cm (Ska2, A14/B34) (Table 5.22; Figure 5.22)

The geochemical signature of nine tephra grains from a single layer in the profile of Ska2 indicates two populations of glass shards. The larger population (seven shards) consists of glass of basic composition with SiO_2 content ranging from 47.7-49.3 % and TiO_2 content >2.4 %. It closely matches a Grimsvötn signature; they are probably derived from G150 (Appendix 6). The subordinate population (two shards) are of silicic composition (SiO2 content >70 %). The geochemical signature of the shards (high SiO_2 content, high K_2O content, low TiO_2, and low MgO content) indicates they are Öræfa tephra. Combining the geochemical data with the stratigraphic position (Table 4.3), this tephra may be Öræfa 1940 (R.C. Chiverrell, personal communication). The age of this layer is ca. 1940 BP.

Table 5.22 Glass chemical data for tephra from A14, 292-294 cm, Ska2 SE Iceland

b 34	SiO2	TiO2	Al2O3	MgO	CaO	MnO	FeO	Na2O	K2O	Total
m1	47.739	2.758	12.538	5.916	10.485	0.211	13.516	2.681	0.391	96.235
	48.41	2.844	12.679	5.33	9.776	0.211	13.722	3.067	0.434	96.473
	48.758	2.984	12.425	5.347	9.747	0.222	13.833	2.919	0.467	96.702
	48.764	2.008	13.343	7.144	11.764	0.198	11.269	2.487	0.299	97.276
	48.788	2.732	12.729	5.936	10.585	0.236	13.113	2.81	0.355	97.284
	48.898	2.701	12.761	5.909	10.308	0.206	13.469	2.798	0.417	97.467
	49.37	2.535	12.801	6	10.306	0.19	12.541	2.751	0.368	96.862
m2	70.701	0.244	13.077	0.015	1.017	0.1	3.303	4.851	3.464	96.772
	71.733	0.239	13.306	0.004	0.923	0.092	3.157	4.899	3.45	97.803

Skaftfellsheidi Profile 2 298-300 cm (Ska2, A15/B35) (Table 5.23; Figure 5.23)

Ten shards from a 2-cm thick tephra layer have a basic composition, with SiO_2 content ca. 45.3 %. The geochemical signature, FeO (12-12.6 %), Ti_2O (1.7-1.9 %), CaO (ca. 11.7 %), K_2O (ca. 1.9 %), and MgO (6.8-7.2 %), strongly suggest the tephra shards are derived from a Veidivötn eruption. ED and SC values (Appendix 6)

indicate that this tephra layer may be SvV (Haflidason *et al.*, 2000). The age of this layer is ca. 2500 BP.

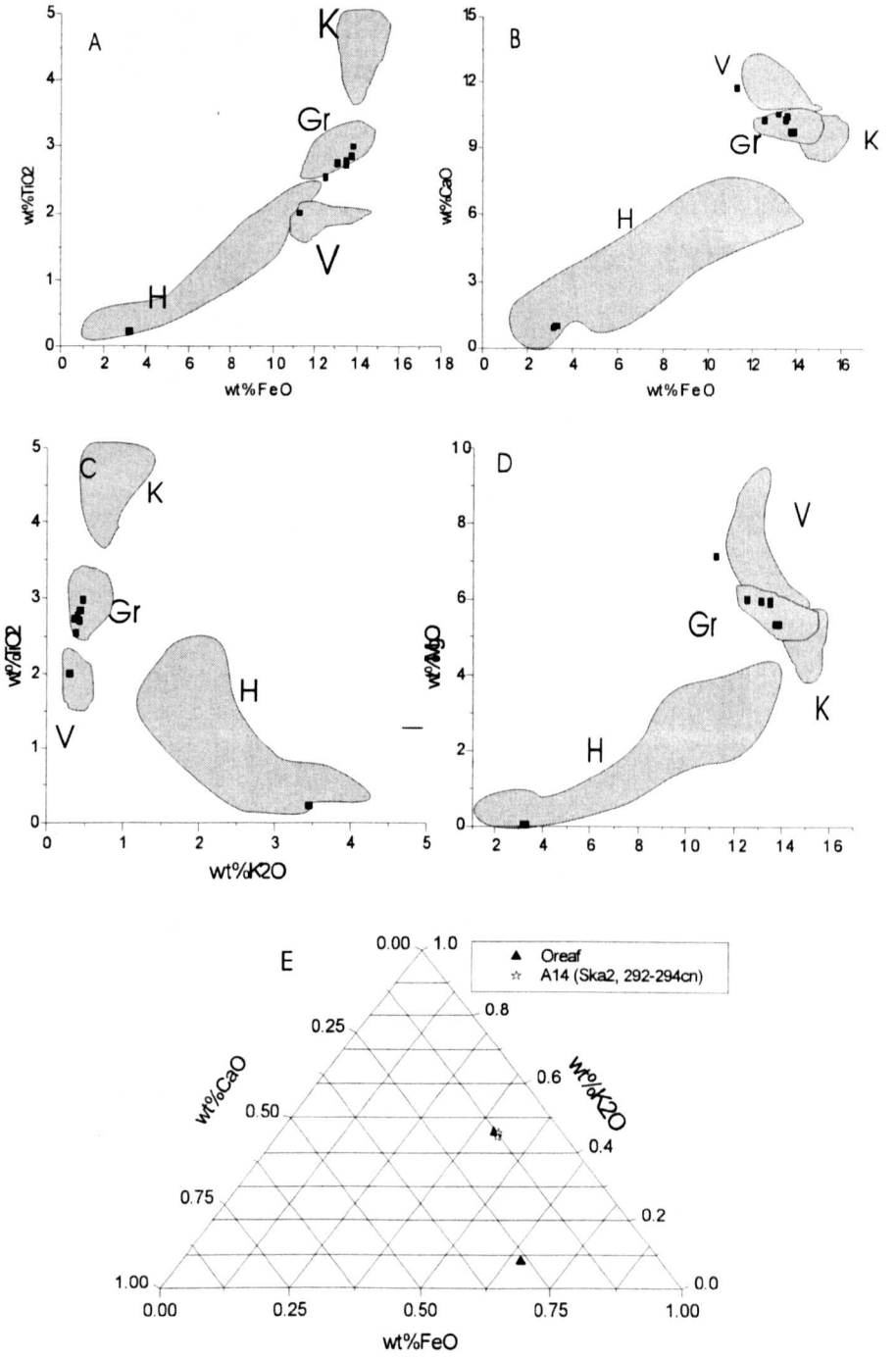

Figure 5.22 Binary plots of geochemical data of A14, 292-294 cm, Ska2, SE Iceland. Ternary plot (E) matches A14 to O1949BP. The volcanic system names are abbreviated as follows: Gr, Grimsvötn; H, Hekla; A, Askja; K, Katla; Th, Thordarhrna; V, Veidivötn, E, Eyjafjallajökull; O, Öræfajökull, and B, B03.

Table 5.23 Glass geochemical data for tephra from A15, 298-300 cm, Ska2 SE Iceland

b 35	SiO2	TiO2	Al2O3	MgO	CaO	MnO	FeO	Na2O	K2O	Total
	47.685	1.699	13.272	7.221	11.907	0.203	12.073	2.317	0.195	96.572
	47.693	1.855	12.857	6.862	11.641	0.195	12.419	2.553	0.189	96.264
	47.694	1.846	13.041	6.885	11.649	0.213	12.642	2.503	0.199	96.672
	47.921	1.862	12.974	6.878	11.819	0.208	12.614	2.321	0.2	96.797
	48.023	1.863	13.133	6.86	11.737	0.214	12.509	2.42	0.2	96.959
	48.558	1.866	13.004	6.847	11.863	0.204	12.675	2.495	0.163	97.675
	48.748	1.857	13.072	6.819	11.778	0.223	12.631	2.473	0.181	97.782
	48.88	1.871	13.176	6.836	11.724	0.211	12.643	2.475	0.202	98.018
	49.019	1.892	13.158	6.905	11.656	0.21	12.474	2.589	0.199	98.102
	49.201	1.88	12.969	6.787	11.59	0.186	12.515	2.546	0.194	97.868
mean	48.3422	1.8491	13.0656	6.89	11.7364	0.2067	12.5195	2.4692	0.1922	97.2709

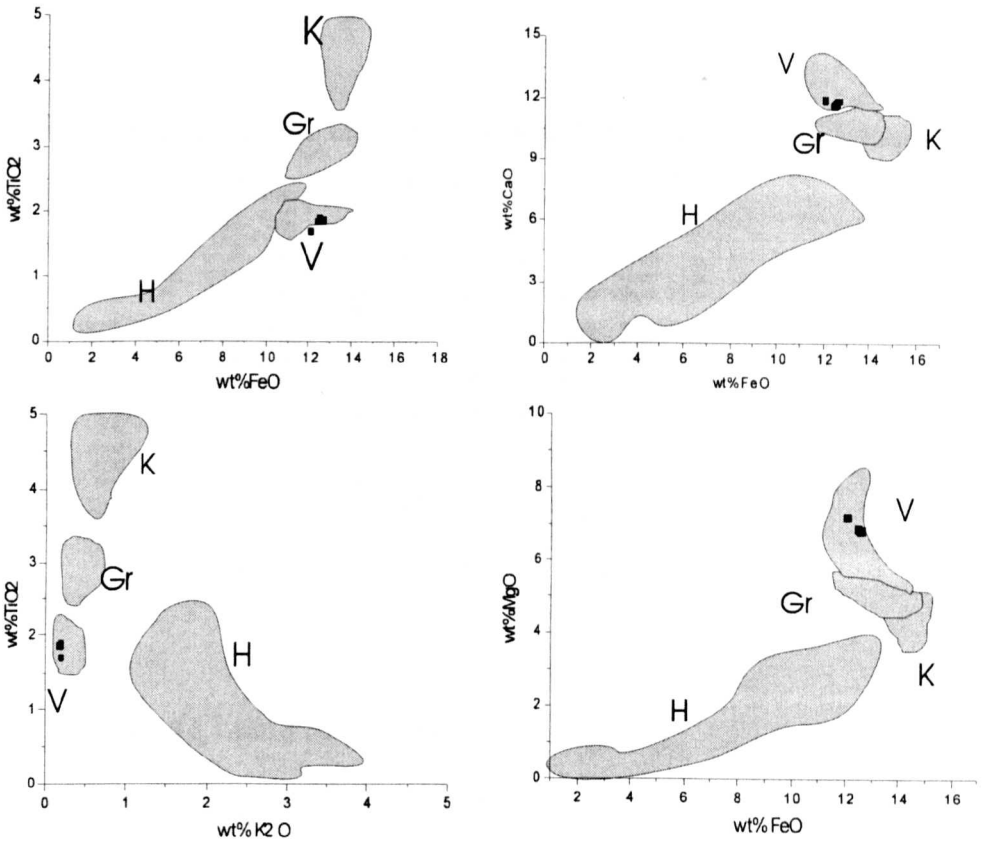

Figure 5.23 Binary plots of chemical data of A15, 298-300 cm, Ska2, SE Iceland, showing the tephra shards in this layer are mainly derived from Veidivötn.

Skaftfellsheidi Profile 2 354-356 cm (Ska2, A16/B36) (Table 5.24; Figure 5.24)

The geochemical signature of twenty shards indicates that this single white tephra layer contains shards derived from three separate eruptions, labelled A, B and C. The largest population (eleven shards, group C) consists of glass of silicic composition (with SiO_2 content >70 %, C). It closely matches a Hekla signature with low MgO content (<0.05 %), and low FeO content (<2 %). ED and SC values (Appendix 6)

indicate that this tephra may be H4 (3830 BP). Six shards (Group A) consist of glass of basic (composition with SiO_2 content ca. 45.7 % and TiO_2 content <2.4 %). It closely matches Veidivötn. The last population (four shards) are of basic composition (with SiO_2 content ca. 46 % and TiO_2 content >2.4 %). However its titanium content is very high, indicating that it may originate from Grimsvötn. In short, the age of this layer is ca. 3839BP.

Table 5.24 Glass chemical of tephra from A16, 354-356 cm, Ska2 SE Iceland

b 36	SiO2	TiO2	Al2O3	MgO	CaO	MnO	FeO	Na2O	K2O	Total	Mearsred
A	47.404	1.955	13.392	7.324	11.89	0.178	10.968	2.508	0.26	95.879	m
	47.722	1.76	13.036	6.842	11.848	0.197	12.241	2.275	0.178	96.099	m
	48.528	1.777	13.065	6.884	11.492	0.208	12.304	2.473	0.172	96.903	m
	48.663	2.456	12.917	6.107	10.565	0.193	12.831	2.735	0.34	96.807	m
	48.741	1.84	12.985	6.803	11.64	0.195	12.306	2.297	0.195	97.002	m
B	49.116	3.895	12.58	4.41	8.537	0.2	13.514	3.503	1.038	96.793	m
	46.045	4.399	12.204	4.984	9.668	0.202	15.124	3.114	0.771	96.511	m
	46.313	4.395	12.129	5.004	9.657	0.209	15.028	3.145	0.765	96.645	m
	46.483	4.469	12.308	4.954	9.529	0.222	14.485	3.248	0.762	96.46	m
C	71.48	0.1	12.53	0	1.32	0.09	1.82	3.96	2.8	94.1	e
	72.74	0.33	12.52	0.01	1.37	0.1	1.84	3.89	2.73	95.53	e
	71.57	0.13	12.53	0.04	1.23	0.13	1.83	3.99	2.72	94.17	e
	72.41	0.31	12.63	0.02	1.35	0.09	1.89	4.18	2.94	95.82	e
	71.14	0.08	12.57	0.01	1.38	0.13	2.03	4.09	2.9	94.33	e
	71.72	0.11	12.32	0.01	1.32	0.08	1.8	4.03	2.66	94.05	e
	73.68	0.1	12.43	0.04	1.29	0.11	1.82	4.39	2.85	96.71	e
	71.41	0.12	12.5	0.04	1.33	0.08	1.89	3.85	2.77	93.99	e
	73.8	0.11	12.93	0.02	1.45	0.12	1.84	4.37	2.8	97.44	e
	73.19	0.14	12.77	0.03	1.35	0.1	1.93	4.31	2.88	96.7	e
	73.66	0.14	12.83	0.03	1.44	0.16	1.83	4.16	2.85	97.1	e

5.2.6 Jokulsa I Loni Profile 1 and 2

Jokulsa I Loni Profile 1 38-40cm (JL1 38) (Table 5.25; Figure 5.25)

The geochemical data from two shards suggests that this 2 cm-thick black tephra layer contains shards derived from one eruption. The shards are of silicic composition, with SiO_2 content >60 %. The geochemical signature suggests an Eyjafjalljökull source, with high SiO_2 content (>60 %), moderate K_2O content (2-2.4 %), low TiO_2 content (<0.3 %), low FeO content (<4 %), low CaO content (<4 %) and low MgO content (<0.7 %). ED and SC values (Appendix 6) suggest the shards are derived from Eyjafjalljökull 1821 and hence the age of this layer is ca. AD 1821.

Table 5.25 Glass geochemical data of tephra from Jokulsa I Loni Profile 38-40 cm, SE Iceland.

JL1(38)	SiO2	TiO2	Al2O3	FeO	MnO	MgO	CaO	Na2O	K2O	Total
	64.24	0.04	17.07	2.26	0.03	0.03	0.62	6.94	4.84	96.07
	71.88	0.26	12.88	3.15	0.1	0.04	1	4.91	3.36	97.58

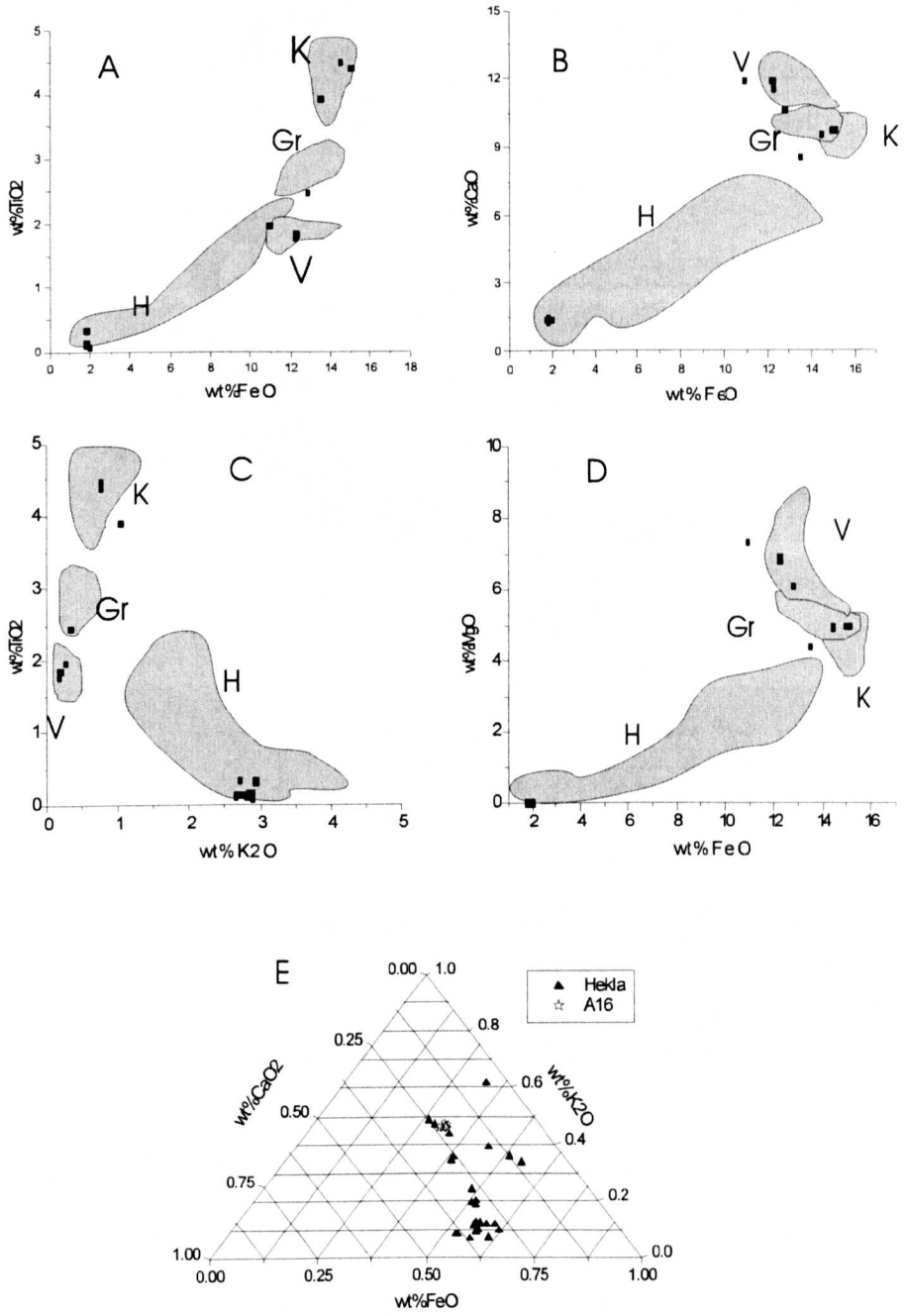

Figure 5.24 Binary and ternary plots of chemical data of A16, 298-300 cm, Ska2, SE Iceland. Triangular plot (E) matches A14 to Hekla4. The volcanic system names are abbreviated as the follows: Gr, Grimsvötn; H, Hekla; A, Askja; K, Katla; Th, Thordarhrna; V, Veidivötn, E, Eyjafjallajpkull; O, Öræfi, and ★, A16.

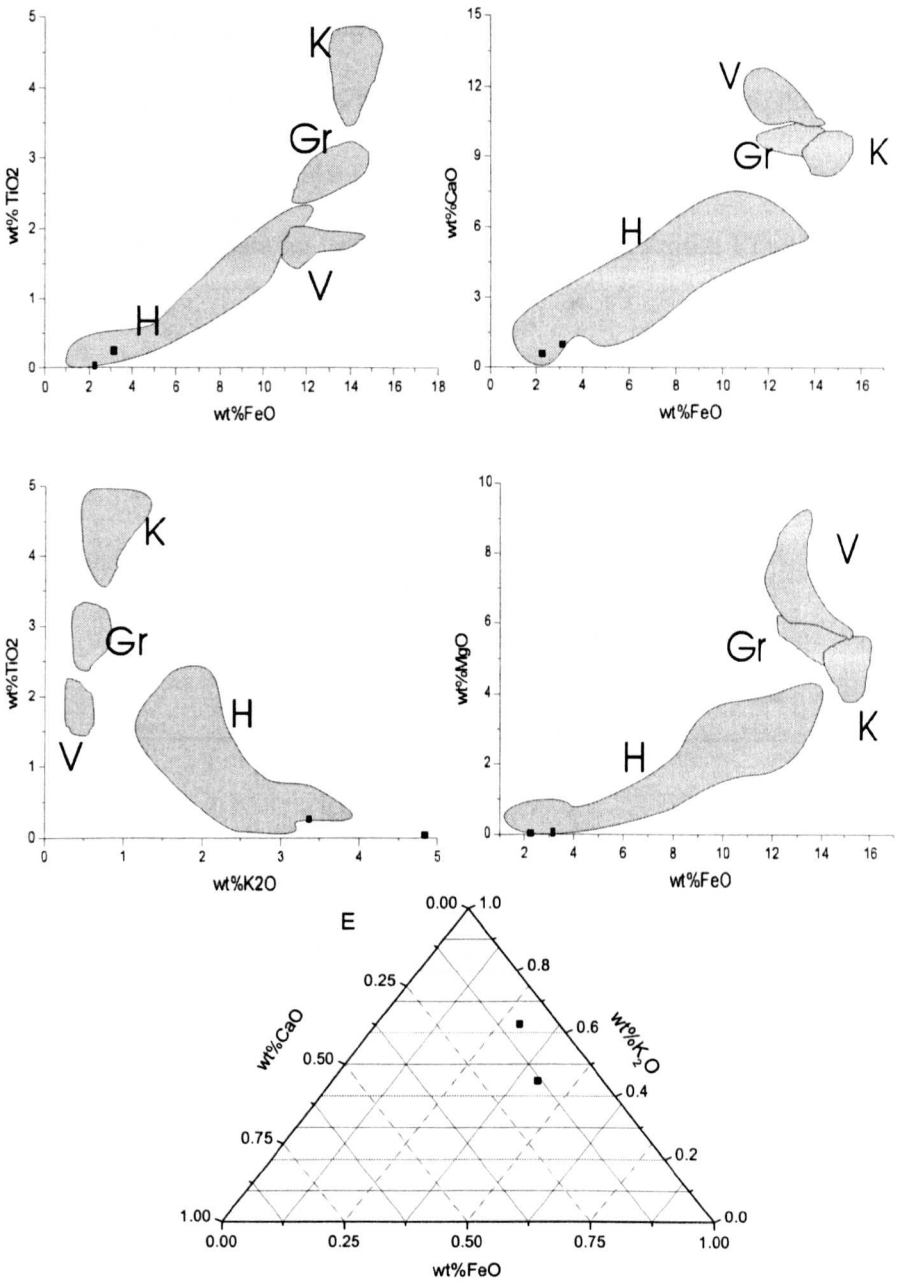

Figure 5.25 Binary and ternary plots of chemical data of Jokulsa I Loni Profile 1 38-40 cm, SE Iceland, showing the tephra shards in this layer are mainly derived from Hekla.

Jokulsa I Loni Profile 1 173-175 cm (JL1 174) (Table 5.26; Figure 5.26)

The geochemical character of ten shards indicates this 18 cm-thick coarse black tephra layer contains shards derived from one eruption. All the shards are of basic composition, with SiO_2 content ranging from 45.1 % to 50.6 %. The content of SiO_2 (50.5 %), TiO_2 (1.9 %), CaO (11.1 %), K_2O (0.2 %) and MgO (6.4 %) indicate that

they probably originate from Veidivötn. The ED and SC values (Appendix 6) suggest they are derived from Veidivötn 1707, and their age is therefore ca. AD 1707.

Table 5.26 Glass chemical data for tephra from Jokulsa I Loni Profile 173-175 cm, SE Iceland.

JL1(174)	SiO2	TiO2	Al2O3	FeO	MnO	MgO	CaO	Na2O	K2O	Total
	48.14	1.77	13.18	12.31	0.19	6.45	11.26	2.56	0.46	96.32
	49.82	2.17	12.96	13.48	0.24	5.64	11.02	2.87	0.15	98.35
	49.16	1.83	13.43	12.13	0.28	6.67	11.39	2.53	0.16	97.58
	49.8	2.1	13.36	13.92	0.23	5.22	10.31	2.59	0.25	97.78
	48.27	2.16	11.69	13.29	0.32	8.65	12.57	1.9	0.17	99.02
	48.37	1.78	12.93	11.55	0.16	6.37	11.08	2.42	0.2	94.86
	50.26	2.02	13.72	12.58	0.22	6.42	11.39	2.63	0.25	99.49
	49.73	1.88	13.62	12.38	0.26	6.18	11.5	2.51	0.25	98.31
	49.74	1.85	13.64	12.56	0.22	6.4	11.37	2.46	0.22	98.46
	50.59	2.16	13.09	12.34	0.25	6.44	11.86	2.95	0.2	99.88
Mean	49.388	1.972	13.162	12.65	0.237	6.444	11.375	2.542	0.231	98.005

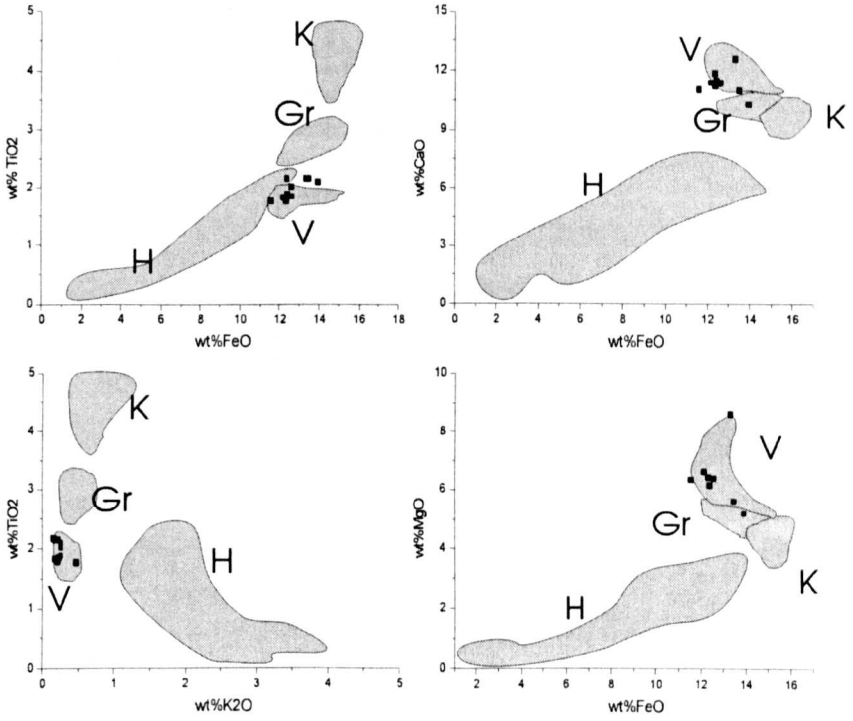

Figure 5.26 Binary plots of chemical data of Jokulsa I Loni Profile 1 173-175 cm, SE Iceland, showing the tephra shards in this layer are mainly derived from Veidivötn.

Jokulsa I Loni Profile 1 185-186 cm (JL1 186) (Table 5.27; Figure 5.27)

The geochemical signature of eleven shards indicates that this 1 cm-thick fine, black tephra layer comprises shards derived from several eruptions. All the shards are of

basic composition, with SiO_2 content ca. 45.3%. The content of FeO (ca. 13.1 %), TiO_2 (ca. 3.1 %), CaO (ca. 10.3 %), K_2O (ca. 0.6 %) and, MgO (ca. 5.4 %) suggest these shards have the Grimsvötn signature. The ED and SC values (Appendix 6) suggest they may originate from G1616; therefore the age is ca. AD 1600.

Table 5.27 Glass geochemical data for tephra from Jokulsa I Loni Profile 185-186 cm, SE Iceland.

JL1(186)	SiO2	TiO2	Al2O3	FeO	MnO	MgO	CaO	Na2O	K2O	Total	Group
	46.9	4.88	12.64	14.86	0.22	4.76	9.86	2.77	0.79	97.68	a
	48	4.48	12.87	13.97	0.22	4.89	10.01	3.1	0.64	98.18	a
	45.9	3.75	14.42	13.75	0.26	3.69	9.47	3.21	0.54	94.99	a
	48.39	3.63	13.25	11.83	0.24	6.33	11.13	2.47	0.23	97.5	a
	49.24	3.37	12.72	14.28	0.19	3.95	9.29	2.57	0.5	96.11	b
	48.66	3.05	12.72	14.14	0.26	5.21	9.72	2.92	1.79	98.47	b
	48.84	2.71	13.15	12.39	0.29	5.17	9.76	2.98	0.49	95.78	b
	49.04	2.56	13.18	12.63	0.25	6.07	10.51	2.73	0.37	97.34	b
	48.51	2.26	13.49	11.47	0.21	6.56	11.02	2.57	0.31	96.4	c
	48.62	1.86	13.34	12.44	0.21	6.43	11.07	2.57	0.21	96.75	c
	49.14	1.81	13.45	12.4	0.35	6.38	11.3	2.48	0.23	97.54	c

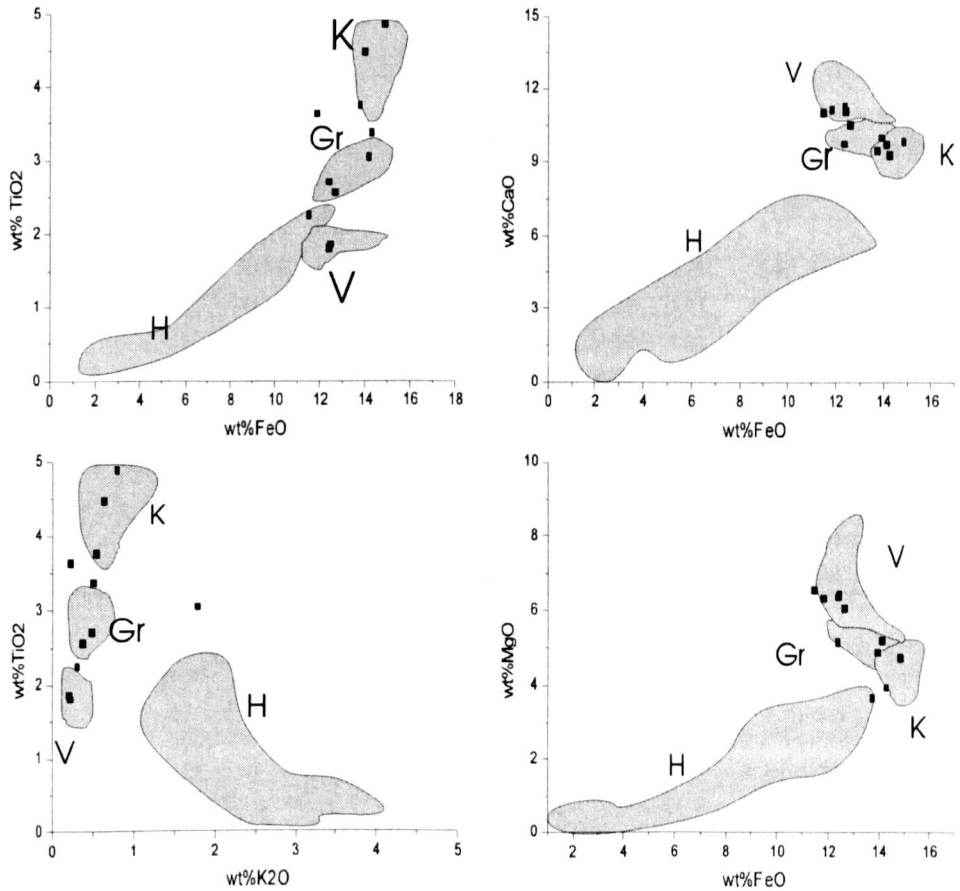

Figure 5.27 Binary plots of geochemical data of Joulsa I Loni Profile 1 185-186 cm, SE Iceland, showing the tephra shards in this layer are mainly derived from three sources.

Jokulsa I Loni Profile 1 189-190 cm (JL1 190) (Table 5.28; Figure 5.28)

The geochemical data of thirteen shards indicate that this 1 cm-thick fine, white tephra layer contains shards derived from one eruption. The tephra is of silicic composition, with SiO_2 content ranging from 71 % to 73 %. The geochemical signature is suggestive of an Öræfajökull source, with high SiO_2 content (>70 %), high K_2O content (>3 %), low FeO content (ca. 3 %), low CaO content (ca. 1 %) and, low TiO2 content (ca. 0.25 %). ED and SC values (Appendix 6) confirm that the shards are from Öræfajökull 1362, and hence the age of this tephra layer is AD 1362.

Table 5.28 Glass geochemical data for tephra from Jokulsa I Loni Profile 1 189-190cm, SE Iceland.

JL1(190)	SiO2	TiO2	Al2O3	FeO	MnO	MgO	CaO	Na2O	K2O	Total
	71.87	0.26	13.3	3.18	0.07	0.03	1.02	4.86	3.41	98
	71.92	0.19	12.9	3.19	0.08	0.04	0.98	4.28	3.5	97.08
	72.26	0.21	13.14	3.37	0.1	0.03	1.04	4.85	3.39	98.39
	72.15	0.27	13.27	3.08	0.11	0.04	1.02	4.43	3.34	97.71
	71.48	0.26	13.11	3.23	0.13	0.02	0.95	4.7	3.29	97.17
	71.94	0.24	13.13	3.02	0.1	0.04	1.04	4.8	3.43	97.74
	71.29	0.25	12.93	3.11	0.14	0.03	1.01	4.56	3.45	96.77
	72.35	0.28	13.19	3.5	0.13	0.02	1.02	4.15	3.45	98.09
	70.62	0.25	12.88	2.85	0.13	0.04	1.01	4.59	3.38	95.75
	71.44	0.24	13.11	3.06	0.14	0.04	0.99	4.25	3.45	96.72
	71.93	0.29	13.18	3.28	0.15	0.05	1.06	4.3	3.42	97.66
	71.84	0.24	13.01	3.17	0.07	0.02	1	4.61	3.33	97.29
	71.38	0.29	13	3.1	0.09	0.04	1.03	4.59	3.35	96.87
Mean	71.72846	0.252	13.0885	3.165	0.1108	0.034	1.0131	4.5362	3.399	97.3262

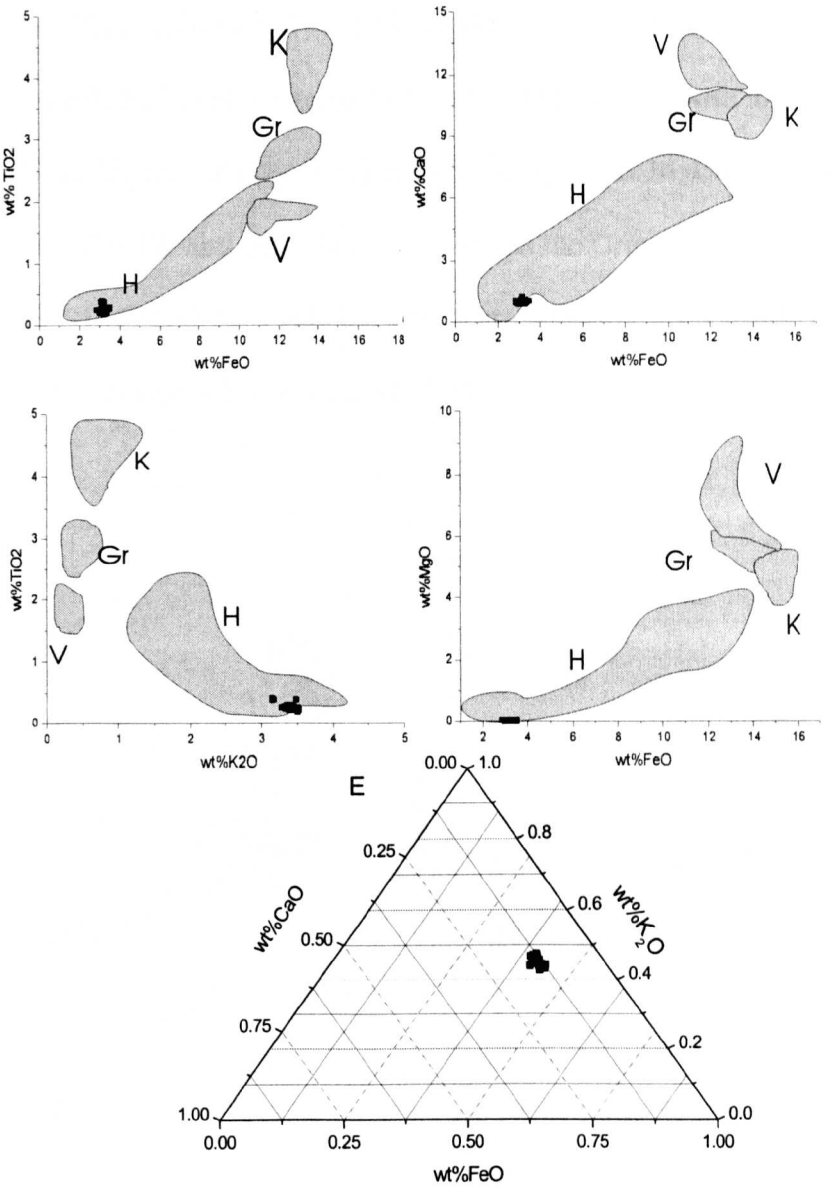

Figure 5.28 Binary and ternary plots of geochemical data of Jokulsa I Loni Profile 1 189-190 cm, SE Iceland, showing the tephra shards in this layer are mainly derived from Öræfajökull 1362.

5.3.6 Jokulsa I Loni Profile 2

Jokulsa I Loni Profile 2 74-76 cm (JL2 74) (Table 5.29; Figure 5.29)

The geochemical signature of eleven shards indicates that this 4 cm-thick black tephra layer comprises shards derived from two separate eruptions. All the shards are of basic composition, with SiO_2 content less than 51%. Two shards (labelled a in Table 5.29) have the Grimsvötn signature, with contents of FeO (ca. 15 %), TiO_2 (ca.

3 %), CaO (ca. 9 %), K_2O (ca. 0.4 %) and, MgO (ca. 4 %). The other nine shards (labelled b in Table 5.29) are suggestive of a Veidivötn source, with lower TiO_2 content (<2.1 %), higher CaO content (ca. 11 %) and, higher MgO content (ca. 6 %) than the former. The ED and SC values indicate that the Grimsvötn tephra may originate from G1659 and the Veidivötn tephra are probably from V1697 or V1706. Thus, the age of this tephra layer is ca. AD 1700.

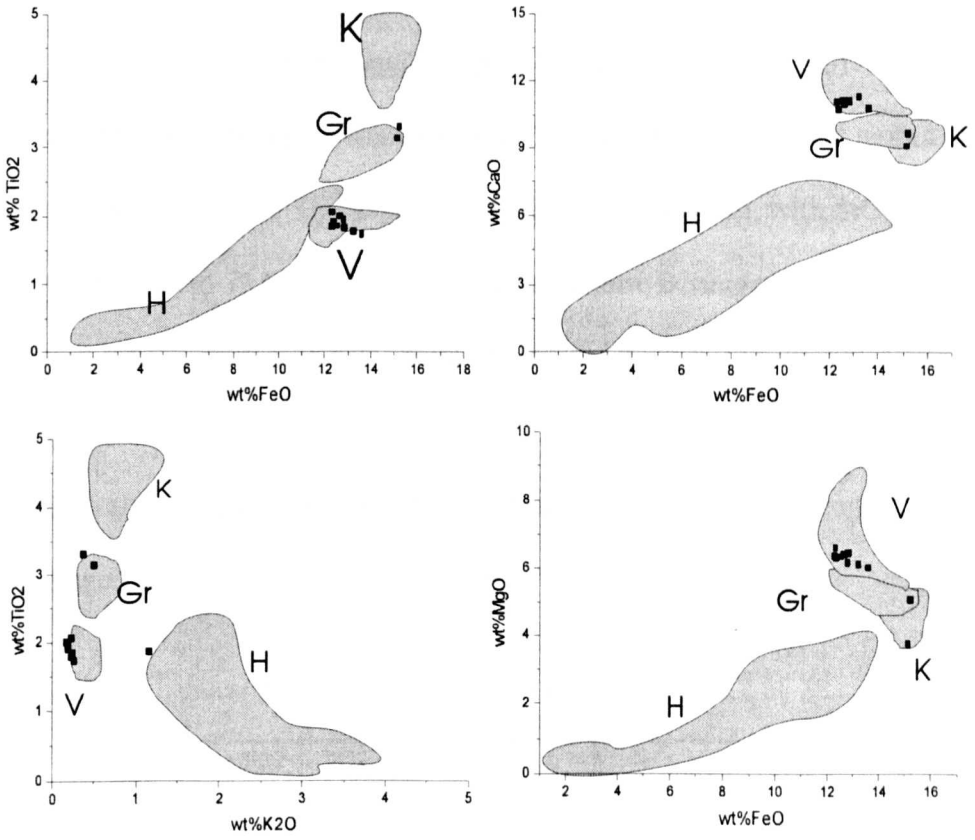

Figure 5.29 Binary plots of chemical data for Jokulsa I Loni Profile 2 74-76 cm, SE Iceland, showing the tephra shards in this layer are mainly derived from two sources.

Table 5.29 Glass geochemical data of tephra from Jokulsa I Loni Profile 2 74-76 cm, SE Iceland.

JL2 (74)	SiO2	TiO2	Al2O3	FeO	MnO	MgO	CaO	Na2O	K2O	Total	Group
	48.24	3.32	11.96	15.22	0.27	5.07	9.65	2.76	0.36	96.85	a
	50.09	3.15	12.34	15.13	0.51	3.78	9.11	3.07	0.49	97.67	a
	48.14	2.06	13.1	12.28	0.21	6.38	11.07	2.51	0.22	95.97	b
	48.77	2	13.11	12.62	0.23	6.44	11	2.54	0.17	96.88	b
	48.97	1.95	12.99	12.79	0.25	6.2	11.1	2.61	0.19	97.05	b
	48.39	1.91	13.17	12.37	0.18	6.35	10.76	2.65	0.18	95.96	b
	49	1.86	13.03	12.53	0.25	6.37	11.14	2.48	1.15	97.81	b
	48.91	1.85	13.13	12.31	0.25	6.63	11.08	2.54	0.24	96.94	b
	49.1	1.83	13.4	12.8	0.24	6.48	11.19	2.07	0.25	97.36	b
	49.07	1.78	13.9	13.2	0.22	6.14	11.36	2.65	0.22	98.54	b
	49.79	1.73	13.46	13.58	0.27	6.05	10.79	2.19	0.26	98.12	b

Jokulsa I Loni Profile 2 86-88 cm (JL2 86) (Table 5.30; Figure 5.30)

The geochemical data from ten shards imply that this 2 cm-thick white tephra layer is derived from one eruption. This tephra is of silicic composition, with SiO_2 content ranging from 69 % to 73 %. The geochemical signature is suggestive of an Öræfajökull source, with high SiO_2 content (>69 %), high K_2O content (>3 %), low FeO content (ca. 3 %), low CaO content (ca. 1 %) and, low TiO_2 content (ca. 0.2 %). ED and SC values (Appendix 6) confirm that the tephra shards are Öræfi 1362, and hence the age of this tephra layer is AD 1362.

Table 5.30 Glass chemical data of tephra from Joulsa I Loni Profile 2 86-88 cm, SE Iceland.

JL2 (86)	SiO2	TiO2	Al2O3	FeO	MnO	MgO	CaO	Na2O	K2O	Total
	71.98	0.21	13.07	3.09	0.14	0.03	0.92	4.7	3.44	97.58
	71.94	0.39	12.92	3.06	0.13	0.04	1.07	4.35	3.32	97.22
	70.97	0.26	12.89	3.14	0.15	0.04	1	4.73	3.59	96.77
	71.93	0.23	12.87	3.08	0.13	0.02	1.02	4.74	3.29	97.31
	71.63	0.29	13.12	3.16	0.09	0.04	1.02	4.63	3.45	97.43
	69.3	0.2	13.07	3.22	0.14	0.01	0.95	4.69	3.39	94.97
	71.29	0.27	13.15	3.17	0.08	0.01	0.98	4.68	3.49	97.12
	71.33	0.21	12.87	3.13	0.06	0.05	1.04	4.34	3.48	96.51
	71.47	0.31	13.21	3.67	0.09	0.03	0.97	4.95	3.36	98.06
	69.7	0.24	12.66	3.12	0.1	0.03	0.99	4.45	3.36	94.65
Mean	71.154	0.261	12.983	3.184	0.111	0.03	0.996	4.626	3.417	96.762

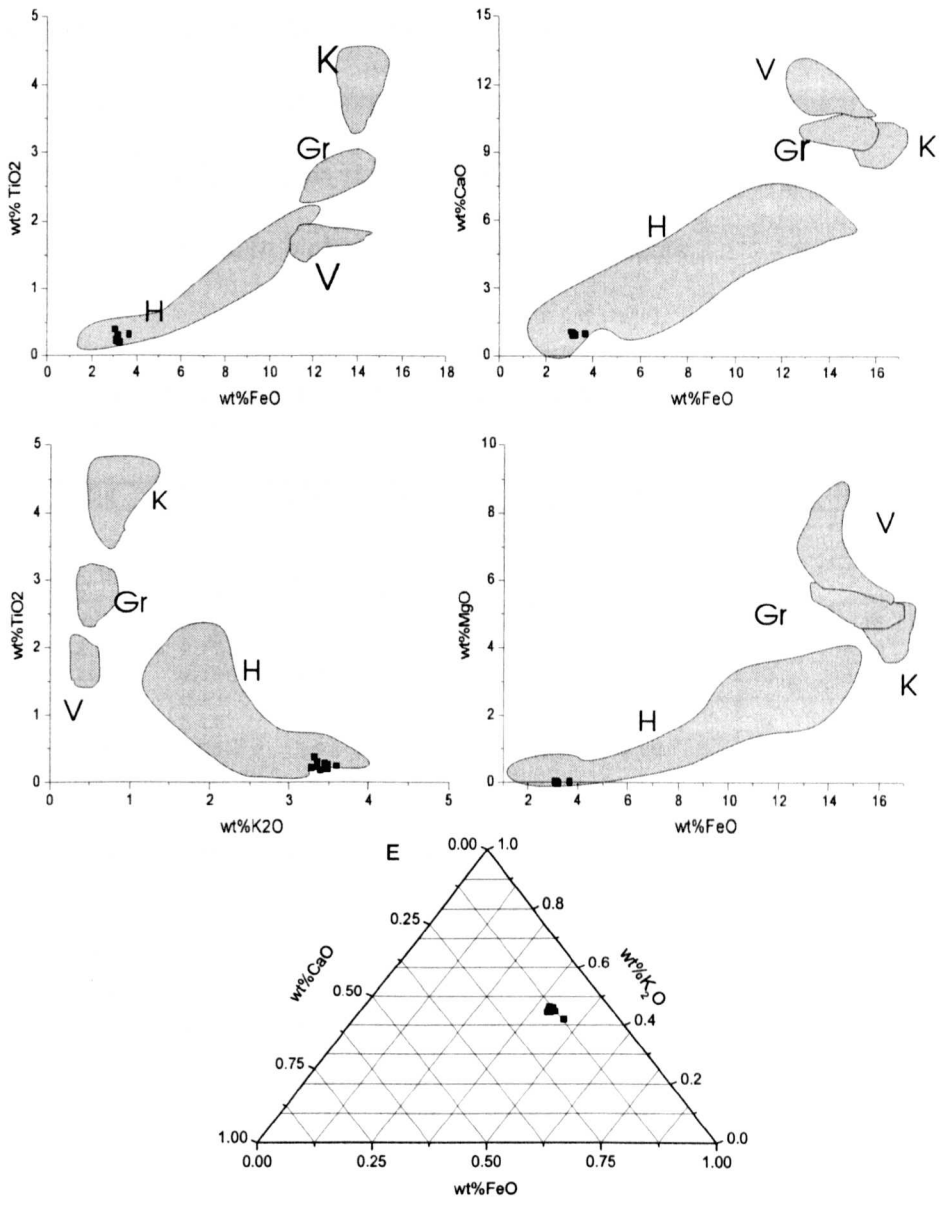

Figure 5.30 Binary and ternary plots of chemical data of Jokulsa I Loni Profile 2 86-88 cm, SE Iceland, showing the tephra shards in this layer are mainly derived from Öræfajökull 1362.

5.4 Discussion

5.4.1 Comparison of Öræfajökull 1362 tephra shards present in different depositional environments

A series of analyses was performed to compare silicic tephra from the Öræfajökull 1362 eruption, deposited in the two loessial soil profiles (i.e. JL1 and JL2) and one peat profile, Lax, in this study. The results (Table 5.31, Figs. 5.31 and 5.32) confirm

that the tephra layers (i.e. Lax: 36-38 cm; JL1: 189-190 cm and, JL2: 86-88 cm) contain tephra shards derived from the eruption of Öræfa 1362, which are strongly supported by the PCO analysis results (Table 5.1) and, (2) the Öræfa tephra shards are geochemically stable in both depositional environments.

Table 5.31 Geochemical data for tephra shards for Öraefajökull 1362 from Lax, JL1 and JL2, SE Iceland, and one set of data from Sigurdasson (1982).

	SiO2	TiO2	Al2O3	MgO	CaO	MnO	FeO	Na2O	K2O
Lax(38)	72.77	0.23	12.73	0.01	1.04	0.05	3.25	4.75	3.46
	72.13	0.24	13.17	0	1.02	0.09	3.42	4.63	3.41
	72.81	0.16	13.06	0	0.97	0.04	3.53	4.85	3.35
	73.2	0.17	12.95	0.02	1.04	0.09	3.21	4.75	3.59
	72.71	0.17	12.94	0.04	1.03	0.07	3.35	4.76	3.32
	72.45	0.19	13.09	0.03	0.94	0.11	3.13	4.47	3.52
	72.68	0.19	13.31	0.01	1	0.06	3.18	4.76	3.54
	73.25	0.17	13.07	0.03	1.14	0.08	3.16	4.54	3.71
	72.3	0.25	12.93	0.03	1.13	0.09	2.99	4.57	3.6
JL1(190)	71.87	0.26	13.3	0.03	1.02	0.07	3.18	4.86	3.41
	71.92	0.19	12.9	0.04	0.98	0.08	3.19	4.28	3.5
	72.26	0.21	13.14	0.03	1.04	0.1	3.37	4.85	3.39
	72.15	0.27	13.27	0.04	1.02	0.11	3.08	4.43	3.34
	71.48	0.26	13.11	0.02	0.95	0.13	3.23	4.7	3.29
	71.94	0.24	13.13	0.04	1.04	0.1	3.02	4.8	3.43
	71.29	0.25	12.93	0.03	1.01	0.14	3.11	4.56	3.45
	72.35	0.28	13.19	0.02	1.02	0.13	3.5	4.15	3.45
	70.62	0.25	12.88	0.04	1.01	0.13	2.85	4.59	3.38
	71.44	0.24	13.11	0.04	0.99	0.14	3.06	4.25	3.45
	71.93	0.29	13.18	0.05	1.06	0.15	3.28	4.3	3.42
	71.84	0.24	13.01	0.02	1	0.07	3.17	4.61	3.33
	71.38	0.29	13	0.04	1.03	0.09	3.1	4.59	3.35
JL2 (86)	71.98	0.21	13.07	0.03	0.92	0.14	3.09	4.7	3.44
	71.94	0.39	12.92	0.04	1.07	0.13	3.06	4.35	3.32
	70.97	0.26	12.89	0.04	1	0.15	3.14	4.73	3.59
	71.93	0.23	12.87	0.02	1.02	0.13	3.08	4.74	3.29
	71.63	0.29	13.12	0.04	1.02	0.09	3.16	4.63	3.45
	69.3	0.2	13.07	0.01	0.95	0.14	3.22	4.69	3.39
	71.29	0.27	13.15	0.01	0.98	0.08	3.17	4.68	3.49
	71.33	0.21	12.87	0.05	1.04	0.06	3.13	4.34	3.48
	71.47	0.31	13.21	0.03	0.97	0.09	3.67	4.95	3.36
	69.7	0.24	12.66	0.03	0.99	0.1	3.12	4.45	3.36
nown Orea	71.46	0.22	13.13	0	0.99	0.05	3.16	5.45	3.53

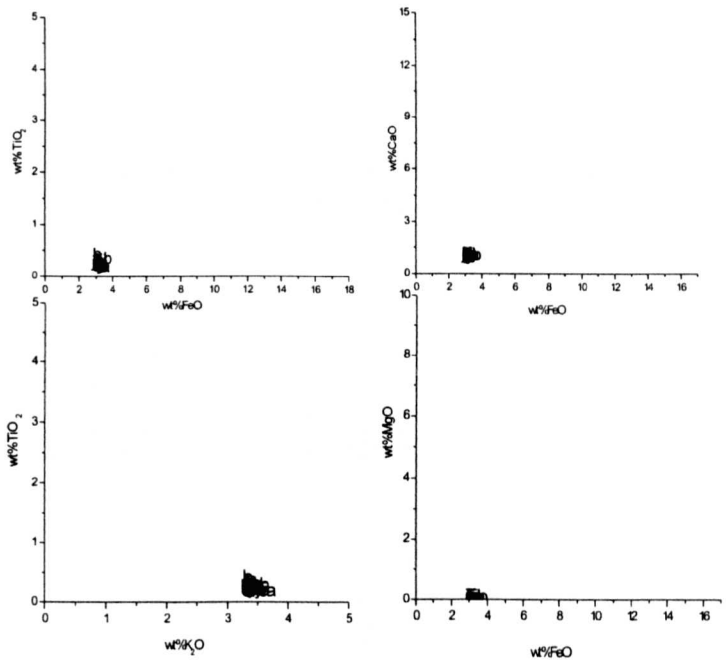

Figure 5.31 Binary plot of chemical data of Öræfa 1362 from 3 sections: Lax (a), JL1 (j) and JL2 (b), SE Iceland.

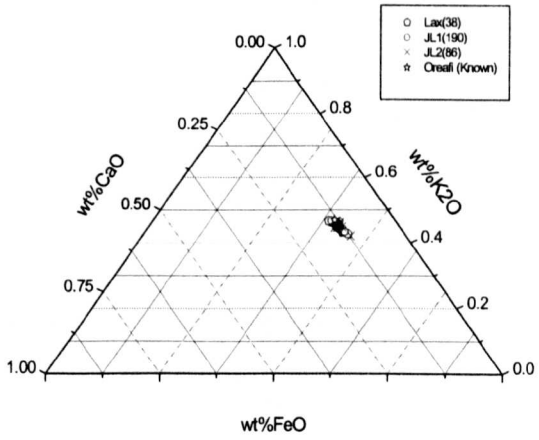

Figure 5.32 Ternary plot for tephra layers in three profiles (Lax, JL1 and JL2) ascribed to Öræfajökull 1362.

5.4.2 Comparison of Grimsvötn 150 tephra shards in different depositional environments

The author also made a comparison of the consistency of the geochemical signature of basic tephra shards (from Grimsvötn 150) in different depositional environments. The results (Table 5.32 and Figure 5.33) demonstrate that the geochemistry of basic

tephra shards is fairly consistent in both environments. However, it is less concentrated than that of Öræfajökull 1362, especially in Ska, the first study area. This may support the suggestion that silicic shards are more stable than basic shards (Dugmore *et al.*, 1992).

Table 5.32 Geochemical character of tephra shards for G150 from Lax (a), Ska2 (b) and JL1 (d), SE Iceland,

	SiO2	TiO2	Al2O3	MgO	CaO	MnO	FeO	Na2O	K2O	label
Lax(154)	47.9	2.67	12.8	5.69	10.54	0.16	12.17	2.59	0.35	a
	48.76	2.73	12.85	5.9	10.48	0.18	12.77	2.73	0.39	a
	48.2	2.61	12.84	6.02	10.62	0.2	12.68	2.8	0.32	a
	48.61	2.6	12.75	5.85	10.45	0.21	12.86	2.63	0.37	a
	48.61	2.74	12.72	5.84	10.77	0.19	12.96	2.89	0.3	a
	48.63	2.65	12.95	5.89	10.68	0.27	12.63	2.8	0.41	a
	48.4	2.68	12.78	5.82	10.89	0.2	12.78	2.72	0.35	a
	48.75	2.53	12.84	6.07	10.71	0.21	13.24	2.73	0.41	a
	48.87	2.53	12.89	5.98	10.78	0.23	12.77	2.79	0.34	a
Ska2-275(B20)	48.63	3.20	12.09	4.99	9.16	0.24	14.80	3.00	0.49	c
	49.73	3.67	11.92	3.94	7.84	0.27	14.89	3.39	0.58	c
	48.64	3.33	12.11	4.93	9.30	0.22	14.74	2.94	0.47	c
	49.48	2.50	12.81	5.44	9.90	0.20	12.79	3.04	0.42	c
	48.62	2.53	12.69	6.20	10.71	0.21	12.91	2.67	0.39	c
	52.53	2.54	13.91	3.47	7.04	0.29	12.08	3.86	1.09	c
	48.64	3.03	12.27	5.41	9.70	0.23	14.23	2.95	0.37	c
	49.47	*2.97*	*12.54*	*4.91*	*9.09*	*0.24*	*13.78*	*3.12*	*0.54*	*c*
Jl1-319(B23)	48.47	2.63	12.97	6.22	10.75	0.22	12.91	2.77	0.36	d
	48.09	2.46	12.97	6.06	10.46	0.20	12.98	2.71	0.38	d
	48.30	2.61	12.72	6.09	10.37	0.22	13.11	2.70	0.35	d
	49.27	2.59	13.02	6.16	10.45	0.21	12.75	2.81	0.35	d

5.5 Tephrochronology of the sites from SE Iceland

Tephrochronology is the study of volcanic ash for the purpose of correlating and dating volcanic and other geologic events. Large magnitude eruptions can disperse tephra up to thousands of kilometres from the vent, producing a near instantaneous marker horizon. The key to tephrochronology is the identification and correlation of tephra horizons. In the site of deposition, tephra layers can often be identified by their lithology, stratigraphic position and mineralogy. The known records of tephrochronology for the study areas are presented in Appendix 4, which provides an overview of present knowledge regarding the geochemical signature and dating of

the tephra layers in Iceland for the last 5000 years BP. The tephrochronology of all of the study sites is summarised in Figure 5.34.

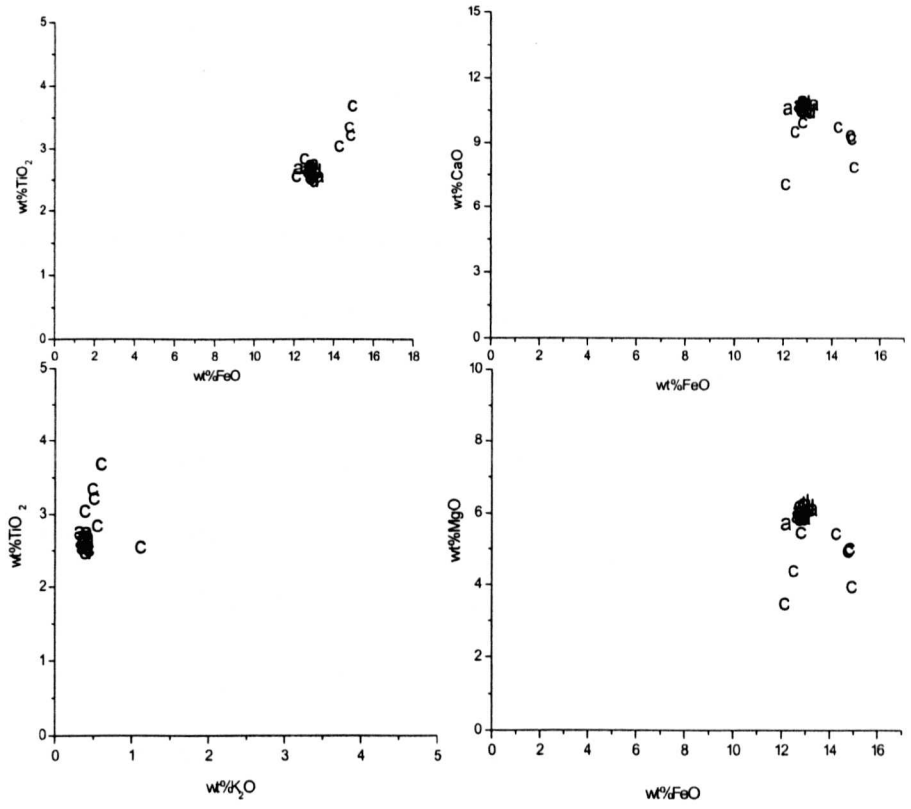

Figure 5.33 Binary plot of chemical data of G150 from 3 sections: Lax (a), Ska2 (c), and JL1(d), SE Iceland.

5.5.1 Ska2

Figure 5.34 and Table 5.1 show the results of the age of tephra layers identified in Ska2. There are four tephra layers that can be identified unambiguously in the Ska2 soil profile. They are Öræfajökull 1727, Öræfajökull 1362, G1354 and H4. The age of other tephra layers can be inferred from their geochemical signature and stratigraphic position within the initially dated profile.

There have only been two eruptions of Öræfajökull in historical time (after AD 870, Larsen *et al.*, 1999). The AD 1362 Öræfa tephra is present in this profile at 188-192

cm. The distinctive white tephra layer produced by this eruption has been used previously as a stratigraphic marker for SE Iceland (Thorarinsson, 1958, Gonzalez *et al.*, 1999). Another set of white tephra shards from the eruption of Öræfajökull at a depth of 84-86 cm should reflect the Öræfajökull AD 1727 eruption. These conclusions are also strongly supported by the Euclidean distance and similarity results (Appendix 6). On the other hand, the results of Euclidean distance and similarity also demonstrate that the PCO methods work well.

Hekla4 tephra is present at a depth of 354-356 cm in the soil profile of Ska2 (Fig. 5.33). This is supported by their lithology, stratigraphic position, geochemical signature and the PCO results. Hekla4 is in the process of becoming one of the best-dated isochrones in northwest Europe (Dugmore *et al.*, 1995). The original radiocarbon dating in Iceland was undertaken by Throrainsson *et al.* (1964). The age of the Hekla4 eruption lies close to 3830 radiocarbon years BP (Dugmore *et al.*, 1995).

5.5.2 Lax

The age of tephra layers, based on the geochemical results, in Lax was summarised in Table 5.1. Four tephra layers can be readily identified in the peat profile. They are Katla 1918AD, Öraefa 1362, T-c AD 550, and G 150AD. The Katla 1918 AD is at the depth of 17-19cm (Table 5.2 and Fig. 5.2). Öraefa 1362, the white layer, as a stratigraphic maker, appears at a depth 36-38 cm (Table 5,3 and Fig.5.3). T-c AD 550 is present at the depth of 121-123 cm. The last one, G150, is at depth of 153-154cm (Table 5.5 and Figure 5.5) The age of other tephra layers can be inferred from their stratigraphic position within the dated profile.

5.5.3 JL1 and JL2

The ages of tephra layers, based on the geochemical results, in JL1 and JL2, were summarised in Table 5.1. Four tephra layers can be defined in JL1, and two can be confirmed in JL2. Öræfajökull 1362, an established lithological marker, was found at a depth 189-190 cm in JL1 and at a depth 86-88 cm in JL2.

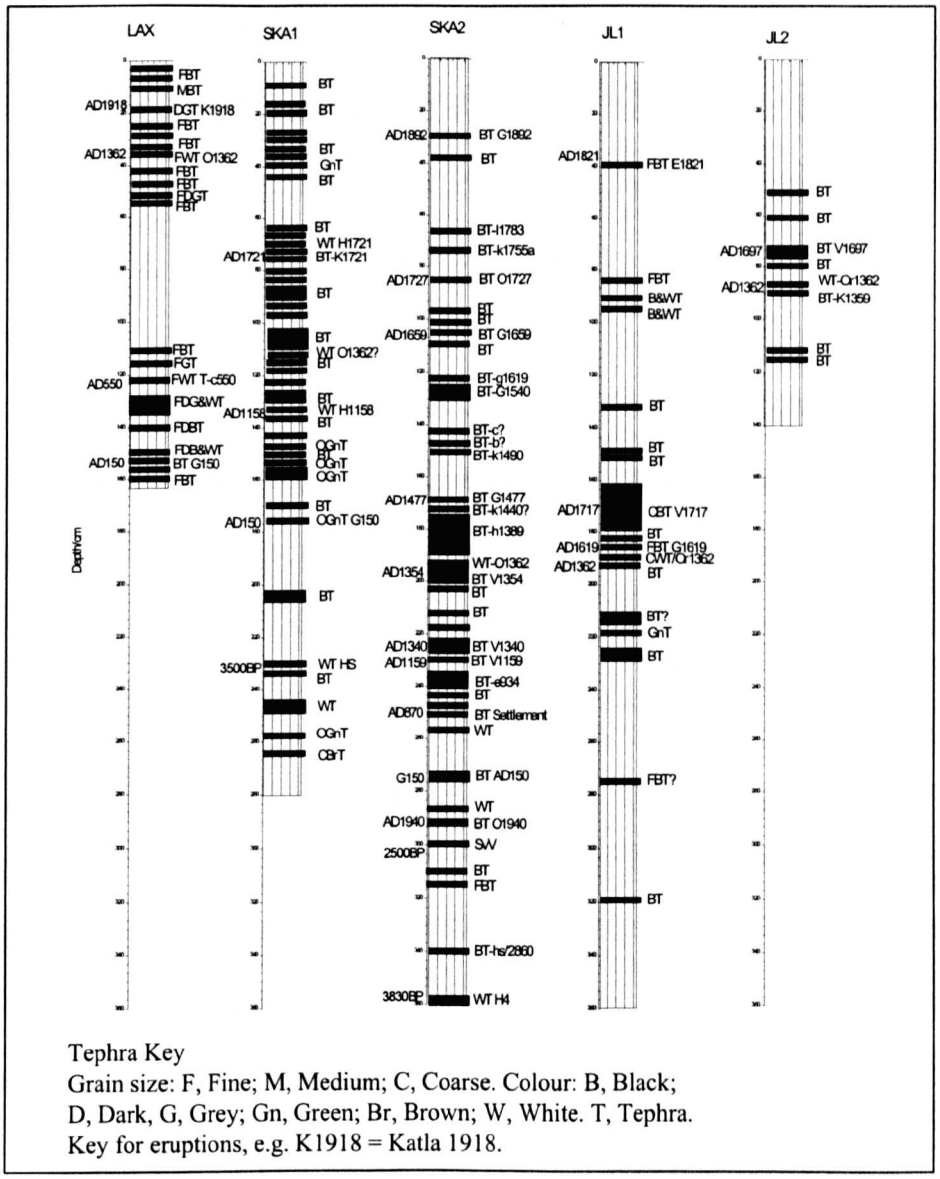

Figure 5.34 Tephrochrological framework for Lax, Ska1, Ska2, JL1 and JL2, SE Iceland.

5.6 Summary

The EPMA measurement results in this study demonstrate that the geochemistry may provide useful information for characterizing and correlating tephra layers from one section to the next. Results show that the EPMA measurements are consistent between the Edinburgh and Manchester Laboratories.

The density separation procedure has been shown to be successful in extracting microtephra particles from bulk samples. The tephra shards from two different densities of 2.4-2.6 gcm^{-3} and 2.6-2.8 gcm^{-3} have almost the same geochemical signature. It was therefore decided to isolate the tephra shards with a relative density between 2.4 to 2.8 gcm^{-3} in order to maximise the concentration of microtephra particles.

The results indicate that (1) the tephra layers (i.e. Lax: 36-38 cm; JL: 189-190 cm and, JL2: 86-88 cm) contain tephra shards derived from the eruption of Öræfajökull 1362 and (2) the silicic tephra shards are geochemically stable in soil and peat environments. A second comparison of the consistency of the geochemical signature of basic tephra shards in different environments was performed on the Grimsvötn 150. The results demonstrate that the geochemistry of the basic tephra shards are fairly consistent in both soil and peat environments. However, it is less concentrated than that of Öræfajökull 1362, especially in Ska, the first study area. This could be because silicic shards are more geochemically stable than basic shards. Finally, the geochemical results have been used to establish a tephrochronology for the five study profiles.

Chapter 6 Results of rock magnetic and XRF measurements of the peat sections

6.1 Introduction

This chapter presents the results of bulk sample rock magnetic and XRF measurements of the two peat sections, Lax and Ska1, from SE Iceland. Most of the results are presented as down-core plots.

6.2 Rock magnetic results

6.2.1 Lax

Table 6.1 gives the range and mean for each of the basic magnetic parameters for all of the sites studied. Rock magnetic measurements of bulk samples from Lax are plotted against depth in Figure 6.1. χ_{lf} has quite high values, at ca. $360\times10^{-8}m^3kg^{-1}$, at the top of the profile (from 0 to 12 cm). The values generally decrease to ca. $100\times10^{-8}m^3kg^{-1}$ at a depth of 25 cm. The values then remain stable at ca. $60\times10^{-8}m^3kg^{-1}$ from 25cm to 56 cm. This is followed by another interval of stable values at ca. $30\times10^{-8}m^3kg^{-1}$ from 56 cm to the end of the profile except three peaks at depths of 112 cm, 122 cm, and 145 cm. SOFT (with values in the range of $48.5\text{-}1583.1\times10^{-5}Am^2kg^{-1}$), χ_{fd} (with an average value of $5.2\times10^{-8}m^3kg^{-1}$), χ_{ARM} (with values ranging from $58.3\text{-}1039.6\times10^{-8}m^3kg^{-1}$), and SIRM (average value $3021.3\times10^{-5}Am^2kg^{-1}$) follow fairly similar trends to χlf. χ_{fd} % remains almost constant at a level of ca. 5.3 throughout the whole profile, with temporary increases to ca. 12 % at depths of 8 cm and 121 cm, and decreases to 1 % at depths of 122 cm and 148 cm. HIRM generally decreases from the top, at ca. $275.3\times10^{-}$

$^{5}Am^{2}kg^{-1}$, to a depth of 56 cm, ca. $250.2\times10^{-5}Am^{2}kg^{-1}$, with one noticeable peak at the depth of 30 cm. There is a sharp decrease to ca. $60\times10^{-5}Am^{2}kg^{-1}$ at 56 cm, and this is followed by a general increase to ca. $275\times10^{-5}Am^{2}kg^{-1}$ at 123cm. This is then followed by a sharp decrease again to ca. $59\times10^{-5}Am^{2}kg^{-1}$ at 109 cm with a significant peak to ca. $133\times10^{-5}Am^{2}kg^{-1}$ at 245 cm. After that, there is another general increase to ca. $300\times10^{-5}Am^{2}kg^{-1}$ at the bottom. The values of SIRM/ARM range from 57.3-287.6, with several noticeable peaks at depths of 132 cm, 140 cm, 150 cm and 158 cm. χ_{ARM}/SIRM has an average value of ca. $0.15\times10^{-3}mA^{-1}$, with an abrupt increase to $0.3\times10^{-3}mA^{-1}$ at 58-65 cm and three notable peaks at 110 cm, 120 cm and 145 cm. The χ_{ARM}/χlf values remain fairly constant at an average of ca. 4.6 from the top to 110 cm, except over the interval 20-40 cm where the values are ca. 5. This is followed by a general increase to 6.0 at 120 cm, an abrupt decrease to ca.2 at 140 cm, and a sharp increase to 6.0 at 145 cm. The values then decrease again to the end of the profile. The SIRM/χ profile is fairly constant at an average of ca. $29.3\times10^{-3}Am^{-1}$ from the top to 56 cm, with two peaks of ca. $60\times10^{-3}Am^{-1}$ at 28 cm and 41 cm. This is followed by an abrupt decrease to ca. $12\times10^{-3}Am^{-1}$ at 195 cm, followed by a general increase to ca. $29.3\times10^{-3}Am^{-1}$ until 122 cm, with an abrupt decrease at 108 cm. There is another large reduction, to ca. $11.2\times10^{-3}Am^{-1}$ at 122 cm, which was followed by three significant peaks, greater than $120\times10^{-3}Am^{-1}$, at 135 cm, 150 cm and 158 cm in the lower part of the profile.

These variations enable three major zones to be distinguished in terms of rock magnetic properties. Zone III (110-162 cm) consisting of the lowest part of the core, is

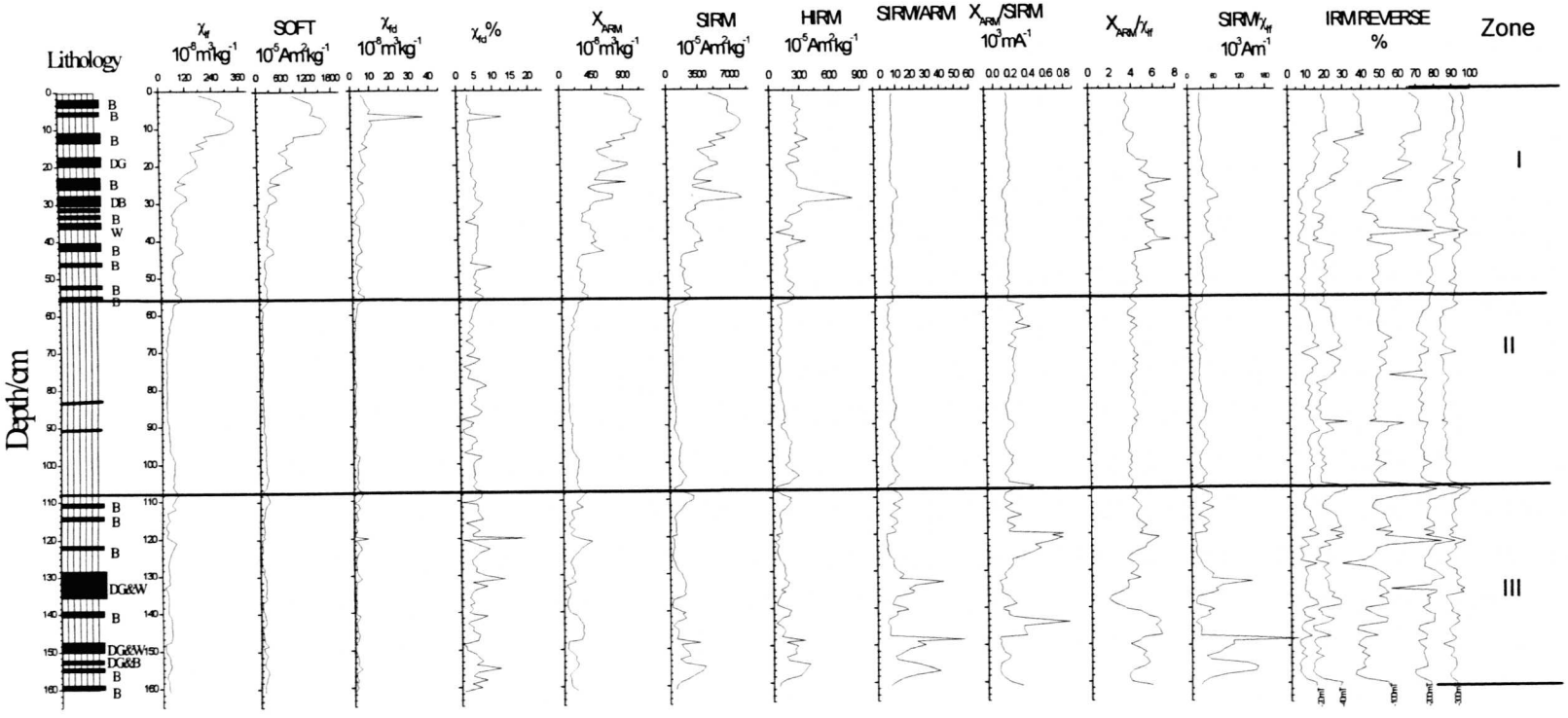

Figure 6.1 Magnetic parameters of Lax, SE Iceland. Tephra colours: B, Black; D, Dark; G, Grey; Gr Green; Br, Brown; W, White. Horizontal shaded zones are some clearly visible tephra layers in the profile.

Table 6.1 Measurement results of the basic magnetic parameters for the five sections.

		XLF	SOFT	XFD	XFD%	XARM	SIRM	HIRM	SIRM/ARM	XARM/SIRM	XARM/XLF	SIRM/XLF	S-20	S-40	S-100	S-300
		$10^{-8}m^3kg^{-1}$	$10^{-5}m^3kg^{-1}$	$10^{-8}m^3kg^{-1}$		$10^{-8}m^3kg^{-1}$	$10^{-5}Am^2kg^{-1}$	$10^{-5}Am^2kg^{-1}$	Am^{-1}	$10^{-3}mA^{-1}$		$10^{-3}mA^{-1}$	%	%	%	%
Lax	Max	341.248	1692.3	37.27	18	1157.55	8134.342	817.65	53.90503	0.830471	7.60405	247.118	21.43	41.36	82.55	98.83
	Min	12.2507	20.843	0	0	42.1525	237.6409	18.54	1.204136	0.018551	1.61279	7.1215	4.201	11.05	27.46	82.01
	Mean	70.104	252.539	3.0008	4.25	301.599	2116.072	163.8157	8.083323	0.176127	4.33879	35.7648	10.49	21.61	50.96	89.71
Ska1	Max	1060.99	7272.68	22.591	7.39	3017.3	16740.41	1221.29	586.3305	0.229513	11.1952	73.3767	43.44	77.28	90.95	102.9
	Min	34.5672	48.995	0.6766	0.81	116.557	1298.131	0	54.7369	0.021426	0.91857	13.5944	2.281	14.92	39.23	88.12
	Mean	150.523	761.568	6.3429	4.31	807.237	5103.915	234.5807	85.16926	0.154481	5.64831	37.3237	13.66	28.12	59.59	95.09
Ska2	Max	492.9469	2565.373	31.90578	7.6783	2717.5	15624.9	8853.75	133.1263	0.211893	11.3664	66.50571	25.29388	44.45471	75.15722	100.4626
	Min	48.3979	172.6055	1.530368	3.044204	250.9531	1981.711	0	59.28848	0.094368	2.536896	15.47831	6.236611	17.11966	41.24176	89.45943
	Mean	184.1496	941.2554	9.837169	5.231613	1065.379	6859.838	3130.005	82.59616	0.154124	5.885952	38.63864	13.62491	27.8604	57.39074	93.70737
JL1	Max	989.141	6651.667	27.499	5.757	3066.015	21141.63	1754.263	133.886	0.244	7.161	71.685	32.04	56.16	84.53	100.24
	Min	167.657	772.253	7.097	1.551	1045.692	6096.853	0	51.438	0.094	2.762	18.405	8.21	19.26	48.98	89.05
	Mean	628.0075	3548.923	16.58571	2.754565	2175.299	14041.62	481.1898	81.3873	0.158672	3.650808	23.76539	25.08576	44.46542	73.35294	96.47701
JL2	Max	1012.696	6560.628	16.69551	5.643341	2856.883	20381.12	2065.021	640.6789	0.219496	7.259019	52.71188	32.27334	54.14693	82.31192	99.53726
	Min	48.57143	218.5522	1.428571	1.151498	180.7721	823.5779	28.50781	57.23481	0.019609	0.407006	16.95602	9.495536	19.51239	48.64364	87.94379
	Mean	644.068	3646.609	12.87515	2.202086	2027.143	13728.73	471.6188	91.52615	0.151678	3.329504	22.40101	26.00979	46.28162	74.13411	96.34749
Scot	Max	6.2E-06				11.07925	56.74531		270.5018	34.40833			85.2		100	
	Min	-1.2E-06				-1.31502	0.032585		-73.5509	-15.7126			0.87		31.3	
	Mean	-7.4E-08				1.662536	2.15852		14.46743	1.834036					81.52	

characterized by considerable variations in most of the ratio parameters (e.g. SIRM/ χ lf, χ_{ARM}/SIRM), indicating that the magnetic grain-size fluctuates significantly through the section, with relatively fine grains probably dominant in most samples. However, the mass-specific parameters (e.g. χ , χ_{fd}, χ_{ARM} and SIRM) show no major variations with depth, implying the concentration of ferrimagnetic minerals is stable. Zone II (56-110 cm), the middle part of the section, is characterized by quite low and stable most parameters, implying the lowest concentrations of ferrimagnetic minerals. Zone I (0-56 cm), the top part, is characterized by no major variations in most of the ratio parameters, indicating that magnetic grain-size changes little through the zone, with relatively coarse grains probably dominant in most samples. However, the mass-specific parameters (e.g. χ , χ_{fd}, χ_{ARM} and SIRM) show considerable variations with depth, together with a rising trend in most cases. Therefore, changes in the concentration of ferrimagnetic minerals are probably responsible for most of the variations. However, HIRM is also variable, thus indicating changes in the concentration of canted antiferromagnetic minerals. Finally, there are a number of significant peaks in the reverse-field IRM/SIRM ratios and other parameters (e.g. HIRM), such as at 18 cm, 28 cm, 56 cm, 99 cm, 121 cm and 154 cm, which roughly coincide with visible tephra layers in the section.

6.2.2 Ska1

Figure 6.2 presents the basic magnetic parameters against depth for Ska1. As was the case for Lax, the values of magnetic concentration parameters of the sections are quite high (Table 6.1), indicating quite high concentrations of ferrimagnetic minerals. Both the mass-specific parameters (e.g. χ , χ_{fd}, χ_{ARM} and SIRM) and the

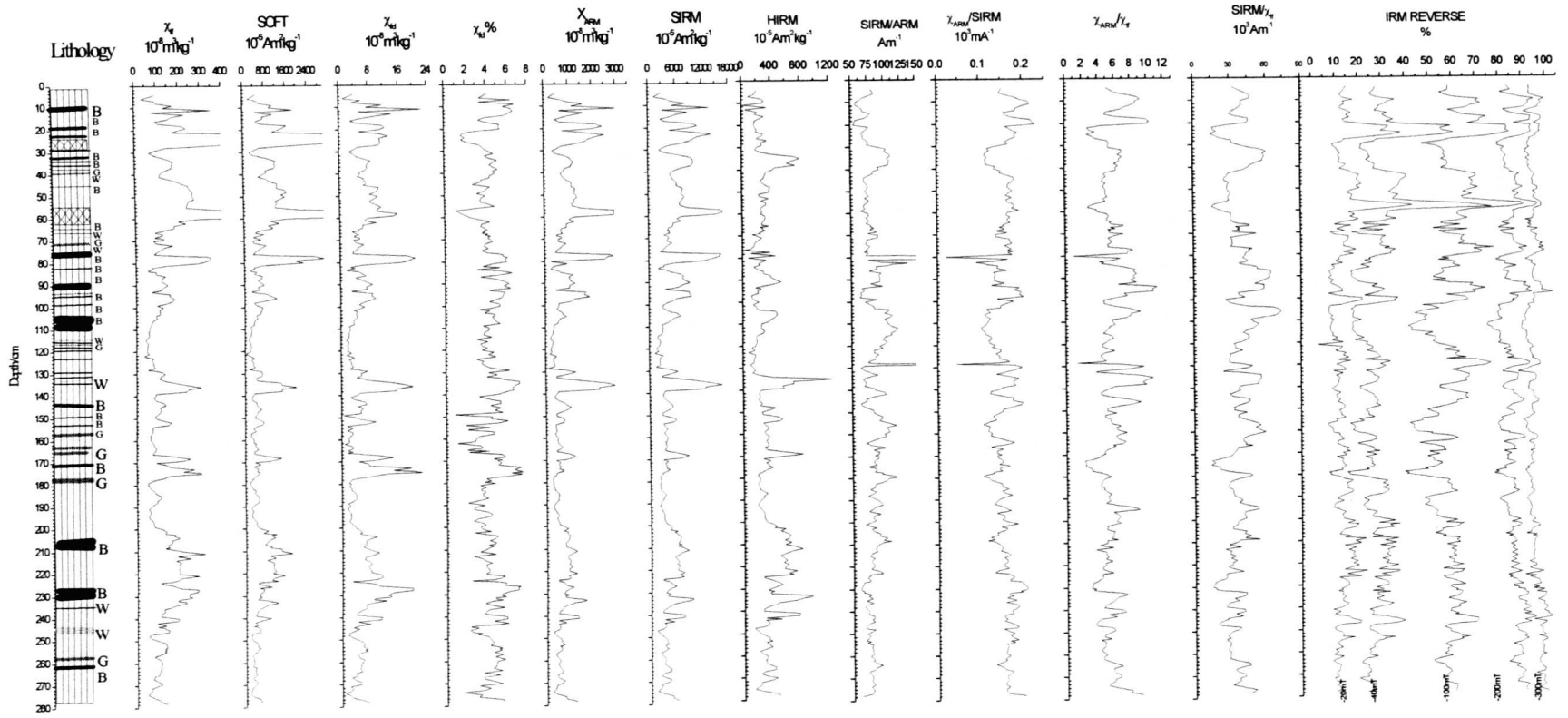

Fig. 6.2 Magnetic parameters for Ska1, SE Iceland. Tephra colour: B, Black; D, Dark; G, Gray; Gr Green; Br, Brown; W, White. Horizontal shaded zones are selected visible tephra layers in the profile.

ratio parameters (e.g. SIRM/χ lf, χ_{ARM}/SIRM) show pronounced variations with depth, and major changes are generally coincident in most parameters, indicating significant variations in both the concentration of the ferrimagnetic minerals and the magnetic mineral grain size. There are many large peaks in reverse-field IRM/SIRM ratios and most parameters, which are clearly associated with visible tephra layers at depths of 20 cm, 35 cm, 52 cm, 67 cm, 78 cm, 90 cm, 98 cm, 13 5cm, 143 cm, 152 cm, 168 cm, 173 cm, 185 cm, 206 cm, 215 cm and 230 cm. The baseline of χ lf, for example, is less than 100 $\times 10^{-8} m^3 kg^{-1}$, but it exceeds 300 $\times 10^{-8} m^3 kg^{-1}$ in some peaks. There are two gravelly layers at depths of 26-27.5 cm and 55-61 cm (Table 3.2 and Fig. 6.2) in this section, which show extremely high values for several of the magnetic concentration parameters.

6.3 Hysteresis loop measurements

6.3.1 Hysteresis loop classification

In this study, high field magnetization curves and hysteresis loops from 127 samples were obtained from selected samples from individual tephra layers. The measurements were made using a VSM (Molyneux Vibrating Sample Magnetometer), following the methods of Lees and Dearing (1999) (Chapter 2, section 2.2.3).

Magnetic hysteresis can be interpreted as a magnetic mineralogical signature on the basis of the shape of the loop. The following section describes a classification scheme of hysteresis loop shapes based on the types of loop encountered in the present work. Figure 6.3 shows representative loops, and these are described and interpreted as follows:

1. Thin saturated loop. Interpretation: dominance by low coercivity ferrimagnets (Fig. 6.3, no. 1).
2. Tall, thin unsaturated loop. Interpretation: dominated by both low coercivity ferrimagnets and paramagnetic minerals (Fig. 6.3, no. 2).

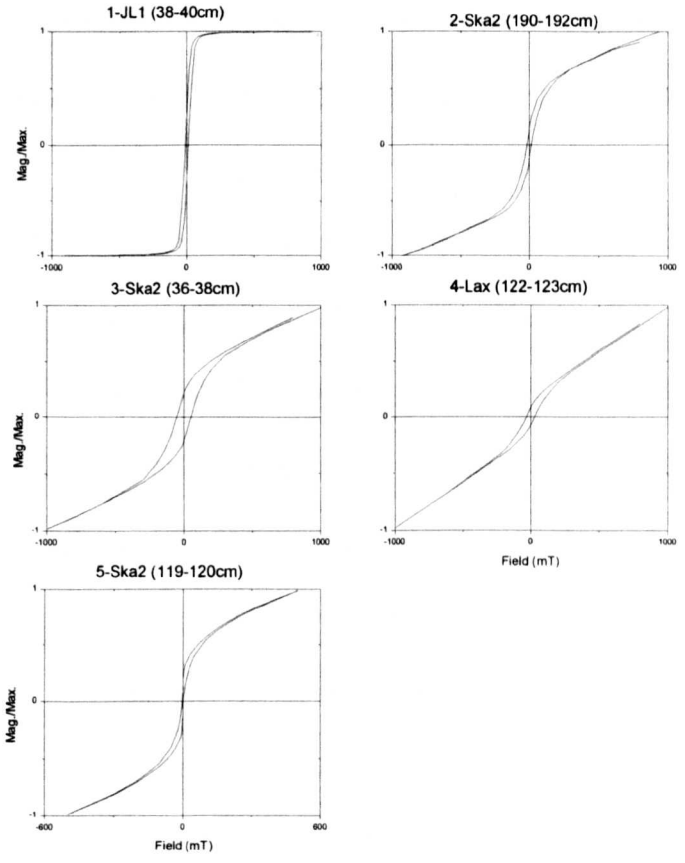

Figure 6.3 Examples of typical high field magnetization hysteresis loops from the five studied profiles: (1) depth 38-40 cm from JL1; (2) depth 190-192 cm from Ska2; (3) depth 36-38 cm from Ska2; (4) depth 122-123 cm from Lax; (5) depth 120cm from Ska2.

3. Wide, unsaturated loop. Interpretation: dominated by higher coercivity ferrimagnets (Fig. 6.3, no. 3);
4. Short, thin, unsaturated loop. Interpretation: dominated by paramagnetic minerals with minor ferrimagnetic content (Fig. 6.3, no. 4).
5. 'Wasp-waisted' loop (cf. Tauxe *et al.*, 1996). Interpretation: dominated by ferrimagnets with a bimodal grain-size distribution (Fig. 6.3, no. 5).

The hysteresis loops of 20 samples from Lax and 30 samples from Ska1 were measured. All of the loops are shown in Appendix 1, while the results are summarized below.

6.3.2 Lax

Table 6.2 classifies the hysteresis loops for the 20 selected samples from Lax, based on the classification shown in Figure 6.3. In general, the loops are thin, exhibit more or less dependence in high fields and none of them shows a trend of flattening up to the maximum field of 1 T used. However, some differences also can be observed for the samples from different tephra layers. The loops of the upper 4 samples (4 cm, 7 cm, 14 cm, and 19 cm) are thin ($(B_0)_c$ values are ~13, ~12, ~14 and ~19 mT, respectively in Table 6.3) and tall (M_s values are 268.9, 262.6, 158.7 and 124.5×10^{-3} Am^2kg^{-1}, respectively in Table 6.3), indicating soft magnetic content (Robinson, 1997). The following 7 samples of Zone I (from 25 cm, 28 cm, 32 cm, 36 cm, 42 cm, 47 cm and 57 cm) exhibit relatively broader loops (~17-50 mT in Table 6.3). Most of the loops of the samples from zone III (from 111 cm, 115 cm, 123 cm, 131 cm, 134 cm, 140 cm, 150 cm and 161 cm) are extremely thin, especially the samples of 44 (123 cm) and 50 (161cm), which exhibit almost no hysteresis loop. Sample 49 (156 cm), is an exception – it has a much broader loop.

Figures 6.4 shows the 'loop2' parameters for 20 selected samples from Lax. They exhibit quite similar patterns to the basic magnetic parameters in the down-core profiles (Figure 6.1). χ_{low}, χ_{low5}, χ_{ferri}, M_s and M_{rs} have a similar variation pattern with depth, showing quite low and stable values in the lower part of this section, and a significant rising trend in the top part. The profile of χ_{high} has a slightly different

form from the former parameters, e.g. at the top of the section, it shows low values. There is an abrupt peak between 28-30 cm in most parameters. χ_{ferri} % decreases with depth while the χ_{para} % increases with depth throughout the whole section, indicating that the paramagnetic component is significant in the lower part of the section . The M_{rs}/M_s ratio ranges between 0.2-0.6, indicating PSD and MD magnetic minerals (Day *et al.*, 1977).

6.3.3 Ska1

The hysteresis loop parameters from VSM measurements for 30 selected samples from Ska1 are presented in Figure 6.4. All samples exhibit thin loops, and fail to saturate (e.g. the sample at 115 cm) at the field of 1T used in the VSM measurements. The differences in loop shape are quite obvious for the samples from the different tephra layers. The loops of most samples, e.g. the samples at depths of 77.5 cm and 205 cm, are relatively broad ($(B_0)_c$ values range from ~12.5-33 mT, Table 6.3) and have slight slope in high fields. The samples from the depths of 128.5 cm, 177 cm, 230 cm 247 cm and 258 cm exhibit very narrow loops and gentle slopes in high fields, which implies that there is some soft content in these horizons (Robinson, 1997). Interestingly, loops of sample at depths of 91 cm and 105 cm are wasp-waisted (Tauxe *et al.*, 1996), implying a bimodal magnetic grain-size distribution.

Table 6.2 Magnetic parameters of T_c and 'loop' from Lax, SE Iceland.

Depth cm		Colour	Grainsize	Lp	Tcc	Tc
3	4	black	fine	1	3	575
6	7	black	fine	1	2	575
12	14	black	middle	1	4	575
17	19	dark grey		1	3	no
23.5	25	black	fine	2	3	no
26	29	dark brown	fine	3	3	no
31	32	black	fine	4	3	no
35	38	white	fine	4	3	575
40	43	black	fine	2	4	575
46	47	black	fine	4	4	no
52	53	dark grey	fine	2	4	no
110	111	black	fine	2	3	no
114	115	grey	fine	4	4	no
121	123	white	fine/needles	4	4	no
128	134	dark grey & white	fine	4	4	no
139	140	dark brown	fine	4	3	no
147.5	150	dark brown &white	fine	4	4	no
155	156	black	fine	3	3	no
159.5	161	black	fine	4	4	no

LP, loop; Tcc, Curie temperature curve; T_c, Curie temperature point. In the column LP, 1~ 5 indicates the different hysteresis loop shape in figure 6.3. In the column Tcc: 1-4 expresses differences in Tc curve shape in Figure 6.6.

Table 6.3 Magnetic hysteresis parameters ('loop2') of VSM analysis of samples from Lax.

Depth	Xlow	Xlow5	Xhigh	Xferri	Xpara%	Xferri%	Ms	Mrs	Mrs/Ms	Mrs/ Xlow	(Bo)cr	(Bo)c	(Bo)cr/(Bo)c
	$10^{-6}m^3kg^{-1}$	$10^{-6}m^3kg^{-1}$	$10^{-6}m^3kg^{-1}$	$10^{-6}m^3kg^{-1}$			$10^{-3}Am^2kg^{-1}$	$10^{-3}Am^2kg^{-1}$			mT	mT	
4	5.14	8.42	0.20	4.94	3.93	96.07	268.91	60.21	0.22	11.70	24.53	13.00	1.89
7	4.63	7.94	0.21	4.42	4.52	95.48	262.63	64.37	0.25	13.91	38.12	12.00	3.18
14	3.15	5.74	0.23	2.92	7.23	92.77	158.70	44.95	0.28	14.27	29.34	14.00	2.10
19	2.61	4.52	0.20	2.42	7.54	92.46	124.50	34.82	0.28	13.32	46.99	19.00	2.47
25	1.41	2.62	0.21	1.21	14.56	85.44	67.40	31.69	0.47	22.43	212.89	29.00	7.34
28	3.72	8.18	0.22	3.51	5.80	94.20	117.45	61.13	0.52	16.43	72.96	50.00	1.46
32	0.89	2.12	0.20	0.69	22.86	77.14	49.69	24.86	0.50	27.79	125.58	38.00	3.30
36	1.09	2.31	0.17	0.92	15.78	84.22	56.09	23.09	0.41	21.20	157.43	27.50	5.72
42	1.55	2.90	0.19	1.36	12.19	87.81	65.89	25.26	0.38	16.30	38.96	24.00	1.62
47	0.79	1.39	0.17	0.62	20.99	79.01	33.32	13.29	0.40	16.82	49.79	15.50	3.21
53	1.17	2.32	0.18	0.99	15.50	84.50	52.63	23.61	0.45	20.25	125.28	29.00	4.32
111	0.81	1.14	0.15	0.65	18.79	81.21	31.81	15.34	0.48	19.05	435.99	30.50	14.29
115	0.45	0.54	0.15	0.30	33.43	66.57	12.71	5.05	0.40	11.17	25.06	15.00	1.67
123	0.46	0.65	0.17	0.30	36.22	63.78	12.09	5.88	0.49	12.66	40.74	21.00	1.94
134	0.67	1.39	0.16	0.51	24.31	75.69	27.06	15.05	0.56	22.38	266.63	32.00	8.33
140	0.38	0.45	0.13	0.25	33.38	66.62	18.76	10.33	0.55	27.04	157.75	35.00	4.51
150	0.60	0.73	0.15	0.45	25.15	74.85	22.34	13.07	0.59	21.74	126.86	37.50	3.38
156	0.83	1.59	0.18	0.66	21.52	78.48	46.67	28.88	0.62	34.60	75.89	48.00	1.58
161	0.41	0.52	0.13	0.27	32.56	67.44	14.76	5.56	0.38	13.69	56.24	17.50	3.21

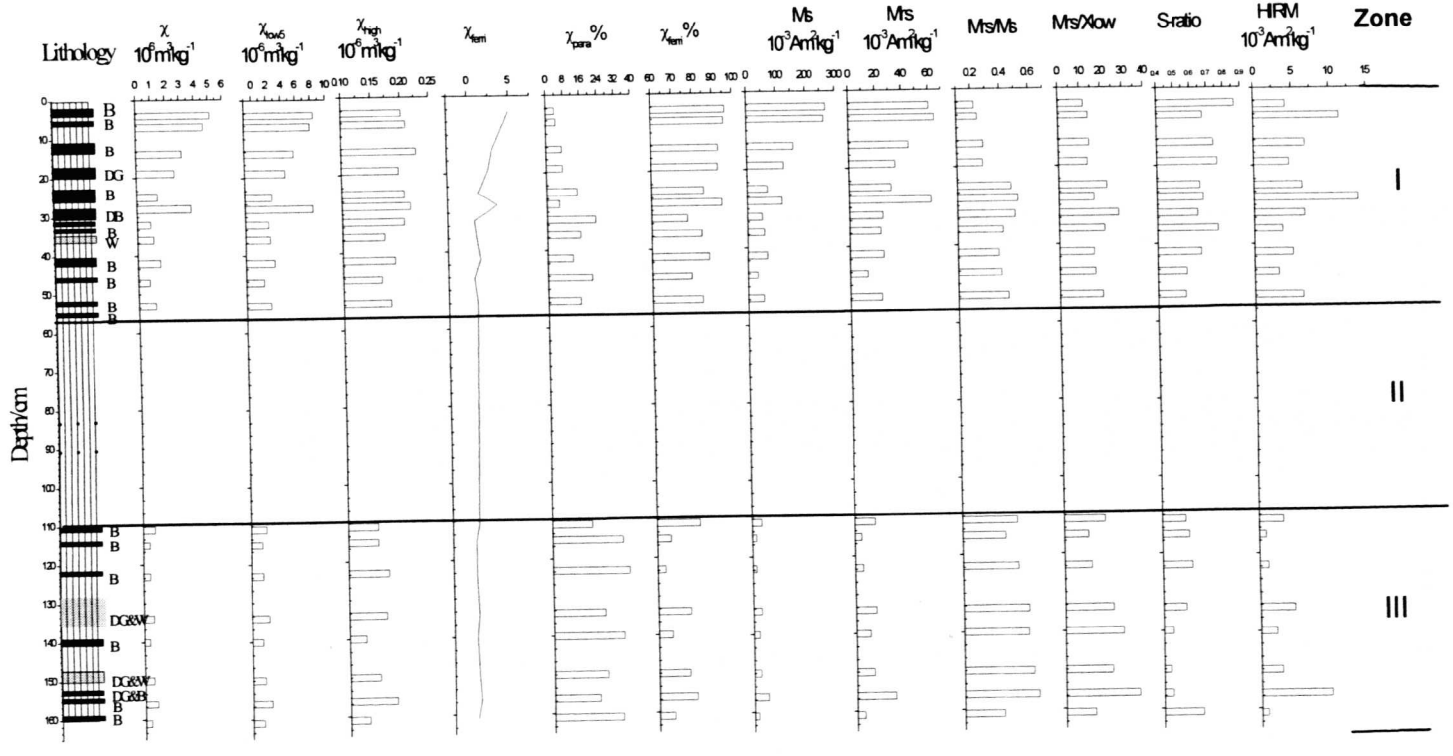

Figure 6.4 Magnetic hysteresis parameters ('loop2') from VSM analysis for Lax, SE Iceland. Tephra colour: B, Black; D, Dark; G, Gray; Gr Green; Br, Brown; W, White. Horizontal shaded zones are selected visible tephra layers in the profile.

Table 6.4 Colour, hysteresis loop type, Curie temperature (T_c) curve type and Curie point for samples from Skal, SE Iceland.

Depth cm		Colour	Lp	Tcc	Tc
8	12	black	2	2	no
17	18	black	2	2	no
20	22	black	2	2	no
27.5	29	black	2	2	no
30.5	32	black	2	2	no
39	40	green	3	3	no
68.5	69	white	2	2	no
69	70	black	2	2	no
75	78	black	3	3	no
82.5	83	black	2	2	no
87	91	black	5	3	no
97	98	black	2	3	no
103	112	black	5	3	no
114	115	black	4	3	no
115	116	white and green	4	2	no
116	117	black	4	2	no
117	118	black	4	2	no
127.5	129	black	2	3	no
133	134	white	4	3	no
143	145	black	2	3	no
151	152	black	2	2	no
153	155	green	2	3	no
155.5	162	green	2	2	no
169	171	black	2	2	no
175.5	179	green	2	2	no
203	208	black	3	2	no
230.5	231	white	1	2	575
243	244	white	2	2	no
246	247	white	2	2	575
257	259	green	2	2	no

LP, loop; Tcc, Curie temperature curve; T_c, Curie temperature point. In column LP, 1-5 indicates the different hysteresis loop shapes in Figure 6.3. In the column Tcc: 1-4 expresses the type of T_c curve shape shown in Figure 6.6.

Table 6. 5 Magnetic hysteresis parameters ('loop2') of VSM analysis of samples from Skal, SE Iceland

Depth	Xlow	Xlow5	Xhigh	Xferri	Xpara%	Xferri%	Ms	Mrs	Mrs/Ms	Mrs/ Xlow	(Bo)cr	(Bo)c	(Bo)cr/(Bo)c
cm	$10^{-6}m^3kg^{-1}$	$10^{-6}m^3kg^{-1}$	$10^{-6}m^3kg^{-1}$	$10^{-6}m^3kg^{-1}$			$10^{-3}Am^2kg^{-1}$	$10^{-3}Am^2kg^{-1}$			mT	mT	
10	3.77	7.82	0.27	3.49	7.23	92.77	147.65	50.70	0.34	13.46	43.67	22.50	1.94
18	4.78	10.02	0.27	4.51	5.55	94.45	173.84	52.10	0.30	10.90	197.70	19.00	10.41
21	2.08	3.83	0.20	1.88	9.63	90.37	92.42	33.27	0.36	16.03	61.03	21.00	2.91
28	2.28	4.29	0.18	2.10	7.87	92.13	99.46	36.18	0.36	15.86	59.18	21.00	2.82
31	1.45	2.83	0.21	1.25	14.29	85.71	68.94	30.37	0.44	20.91	45.23	20.50	2.21
40	1.83	3.41	0.25	1.58	13.66	86.34	99.27	45.54	0.46	24.82	38.15	24.50	1.56
69	1.94	3.17	0.17	1.77	8.83	91.17	102.09	34.53	0.34	17.77	23.35	16.60	1.41
70	1.60	3.91	0.17	1.44	10.40	89.60	48.45	18.90	0.39	11.78	38.76	13.50	2.87
78	7.04	14.88	0.26	6.78	3.68	96.32	329.63	121.51	0.37	17.27	34.54	26.00	1.33
83	1.50	3.01	0.21	1.29	13.83	86.17	63.21	27.82	0.44	18.54	162.64	29.00	5.61
91	3.93	10.04	0.25	3.68	6.36	93.64	120.21	59.00	0.49	15.02	138.54	36.50	3.80
98	2.64	5.04	0.23	2.41	8.80	91.20	115.03	49.98	0.43	18.95	35.96	25.00	1.44
105	1.88	4.61	0.22	1.66	11.80	88.20	98.90	52.93	0.54	28.20	53.68	20.50	2.62
115	0.73	1.71	0.20	0.53	27.36	72.64	31.12	15.87	0.51	21.82	154.26	28.50	5.41
116	0.91	2.28	0.17	0.74	18.60	81.40	39.33	19.75	0.50	21.69	204.31	34.00	6.01
117	1.03	2.26	0.18	0.85	17.70	82.30	39.29	18.93	0.48	18.35	216.77	33.00	6.57
118	1.36	3.14	0.18	1.18	13.31	86.69	36.88	18.00	0.49	13.19	370.23	31.00	11.94
129	1.41	2.17	0.16	1.25	11.54	88.46	52.15	16.79	0.32	11.87	26.72	15.00	1.78
134	3.44	6.26	0.26	3.19	7.49	92.51	173.04	87.49	0.51	25.41	227.59	33.00	6.90
144	1.68	2.52	0.18	1.50	10.52	89.48	73.36	33.04	0.45	19.71	32.89	26.50	1.24
152	2.44	4.83	0.20	2.24	8.33	91.67	115.50	48.70	0.42	19.95	32.96	26.00	1.27
154	1.28	2.28	0.18	1.10	14.30	85.70	60.71	25.80	0.42	20.15	36.62	25.00	1.46
162	1.68	2.99	0.19	1.48	11.53	88.47	77.06	31.53	0.41	18.81	35.55	25.00	1.42
170	1.65	2.60	0.19	1.46	11.70	88.30	67.43	26.56	0.39	16.09	370.00	23.00	16.09
177	1.87	3.20	0.19	1.67	10.27	89.73	71.07	23.24	0.33	12.45	42.20	17.00	2.48
205	2.70	5.00	0.20	2.50	7.56	92.44	130.52	57.64	0.44	21.32	489.72	30.50	16.06
230	3.74	7.32	0.22	3.51	5.99	94.01	150.67	33.34	0.22	8.92	37.68	12.50	3.01
244	2.40	3.78	0.18	2.22	7.68	92.32	105.61	33.57	0.32	13.98	46.88	19.50	2.40
247	0.92	1.58	0.07	0.86	7.21	92.79	36.54	8.17	0.22	8.87	25.73	15.50	1.66
258	1.83	2.80	0.17	1.66	9.37	90.63	72.40	23.47	0.32	12.82	47.41	19.00	2.50

Figure 6.5 shows hysteresis loop2 parameters for 30 selected samples from Skal. Most of the parameters show a similar pattern of variation with depth. The χ_{low} is variable between ~0.7-7 $10^{-6}m^3kg^{-1}$, having high values at depths of 75 cm and 230 cm, which is similar to χ_{low5}, χ_{ferri}, M_s and M_{rs}. The χ_{ferri}% varies from 72.6-94.5 (Table 6.5), and the M_{rs}/M_s ratio ranges between 0.3-0.6 (Table 6.5), indicating the main domain state of the magnetic minerals is PSD (Day *et al.*, 1977). The ratios of M_{rs}/χ_{low} are ca. 20, and are quite stable through the profile. The S-ratio shows remarkably high values in the top two tephra layers, and the values of HIRM are

Fig. 6.5 Magnetic hysteresis parameters ('loop2') from VSM analysis of samples from Ska1, SE Iceland. Tephra colour: B, Black; D, Dark; G, Gray; Gr Green; Br, Brown; W, White. Horizontal shaded zones are selected visible tephra layers in the profile.

typically less then 6×10^{-3} Am^2kg^{-1} in the profile and reach 12×10^{-3} Am^2kg^{-1} in the middle part of the profile.

6.4 Curie temperature analyses

6.4.1 Curie temperature curve classification

Identification of magnetic minerals from Curie temperature measurement is based on the observation of thermal changes in spontaneous magnetization (Chapter 2.2.4). In this study, 127 samples were selected from individual tephra layers for Curie temperature (T_c) measurement, using a VFTB (Chapter 4, section 4.5.2). The results are summarized in Figure 6.6.

Magnetic properties vary with temperature. On heating beyond a critical temperature (the Curie point - T_c), ferrimagnetic or antiferromagnetic materials become paramagnetic and lose magnetization. This can be used as a diagnostic signature of mineral type. Figure 6.6 shows a classification of the types of Curie temperature curve encountered in this study. The types of curve are defined below:

1. Reversible, with T_c ~580°C attained during the heating process, indicating the contribution of magnetite (Fig. 6.6, no. 1).
2. Irreversible, with a T_c ~570-600°C (Fig. 6.6, no. 2), indicating the contribution of magnetite but with mineral transformation/oxidation during the heating process.
3. The distance between heating and cooling is medium without a well-defined T_c (Fig. 6.6, no. 3), indicating domination of the heating/cooling curve by paramagnetic minerals.
4. The distance between heating and cooling is broad without a well-defined T_c (Fig. 6.6, no. 4), indicating a significant paramagnetic mineral contribution,

together with significant mineralogical alteration during heating. A significant difference of magnetization between the heating and cooling limbs indicates mineral transformation/oxidation during the heating process.

In this study, 50 samples from individual tephra layers in the two peat sections, 20 samples from Lax and 30 samples from Ska1, were measured. All of the T_c curves are shown in Appendix II, while the results are summarised below.

6.4.2 Lax

Thermomagnetic curves for 20 selected samples of Lax are classified in Table 6.2. Some common features are observed amongst the M/T curves. Firstly, the cooling curves are all irreversible with respect to the heating curves. Secondly, the magnetization values of the heating curves are less than those of the cooling curves. Thirdly, all the heating curves are straight. The top three samples (depths of 4 cm, 7 cm, and 14 cm) have a clear T_c point at ca. 580°C, indicating magnetite (Table 6.4). The other 17 samples have no clear T_c point, indicating a significant paramagnetic mineral component. The magnetization values of four samples (4 cm, 7 cm, 14 cm and 19 cm) increase above 250°C during heating; 4 samples (28 cm, 32 cm, 111 cm and 134 cm) show no clear increase during heating, and the magnetization values of the other 12 samples increase above 450°C, indicating a different magnetic mineral component in these samples.

6.4.3 Ska1

Table 6.4 classifies the thermomagnetic curves of 30 selected samples from Ska1. The common features of the M/T curves are that the cooling and heating curves are

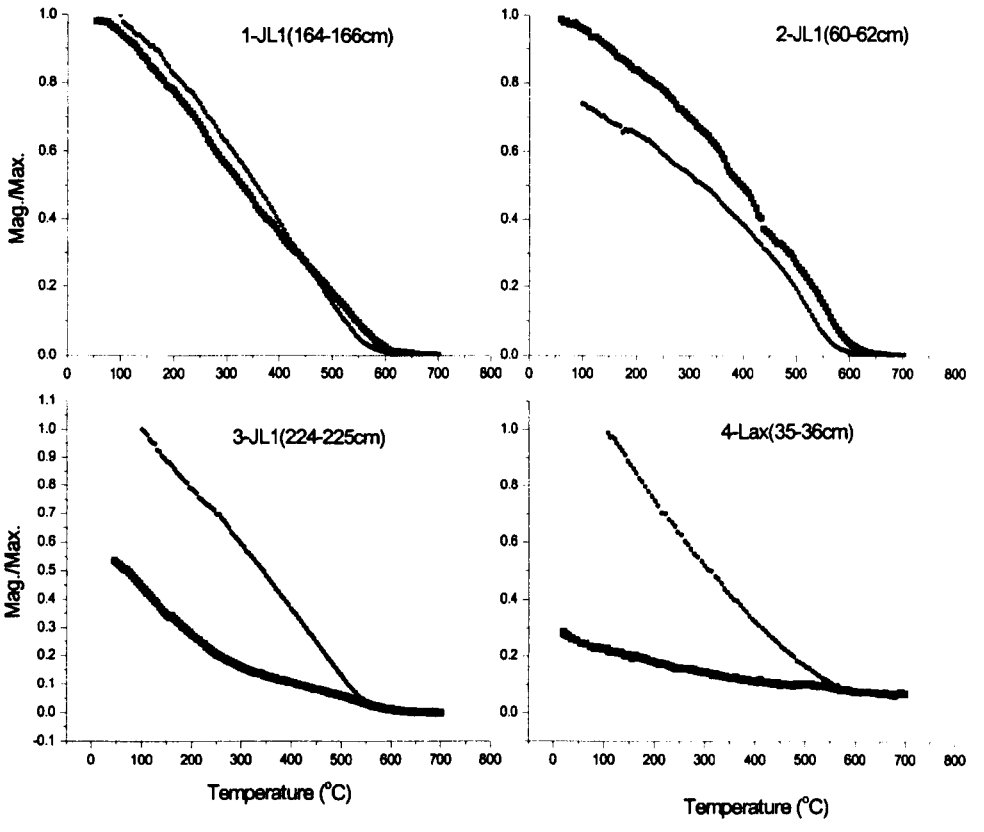

Figure 6.6 Examples of representative high field thermomagnetic curves encountered in this study: (1) JL1, depth 164-166 cm; (2) JL1, depth 60-62 cm; (4) JL1, depth 224-225 cm, and (5) Lax, 35-36 cm.

all irreversible, and the values of the cooling curves are great than those of the heating curves. Only one sample, i.e. 29 (247 cm), has a poorly defined T_c point at about 580°C, indicating magnetite. None of the other 29 samples has a clear T_c point, and almost all show a significant rise in magnetization during cooling, indicating the significant conversion of paramagnetic iron to a ferrimagnetic form.

6.5 Loss-on-ignition and XRF measurements

6.5.1 Loss on ignition

Figure 6.7 shows the loss-on-ignition LOI) values selected samples (from individual tephra layers) of Lax, together with the results of XRF analyses. LOI ranges from 4.8-36.8 % with a mean 15.4 % (Appendix 3). There is a gradual decrease in LOI values moving up the core. The lowest % loss is in the upper part of the section with a value of 4.8 % at the depth of 32 cm. The largest value is at 134 cm depth, where it is 36.8 %. There are relatively high values at depths of 115 cm 140 cm and 161cm.

6.5.2 X-Ray Fluorescence (XRF)

XRF was measured mainly on one peat core (Lax). The concentrations of 14 elements were obtained. In general, the peat cores consist mainly of organic material, as would be expected, together with significant amounts of Si and Al. The results for selected elements for Lax are shown in Figure 6.7. Three major sections can be distinguished based on element concentrations. Zone III exhibits fluctuating concentrations of all elements, with highest values of Fe (~300 mg/g), Ti (~22 mg/g) and S (~11 mg/g). Si, Al, Ca and Ca show higher values at depths of 110-114 cm and 130-140 cm. Fe is quite variable with several distinct peaks at 110 cm, 115 cm, 125 cm, and 145 cm. Ti shows higher values between 107 and 120 cm, and there is a sharp decline at 125 cm; then the trend is that of a slow increase towards the base of the core. Zone II: Fairly uniform values of all elements. Fe, K, Ca and Mn show low concentrations, but S has higher values in the central part. In Zone II (56-110 cm), the concentrations are fairly stable, compared to that of Zone I (0-56 cm) and Zone III (110-160 cm). Zone I is characterized by fluctuating concentrations of most elements, with distinct minima in Si, Al Ca, K and Ti at ~15cm. The minima

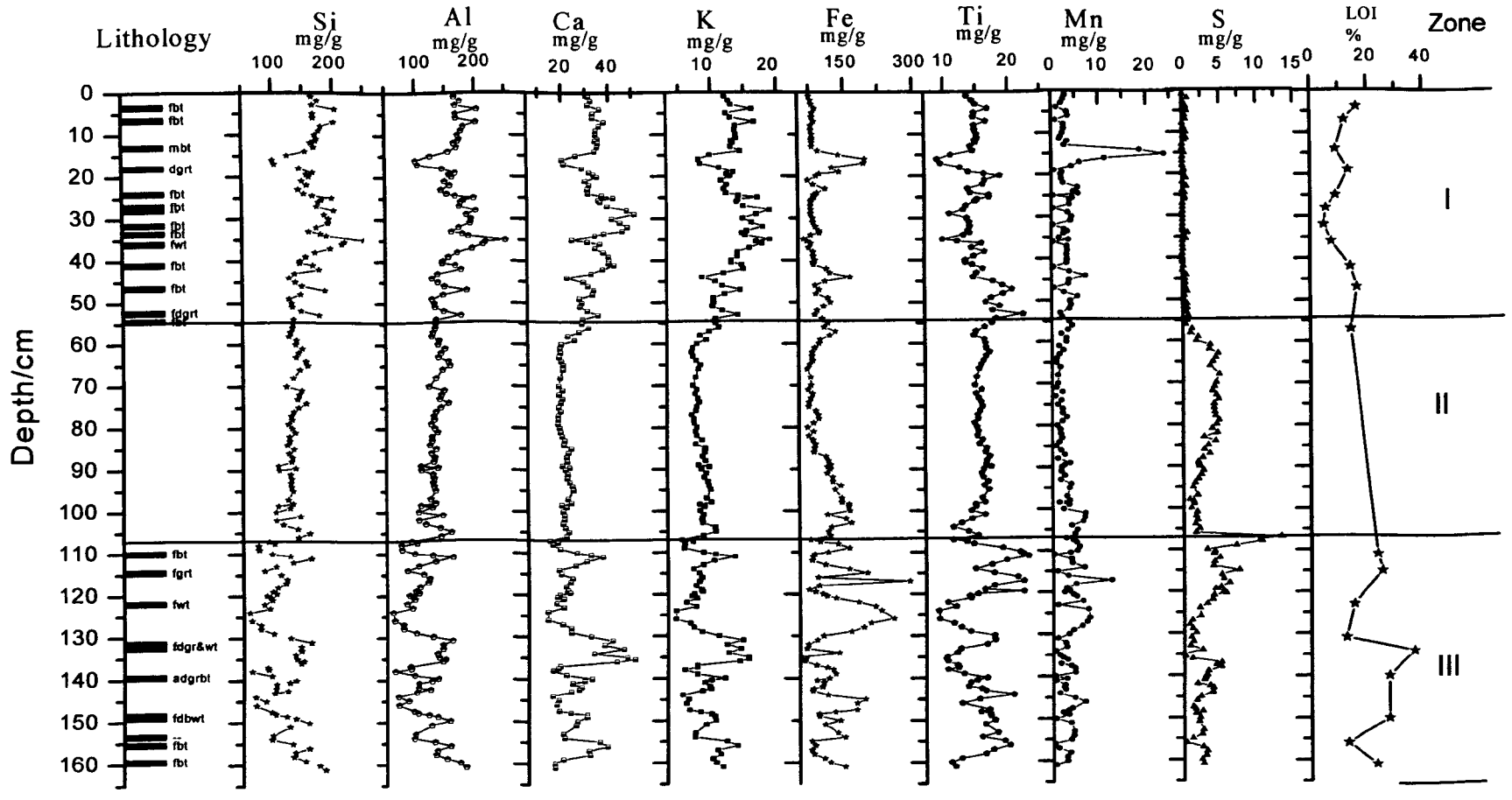

Fig. 6.7 LOI and selected element from XRF analyses of Lax, Iceland. Tephra colour: B, Black; D, Dark; G, Gray; Gr Green; Br, Brown; W, White. Horizontal shaded zones are selected visible tephra layers in the profile.

correspond to peaks in Fe and especially Mn (~25 mg/g). Si, Al, Ca and K have higher values in the central part and lower values in the lower part. S has lower values (<1mg/g) throughout this zone. It is noticeable that the variability in zone I and III coincides with the presence of tephras, and the low and stable element values in zone II relate to the absence of tephras.

The XRF measurements may potentially help characterise tephra, given the significant variations in elemental concentrations within the peat profiles. There are a number of peaks (e.g. at 78-80 cm, 132-136 cm, and 165-175 cm in Ska1), which quite clearly coincide with visible tephra layers in the two peat sections.

6.6 Summary

The results indicate that bulk sample magnetic and XRF measurements may potentially help characterise tephra, given the dramatic variations in magnetic parameters and elemental concentrations within the peat profiles. In general, several points can be made: Firstly, there are a number of peaks (e.g. at 78-80 cm, 132-136 cm, and 165-175 cm in Ska1), which quite clearly coincide with visible tephra layers in the two peat sections. Secondly, the magnetic concentration parameters of the sections are quite high (Table 6.1), indicating the occurrence of high concentrations of ferrimagnetic minerals. Both the mass-specific parameters (e.g. χ , χ_{fd}, χ_{ARM} and SIRM) and the ratio parameters (e.g. SIRM/χ lf, χ_{ARM}/SIRM) show pronounced variations with depth, and major changes are generally coincident in most parameters, indicating significant variations in both the concentration of the ferrimagnetic minerals and in the magnetic mineral grain size. Magnetic hysteresis can be interpreted as a magnetic mineralogical signature on the basis of the shape of the

loop. Bulk tephra can be classified based on the shape of magnetic hysteresis loop and thermomagnetic curves.

Chapter 7 Results of rock magnetic and XRF measurements of the soil sections

7.1 Introduction

This chapter presents the results of magnetic and XRF measurements for the three soil sections, Ska2, JL1 and JL2, from SE Iceland. Most of the results are presented as down-core plots.

7.2 Basic magnetic parameters

7.2.1 Ska2

Magnetic measurements of bulk samples from the soil profile, Ska2, are plotted against depth in Figure 7.1. In detail, χ_{lf} remains fairly stable from 0 to 200 cm, at ca. $200\times10^{-8}m^3kg^{-1}$, except for two slight decreases to ca. $100\times10^{-8}m^3kg^{-1}$ at the depths of 105 cm and 195 cm. This is followed by an abrupt peak reaching to ca. $270\times10^{-8}m^3kg^{-1}$ at the depth of 235 cm. Values then generally decrease again at the depth of 250 cm. There are three dramatic peaks at 275 cm, 310 cm and 345 cm in the basal part of the profile (260-360 cm). SOFT (with values in the range of $223.6\text{-}1860.7\times10^{-5}Am^2kg^{-1}$), χ_{fd} (with an average value of $9.8\times10^{-8}m^3kg^{-1}$), χ_{ARM} (with values ranging from $316.1\text{-}2008.7\times10^{-8}m^3kg^{-1}$), and SIRM (average value $6767.7\times10^{-5}\times Am^2kg^{-1}$) follow fairly similar trends to χ_{lf}. χ_{fd}% remains roughly at ca. 4 throughout the whole profile, with increases to ca. 7.5 at depths of 39 cm and 215 cm, and a decrease to 3 at depths of 195 cm and 255 cm.

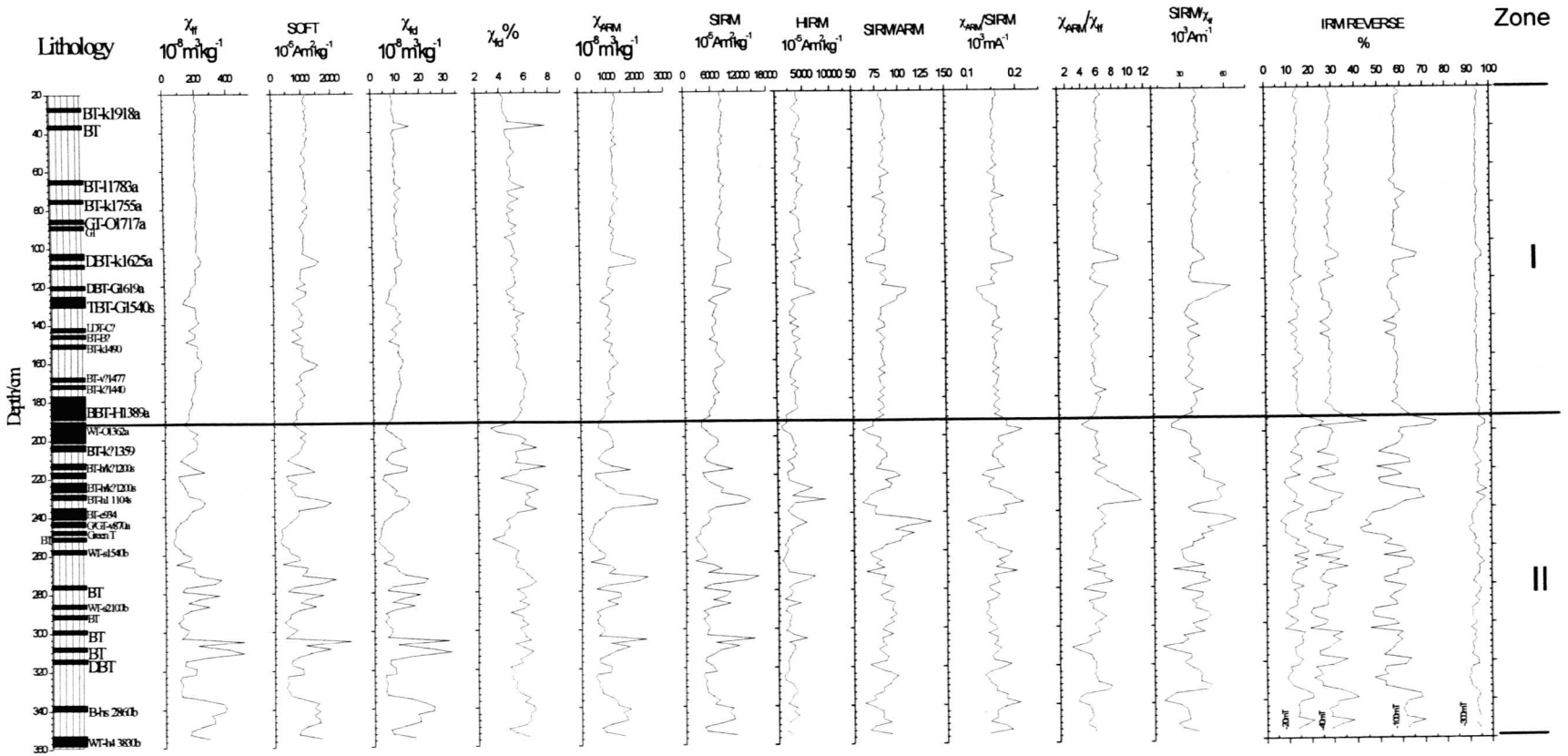

Figure 7.1 Magnetic parameters for Ska2, SE Iceland. Tephra colour: B, Black; D, Dark; G, Gray; Gr Green; Br, Brown; W, White. Horizontal shaded zones are selected visible tephra layers in the profile.

The HIRM ranges from 1277.3-6655.3×$10^{-5}$$Am^2kg^{-1}$, with several noticeable peaks at the depths of 125 cm, 235 cm and 275 cm. SIRM/ARM remains faire stable with a value of ca. 82.9 down the profile. There is a sharp decrease to ca. 60 at 107cm, and this is followed by a general increase to ca. 108 at 123 cm. This is then followed by a sharp decrease again to ca. 59 at 237 cm and a significant peak to ca. 133 at 245 cm. χ_{ARM}/SIRM has an average value of ca. 0.154×10^{-3} mA^{-1}, with an abrupt decrease to 0.09×10^{-3} mA^{-1} at 245 cm and many peaks at 110 cm, 195 cm, 235 cm and 340 cm. The graphs for χ_{ARM}/χ_{lf} and SIRM/χ_{lf} are quite similar to each other, except for a significant increase of χ_{ARM}/χ_{lf} at 235 cm. The χ_{ARM}/χ_{lf} values remain fairly constant at an average of ca. 6. The SIRM/χ profile is fairly constant at an average of ca. 9.3×$10^3$$Am^{-1}$ from 20 cm to 190 cm, with a significant peak at 130 cm; this is then followed by an abrupt decrease at 195 cm. Then, after this, there is a general increase till to 250cm, with an abrupt decrease at 240 cm. There is another large reduction at 313 cm near the base of the profile.

In summary, two major zones can be distinguished in terms of magnetic properties (Fig. 7.1). Zone II (190-360 cm) is characterized by considerable variations in both the mass specific parameters (e.g. χ_{lf}, $\chi_{fd\%}$ and χ_{arm}) and the inter-parametric ratios (e.g. SIRM/ARM and χ_{ARM}/χ_{lf}). The major variations are generally coincident (e.g. at the depth of 230-235 cm in Fig. 7.1), indicating that the variations in the concentration of magnetic minerals and magnetic mineral grain size are responsible for most of variations. Zone I (0-190 cm) is characterized by a lack of major variation in most parameters, indicating that magnetic grain-size and mineral concentrations change little through the

zone, with relatively coarse grains dominant in most samples. Finally, there are a number of peaks, such as at 108 cm, 125 cm, 215 cm, 235 cm, 275 cm, 290 cm, 308 cm, and 338 cm, which are roughly coincident with visible tephra layers in the section.

7.2.2 JL1

Magnetic measurements of bulk samples from soil profile JL1 are plotted against depth in Figure 7.2. χ_{lf} values remain fairly stable at ca. 630×10^{-8} m^3kg^{-1} down the profile until 87 cm, where there is a modest increase to ca. 955×10^{-8} m^3kg^{-1}. This is followed by a general decrease to ca. $566\times10^{-8}m^3kg^{-1}$ until 130 cm. After a general increase to ca. $900\times 10^{-8}m^3kg^{-1}$ from 130 cm to 163 cm, the values show a sharp decrease to ca. $240\times10^{-8}m^3kg^{-1}$ from 163 cm to 180 cm. Then, there are several noticeable peaks at the depths of 196 cm, 210 cm, 235 cm, 255 cm, and 270 cm. After that, the values show a general decrease to the base of the profile. Soft (with values in the range 1023.2-$5684.2\times10^{-5}Am^2kg^{-1}$), χ_{ARM} (with values in the range 1170.7-$2057.7\times10^{-8}m^3kg^{-1}$), and SIRM (with an average of $14552.8\times10^{-5}Am^2kg^{-1}$) follow a fairly similar trend to χ_{lf}. χ_{fd} (with an average of $15.3\times10^{-8}m^3kg^{-1}$) remains fairly stable from the top to 80 cm; an exception is the lower values at the depth of 17-19 cm. This is followed by an abrupt decrease to ca. $13\times10^{-8}m^3kg^{-1}$ at 85 cm and then a sharp increase to ca. $23\times10^{-8}m^3kg^{-1}$ at 91 cm. After this, there is a general decrease to ca. $10\times10^{-8}m^3kg^{-1}$ at 190 cm. This is followed by four peaks at depths of 200 cm, 215cm, 235 cm, and 255 cm. After this, there are many small peaks with a general decrease in values to the base of the profile. χ_{fd}% remains constant at ca. 1.9 from 0-290 cm, with three large peaks at 97 cm, 170-180 cm, and 223-227 cm. This is followed by a general increase to the end.

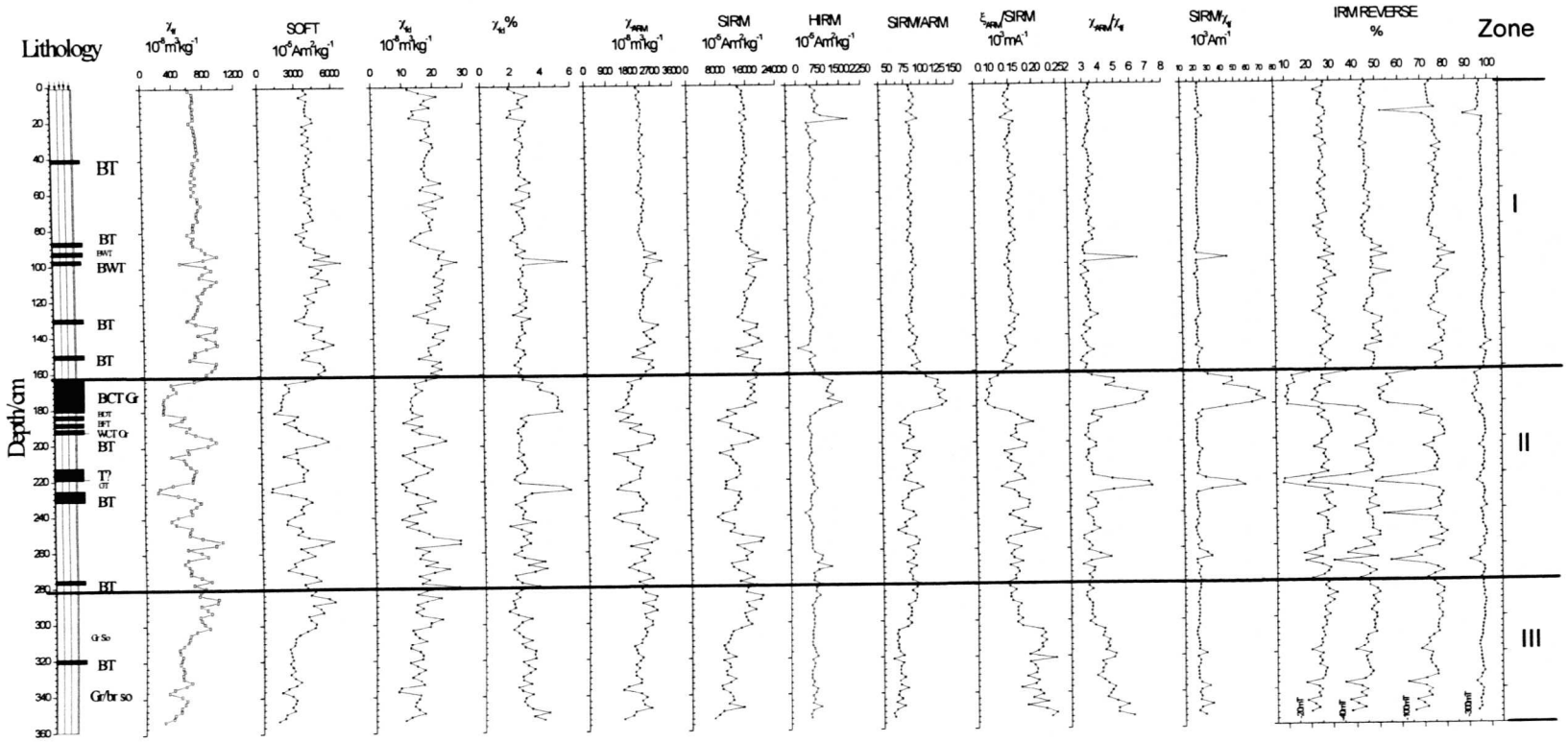

Figure 7.2 Magnetic parameters of JL1, SE Iceland. Tephra colour: B, Black; D, Dark; G, Grey; Gr Green; Br, Brown; W, White. Horizontal shaded zones are selected visible tephra layers in the profile.

HIRM remains fairly stable at the level of ca. $590\times10^{-5}Am^2kg^{-1}$ down through the section with a three noticeable peaks at 20 cm, 160-180 cm, and 260-270 cm. SIRM/ARM has an average value of ca. 83 from 0 to 302 cm, with the exception of a noticeable peak to ca. 123 between 160-180 cm. After this, it remains at ca. 60 until the base of the profile. χ_{ARM} /SIRM remains fairly stable of ca. $0.144\times10^{-3}mA^{-1}$ between 0 – 300cm, with a significant reduction over 160-180 cm. In the lower part of the profile, the values also remain stable with the value of ca. $0.2\times10^{-3}mA^{-1}$. χ_{ARM} / χ_{lf}, with the exception of three significant increases at the depths of 97 cm, 160-180 cm and 200-210 cm, remains fairly constant at an average of ca. 3.5 between 0-300 cm, and this is followed by a general increase to the base of the profile. The SIRM/ χ_{lf} profile is fairly constant at an average of approximately $23\times10^{-3}Am^{-1}$ throughout the profile, with several significant peaks at 97 cm, 160-180 cm, and 200-210 cm.

In general, three points can be made: Firstly, there are a number of peaks, such as at 97-100 cm, 160-180 cm, 200-210 cm, and 275-300 cm, which quite clearly coincide with visible tephra layers in the section. Secondly, the magnetic concentration parameters of the sections are quite high (e.g. χ_{lf} is between 167.7-$981.1\times10^{-8}m^3kg^{-1}$, mean $644.1\times10^{-8}m^3kg^{-1}$), compared to that of the peat section (Lax and Skal, Table 6.1). Thirdly, three major zones can be distinguished in terms of magnetic properties. Zone III (275-360cm) the lowest part, is characterized by 1) a rising trend in most magnetic parameters (e.g. χ_{lf}, χ fd, soft, χ_{ARM}, SIRM, and SIRM/ARM); 2) declining trend for χ_{fd} %, χ_{ARM} / χ_{lf}, SIRM/ χ_{lf} and; 3) the absence of major variations in HIRM, SIRM/ χ_{lf} and IRM-reverse parameters. Zone II (160-275 cm) is characterized by its significant variability of

concentration parameters (e.g. χ_{lf}, χ_{fd}, soft, χ_{ARM} and SIRM) and ratio parameters (e.g. χ_{ARM}/χ_{lf}, SIRM/χ_{lf}) with depth. The major variations of the section are coincident in most cases, indicating that variations in both the concentration and grain-size of magnetic minerals are responsible. There are two major variations among the ratio parameters at 160-190 cm and 220-230 cm, which indicate a significant change in magnetic mineral assemblages. Zone I (0-90 cm), the top part, shows no major variations in most of the parameters, indicating that magnetic grain-size and mineral concentration change little through the section, with relatively coarse grains probably dominant in most parts.

7.2.3 JL2

Figure 7.3 presents the magnetic measurements against depth for the soil profile JL2. The values of magnetic concentration parameters of the sections are again much higher compared to those of the two (see Table 6.1). The whole profile is quite similar to JL1, and can be divided into two zones in term of the magnetic properties: Zone II (135-73 cm), the lower part, is characterized by significant variations in most magnetic parameters (e.g. χ_{lf} and χ_{ARM}, χ_{fd}% and χ_{ARM}/χ_{lf}) and the ratio parameters with depth. The major variations of the section are coincident in most cases, indicating that the concentration of magnetic minerals and the magnetic mineral grain size are probably responsible for most of the variations. Zone I (73-0 cm), the top part, is characterized by the lack of major variations in most parameters, indicating that magnetic grain-size and mineral concentration change little through the section, with relatively coarse grains probably dominant in most parts. The basic magnetic parameters show a number of peaks

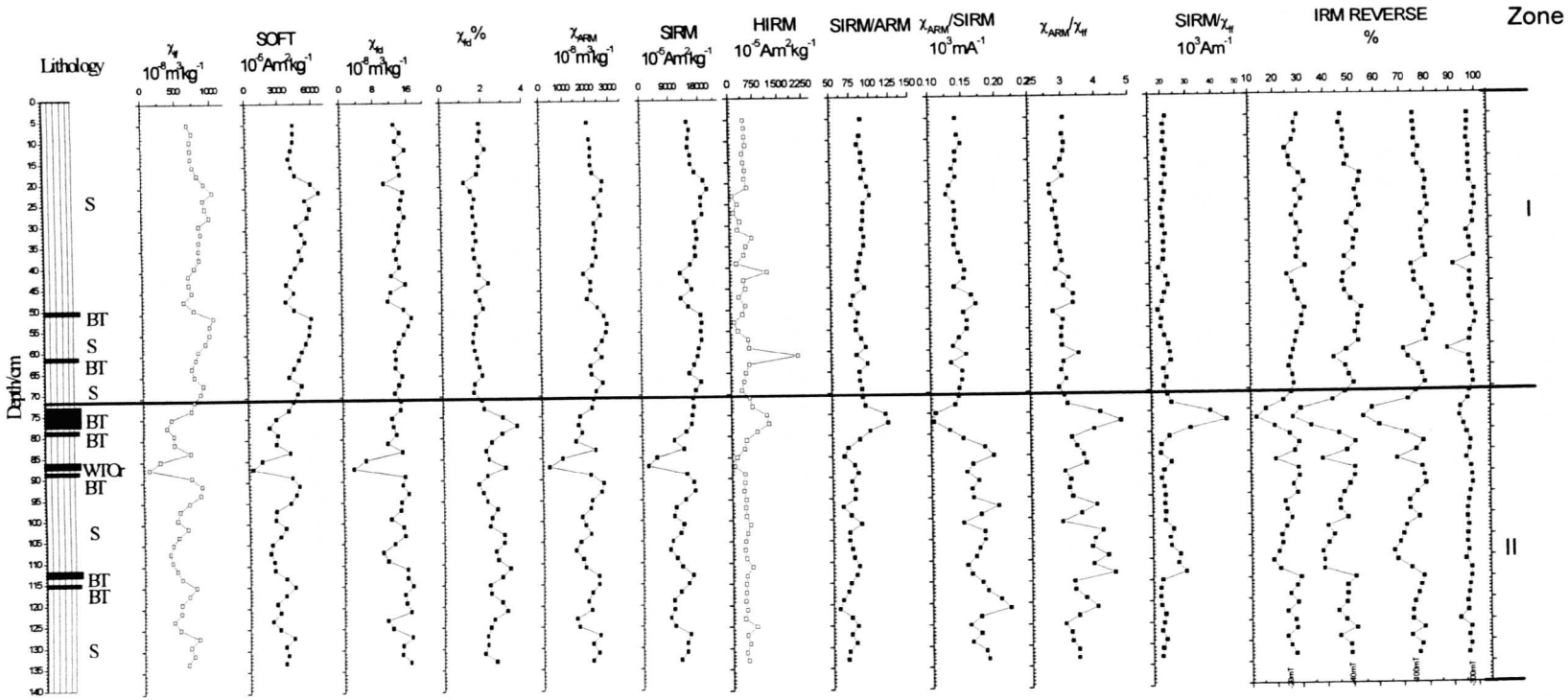

Figure 7.3 Magnetic parameters for JL2, SE Iceland. Tephra colour: B, Black; D, Dark; G, Gray; Gr Green; Br, Brown; W, White; T, Tephra; S, Soil. Horizontal shaded zones are selected visible tephra layers in the profile.

in the section, which are fairly clearly associated with visible tephra layers, e.g. at 52 cm, 75-80 cm, and 85-9 0cm.

7.3 Hysteresis loop measurements

In this study, 77 samples from individual tephra layers in the three soil sections, 47 samples from Ska2, 17 samples from JL1, and 13 samples from JL2, were selected for hysteresis loop measurements. All of the results are given in Appendix 1, whilst a summary is given here as follows:

7.3.1 Ska2

The results of hysteresis loops from VSM analysis for 47 selected tephra layer samples from Ska2 are shown in Table 7.1. All of the loops fail to reach saturation at the maximum field of 1T used, indicating a significant paramagnetic mineral content. Three loops (190-192 cm, 194-196 cm, and 338-340 cm) are quite thin (e.g. $(B_0)_c$ values are 3.4, 7 and 19.5 mT respectively in Table 7.2), and there is one wasp-waisted looped (126-128 cm). The other loops are quite broad (i.e. higher coercivity), indicating either a significant content SSD grain content or some haematite content.

The 'loop2' parameters of the 47 samples of Ska2 are presented in Figure 7.4 and Table 7.2. Most magnetic parameters do not show major variations. χ_{low}, χ_{low5} and χ_{ferri} show similar variations with depth, with high values at 160 cm 280 cm and 34 0cm. The χ_{high} is quite low, while χ_{ferri} % is very high (79.18-96.42 in Table 7.2), compared with the χ_{para} % values (3.58-20.83 in Table 7.2). The M_{rs}/M_s ratio ranges from 0.2-0.5, indicating PSD grain size (Day *et al.*, 1977).

Table 7.1 Magnetic parameters of Curie temperature (Tc) and 'loop' for Ska2, SE Iceland.

Sample position cm	Tephra layer thickness (cm)	Colour	Grain size	Source	Date	Lp	Tcc	Tc
26 ~28	27\28	black	fine	Grimsvotn	1883	3	3	no
ca. 27.5		black	fine			3	3	no
36 ~38	36\36.3	black				3	3	no
66 ~68	66\66.6	black		Laki	1783	3	3	no
ca. 67.1		black		Laki	1783	3	3	no
72 ~74	73.5\74.3	black		Katla	1755	3	3	no
ca. 73.5		black		Katla	1755	3	3	no
84 ~86	84\84.5	grey	coarse	Oraefi	1723	3	3	no
100 ~102	101.5\101.7	black				3	3	no
ca. 102		black				3	3	no
102 ~104	103\105	black				3	3	no
104 ~106	103\105	black		Grimsvotn	1659	3	3	no
108 ~110	108\108.3	black				3	3	no
ca. 120		black	medium & coarse	Grimsvotn	1619	3	3	no
120 ~122	120\121.5	black	medium & coarse	Grimsvotn	1619	3	3	no
126 ~128	124\130	black		Grimsvotn	1540	5	3	no
140 ~142	141\141.5					3	3	no
144 ~146	144\145	black				3	3	no
148 ~150	149\150.9	black	fine	Katla	1490	3	3	no
160 ~162	16\160.5	black	fine			3	3	no
166 ~168	167\167.5	black	fine			3	3	no
168 ~170	168\169	black	coarse & medium	Veidvotn	1477	3	3	no
170 ~172	170\171	black	fine	Katla	1440	3	3	no
172 ~174	172\173	black	fine			3	3	no
178 ~180	176\188	black		Hekla	1389	3	3	no
182 ~184	176\188	balck & white		He&Or	1389	3	3	no
190 ~192	188\200	white	coarse	Oraefi	1362	2	3	575
194 ~196	188\200	white	coarse	Grimsvotn	1354	1	1	575
202 ~204	202\202.3	black				3	3	no
212 ~214	212.5\212.8	black	fine	He/Ka	1200	3	3	no
214 ~216	214.5\214.8	black	fine	He/Ka	1200	3	3	no
218 ~220	218\218.5	black	fine	He/Ka	1200	4	3	no
222 ~224	221\226	black	fine	Veidvotn	1159	3	3	no
228 ~230	228\23	black	nedium & fine	Hekla 1	1104	3	3	no
236 ~238	234\240	black	fine	Eldgja	934	3	3	no
240 ~242	241.5\242	grey & green	fine	Veidvotn	870	3	3	no
248 ~250	248\259	green	fine			4	3	no
254 ~256	255\265.5	black	coarse			4	3	no
256 ~258	256.5\257	white		Skafta	1540b	4	3	no
274 ~276	274\277	black				3	3	no
284 ~286	285\286	white		Oraefi	1940	3	3	no
290 ~292	290\292	black				4	3	no
298 ~300	298\300	black		SvV	2500	4	4	no
306 ~308	307\309	black				3	3	no
312 ~314	313\313.5	black	diffuse			3	3	no
338 ~340	337\340	black	silt	Hs	2860b	2	3	no
354 ~356	355\359	white		H4	3830b	3	4	no

LP, loop; Tcc, Curie temperature curve; Tc, Curie temperature point. In the column LP, 1-5 indicates the different hysteresis loop shape in Chapter 6, Figure 6.3. In column Tcc: 1-4 expresses the type of Tc curve shape in Chapter 6, Figure 6.6.

Table 7.2 Magnetic hysteresis parameters ('loop2') of VSM analysis from Ska2, SE Iceland.

Depth	Xlow	Xlow5	Xhigh	Xferri	Xpara%	Xferri%	Ms	Mrs	Mrs/Ms	Mrs/ Xlow	(Bo)cr	(Bo)c	(Bo)cr/(Bo)c
	$10^{-6}m^3kg^{-1}$	$10^{-6}m^3kg^{-1}$	$10^{-6}m^3kg^{-1}$	$10^{-6}m^3kg^{-1}$			$10^{-3}Am^2kg^{-1}$	$10^{-3}Am^2kg^{-1}$			mT	mT	
27	2.87	5.03	0.22	2.66	7.50	92.50	171.29	71.48	0.42	24.90	33.71	26.50	1.27
27	3.19	5.93	0.27	2.92	8.59	91.41	159.03	71.50	0.45	22.40	37.67	30.50	1.24
37	4.14	6.03	0.26	3.88	6.37	93.63	182.66	72.57	0.40	17.51	34.63	24.50	1.41
67	4.20	6.10	0.29	3.91	6.93	93.07	195.29	82.38	0.42	19.61	34.20	26.00	1.32
67	3.34	5.82	0.28	3.06	8.29	91.71	159.40	74.59	0.47	22.33	55.81	32.00	1.74
73	3.07	5.07	0.22	2.85	7.07	92.93	186.26	77.85	0.42	25.38	36.70	36.50	1.01
74	3.20	5.89	0.26	2.94	8.05	91.95	145.90	59.37	0.41	18.58	33.76	25.50	1.32
85	4.33	6.68	0.30	4.03	6.82	93.18	190.06	77.01	0.41	17.79	22.74	16.00	1.42
101	4.44	5.52	0.31	4.14	6.93	93.07	208.14	84.93	0.41	19.11	33.37	25.00	1.33
102	3.55	6.14	0.23	3.32	6.38	93.62	168.36	70.66	0.42	19.93	34.29	26.50	1.29
103	1.09	2.35	0.21	0.88	18.91	81.09	40.64	18.12	0.45	16.64	17.82	10.00	1.78
105	4.30	6.48	0.29	4.01	6.79	93.21	215.47	93.42	0.43	21.71	41.55	22.00	1.89
109	4.60	6.49	0.36	4.25	7.73	92.27	230.73	104.95	0.45	22.80	39.85	26.50	1.50
120	2.54	5.49	0.25	2.29	9.74	90.26	130.49	26.86	0.21	10.59	103.32	30.00	3.44
121	3.11	5.06	0.25	2.86	8.19	91.81	143.73	60.97	0.42	19.60	44.05	26.00	1.69
126	3.35	5.87	0.34	3.02	10.06	89.94	158.12	48.29	0.31	14.40	36.31	3.50	10.37
140	3.42	4.53	0.26	3.16	7.68	92.32	152.52	61.55	0.40	18.00	41.01	23.50	1.74
145	3.11	5.01	0.24	2.87	7.72	92.28	139.44	56.14	0.40	18.04	44.29	24.00	1.85
149	2.48	4.55	0.29	2.19	11.59	88.41	123.94	57.60	0.46	23.23	40.17	29.00	1.39
161	4.60	7.68	0.26	4.34	5.76	94.24	206.97	80.68	0.39	17.53	34.57	23.00	1.50
167	3.99	5.79	0.28	3.71	7.00	93.00	174.66	73.66	0.42	18.45	40.67	25.00	1.63
169	0.00	4.89	0.00	0.00	7.17	92.83	0.15	0.06	0.40	18.30	35.53	23.50	1.51
171	3.68	5.84	0.26	3.42	7.08	92.92	163.10	64.51	0.40	17.51	89.86	23.00	3.91
173	3.61	4.97	0.27	3.34	7.47	92.53	168.04	67.80	0.40	18.77	40.24	24.00	1.68
179	0.00	4.87	0.00	0.00	8.47	91.53	0.15	0.06	0.44	20.23	58.21	26.00	2.24
183	3.23	5.65	0.25	2.99	7.61	92.39	153.10	61.34	0.40	18.96	39.46	23.50	1.68
191	2.49	3.71	0.17	2.32	6.87	93.13	114.92	41.13	0.36	16.50	187.54	12.50	15.00
195	3.56	5.80	0.13	3.43	3.58	96.42	154.68	26.20	0.17	7.36	31.10	7.00	4.44
203	3.59	5.23	0.25	3.35	6.82	93.18	169.98	68.30	0.40	19.00	97.85	24.00	4.08
213	2.16	2.88	0.20	1.96	9.18	90.82	101.11	37.96	0.38	17.56	35.89	21.50	1.67
216	3.15	3.71	0.27	2.89	8.48	91.52	153.33	58.13	0.38	18.44	33.08	24.00	1.38
219	1.19	1.79	0.25	0.94	20.82	79.18	59.04	25.44	0.43	21.37	80.30	31.00	2.59
223	1.90	3.18	0.25	1.65	13.32	86.68	89.87	42.90	0.48	22.58	114.60	26.00	4.41
229	2.33	4.11	0.28	2.06	11.88	88.12	130.03	65.89	0.51	28.24	41.00	34.00	1.21
237	2.79	4.32	0.25	2.54	9.02	90.98	122.21	50.11	0.41	17.94	35.00	25.00	1.40
241	2.32	3.25	0.21	2.10	9.18	90.82	104.96	39.98	0.38	17.25	32.73	27.00	1.21
249	1.04	1.83	0.21	0.83	20.30	79.70	44.34	21.71	0.49	20.80	105.00	37.00	2.84
255	0.97	1.71	0.19	0.79	19.17	80.83	39.90	19.33	0.48	19.89	89.86	34.00	2.64
257	1.22	1.74	0.22	1.00	17.97	82.03	53.40	21.55	0.40	17.63	41.99	29.50	1.42
275	5.40	6.48	0.33	5.06	6.16	93.84	246.39	116.32	0.47	21.56	194.44	31.50	6.17
285	1.94	2.16	0.24	1.70	12.32	87.68	99.16	40.40	0.41	20.86	49.26	27.50	1.79
291	1.28	1.65	0.22	1.07	16.87	83.13	68.22	25.59	0.38	19.97	32.69	28.00	1.17
299	1.59	1.94	0.22	1.37	13.74	86.26	88.72	33.63	0.38	21.11	261.78	24.00	10.91
307	2.90	2.72	0.26	2.65	8.80	91.20	124.37	36.45	0.29	12.56	160.48	24.00	6.69
313	3.68	4.17	0.25	3.43	6.71	93.29	126.18	32.76	0.26	8.91	35.01	19.50	1.80
339	5.94	7.83	0.24	5.69	4.11	95.89	219.61	39.76	0.18	6.69	73.55	39.00	1.89
355	3.94	4.16	0.23	3.71	5.85	94.15	176.98	68.87	0.39	17.46	64.77	27.50	2.36

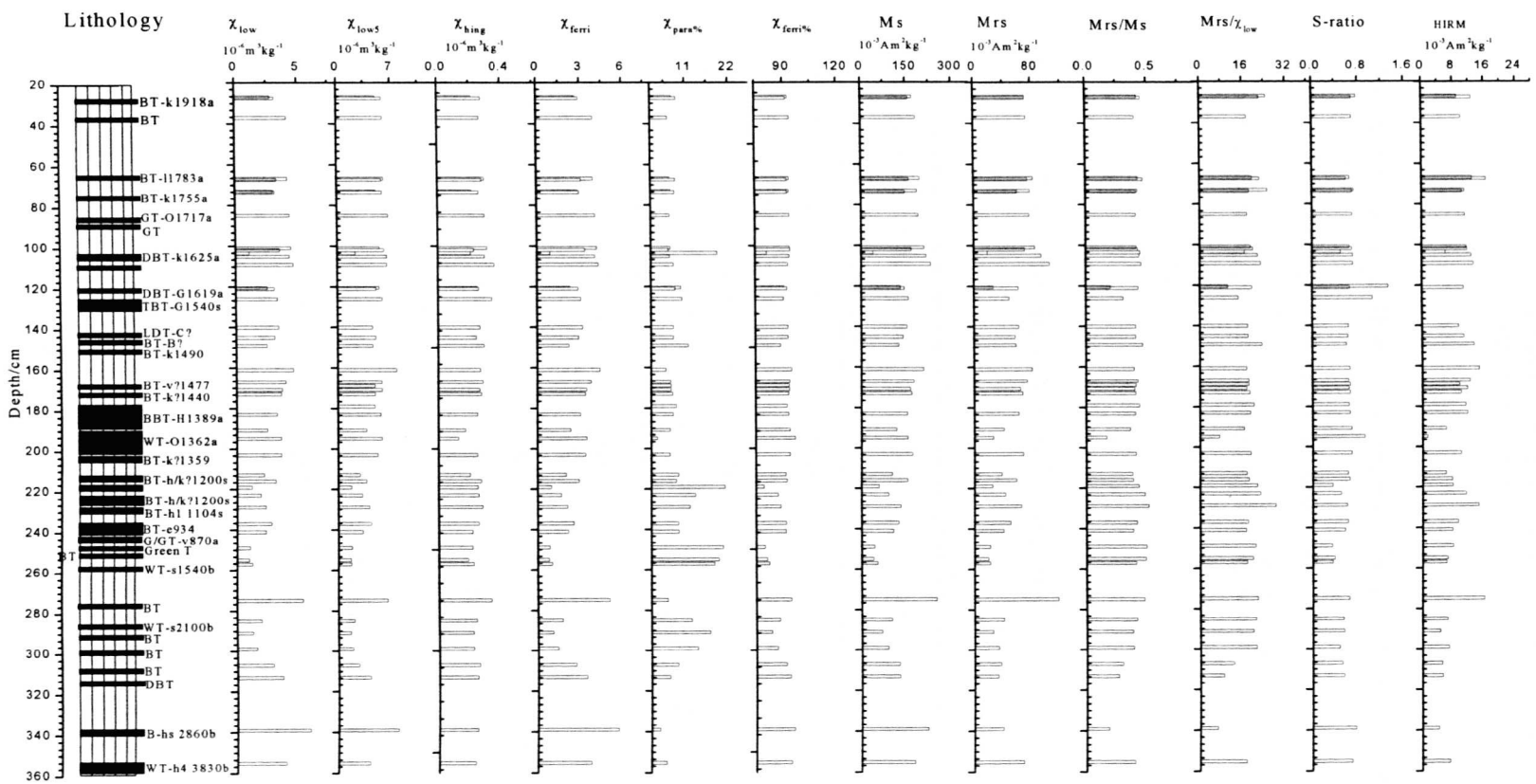

Figure 7.4 Magnetic hystersis parameters (Loop2) from VSM for Ska2, SE Iceland. Tephra colour: B, Black; D, Dark; G, Grey; Gr Green; Br, Brown; W, White. Horizontal shaded zones are selected visible tephra layers in the profile.

7.3.2 JL1

The hysteresis loops from VSM analysis for 17 selected samples from JL1 are shown in Table 7.3. In general, the loops are quite thin. The difference can be read for the samples from different tephra layers: The loops of three samples, 9 (183-185 cm), 13 (224-226 cm)

Table 7.3 Magnetic parameters of Tc and 'loop' for JL1, SE Iceland.

Sample position cm		Tephra layer thickness (cm)	Clolour	Size	Source	Date	Tc	Tcc	Lp
38	40	38\4	black				575	2	1
60	62	0.00					575	2	1
84	86	85\85.5	black				575	2	1
90	92	90\92	black & white		Oraefi	1723	575	2	1
94	96	94\94.5	black & white				575	2	1
130	132	131\132	black				575	2	1
150	152	151\151.5	black				575	2	1
164	166	161\179	black	coarse	Grimsvon		575	1	1
173	173	161\179	black	coarse	Grimsvon		575	1	2
183	185	0.00					no	2	4
186	187	0.00					575	3	1
190	192	190\190.25	black	diffuse	katla		575	1	1
212	214	212\216	brown				575	2	1
224	226	224\229	black	fine			no	3	3
228	230	224\229	black	fine			no	3	3
274	276	274\275	black				575	2	1
318	320	318\320	black				575	2	1

LP, loop; Tcc, Curie temperature curve; Tc, Curie temperature point. In the column LP, 1-5 indicates the hysteresis loop shape (see Chapter 6, Figure 6.3). In the column Tcc: 1-4 indicates the Tc curve shape (see Chapter 6, Figure 6.6).

and 14 (230 cm), are broad and short. Most of the other loops are very thin and tall - ($(B_0)_c$ values ranges from 10-43.5 mT and M_s ranges from 12-128$\times 10^{-3}$Am^{2}kg^{-1} in Table 7.4), and show a trend of flattening up to the maximum field of 1T used, especially in the case of sample no. 1 (depth 38-40 cm).

Table 7.4 presents the 'loop2' parameters of the 17 selected samples from JL1. One special characteristic should be mentioned here. The values of χ_{ferri} % are very high in most of the tephra layers, even reaching 100 % in some cases (e.g. at depths of 62 cm, 84 cm, and 152 cm).

7.3.3 JL2

The hysteresis loops from VSM analysis for 8 selected samples (nos. 48-55 in Appendix 2) and 5 pure tephra samples (nos. 56-60 in Appendix 2) from JL2 are summarized in Table 7.5. All samples exhibit thin loops, and are saturated (e.g. at the depth of 50-52 cm) at the maximum field of 1T used. The differences in the loop shapes are quite obvious for the samples from the different tephra layers. The loops of no 60 (JL2 126 cm) and 57(JL2 82-83 cm) are broad and do not reach saturation at the maximum field of 1T. The other 11 loops are thin and tall ($(B_0)_c$ ranges from 2.5-24 mT and M_s ranges between 0.16-161.9$\times 10^{-3}$Am^{2}kg^{-1}). Two wasp-waisted loops are observed for the samples at depths of 74-76 cm and 77-79 cm.

Table 7.4 Magnetic hysteresis parameters ('loop2') of VSM analysis from JL1, SE Iceland.

Depth	Xlow	Xlow5	Xhigh	Xferri	Xpara%	Xferri%	Ms	Mrs	Mrs/Ms	Mrs/ Xlow	(Bo)Cr	(Bo)c	(Bo)cr/(Bo)c
	$10^{-6}m^3kg^{-1}$	$10^{-6}m^3kg^{-1}$	$10^{-6}m^3kg^{-1}$	$10^{-6}m^3kg^{-1}$			$10^{-3}Am^2kg^{-1}$	$10^{-3}Am^2kg^{-1}$			mT	mT	
40.00	10.11	25.23	0.02	10.09	0.21	99.79	462.39	123.37	0.27	12.20	32.38	11.00	2.94
62.00	11.25	27.18	-0.01	11.26	-0.06	100.06	507.22	141.65	0.28	12.59	29.28	12.50	2.34
84.00	2.70	6.67	-0.01	2.70	-0.30	100.30	9.48	12.19	1.29	4.52	27.77	13.50	2.06
92.00	14.27	35.42	0.02	14.25	0.15	99.85	481.98	152.99	0.32	10.72	33.93	10.00	3.39
96.00	12.47	33.31	-0.02	12.49	-0.17	100.17	448.11	143.45	0.32	11.50	29.76	12.50	2.38
132.00	11.75	25.96	0.02	11.73	0.17	99.83	522.05	129.93	0.25	11.06	29.62	12.50	2.37
152.00	9.29	21.86	-0.03	9.32	-0.29	100.29	484.05	118.30	0.24	12.73	27.93	13.50	2.07
166.00	14.25	31.52	0.07	14.18	0.49	99.51	449.89	96.31	0.21	6.76	26.41	14.50	1.82
173.00	4.60	9.16	0.16	4.43	3.58	96.42	440.86	131.42	0.30	28.58	176.79	20.50	8.62
185.00	1.28	3.33	0.23	1.04	18.27	81.73	63.61	34.02	0.53	26.64	55.97	29.50	1.90
187.00	16.61	39.18	0.00	16.61	0.02	99.98	513.88	198.62	0.39	11.96	31.16	11.50	2.71
190.50	3.19	6.82	0.22	2.97	6.92	93.08	191.80	46.90	0.24	14.68	23.50	16.50	1.42
214.00	11.16	27.61	0.08	11.09	0.69	99.31	465.89	114.80	0.25	10.28	30.02	12.00	2.50
226.00	2.78	5.57	0.31	2.47	11.01	88.99	176.03	91.10	0.52	32.77	132.67	43.50	3.05
230.00	3.07	6.23	0.30	2.77	9.81	90.19	189.10	91.04	0.48	29.64	96.46	39.50	2.44
276.00	13.32	30.60	0.05	13.27	0.38	99.62	511.17	134.37	0.26	10.09	30.77	11.50	2.68
320.00	7.68	13.46	0.28	7.39	3.71	96.29	380.57	100.72	0.26	13.12	23.68	16.50	1.44

Table 7.6 and Figure 7.5 present the 'loop2' parameters for the 8 selected samples and 5 pure tephra samples from JL2. Most of the parameters show a similar pattern of variation with depth. χ_{low} ranges from 0.02-12.87×$10^{-6}m^3kg^{-1}$, and shows high values at depths of 6 1 cm and 115 cm, which is similar to χ_{low5}, χ_{ferri}, Ms and Mrs. The χ_{ferri}% varies from 85.8-99.9 % (Table 6.6). The M_{rs}/M_s ratios vary from 0.2-0.5, indicating a PSD magnetic grain size (Day *et al.*, 1977).

Table 7.5 Magnetic parameters of T_c and 'loop' from JL2, SE Iceland.

Sample position (cm)		Tephra layer thickness (cm)	Colour	Source	Date	Tc	Tcc	Lp
50	~52	50\51	black			575	1	1
60	~62	61\61.5	black			575	1	1
74	~76	73\77	black			575	2	1
77	~79	78\79	black			575	1	1
86	~88	86\88	white	Oraefi	1362	575	1	1
88	~90	88\88.5	black	Katla	1359	575	2	1
112	~114	112\113	black			575	2	1
114	~116	115\116	black			575	1	1
	ca. 78		black			575	2	5
	ca. 82.5		black			no	3	3
	ca. 87		white			575	1	1
	ca. 88		black			575	1	1
	ca. 126		black			no	3	3

LP, loop; Tcc, Curie temperature curve; T_c, Curie temperature point. In the column LP, 1-5 indicates the hysteresis loop shape (see Chapter 6, Figure 6.3). In the column Tcc: 1-4 indicates the T_c curve shape (see Chapter 6, Figure 6.6).

7.4 Curie temperature analyses

In this study, 77 samples from individual tephra layers in the three soil sections, 47 samples from Ska2, 17 samples from JL1, and 13 samples from JL2, were selected for thermomagnetic analysis. All of the results are shown in Appendix 2, while a summary is given here, as follows.

7.4.1 Ska2

The results of thermomagnetic measurements of 42 selected samples and 5 (nos. 43-47) pure tephra samples from Ska2 are shown in Table 7.1. The M-T curves show some common features. Firstly, the cooling curves are all irreversible with respect to the heating curves. Secondly, the magnetization values of the heating curves are less than

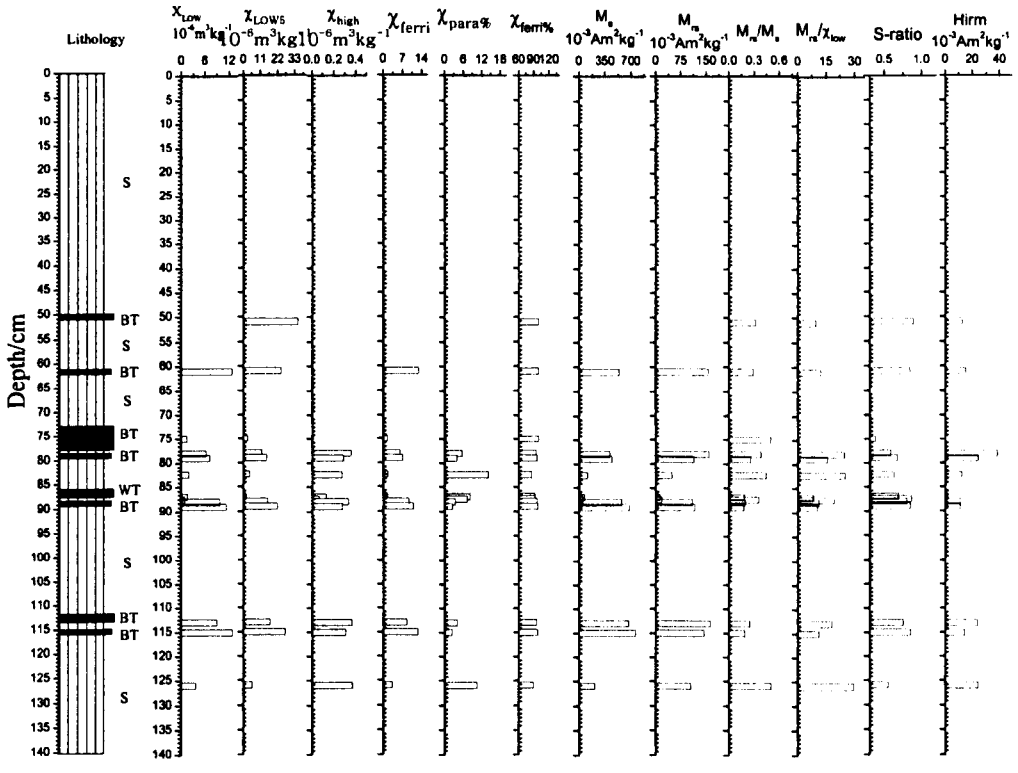

Figure 7.5 Magnetic hysteresis parameters ('loop2') from VSM for JL2, SE Iceland. Tephra colour: B, Black; D, Dark; G, Gray; Gn Green; Br, Brown; W, White. Horizontal shaded zones are selected visible tephra layers in the profile.

those of the cooling curves. Samples 22 and 41 show an unclear T_c point of 580 °C, indicating magnetite (Chapter 2.2.4). All of the other curves have no clear T_c point, indicating the predominance of paramagnetic minerals. The significant differences between the heating and cooling curves indicate that magnetic mineral transformation /oxidation occurred during the heating process. The magnetization value of four samples (nos. 13, 24, 25 and 44) increase after 250 °C during the heating process; in one sample (e.g. no. 26) values increase after 450° C during heating. The heating curve for sample

no. 43 shows three distinct magnetization increases at temperatures of ca. 200 °C, 300 °C and 450 °C.

7.4.2 JL1

The results of thermomagnetic measurements of the 17 selected samples from JL1 are summarised in Table 7.3. Most of the curves in this section have a T_c point at ca. 580 °C during the heating progress; three samples (depths of 183 cm 225 cm and 230 cm), and even the sample at depth of 173 cm, which have no clear T_c point. The cooling curves of only four samples (i.e. at the depths of 29 cm, 85 cm, 165 cm and 190 cm) are reversible. The magnetization values of heating curves of four samples (i.e. at the depths of 173 cm, 183 cm, 225 cm and 230 cm) and even the sample at depth of 165 cm are less than that of the cooling curves.

7.4.3 JL2

The results of thermomagnetic measurements of 13 selected samples from JL2 are summarised in Table 7.5. There is no clear T_c point for samples 57 (JT82-83) and 60 (JT126), indicating the predominance of paramagnetic minerals. All of the other curves have a T_c point of ca. 570 °C during the heating process, indicating the contribution of magnetite (See Chapter 2.2.4). Most of the samples (e.g. nos. 52 and 58) have reversible curves. In the case of two samples (nos. 56 and 59) the magnetization values of the heating curves are less than those of the cooling curves.

7. 5 Loss-on-ignition and XRF results

7.5.1 LOI

The loss-on-ignition (LOI) values for selected samples from the soil profiles, Ska2 and JL2, are relatively low; this is especially so for JL2, where the mean value is 7.2 % (see Appendix 3). The low values are unsurprising given the fact that the sandy nature of the soils. However, despite the fact that inorganic appearance of the sediments in the soil profiles, there are several significant variations in percentage loss-on-ignition within the profile (Fig. 7.6). The largest value, at 18 %, is at 355 cm depth in Ska2. The lowest value, at 1.2 %, is at the top of Ska2. There are obvious peaks at the depths of 121 cm, 140 cm, 203 cm, 21 6cm, 241 cm, 285 cm and 307 cm (Fig. 7.6; Appendix 3).

7.5.2 XRF

XRF analyses were conducted on one soil profile (Ska2). The concentrations of 14 elements were measured. The results of selected element concentrations for Ska2 are shown in Figure 7.6. The Si content of the sediments remains fairly stable down the profile until 180 cm, where there is a noticeable peak of ca. 240 mg/g; it then decreases down the profile until a depth of 220 cm, and after that there is a general increase to ca. 250 cm. At the base of the profile there are three peaks, at 320 cm, 340 cm and 355 cm. K follows a similar trend to Si. There are many small peaks in Al concentration, together with a large reduction in concentration at 235 cm. The Ca content is fairly uniform from 0-120 cm, at ca. 30 mg/g; below there is a sharp increase to 50 mg/g and the values then decrease with depth to 140 cm. The Ca concentration shows a reduction at 193 cm, followed by a general increase to 240 cm, after which there is a decline to the base of the profile. The profiles for Fe and Ti are

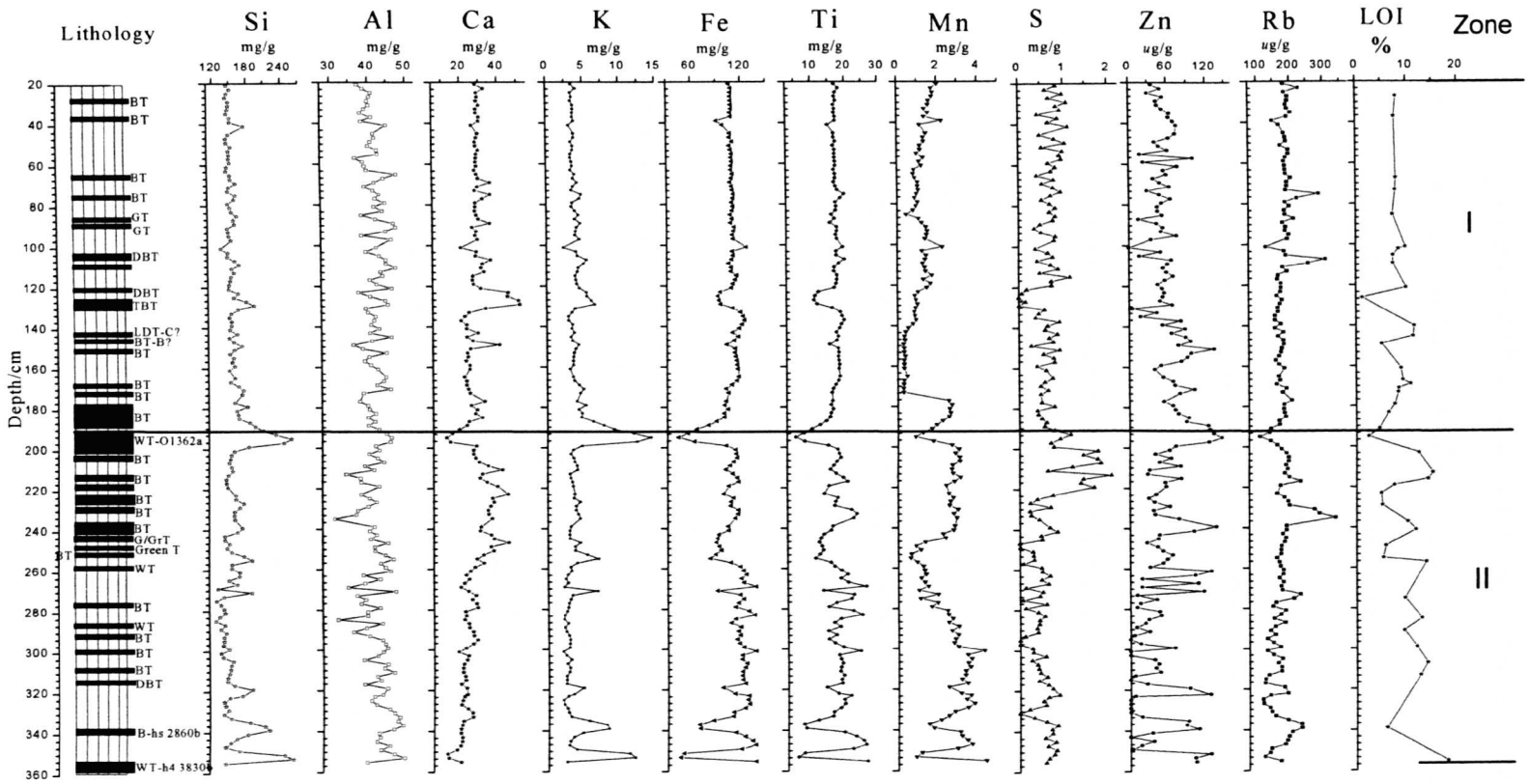

Figure 7.6 Selected elements from XRF analyses of Tephra layers from Ska2, Iceland. Tephra colour: B, Black; D, Dark; G, Gray; Gr Green; Br, Brown; W, White. Horizontal shaded zones are selected visible tephra layers in the profile.

similar to each other, with their concentrations remaining fairly stable down the profile, but with reductions at 40 cm, 130 cm, 200 cm, 340 cm and 355 cm. The concentration of Mn is quite variable, with a pattern of declining values from 0-83 cm and 100-180 cm, with higher values in between these intervals and a sharp increase below 180 cm. The Mn concentration is generally stable from 180-240 cm.

It is clear that the presence of tephras has a considerable influence on the element concentrations, which in general are relatively uniform in the intervals where tephras are absent. White tephra layers, at ~195 cm, ~285 cm and ~355 cm, show distinct peaks in Si, Al, K and Zn, and distinct minima in Ca, Fe and Ti. However, black tephras, at depths of ~128 cm and ~339 cm, show higher values of Si, Al, Ca, K, and Zn, and lower values of Fe, Ti and Mn.

7.6 Summary

In general, there are a number of peaks in magnetic parameters and elemental concentrations (e.g. at 97-100 cm, 160-180 cm, 200-210 cm, and 275-300 cm in JL1), which clearly coincide with visible tephra layers in the three soil sections. The magnetic concentration parameters of the sections are quite high (e.g. χ_{lf} ranges between 48.4-492.9$\times10^{-8}m^{3}kg^{-1}$, and averages 184.1$\times10^{-8}m^{3}kg^{-1}$, in Ska2), compared to that of the peat section (Lax and Ska1, Table 6.1), indicating the occurrence of high concentrations of ferrimagnetic minerals. Magnetic hysteresis can be interpreted as a magnetic mineralogical signature on the basis of the shape of the loop. Bulk tephra can be classified based on the shape of magnetic hysteresis loop and thermomagnetic curves.

Chapter 8 Magnetic characteristics of tephra in the study sections from SE Iceland

8.1 Introduction

This chapter is divided into two main parts: The first part, section 8.2 and 8.3, summarizes the magnetic properties of the tephras in the studied sections and then uses those properties to infer the types of magnetic mineral assemblages present. The second part uses the tephrochronology established in Chapter 5 to test the ability of the magnetic properties to characterise, or 'fingerprint', the tephras generated by individual volcanic eruptions.

8.2 Magnetic properties of tephra layers

Two areas, near the glacier Vatnajökull, were studied in SE Iceland (Chapter 4, Fig. 4.1), in the proximity of volcanoes. The first study area is located in Skaftafell National Park (Ska), which is near the western outlet of Oraefa glaciers. Two sections, Ska1 and Ska2, were studied from Skaftafellsheidi. Jokulla I Loni (JL) is the second study area; three sections, JL1, JL2 and Lax, were studied in this area.

Tables 8.1 and 8.2 summarize the magnetic parameters for all of the tephra layers, showing the different magnetic signatures in the five sections: Lax, Ska1, Ska2, JL1 and JL2. JL1 and JL2 show high values of χ_{lf} and SOFT, slightly higher values of χ_{fd}

and χ_{ARM}, and lower values of χ_{fd}% and HIRM, compared to Ska1 and Ska2, which indicates that the dominant magnetic mineral is magnetite in the JL area. Ska2 exhibits high values of HIRM and low values of χ_{lf}, suggesting that haematite is a significant component of the magnetic mineralogy here. The tables indicate that the dominant magnetic mineral is magnetite in Lax and Ska1, two peat sections, characterised by low values of the magnetic concentration parameters, and therefore low concentrations of magnetic minerals. This could be due to simple dilution of the magnetic minerals of the organic matrix, and perhaps also to the dissolution of magnetic minerals in the peat environment (Williams, 1992). By comparing the two peat cores, it can be concluded that the magnetic mineral concentration is higher in Ska1 than in Lax.

Table 8.1 Summary of the magnetic measurements of tephra layers of JL2, JL1, Ska2, Ska1 and Lax, SE Iceland.

		Xlf	SOFT	Xfd	Xfd%	Xarm	SIRM	HIRM	SIRM/ARM	Xarm/SIRM	Xarm/Xlf	SIRM/Xlf	S20	S40	S100	S300
		$10^{-8}m^3kg^{-1}$	$10^{-5}Am^2kg^{-1}$	$10^{-8}m^3kg^{-1}$	%	$10^{-8}m^3kg^{-1}$	$10^{-5}Am^2kg^{-1}$	$10^{-5}Am^2kg^{-1}$	Am^{-1}	$10^{-3}mA^{-1}$		10^3Am^{-1}	%	%	%	%
JL2	Mean	447.49	2646.28	10.78	2.91	1617.63	11455.74	621.06	87.97	0.15	4.05	28.65	22.20	39.65	67.13	94.67
8	Minimum	48.57	218.55	1.43	1.65	180.77	823.58	28.51	57.23	0.11	2.70	16.96	9.50	19.51	48.64	87.94
	Maximum	1011.25	5790.77	16.70	5.64	2727.58	18178.41	2065.02	117.71	0.22	7.26	52.71	31.86	54.04	81.82	98.00
	SD	294.60	1746.87	5.00	1.18	845.58	5666.87	538.28	16.70	0.03	1.25	11.21	7.40	11.53	11.38	2.89
JL1	Mean	555.44	3119.89	15.30	3.05	2057.70	14552.77	587.55	90.95	0.14	4.05	30.70	21.68	40.17	69.79	96.00
21	Minimum	237.69	1023.19	11.73	1.94	1170.68	10152.14	291.38	63.89	0.09	2.97	19.18	9.15	22.72	50.72	91.74
	Maximum	955.22	5684.98	23.30	5.22	2842.89	19030.30	1473.02	133.89	0.20	6.73	71.69	29.87	52.27	80.47	97.97
	SD	201.02	1158.34	3.24	1.02	392.71	2793.20	306.93	20.90	0.03	1.16	16.39	7.10	9.87	10.06	1.70
Ska2	Mean	179.37	931.10	9.84	5.33	1054.95	6767.61	2993.87	82.92	0.15	5.98	39.31	13.60	27.95	57.39	93.62
44	Maximum	394.36	1860.65	24.77	7.52	2008.68	13061.80	6655.32	114.66	0.20	8.94	57.66	20.77	40.34	68.53	95.87
	Minimum	57.28	223.62	2.28	3.98	316.13	2523.17	1277.33	61.54	0.11	3.35	16.42	6.24	17.12	41.24	89.64
	SD	72.39	366.16	4.82	0.71	401.78	2350.42	1093.18	10.26	0.02	1.09	7.61	2.51	3.90	5.11	1.14
Ska1	Mean	141.61	746.44	6.62	4.57	885.97	5692.27	294.69	91.70	0.15	6.09	41.84	12.33	26.13	59.11	94.43
45	Minimum	44.72	142.12	0.68	0.81	116.56	1831.80	0.00	57.33	0.04	1.29	16.14	6.80	17.17	42.10	88.12
	Maximum	605.35	3265.86	19.63	7.09	2928.26	16354.13	1221.29	287.57	0.22	10.62	61.23	33.43	59.95	83.55	100.00
	SD	96.28	645.53	4.45	1.22	670.62	3509.83	217.02	34.33	0.03	2.04	11.58	4.26	7.11	9.15	2.81
Lax	Mean	89.28	343.74	5.24	5.35	395.81	3021.25	220.56	9.74	0.15	4.62	46.28	9.72	21.01	50.71	91.57
22	Minimum	13.39	48.52	0.17	1.25	58.31	536.63	39.00	1.97	0.03	3.11	11.23	5.01	12.05	37.43	88.08
	Maximum	296.24	1583.12	37.27	12.58	1039.55	7545.63	644.78	32.43	0.52	6.62	154.12	20.98	39.69	71.46	96.66
	SD	78.70	414.94	7.47	2.32	290.62	2096.96	125.70	7.65	0.10	0.99	35.92	4.46	7.79	10.14	2.35

Table 8.2 Summery of the VSM measurements ('loop2') of the tephra layers from Lax, Ska1, Ska2, JL1 and JL2, SE Iceland.

	Parameter	Xlow	Xlow5	Xhigh	Xferri	Xpara%	Xferri%	Ms	Mrs	Mrs/Ms	Mrs/Xlow	(Bo)cr	(Bo)c	(Bo)cr/(Bo)c
Lax	Mean	1.62	2.92	0.18	1.44	18.75	81.25	75.97	26.65	0.43	18.78	110.90	26.71	3.97
19	Minimum	0.38	0.45	0.13	0.25	3.93	63.78	12.09	5.05	0.22	11.17	24.53	12.00	1.46
	Maximum	5.14	8.42	0.23	4.94	36.22	96.07	268.91	64.37	0.62	34.60	435.99	50.00	14.29
	SD	1.49	2.71	0.03	1.47	10.42	10.42	78.10	18.90	0.12	6.25	104.28	11.49	3.16
Ska1	Mean	2.26	4.45	0.20	2.06	10.75	89.25	96.39	37.82	0.40	17.16	111.00	23.65	4.30
30	Minimum	0.73	1.58	0.07	0.53	3.68	72.64	31.12	8.17	0.22	8.87	23.35	12.50	1.24
	Maximum	7.04	14.88	0.27	6.78	27.36	96.32	329.63	121.51	0.54	28.20	489.72	36.50	16.09
	SD	1.34	2.96	0.04	1.31	4.69	4.69	59.51	23.08	0.08	4.83	121.35	6.39	4.16
Ska2	Mean	2.97	4.60	0.24	2.74	9.33	90.67	137.42	54.11	0.40	18.71	63.78	25.40	2.88
42	Minimum	0.00	1.65	0.00	0.00	3.58	79.18	0.15	0.06	0.17	6.69	22.74	3.50	1.01
	Maximum	5.94	7.83	0.36	5.69	20.82	96.42	246.39	116.32	0.51	28.24	261.78	39.00	15.00
	SD	1.33	1.70	0.07	1.29	4.21	4.21	59.07	25.88	0.07	4.15	51.45	6.90	2.94
JL1	Mean	8.81	20.54	0.10	8.71	3.21	96.79	370.48	109.48	0.38	15.28	49.30	17.71	2.71
17	Minimum	1.28	3.33	-0.03	1.04	-0.30	81.73	9.48	12.19	0.21	4.52	23.50	10.00	1.42
	Maximum	16.61	39.18	0.31	16.61	18.27	100.30	522.05	198.62	1.29	32.77	176.79	43.50	8.62
	SD	4.94	12.21	0.12	5.02	5.31	5.31	171.29	46.00	0.26	8.48	44.00	10.10	1.61
JL2	Mean	6.45	15.08	0.23	6.22	5.16	94.84	376.35	95.24	0.29	16.24	39.57	11.58	3.93
12	Minimum	0.02	1.21	0.00	0.02	0.06	85.77	0.50	0.16	0.17	8.40	15.30	2.50	1.39
	Maximum	12.87	35.05	0.37	12.77	14.23	99.94	765.79	161.93	0.50	29.48	61.76	24.00	6.86
	SD	4.75	10.69	0.14	4.70	4.22	4.22	276.12	59.98	0.11	7.02	16.16	5.26	1.79

The magnetic susceptibility χlf represents the total contribution of Fe-bearing minerals in the mineral assemblage, and is normally controlled by the total ferrimagnetic concentration (Thompson and Oldfield, 1986). Dearing *et al.*'s (1996, 1999) work indicates that ferrimagnetic minerals dominate magnetic mineral assemblages (i.e. values as $10^{-8}m^3kg^{-1}$). Magnetic susceptibility is controlled by the following factors, in order of decreasing importance: mineral concentration (χ_{lf} varies by a factor of 20,000-30,000), mineral composition (χ_{lf} varies by a factor of 300-400) and crystal size and shape (χ_{lf} varies by a factor of <200) (Dearing *et al.*, 1999). The values of magnetic susceptibility, vary from 12.3 to 341.2 (average 70.1) in Lax, and from 34.6 to 1061.0 (average 150.5) in Ska1 (Table 6.1), are high, especially in the tephra layers. It might be

that the mineral crystal size and shape control the magnetic parameters in both peat profiles. However, the situation is more complex in the loess-soil sections than that in peat. The mineral crystal size and shape control the magnetic parameters in Ska2, whereas the mineral composition controls the magnetic parameters in Jl1 and JL2. This is due to the fact that the magnetic susceptibility value varies from 48.4 to 492.9 (average 184.4) in Ska2, from 167.5 to 989.1 (average 628.0) in JL1, and from 48.6 to 1012.7 (average 644.1) in JL2 (Table 8.1).

8.2.2 Factor analysis of the magnetic data

Factor analysis is a multivariate statistical technique of data reduction and is concerned with explaining correlations amongst original variables (Chapter 4.6). This section uses the method to investigate associations within two types of magnetic parameter: (i) mass-specific parameters (i.e. χ_{lf}, SOFT, χ_{fd}, χ_{ARM}, SIRM, HIRM) and (ii) magnetic inter-parametric ratios (i.e. SIRM/ARM, χ_{arm}/SIRM, χ_{ARM}/χ_{lf}, SIRM/χ_{lf}, S_{-20}, S_{-40}, S_{-100}, and S_{-300}). The SPSS package was used for the analysis. Results are presented of the factor analysis of one peat section (Lax) and one soil section (Ska2). The results for the other sections are given in Appendix 4.

8.2.2.1 Lax

The factor analysis results of Lax are shown in Tables 8.3-8.6. Table 8.3 shows that two factors account for 93 % of the total original variance of six mass specific parameters. Factor 1 explains ~81 % of the variance, and consequently, most variables are strongly

related to this factor. The SIRM, χ_{ARM}, χ_{lf}, and SOFT show the highest loading on factor 1 (Table 8.4). Factor 2, in contrast, explains only 12.37 % of the variance, and is mainly associated with HIRM. In the case of the factor analysis of the inter-parametric ratios, three factors (with eigenvalues >10) explain 76.2 % of the total original variance (Table 8.5). Factor 1 shows the strongest correlations with S_{-40} and S_{-100}; factor 2 shows the strongest correlations with χ_{ARM}/χ_{lf}; and factor 3 shows the strongest correlation with of χ_{ARM}/SIRM (Table 8.6).

Table 8. 3 Results of factor analysis of the mass-specific magnetic parameters for Lax - total variance explained.

Total Variance Explained-Lax

Component	Initial Eigenvalues			Extraction Sums of Squared Loadings			Rotation Sums of Squared Loadings		
	Total	% of Variance	Cumulative %	Total	% of Variance	Cumulative %	Total	% of Variance	Cumulative %
1	4.835	80.582	80.582	4.835	80.582	80.582	3.921	65.348	65.348
2	.742	12.370	92.952	.742	12.370	92.952	1.656	27.605	92.952
3	.308	5.128	98.080						
4	7.728E-02	1.288	99.368						
5	2.956E-02	.493	99.860						
6	8.372E-03	.140	100.000						

Extraction Method: Principal Component Analysis.

Table 8.4 Results of factor analysis of the mass-specific magnetic parameters for Lax - component matrix.

Component Matrix--Lax[a]

	Component	
	1	2
XLF	**.960**	-.211
SOFT	.953	-.199
XFD	.838	-.242
XARM	**.964**	-8.44E-02
SIRM	**.969**	.192
HIRM	.658	**.746**

Extraction Method: Principal Component Analysis.

a. 2 components extracted.

Table. 8.5 Results of factor analysis of the magnetic inter-parametric ratios for Lax - total variance explained

Total Variance Explained--Lax

Component	Initial Eigenvalues			Extraction Sums of Squared Loadings		
	Total	% of Variance	Cumulative %	Total	% of Variance	Cumulative %
1	3.123	39.038	39.038	3.123	39.038	39.038
2	1.505	18.818	57.856	1.505	18.818	57.856
3	1.470	18.381	76.237	1.470	18.381	76.237
4	.896	11.202	87.439			
5	.409	5.110	92.549			
6	.380	4.746	97.295			
7	.146	1.825	99.120			
8	7.043E-02	.880	100.000			

Extraction Method: Principal Component Analysis.

Table 8.6 Results of factor analysis of the magnetic inter-parametric ratios for Lax - component matrix.

Component Matrix--Lax[a]

	Component		
	1	2	3
XFD100	-4.20E-02	.516	-.130
XARMSIRM	.268	.340	**-.794**
XARMXLF	-.237	**.793**	-8.56E-02
SIRMXLF	-.534	.108	.699
S20	.883	-.273	6.151E-02
S40	**.943**	-6.33E-02	.119
S100	.902	.213	.155
S300	.475	.600	.534

Extraction Method: Principal Component Analysis.

a. 3 components extracted.

8.2.2.2 Ska2

Tables 8.7-8.10 show factor analysis results for the magnetic concentration parameters for Ska2. Two factors account for 92 % of the total original variance (Table 8.7). Factor 1 is associated with all six parameters, especially χ_{ll}, χ_{ARM}, and χ_{fd}. In contrast, factor 2 is strongly correlated with HIRM and SIRM. Tables 8.9 and 8.10 give the factor analysis results for the inter-parametric ratio parameters for Ska2. Three factors, with eigenvalues >10, account for 75.5% of the total original variance (Table 8.9). Factor 1 is strongly

correlated with S_{-20} and S_{-40}; factor 2 has the strongest correlation with χ_{ARM}/χ_{lf} and factor 3 has a the strongest correlation with χ_{fd}% (Table 8.10).

Table 8.7 Results of factor analysis of the mass-specific magnetic parameters for Ska2 - total variance explained.

Total Variance Explained--Ska2

Component	Initial Eigenvalues			Extraction Sums of Squared Loadings			Rotation Sums of Squared Loadings		
	Total	% of Variance	Cumulative %	Total	% of Variance	Cumulative %	Total	% of Variance	Cumulative %
1	4.578	76.294	76.294	4.578	76.294	76.294	3.904	65.058	65.058
2	.940	15.662	91.956	.940	15.662	91.956	1.614	26.897	91.956
3	.342	5.694	97.650						
4	8.324E-02	1.387	99.037						
5	3.712E-02	.619	99.656						
6	2.065E-02	.344	100.000						

Extraction Method: Principal Component Analysis.

Table 8.8 Results of factor analysis of the mass-specific magnetic parameters for Ska2 - component matrix.

Rotated Component Matrix--Ska2

	Component	
	1	2
XLF	**.963**	.101
SOFT	.904	.335
XFD	.943	6.418E-02
XARM	.811	.483
SIRM	.774	.584
HIRM	.115	**.956**

Extraction Method: Principal Component Analysis.
Rotation Method: Varimax with Kaiser Normalization.
a. Rotation converged in 3 iterations.

Table 8.9 Results of factor analysis of the magnetic inter-parametric ratios for Ska2 - total variance explained.

Total Variance Explained--Ska2

Component	Initial Eigenvalues			Extraction Sums of Squared Loadings		
	Total	% of Variance	Cumulative %	Total	% of Variance	Cumulative %
1	4.118	51.471	51.471	4.118	51.471	51.471
2	1.575	19.691	71.162	1.575	19.691	71.162
3	1.069	13.367	84.529	1.069	13.367	84.529
4	.670	8.373	92.901			
5	.318	3.969	96.870			
6	.137	1.715	98.585			
7	9.817E-02	1.227	99.812			
8	1.501E-02	.188	100.000			

Extraction Method: Principal Component Analy sis.

Table 8.10 Results of factor analysis of the magnetic inter-parametric ratios for Ska2 - component matrix.

Component Matrix–Ska2

	Component		
	1	2	3
XFD100	.115	.288	**.882**
XARMSIRM	.780	.394	.166
XARMXLF	-.359	**.906**	-7.86E-02
SIRMXLF	-.786	.534	-.197
S20	**.925**	-.137	-.115
S40	.918	8.593E-02	-3.27E-02
S100	.888	.333	-5.33E-02
S300	.512	.306	-.449

Extraction Method: Principal Component Analysis.
a. 3 components extracted.

8.2.2.3 Significance of the factor analysis results

The factor analysis results show that for both the magnetic concentration parameters and the inter-parametric ratios, a large proportion of the statistical variance can be summarised by a small number of factors. However, the most parsimonious reduction of the data is achieved in the case of the magnetic concentration parameters: for Lax and Ska2 respectively, ~93% and ~92% of the statistical variance are explained by the first two factors. In the case of the magnetic inter-parametric ratios, the values are ~58% for Lax and ~71% for Ska2.

In the case of the factor analysis of the magnetic concentration parameters, at both sections χ_{lf} has the highest loading with factor 1 and HIRM has the highest loading with factor 2. This indicates that the variations in the concentration of ferrimagnetic and canted antiferromagnetic minerals, probably magnetite and hematite respectively, dominate the parameters. These conclusions are similar to those based on both cluster analysis and factor analysis of soil samples by Lees (1994, 1999).

In the case of the factor analysis of the magnetic inter-parametric ratios for Lax, S_{-40} and S_{-100} have the highest loading on factor 1; χ_{ARM}/χ_{lf} has the highest loading on factor 2; and χ_{fd}% as the highest loading on factor 3. In the case of Ska2, S_{-40} has the highest loading on factor 1; χ_{ARM}/χ has the highest loading on factor 2; and χ_{fd}% has the highest loading on factor 3. One explanation for the slight difference could be that the magnetic material in the Lax peat section should be associated entirely with air-fall tephra; in contrast, in the Ska2 soil section there will be a significant 'background' contribution from local soil, as well as from air-fall tephra. Another possible explanation is that the magnetic material in the peat section has been affected by dissolution in the peat environment (Williams, 1992).

The factor analysis results demonstrate that χ lf and HIRM are most important among the mass specific parameters. And S20, S40 and χ_{ARM}/χ lf are quite important in the ratio parameters.

8.3 Inferred magnetic mineralogy

Factor analysis of the magnetic concentration data showed that χ_{lf} and HIRM are especially significant parameters, reflecting variations in the concentration of ferrimagnetic and canted antiferromagnetic material, respectively. Therefore, for these samples bi-variate plots of χ_{lf} and HIRM should provide a simple means of displaying the magnetic mineral variability. Figure 8.1 shows the plot of HIRM versus χ_{lf} for all of the tephra layers from the five sections, Lax, Ska1, Ska2, JL1 and JL2. JL1 and JL2, the two soil sections, show relatively high values of χ_{lf} and relatively lower values of

HIRM. This indicates that the dominant magnetic minerals are ferrimagnetic, probably magnetite. In contrast, Ska2 exhibits lower values of χ_{lf} and higher values of HIRM, respectively. This suggests that in this section, canted antiferromagnetic material, probably hematite is a more significant component of the magnetic mineralogy than that at JL1 and JL2. Figure 8.1 also shows that at Lax and Ska1, the dominant magnetic mineral type is ferrimagnetic, and that the concentrations of ferrimagnetic material are much lower than in the soil profiles. This is likely to be due to simple dilution by the organic matrix, but could also reflect dissolution of magnetic material, suggested in section 8.2. Finally, it can be seen that the concentration of magnetic minerals is higher in Ska1 than in Lax.

The parameters of S-100 and χ ferri % are particularly useful in discriminating ferrimagnetic components (Snowball, 1993). The magnetic measurement results for the tephra layers in the five sections show that the value of χ ferri ranges from 0.03 to 11.1 $\times 10^{-8} m^3 kg^{-1}$ (Tables 5.2-5.6), indicating that the total contribution of ferrimagnetic material to the magnetic susceptibility is significant. χ para% (~4-21 %) and the values of χ ferri % (~80-96 %) and χ lf (>$50\times10^{-8} m^3 kg^{-1}$, with the exception of one sample) also suggest that the dominant magnetic minerals in tephra are ferrimagnetic.

The full hysteresis loops of the 127 tephra layers samples, which are shown in Appendix 1 and Chapters 6 (Tables 6.2, and 6.4) and Chapter 7 (Tables 7.1, 7.3 and 7.5) show that there is a ferrimagnetic component in some tephra layers, whose loops are shown as quite thin. For example, the loops of the samples from depth 14 cm at Lax and from

depth 38-40 cm at JL1 (Appendix 1), these loops rise steeply, and saturate at 300 mT. However, most loops indicate that there is a significant paramagnetic component in the majority of samples, whose loops' width is only between +/-200mT. In addition, some of the curves (e.g. the loops from depths of 123 cm and 161 cm at Lax and 115 cm at Ska1) are only between +/-100mT in field, which show paramagnetic minerals (Appendix 1).

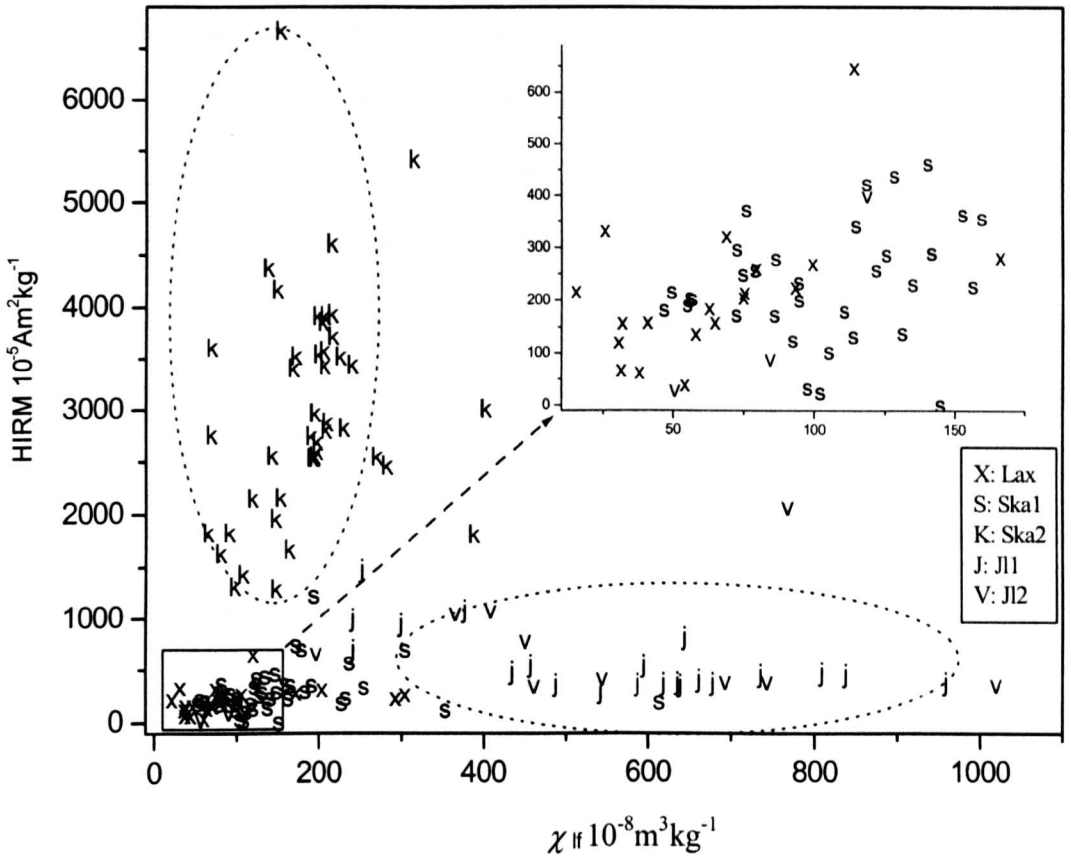

Figure 8.1 Scatter plot of HIRM against χ lf for the five sections: Lax, Ska1, Ska2, JL1 and JL2, SE Iceland, the detail within the marked area is shown on an expended scale in the upright corner.

Some of the reversible curves, such as the curves of samples from the depths 230 cm and 247 cm at Ska1 and samples from the depth of 4cm and 32cm at Lax (Appendix 2), with Curie temperature (*Tc*) close to 580 °C, are probably pure magnetite. Most of the reversible curves in the figures, which show no clear *Tc*, suggest a significant contribution from paramagnetic minerals (Appendix 2).

In summary, there are some magnetite components in some of the tephra layers (e.g. at the top of the Lax section). The 'loop2' parameters show the dominant magnetic minerals are ferrimagnetic, and the factor analysis results demonstrate the magnetic properties are dominated by ferrimagnetic and canted antiferromagnetic minerals, probably also magnetite and haematite. At the same time, the thermomagnetic curves, which have no clear *Tc*, and most of the hysteresis loops, which are extremely narrow (only between +/-200mT), show that there are abundant paramagnetic mineral contributions to the tephra.

8.4 Magnetic mineral grain size

Magnetic properties can also give the information about the magnetic grain size or domain configuration of the dominant magnetic constituents of samples, particularly in the case of ferrimagnetic minerals. It is usually possible to distinguish between samples of dominantly MD, PSD, SD and SP magnetic composition. Some magnetic parameters are concentration independent (Robinson, 1997), and reflect the relative proportions of different grain sizes. Such parameters are usually either ratios of two magnetic parameters, which are primarily concentration-dependant (Robinson, 1997), or are

values for magnetic fields at which samples attain characteristic states of magnetization during a systematic analysis of the incremental acquisition, or coercive-remagnetization, of a sample. Those parameters include SIRM/χ, χ_{ARM}/χ, χ_{ARM}/SIRM, SIRM/ARM and χ_{fd} %, and they are, primarily, influenced by either the mineralogical or granulometric composition of a sample's magnetic assemblage, rather than by its bulk concentration of magnetic constituents.

High values of χ_{fd} % indicate the presence of ferrimagnetic grains lying at the stable single domain/superparamagnetic boundary (~0.02 μm). The χ_{fd} % values are intermediate (~2.0-10.0 %), which indicate there might be an admixture of SP and coarse grains, or SP grains < 0.005 μm (Dearing, 1999) in these five sections. In detail, there are a few layers (e.g. 134-138 cm, 172-176 cm, and 226-228 cm in Ska1- Chapter 6, Fig. 6.2) which have a significant proportion of SP grains with χ_{fd} % values >6. But for most layers, whose values of χ_{fd} % is less than 5, SP grains do not significantly influence the assemblage (e.g. Chapter 6, Figs. 6.1-6.2; Chapter 7, Figs. 7.1-7.3).

Magnetic materials can also be classified by determining their magnetization and coercivity ratios (Day *et al.*, 1977; Thompson and Oldfield, 1986). Single domain (SD) grains are characterized by $M_{rs}/M_s>0.5$, and $(B_0)_{cr}/(B_0)_c<1.5$, and multidomain (MD) grains are characterized by $M_{rs}/M_s<0.1$ and $(B_0)_{cr}/(B_0)_c>4$. Accordingly, these hysteresis properties for the five sections are plotted on a "Day plot" (Day *et al.*, 1977) with the regions for the SD, PSD and MD behaviour are highlighted (Figure 8.2). These plots show that most of the magnetic grains are PSD.

Figure 8.3 compares the χ_{fd}% and χ_{ARM}/SIRM data with the results of a quantitative mixing model (Dearing *et al.*, 1997; Xie *et al.*, 2000). These results conform that most of the common magnetic minerals are PSD and MD in these samples (Dearing *et al.*, 1997).

Figures 8.2 and 8.3 also indicate that most of the magnetic minerals are PSD and MD in these samples (Day *et al.*, 1977; Thompson and Oldfield, 1986; Dearing *et al.*, 1997). In addition, both the mass specific (e.g. χ, χ_{fd}, χ_{ARM} and SIRM) and the ratio parameters (e.g. SIRM/χ_{lf}, χ_{ARM}/SIRM) indicate the predominance of MD ferrimagnetic grain components (Chapter 6, Figs. 6.1-6.2; Chapter 7, Figs. 7.1-7.3).

8.5 Comparison of the magnetic properties of individual volcanic eruption events

Several volcanic eruption events have been defined based on their geochemical composition and position within the profiles (Chapter 5). Here, the magnetic signatures of the tephra derived from the same eruption event are compared in order to check the consistency of its magnetic hysteresis parameters and *Tc* curves.

The results of hysteresis loop and *Tc* curves measurements of bulk samples are shown in Table 8.11 and Figures 8.4 and 8.5, respectively. The hysteresis loops of bulk tephra from Oreafa 1362 from the Lax peat section are quite different from those from the three

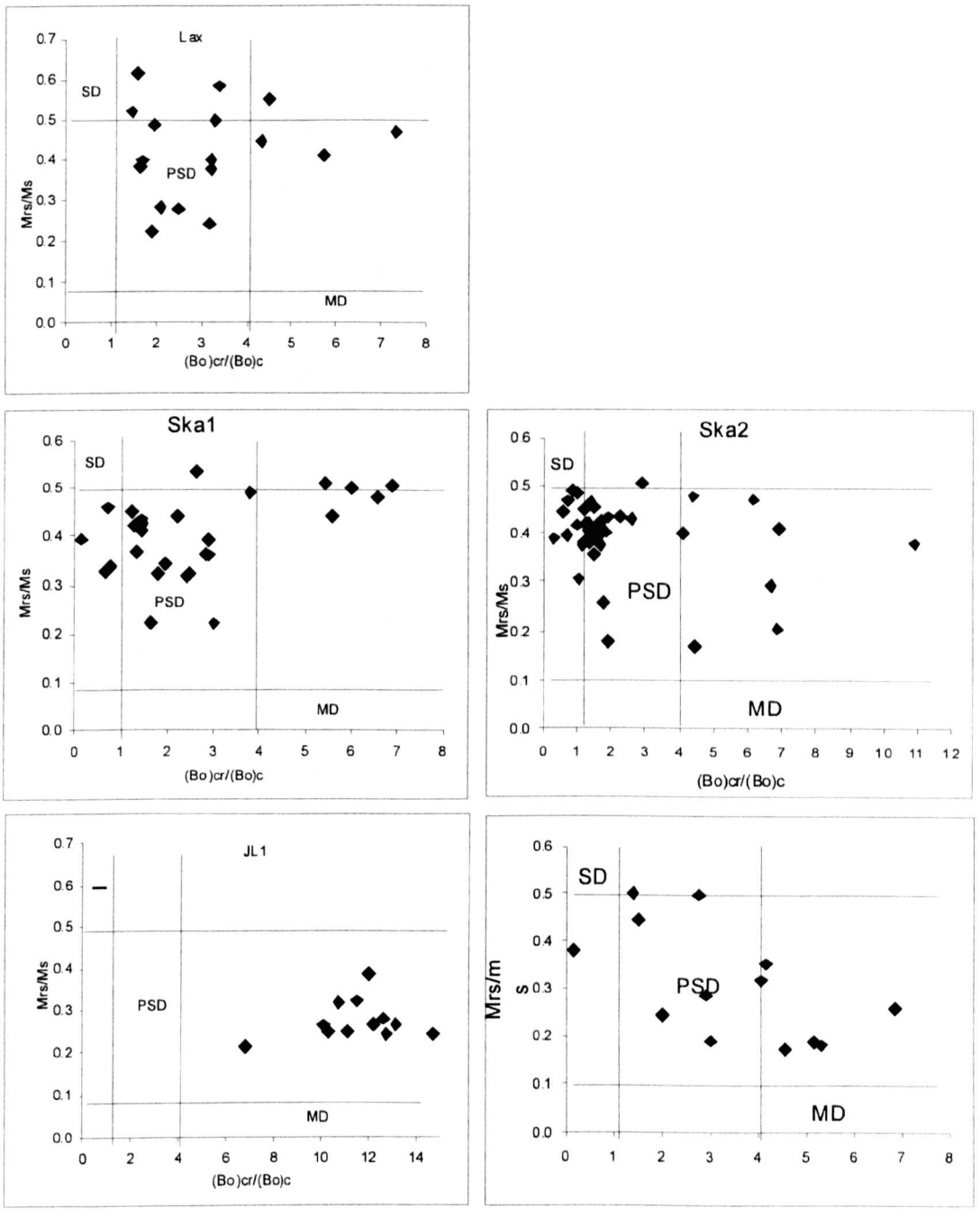

Fig 8.2 Magnetic mineral grain size of the five profiles/cores (Lax, Ska1, Ska2, Jl1 and Jl2), SE Iceland (After Day et al, 1977; Thompson and Oldfield, 1986).

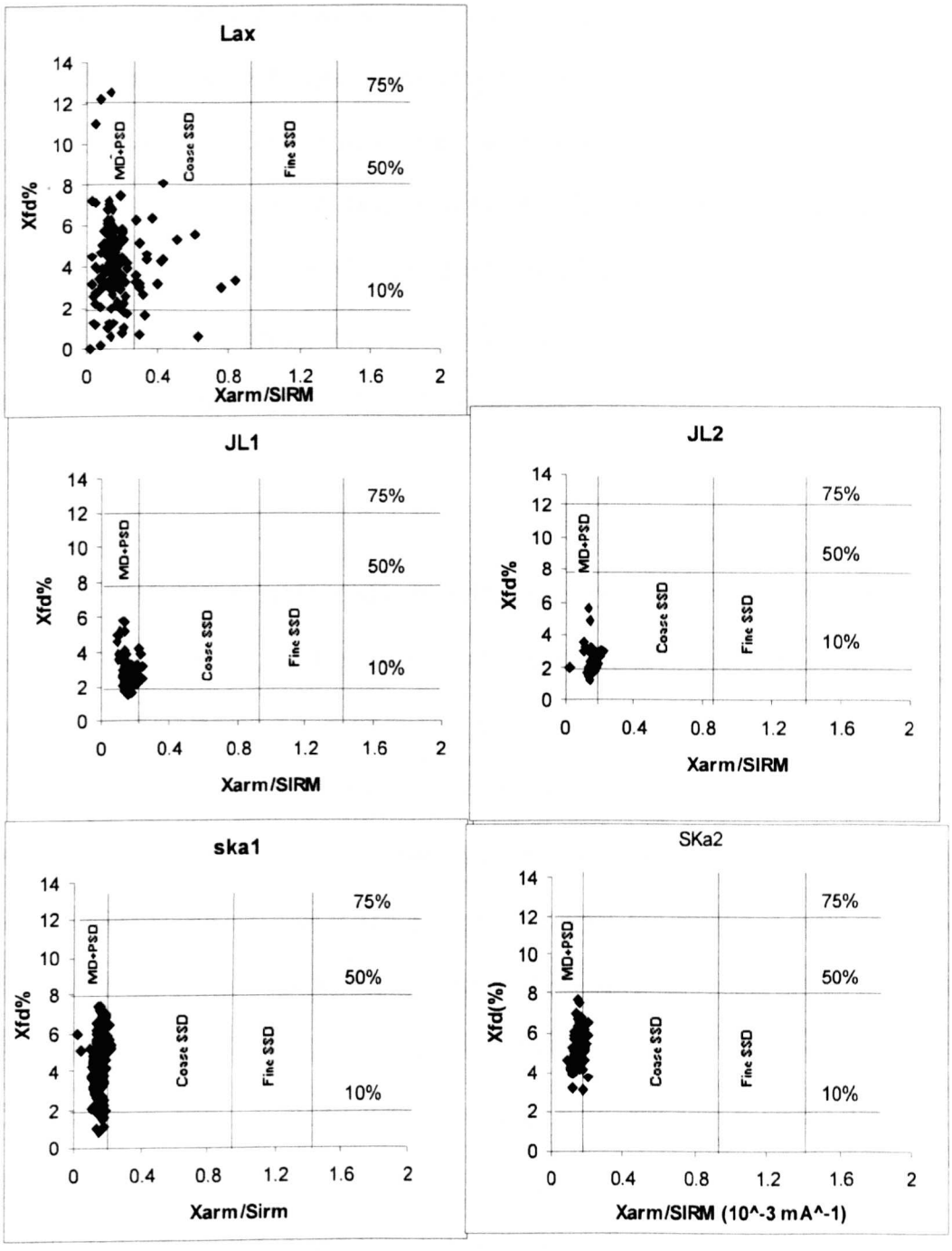

Fig 8.3 Ferrimagnetic grain size analysis of Icelandic tephra samples. The pot of Xfd versus Xarm/SIRM (Dearing et al., 1997; Xie, 2000)

soil sections Ska2, JL1 and JL2 (Figure 8.4). This could be the result either of the dissolution of magnetic minerals and/or to the presence of 'background' locally-derived material in addition to the air-fall tephra in the soil sections. The hysteresis loops of the tephra from same volcanic centre, for example, the Grimsvötn G650 (175.5-178.5 cm in Ska1), G1982 (26-28 cm at Ska2) and G1354 (194-196 cm at Ska2), have different shapes. At the same time, the bulk tephra from different volcanic centres, for example, G1892 (26-28 cm at Ska2) and O1727 (84-86 cm at Ska2) have very similar loops. In addition, the *Tc* curve of Öraefa 1362 from Lax is different from the *Tc* curves from Ska2, JL1 and JL2 (Figure 8.5).

A further analysis was performed to investigate the hysteresis properties of tephra samples, which had been subject to a density separation procedure (see Chapter 4, section 4.53). This would be expected to reduce the possible problem of local 'contamination' of the air-fall tephras in the soils. The results of the VSM analysis (Fig. 8.6) indicate that the shape of the loops of the bulk sample is in fact quite similar to that of the sub-sample with density >2.8 g/ml. For example, the sample at depth 26-28 cm from Ska2 was divided into four sub-samples of densities <2.4 g/ml, 2.4-2.6g/ml, 2.6-2.8g/ml and >2.8g/ml. In addition, the bulk sample of this layer was measured as well. If the sub-sample with density 2.4-2.8 g/ml is taken to consist of pure tephra shards (Turney, 1996; 1998), and the sub-sample with density >2.8 g/ml is taken to represent locally-derived material, then this probably indicate that the background materials dominate the bulk sample.

The results obtained in the present study imply that the hysteresis and *Tc* characteristics of the same tephra layer at different sites are insufficiently consistent to provide a reliable basis for correlating tephra layers from one profile to the next (Figures 8.4 and 8.5 and Table 8.11). This conclusion is similar to that of previous work, which was based on magnetic characterization of bulk samples (e.g. Robertson, 1993; Gonzalez *et al.*, 1999). Gonzalez *et al.* (1999) suggested that reason for this could be either because the same number of tephras is not represented in studied profiles and/or because significant changes in magnetic grain size of the same tephra layer occur over short distances. Based on the experimental results, the present writer believes that the reason for the lack of consistency of the magnetic signatures of the bulk samples is the presence of locally derived material.

The character of tephra layers are readily described in field in term of their colouration, degree of weathering, lithic content, granulometric parameters, sedimentary structures, distribution, thickness, and stratigraphic context, which may provides sufficient control for identification and correlation in regions close to source vents. The former part indicates that bulk tephra analyses do not satisfy this condition

Table 8.11 Summary of the magnetic signatures of bulk tephra samples from known volcanic eruptions.

Profile	Depth (Cm)	Name	color	Loop type	Tc type	Tcc
Lax	17 ~19	K1918	dark grey	1	3	n
	35 ~37.5	O1362	white	4	3	575
	121 ~123	Vt-c 550	white	4	4	n
Ska1	75 ~77.5	K1721	black	3	3	n
	133 ~134	H1158	white	4	3	n
	175.5 ~178.5	G650	green	2	2	n
	230 ~231	HS	white	1	2	575
Ska2	26 ~28	G1982	black	3	3	n
	84 ~86	O1727	grey	3	3	n
	104 ~106	G1659	black	3	3	n
	168 ~170	V1477	black	3	3	n
	194 ~196	G1354	white	1	1	575
	222 ~224	V1340	black	3	3	n
	228 ~230	G1159	black	3	3	n
	256 ~258	V870	white	4	3	n
	274 ~276	G150	black	3	3	n
	298 ~300	SW	black	4	4	n
	354 ~356	H4	white	3	4	n
JL1	38 ~40	E1821	black	1	2	575
	173 ~173	V1717	black	2	1	575
	189 ~190	O1362	white	1	1	575
JL2	74 ~76	V1697	black	1	2	575
	86 ~88	O1362	white	1	1	575

Note: LP, loop; Tc, Curie temperature curve; Tcc, Curie temperature point; n, no Tc point. In column LP, 1~-5 indicates the hysteresis loop type (see Chapter 6, Figure 6.3). In column Tcc: 1-4 indicates the Tc curve type (See Chapter 6, Fig. 6.6).

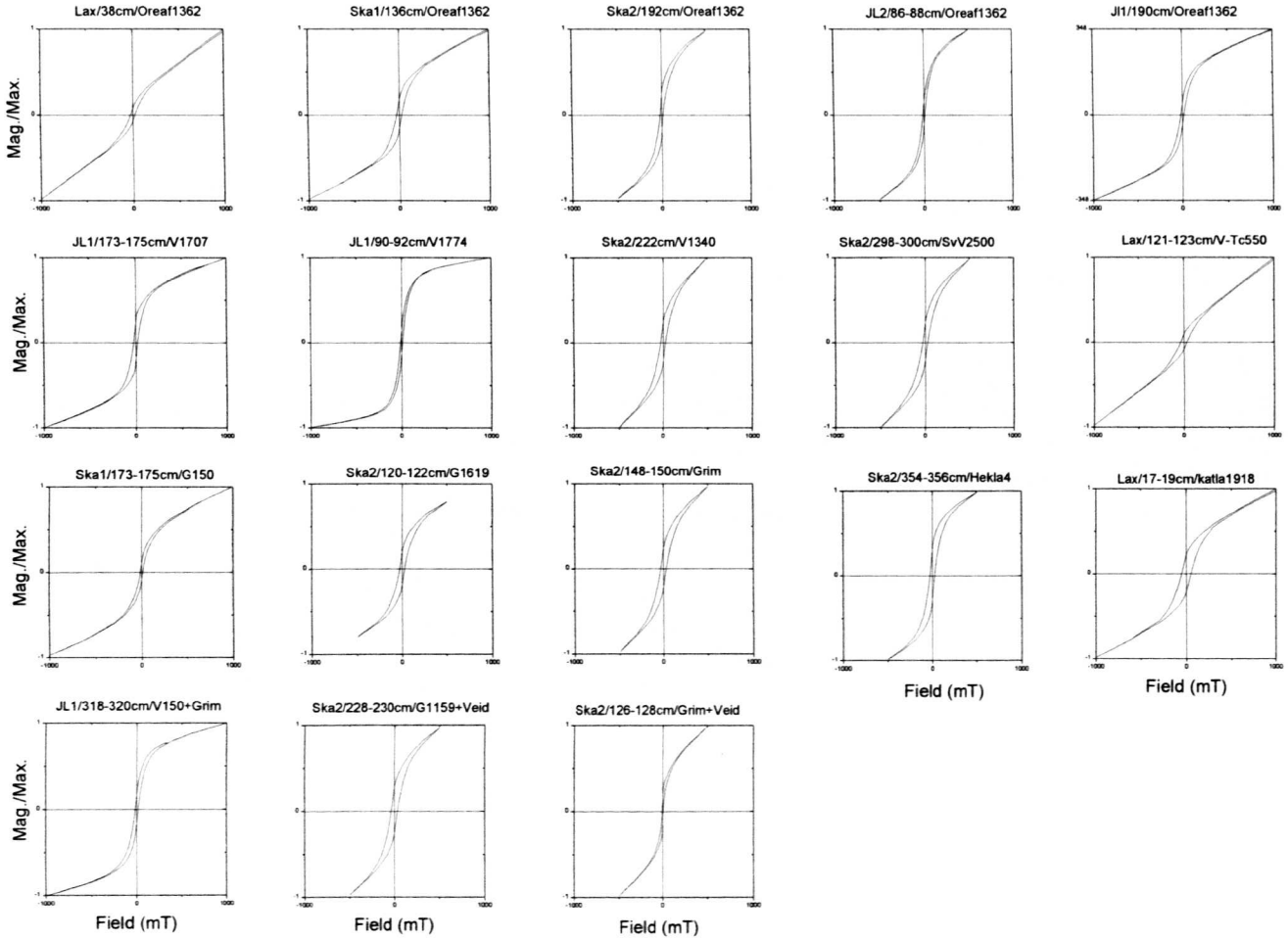

Figure 8.4 Comparing magnetic hysteresis loops of same tephra events.

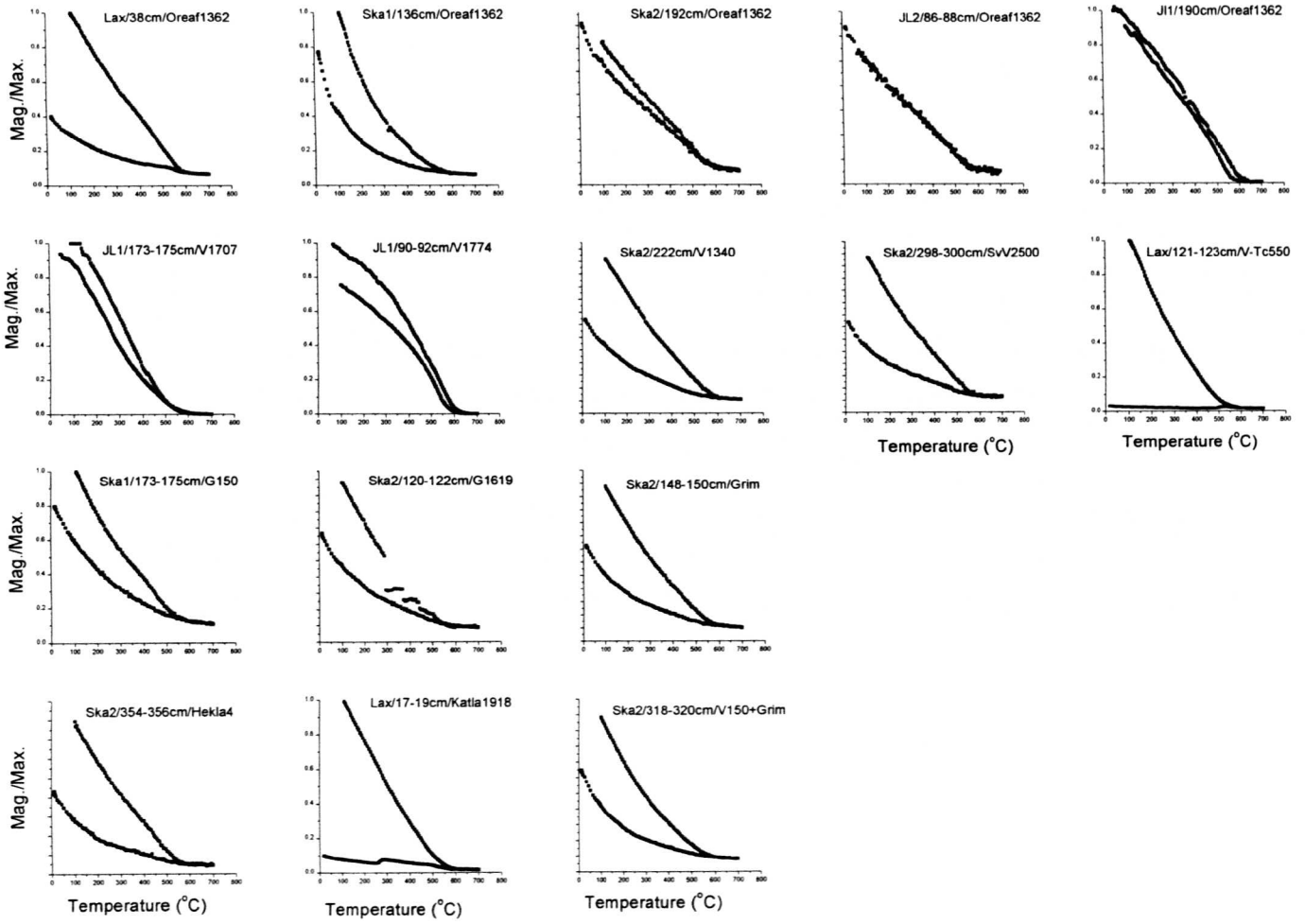

Figure 8.5 Comparison of themomagnetic curves of same tephra events.

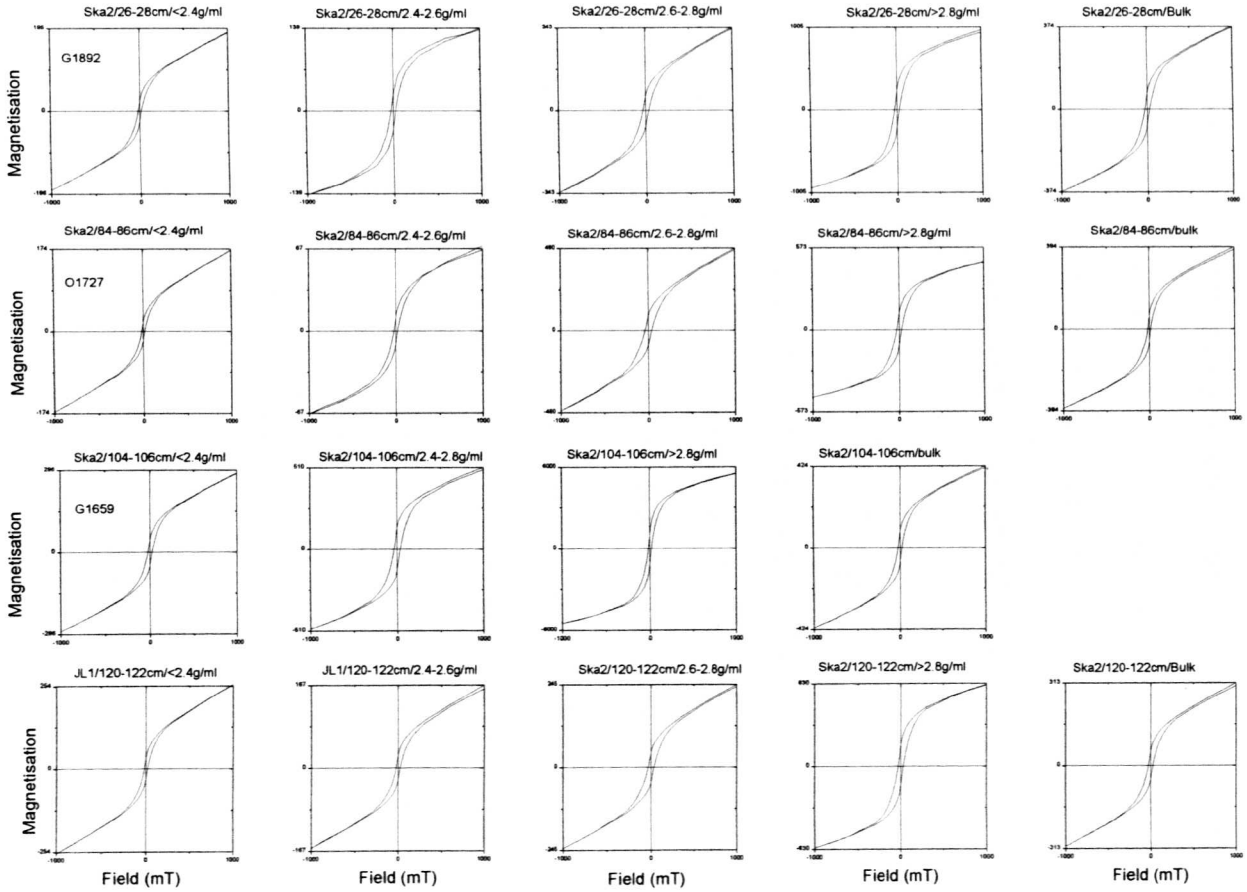

Figure 8.6 Magnetic hysteresis loops of same tephra events with different density.

8.6 Correlation of the tephra layers using multivariate statistical analysis

The previous section showed that the use of hysteresis loop and Curie temperature analysis of the density-separated tephra shard samples did not produce convincing results in term of establishing consistent magnetic 'fingerprints' for the same tephra present at more than one site. This section describes an alternative approach, based on the multivariate analysis of bulk tephra samples.

Principal coordinates analysis (PCO, Kovach, 1995) was applied to 15 magnetic properties from selected tephra layers from the 5 sections to get the distance and similarities between the measurement results directly, and the eigenvectors represent the scores for the samples (Chapter 4). The magnetic properties are: χ_{lf}, SOFT, χ_{fd}, $\chi_{fd\%}$, χ_{ARM}, SIRM, HIRM, SIRM/ARM, χ_{ARM}/SIRM, χ_{ARM}/χ_{lf}, SIRM/χ_{lf}, S_{-20}, S_{-40}, S_{-100}, and S_{-300}. The similarity and distance measures can then be used to help correlation of tephra layers from one section to the next in a multidimensional scaling. Prior to the analysis, each magnetic parameter was normalised so that it ranged from 0-1. The complete PCO analysis results are shown in Appendix 7.

The results of SC and ED analysis to correlate the two soil sections of JL1 and Jl2 are shown in Table 8.12. The title row in the table shows the tephra layers in JL2, and the first column is the depth of tephra layers in JL1. The numbers in the table are the ED and SC values calculated between different tephra layers in the two sections, with lower values in ED and higher values in SC, indicating greater similarity, respectively. With guidance provided by tephra layer stratigraphic relationships, tephra colour, and

geochemical measurements, the tephra layers can be correlated quite well between the two sections. The analysis was repeated for Ska2 and JL1, and between each pair of the five sections (the results are shown in Appendix 7). However, the correlation becomes more difficult and the results less convincing due to the greater distance between the two study sites. This is presumably because the tephra has been subjected to sedimentary fractionation. Such information includes local value, providing data pertinent to location of the source vent as well.

Figure 8.7 shows the lithology of the two peat cores and three soil profiles together, based on stratigraphic relationships, tephra colour, magnetic and geochemical properties, and the results of calculating ED and SC. It is not very difficult to correlate tephra layers from one section to the next within the same study area on the basis of the magnetic properties, as in the case of JL1 and JL2. However, in the case of sections from different locations, it is much more difficult to correlate all of the tephra layers between sections. Using several distinctive tephra layers as lithological marker layers (e.g. the AD 1362 Oraefa tephra), most of the tephra layers in the five sections can be roughly correlated from one section to another. Tephra layer correlation was performed first time here using magnetic measurements. It demonstrates that magnetic techniques do have the potential to facilitate identification and correlation of distal tephra.

Table 8.12 Similarity cofficient (SC) and Euclidean distance (ED) between tephra layers from JL1-JL2, SE Iceland.

JL1 \ JL2		51 cm	61 cm	75 cm	79 cm	87 cm	89 cm	113 cm	115 cm
39 cm	ED	0.06005	0.09235	0.11775	0.07654	0.09501	0.03014	0.04747	0.04399
	SC	0.99849	0.99618	0.99379	0.99741	0.99587	0.99962	0.999	0.99921
85 cm	ED	0.07931	0.09859	0.10558	0.06426	0.08298	0.04962	0.02797	0.05902
	SC	0.99734	0.99566	0.99496	0.99815	0.99682	0.99894	0.99965	0.99856
91 cm	ED	0.04454	0.09232	0.12958	0.08936	0.10705	0.01647	0.06462	0.03706
	SC	0.99918	0.99617	0.99252	0.99648	0.9948	0.99989	0.99816	0.99943
93 cm	ED	**0.02057**	0.10425	0.15437	0.11425	0.12623	0.01343	0.08656	0.02692
	SC	**0.99983**	0.99512	0.9895	0.99432	0.99288	0.99992	0.99675	0.99968
131 cm	ED	0.0738	0.09787	0.11022	0.06883	0.08608	0.04424	0.0336	0.05383
	SC	0.9977	0.99572	0.99452	0.99789	0.99659	0.99916	0.9995	0.99881
149 cm	ED	0.07179	0.09737	0.10735	0.06648	0.08896	0.0426	0.03634	0.05623
	SC	0.99785	0.99577	0.99479	0.99802	0.99635	0.99924	0.99941	0.9987
151 cm	ED	0.06578	**0.08016**	0.10858	0.06814	0.09219	0.03637	0.05046	0.05319
	SC	0.99819	**0.99714**	0.99472	0.99795	0.9961	0.99944	0.99886	0.99882
171 cm	ED	0.20653	0.16716	**0.03787**	0.0751	0.12031	0.17771	0.11154	0.19169
	SC	0.98123	0.98771	**0.99933**	0.99739	0.99336	0.98594	0.99429	0.98382
181 cm	ED	0.22877	0.18414	0.06171	0.0964	0.12995	0.19913	0.12954	0.21133
	SC	0.97676	0.98495	0.99819	0.99565	0.99223	0.98219	0.99224	0.98016
185 cm	ED	0.05864	0.08562	0.12444	0.08262	0.09277	0.02828	0.05273	0.03569
	SC	0.99853	0.99671	0.99313	0.99702	0.99611	0.99965	0.9988	0.99948
189 cm	ED	0.08101	0.09953	0.13692	0.09608	**0.09443**	0.0568	0.05754	0.04832
	SC	0.9971	0.99554	0.99172	0.99598	**0.99602**	0.99855	0.9986	0.99898
191 cm	ED	0.03864	0.095	0.14098	0.09971	0.10809	**0.01005**	0.06971	0.02193
	SC	0.99937	0.99594	0.99122	0.99567	0.99476	**0.99996**	0.9979	0.9998
215 cm	ED	0.06064	0.09433	0.12402	0.08226	0.0937	0.03124	**0.04813**	0.03821
	SC	0.99844	0.996	0.99314	0.99702	0.99601	0.99958	**0.999**	0.9994
219 cm	ED	0.04523	0.09292	0.14497	0.10311	0.10858	0.02168	0.0703	**0.01568**
	SC	0.99911	0.99612	0.99077	0.99541	0.99475	0.99979	0.9979	**0.9999**
227 cm	ED	0.14461	0.1269	0.06114	0.03885	0.07348	0.11452	0.03877	0.12337
	SC	0.99094	0.99291	0.99824	0.99929	0.99751	0.99425	0.99932	0.99345
275 cm	ED	0.03964	0.09372	0.13775	0.09669	0.10971	0.00999	0.06776	0.02555
	SC	0.99934	0.99605	0.9916	0.99592	0.99458	0.99996	0.99801	0.99973
319 cm	ED	0.12463	0.10514	0.09371	0.06	0.07185	0.09472	0.03518	0.09658
	SC	0.9932	0.99508	0.99601	0.99836	0.99761	0.996	0.99943	0.99595

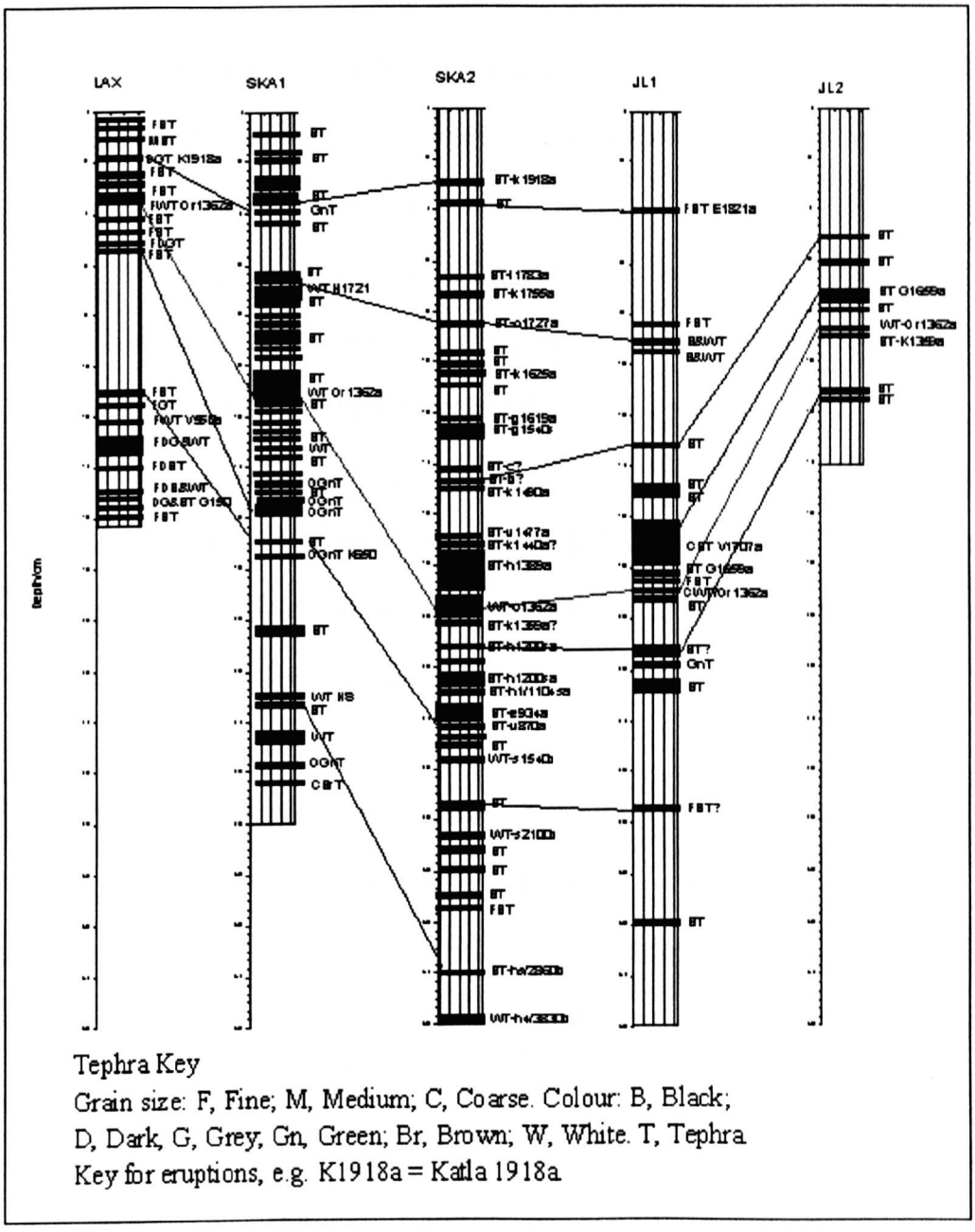

Figure 8.7 Correlation of tephra layers between the 5 sections of Lax, Ska1, Ska2, JL1 and JL2, SE Iceland, based on stratigraphic relationships, tephra colour, magnetic and geochemical measurements properties and SC and ED analysis.

8.7 Summary

The primary objective of this study was to investigate the application potential of magnetic techniques to characterize Icelandic tephra. This chapter focuses on the magnetic characteristics of tephra in terms of the response of magnetic parameters to the differences in composition and granulometry of the magnetic mineral assemblages present. Magnetic parameters provide indications of magnetic concentrations, magnetic mineralogy and magnetic grain sizes (See Chapter 2). Interpretation of magnetic parameters is complicated by the fact that they are influenced by three controls (i.e. mineral type, mineral concentration and grain size). Mineral type and the concentration of minerals (especially ferrimagnetic minerals) affect direct measurements whereas ratios of certain magnetic parameters can eliminate the effects of concentration and mineral type and indicate grain size.

Results of the magnetic measurements of the three soil sections show that magnetic techniques have advantages for studying the properties of tephra (chemical composition / mineralogy / grain size), which might be dependent on their volcanic centres and regional contribution. It is concluded that the main magnetic minerals in the tephras are ferrimagnetic minerals (e.g. magnetite) and canted antiferromagnetic minerals (e.g. haematite), with abundant paramagnetic material also present. Cross plots of M_{rs}/M_s vs. $(B_0)_{cr}/(B_0)_c$ and χ_{fd} % vs. χ_{ARM}/SIRM indicate the main magnetic grain sizes in these tephras are PSD and MD.

The results indicate that the fingerprint of both hysteresis and Curie temperature properties are insufficiently consistent within layers to provide a sound basis for correlating tephra layers from one profile to the next, which is similar to the results of previous work (e.g. Robertson, 1993; Gonzalez *et al.*, 1999). It is suggested that the reason the magnetic signatures of bulk samples could not be directly used to correlate thin tephras in Iceland is because of the presence of locally-derived material in addition to the air-fall tephra. However, initial correlation of tephra layers was achieved, using all the measured magnetic parameters, by the use of the statistical measures of Similarity Coefficient (SC) and Euclidean Distance (ED). It demonstrates that magnetic techniques do have the potential to assist in the identification and correlation of distal tephra layers.

Chapter 9 Late Holocene environmental change in SE Iceland

9.1 Introduction

This chapter tries to make a contribution to the knowledge of the late Holocene environmental history of Iceland. Two themes are considered: the relationship of changes in loessial soil accumulation rates (made possible by the tephrochronology established in Chapter 5) to the record of human settlement of Iceland (section 9.2); and the possible relationship of changes in magnetic properties of the soil sections to climatic variations (section 9.3).

9.2 Environmental implications of changes in loessial soil accumulation rates

The scale of soil erosion in Iceland, especially since the time of initial human settlement, is generally well known (Dugmore and Buckland, 1991); however, the detailed patterns of change are less clear. The results of the present study make it possible to examine in more detail the patterns of erosion and corresponding soil accumulation on a local scale. The presence of numerous tephra layers within these profiles offers a means of determining sediment accumulation and therefore of inferring rates of erosion.

In this study, accumulation rates were calculated between tephra dates in the three long sections of Ska1, Ska2 and JL1 (Figure 9.1). In Ska2, accumulation rates increase from low values of 0.02 cm/yr at the base of the profile to intermediate values (0.04 to 0.06

cm/yr) between 1200 BP and 900 BP, followed by high values between 1000 BP and 500 BP (up to 1.4 cm/yr). The variations of accumulation rate are quite similar in the other soil section JL1 (Fig. 9.1). However, in the peat section, Ska1, the accumulation rates are relatively stable until 500 BP in comparison with the two soil sections (Figure 9.1).

Runolfsson (1978) reported that about half of the pre-existing soil cover has been stripped away since the Norse colonisation of Iceland. Soil erosion has been extensive and acute, turning some 20,000 km^2 of formerly vegetated land into semi-desert and creating patchworks of erosion in much of the surviving grassland (Dugmore and Buckland, 1991). Winds are particularly important in Iceland, if not the most important agent of soil erosion and accumulation. Aeolian sediments can form deposits several metres deep (Thorarinsson, 1961; Bjarnarson, 1978; Dugmore and Buckland, 1991).

The impact of settlement (Landnàm) on the vegetation of Iceland was extensively studied by Einasson (1961) and Hallsdóttir (1996). The correlation between destruction of the vegetation cover and ensuing soil erosion is immediately apparent in any comparison of these two lines of study. A regional scale model of soil erosion in south Iceland, based on the interpretation of aeolian sediment accumulation rates at site up to 500 m above sea level, was proposed by Dugmore and Buckland (1991). A dramatic acceleration of aeolian sediment accumulation rates, following Norse settlement, clearly indicated the primary role of anthropogenic impact in post-settlement soil erosion and they concluded that spatial variations in erosion relate directly to the intensity of settlement (Dugmore and Buckland, 1991).

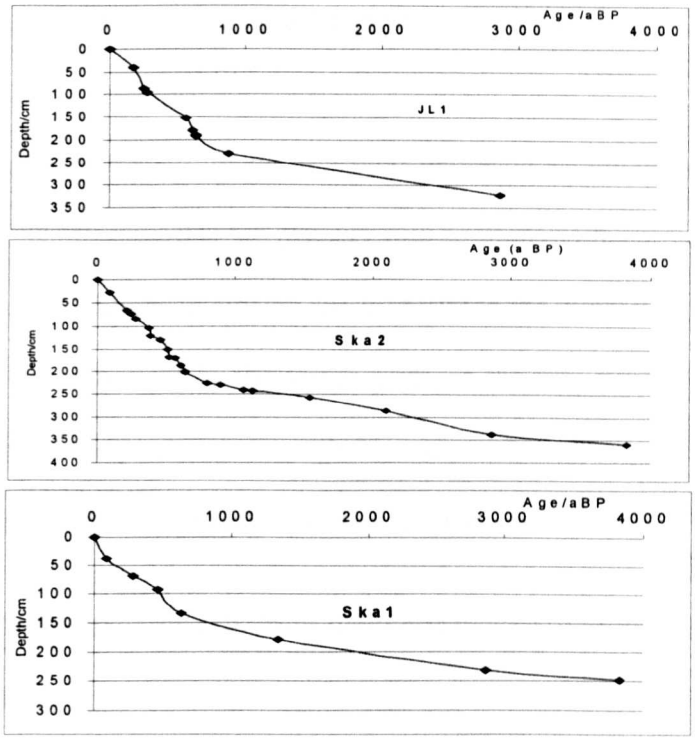

Figure 9.1 Age-depth curves for Ska1, Ska2 and JL1, SE Iceland, based on the tephrochronology.

Recently, a study of late Holocene (ca. 4 ka) marine and terrestrial environmental change in Reykarfördur (Andrews *et al.*, 2001), indicated a major environmental change close to 1000 ^{14}C year ago, which approximately coincided with the onset of the settlement of Iceland. However, they argued it was only a response to natural environmental changes as opposed to the settlement of that area in their study. More recently, a study on the spatial and temporal pattern of land degradation in northeastern Iceland during the Holocene by Ólafsdóttir *et al.* (2002) highlighted three substantial degradation phases, two of which occurred prior to the recorded Norse settlement, ca. 5000 BP and ca. 2500 BP. Their results demonstrated the role of climate in modifying land cover, hence

triggering land degradation without anthropogenic influence. But anthropogenic activity probably had a significant role in the third degradation phase in the sixteenth century AD.

In this study, the dramatic acceleration of aeolian sediment accumulation rates following Norse settlement clearly indicates the primary role of human impact on soil erosion and suggests that spatial variations in erosion should relate to the intensity of settlement. Thus the higher sedimentation rates in the upper parts of the two profiles, with the stable accumulation rates of the peat section, probably reflect the influence of Landnam at 897 AD. This is strongly supported by the results of Dugmore and Buckland (1991).

9.3 Possible relationship of variations in magnetic properties and organic content of the study sections to climate

Time series of selected magnetic parameters, organic content (LOI) for Ska2, together with a temperature record for Iceland (Gudmundsson, 1997; Olafsdottir *et al.*, 2002), are shown in Figure 9.2. Magnetic susceptibility (χ_{lf}) shows a pattern of slightly decreasing values from the top of the profile until 900 BP, at which point there is a noticeable peak. It then decreases again down the profile with a series of distinct peaks at ~1300 –1800 AD, ~2300-2700 BP and ~3400-3700 BP. χ_{ARM} and SIRM follow a similar trend to χlf. The χ_{fd} % remains fairly stable through the profile, with two sharp decreases at ~700 AD and ~800 AD, and general decreases between ~100-1400 AD and ~2900-3300 AD. LOI shows a fairly contrary trend from the temperature variations throughout the late Holocene.

Figure 9.3 shows a comparison of the χ_{lf} records for the three profiles, Ska2, JL1 and Lax, together with the temperature record. In general, the susceptibility of JL1 shows significantly higher values than Ska2, perhaps reflecting local inputs of magnetic material; Lower values for Lax than that of soil sections presumably reflect organic dilution (Chapter 8). Based on the temperature record, several major sections can be distinguished: During the relatively warm period of 4000-3500 BP. Magnetic susceptibility of Ska2 shows high value, which coincide with temperature peak during a warm period. The very low value around 3000 BP might match a relatively severe environment (Gudmundsson, 1997) with the glacier advances (Mackintosh *et al.*, 2002).

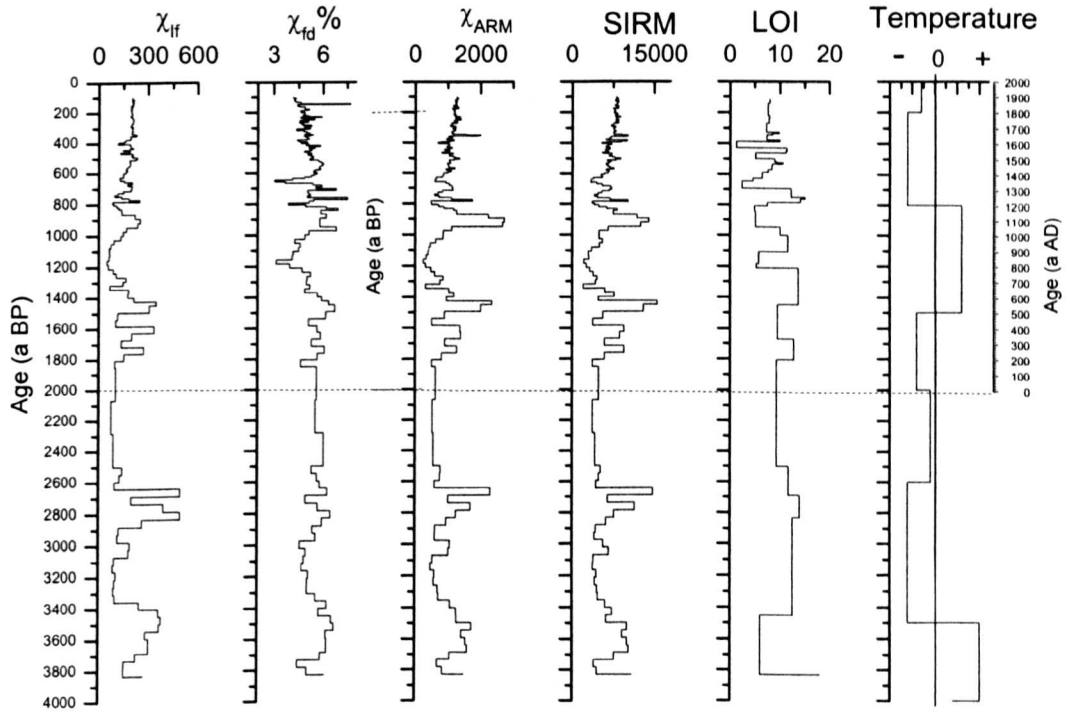

Figure 9.2 Selected magnetic parameters and LOI for Ska2, together with a temperature record. The temperature record is based on Gudmundsson (1997) and Olafsdottir *et al.*, (2002).

During the relatively cold but improved period of 2600-2000 BP, the Ska2 magnetic susceptibility remains low and stable. The sharp decrease after 2600 BP, coincides with a period of land degradation in north eastern Iceland (Olafsdottir *et al.*, 2002), might indicate a severe environment in south eastern Iceland as well. The very low value at 2000 AD might be a sign of another period of glacier advance (Gudmundsson, 1997; Mackintosh *et al.*, 2002).

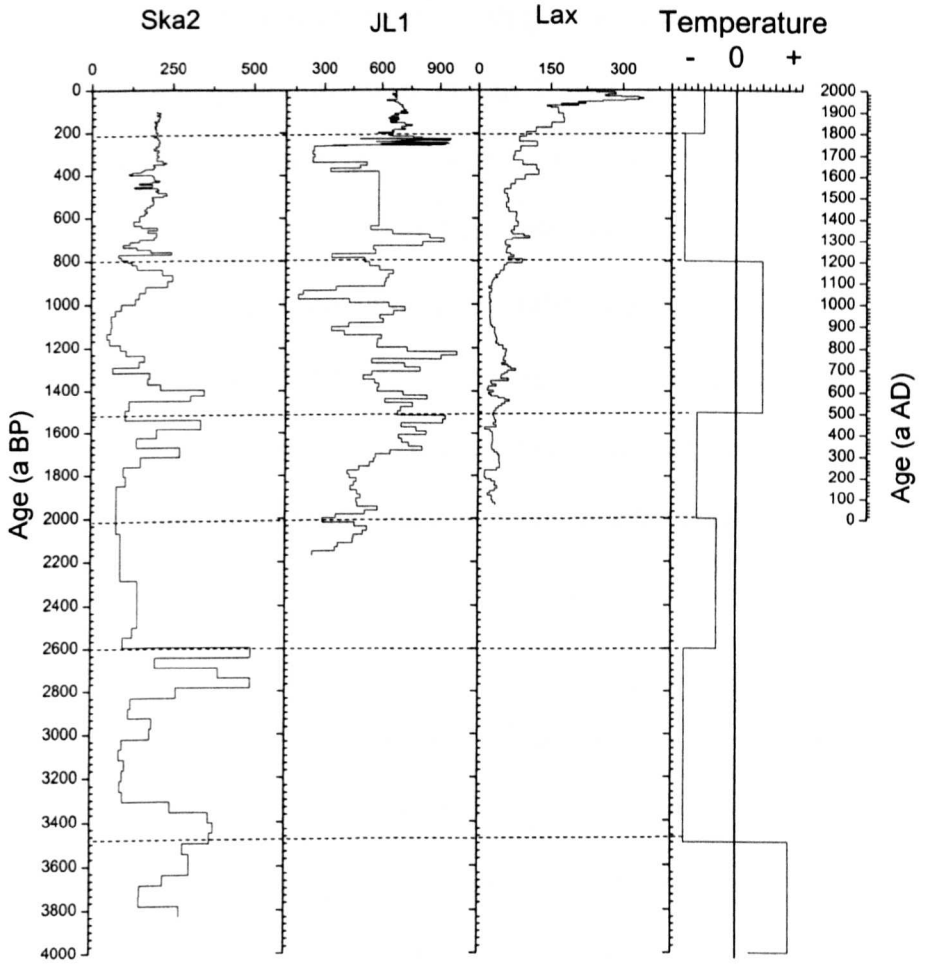

Figure 9.3 Comparison of magnetic susceptibility records for Lax, JL1 and Ska2 with temperature. The temperature record is based on Gudmundsson (1997) and Olafsdottir *et al.*, (2002).

During the relatively cold period of ~2000-1500 BP, the magnetic susceptibility of Ska2, JL1 and Lax show a general increase which might coincide with a improved environment. During the warm period of 1500-800 BP (500-1200AD), the magnetic susceptibility of all the three profiles Ska2, JL1 and Lax show a decreasing trend followed by a generally increasing trend. At the same time, the magnetic susceptibility of JL1 shows dramatic variations with many sharp peaks. Gudmundsson (1997) reports that there were specific glacier advances during 1500-1200 BP, while Mackintosh *et al.* (2002) suggest that the colder period was centred on ~1400 BP. In this study, the magnetic susceptibility of JL1 and Lax show quite low values around 1400AD; however, the Ska2 magnetic susceptibility shows a low value at ~1500AD followed by quite a high value at ~ 1400AD. One reason for this discrepancy could be an error(s) in the age control points for the tephra layers. The low magnetic susceptibility values of the three profiles around 1000 BP coincide with the cooler climate of the 10th century (Mackintosh et al., 2002).

During the relatively cold period of 800-200 BP (1200-1800AD), the magnetic susceptibility of Ska2 and Lax generally increase; however, in JL1 the values generally decrease. The low value of magnetic susceptibility in Ska2 around 600 BP might indicate the colder period around 14th century (Mackintosh *et al.*, 2002). Then, in JL1 the magnetic susceptibility shows a very low value between 300-250 AD, followed by several distinct peaks during ~200-250 AD which might reflect the fact that the climate of the 17th, 18th and 19th centuries was dominated by decadal-scale climatic variability,

associated with changes in sea ice extent A warming occurred between 1700 AD and 1750 AD, while the coldest period in historic times occurred between 1750 and 1800. (Mackintosh *et al.*, 2002). In the most recent interval in the profiles, corresponding to a period of relative cold after 200 AD, the magnetic susceptibility of Ska2 shows fairly stable value; JL1 shows a general trend of decreasing values, while Lax shows a dramatic increase.

The results of this study suggest that climate might have some influence on the magnetic susceptibility records of the sections from SE Iceland. Higher magnetic susceptibility seem to correspond to warmer conditions, and lower susceptibility values to colder conditions. However, the cause of this relationship is unclear. In Chinese loess, the production of secondary ferrimagnetic minerals during pedogenesis has been well-documented as the origin of the relationship between loess magnetic susceptibility and climate. However, this mechanism seems unlikely to be the cause of the loessial soils in SE Iceland, in which pedogenesis has been minimal. Clearly further research is needed to establish the reason for the linkage.

9.5 Summary

Iceland offers a unique opportunity to study the role of human activity in land degradation processes because of the late and well documented human colonisation some 1100 years ago. In this study, the dramatic acceleration of aeolian sediment accumulation rates following Norse settlement clearly indicates the primary role of human impact on soil erosion and suggests that spatial variations in erosion should relate to the intensity of

settlement. Thus the higher sedimentation rates in the upper parts of the two profiles, with the stable accumulation rates of the peat section, probably reflect the influence of Landnam at 897 AD. This is strongly supported by the results of Dugmore and Buckland (1991). A possible relationship between magnetic susceptibility and a temperature record is observed in some of the study profiles, with higher (lower) susceptibility values corresponding to higher (lower) temperatures. Further work is needed to determine the reasons for this relationship.

Chapter 10 Summary

10.1 Conclusions

This study shows that peat and loessial soil deposits in Iceland are useful archives for studying tephra. The tephras are both abundant and clearly visible in terms of colour, reflecting their different sources, in the five profiles from SE Iceland. Iceland is one of the few volcanically extraordinarily active areas in the world, where peat formation and formation of loess-soil are very rapid (Thorarinsson, 1981a). This means that the soil cover thickens so quickly that tephra layers of small difference in layer/age are separated in the soil sections. In addition, Iceland is a country where relatively reliable written records of volcanic eruptions are more abundant and go farther back than in most volcanic areas (Grattan and Pyatt, 1999; Sadler and Grattan, 1999). It is thus an ideal area for tephra study.

A density separation procedure has been shown to be successful in extracting microtephra particles from bulk samples. The tephra shards from two different densities of 2.4-2.6 g/ml and 2.6-2.8 g/ml have almost the same geochemical signature. It was therefore decided to isolate the tephra shards with a relative density between 2.4 to 2.8 g/ml in order to maximise the concentration of microtephra parties in this study. Two EMPA systems were used (one at the University of Edinburgh and the other at the University of Manchester). Overall the results of duplicate measurements show little difference, demonstrating that the two sets of EPMA measurements highly comparable between Edinburgh and Manchester.

The geochemical signatures of tephra shards indicate that the tephra layers (i.e. Lax: 36-38 cm; JL1: 189-190 cm and, JL2: 86-88 cm) contain shards derived from the eruption of Öræfajökull 1362, and that the silicic tephra shards are geochemically stable in soil and peat environments. The comparison of the consistency of the geochemical signature of basic tephra shards of the Grimsvötn 150 eruption demonstrates that the geochemistry of the basic tephra shards are fairly consistent both in soil and peat environments. However, it is less concentrated than that of Öræfajökull 1362, especially in Ska, the first study area. This suggests that the silicic shards are more stable than basic shards. The geochemical results have been used to establish a tephrochronology for the five profiles studied.

This study indicates that the main magnetic minerals in the tephras are ferrimagnetic (e.g. magnetite) and canted antiferromagnetic (e.g. haematite). There is also a significant amount of paramagnetic material in many of the samples. Cross plots of M_{rs}/M_s vs. Bcr/Bc and χ_{fd} % vs. χ_{ARM}/SIRM indicate that the main ferrimagnetic grain sizes in the tephras are PSD and MD.

The results demonstrate that magnetic techniques can be used to characterize tephra in terms of the response of magnetic parameters to the differences in composition and granulometry of magnetic mineral assemblage. Magnetic parameters provide indications of magnetic concentrations, magnetic mineralogy and magnetic grain sizes. However, interpretation of magnetic parameters is complicated by the fact that they are influenced by three controls (i.e. mineral type, mineral concentration and grain size). Mineral type

and the concentration of minerals (especially ferrimagnetic minerals) affect direct measurements whereas ratios of certain magnetic parameters can eliminate the effects of concentration and mineral type and indicate grain size.

One of the main conclusions of this work is that the results highlight the problems of using the magnetic signatures of bulk samples from thin tephras for correlation purposes, probably because of the presence of detritus material derived from parental background, in addition to the air-fall tephra. The use of hysteresis loop and thermomagnetic analyses of density-separated tephra shards, which should have minimized the problem of local contamination , were also not particularly successful for correlating tephras; however, some success was achieved in correlating the profiles of JL1 and JL2, which are located close to each other. Thus it seems that the 'fingerprints' of hysteresis and thermomagnetic properties are not sufficiently consistent to provide reliable correlations over widely separated profiles. These conclusions are similar to those of previous workers (e.g. Robertson, 1993; Gonzalez *et al.*, 1999). However, initial correlation of tephra layers was achieved, using all the measured magnetic parameters, by the use of the multivariate statistical measures of Similarity Coefficient (SC) and Euclidean Distance (ED). Tephra layer correlation was performed first time here using magnetic measurements. This demonstrates that magnetic techniques can potentially assist in the identification and correlation of distal tephra

Iceland offers a unique opportunity to study the human role in land degradation processes because of the late and well-documented occurrence of human settlement 1100 years ago. In this study, sedimentation rates for the profiles were calculated based

on dated tephra layers in the three long sections of Ska1, Ska2 and JL1. The higher sedimentation rates in the upper parts of the profiles are interpreted as reflecting the influence the start of human settlement (Landnam) 897 AD, and support the results of Dugmore and Buckland (1991).

A possible relationship between magnetic susceptibility and a temperature record is observed in some of the study profiles, with higher (lower) susceptibility values corresponding to higher (lower) temperatures. Further work is needed to determine the reasons for this relationship.

10.2 Suggestions for future research

This study demonstrates that (1) magnetic techniques can be used to characterize tephra in terms the response of magnetic parameters to the differences in composition and granulometry of magnetic mineral assemblages; (2) however, the 'fingerprint' of both hysteresis and Curie temperature properties are insufficiently consistent within layers to provide an obviously sound basis for correlating tephra layers from one profile to the next and; (3) Some success was achieved in correlating tephra layers, using a range of magnetic parameters, by the use of multivariate statistical measures of similarity: the Similarity Coefficient (SC) and Euclidean Distance (ED). The magnetic techniques can potentially assist in the identification and correlation of distal tephras. Is this a paradox? To overcome this problem, more basic work is needed in the future, in particular characterising *pure* tephra from different volcanic centres using magnetic measurements.

It might be necessary to measure the geochemistry of more samples, to support the use of magnetic parameters.

This study suggests that climate might have some influence on the magnetic susceptibility records of the sections from SE Iceland. Higher magnetic susceptibility seems to correspond to warmer conditions, and lower susceptibility values to colder conditions. However, the cause of this relationship is unclear. In Chinese loess, the production of secondary ferrimagnetic minerals during pedogenesis has been well-documented as the origin of the relationship between loess magnetic susceptibility and climate. However, this mechanism seems unlikely to be the cause of the loessial soils in SE Iceland, in which pedogenesis has been minimal. Clearly further research is needed to establish the reason for the linkage.

XRF was performed on the five profiles, but due to the time and personal energy limited, little further analysis was done at present. It might be useful to study the association between the results of XRF and magnetic measurements in the five sections.

References

Anderson DE, at el., 1998, Evidence for abrupt climatic change in northern Scotland between 3900 and 3500 calendar years BP, *The Holocene*, **8**(1), 97-103.

Andrews JT, Caseldine C, Weiner NJ and Hatton J, 2001, Later Holocene (ca.4Ka) marine and terrestrial environmental change in Reykjarfjordur, north Iceland: Climate and/or settlement, *Journal of Quaternary Science*, **16**(2), 133-143.

Appleby PG, Nolan PJ, Gifford DW, Godfrey MJ, Oldfield F, Anderson NJ & Battarbee RW, 1986, 210Pb dating by low-background gamma counting, *Hydrobiologia*, **43**, 21-27

Bailey ME, Dunlop DJ, 1983, Alternating-field characteristics of pseudo-single-domain (2-14 MU-M) and multidomain magnetite, *Earth Planet SC LETT.*, **63**(3), 335-352.

Baker, A. et al, 1995, The Hekla 3 volcanic eruption record in a Scottish speleothem, *The Holocene*, **5**(3), 336-342.

Banerjee SK, King JW and Marvin J, 1981, A rapid method for magnetic granulometry with applications to environmental studies, *Geophysics Research Letter*, **8**, 333-336.

Battarbee RW, Flower RJ, Stevenson AC, et al., 1988, Diatom and chemical evidence for reversibility of acidification of Scottish lochs, *Nature*, **332** (6164): 530-532.

Bergthorsson, P, 1969, Forecasting drift ice at Iceland by means of Jan Mayen air temperature, *Jokull*, **19**, 44-52.

Bjarnarson AH, 1978, Erosion, tree growth and land regeneration in Iceland. In: Holdgate MW and Woodman MJ (eds.), The breakdown and restoration of ecosystems, 241-248. Plenum, London.

Blake S, 1984, Magma mixing and hubridization processes at the alkalic, silicic, torfajokull central volcano triggered by tholeiitic Veidivotn fissuring, south Iceland, *J Volcanol Geoth Res.*, **22**(1-2), 1-31.

Bloemendal J, Oldfield F and Thompson R, 1979, Magnetic measurements used to assess sediment influx at Llyn Goddionduon, *Nature*, **280**, 50-53.

Bloemendal J, Barton CE, and Radhakrishnamurty C, 1985, Correlation between Rayleigh loops and frequency-dependent and quadrature susceptibility: application to magnetic granulometry of rocks, *Journal of Geophysical Research B: Solid Earth*, **90**, 8789–8792.

Bloemendal J, Lamb B, and King JW, 1988, Paleoenvironmental implications of rock-magnetic properties of Late Quaternary sediment cores from the eastern equatorial Atlantic, *Paleoceanography*, **3**, 61–87.

Bloemendal J, and deMenocal PB, 1989, Evidence for a change in the periodicity of tropical climate cycles at 2.4 Myr from whole-core magnetic susceptibility measurements, *Nature*, **342**, 897–900.

Bloemendal J, King JW, Hall FR, and Doh ST, 1992, Rock magnetism of Late Neogene and Pleistocene deep-sea sediments: relationship to sediment source, diagenetic processes, and sediment lithology, *Journal of Geophysical Research B: Solid Earth*, **97**, 4361–4375.

Bloemendal J, King JW, Hunt A, deMenocal PB, and Hayashida A, 1993, Origin of the sedimentary magnetic record at Ocean Drilling Program sites on the Owen Ridge, western Arabian Sea, *Journal of Geophysical Research B: Solid Earth*, **98**, 4199–4219.

Bogaard van den B, Dorfler W, Sandgren P, Schmincke HU, 1994, Correlating the Holocene records: Icelandic tephra found in Schleswig-Holstein (Nothern Germany), *Naturwissenschaften* **81**,554-556.

Boygle J, 1999, Variability of tephra in lake and catchment sediments, Svinavatn, Iceland, *Global Planet Change*, **21**(1-3), 129-149.

Boyle JF, 2000, Rapid elemental analysis of sediment samples by isotope source XRF, *Journal of Paleolimmoloyg*, **23**,213-221.

Bradshaw R and Thompson R, 1985, The use of magnetic measurements to investigate the mineralogy of Icelandic lake sediments and to study catchment processes, *Boreas*, **14**, 203-215.

Canfield DE, and Berner RA, 1987, Dissolution and pyritization of magnetite in anoxic marine sediments, *Geochimica et Cosmochimica Acta*, **51**, 645–659.

Chambers FM, et al., 1997, A 5500-year proxy-climate and vegetation record from blanket mire at Talla Moss, Borders, Scotland, *The Holocene*, **7**(4), 391-399.

Charleworth SM and Less JA, 1997, The use of mineral magnetic measurements in polluted urban lakes and deposited dusts, Coventry UK, *Physics and Chemistry of the Earth*, **22**, 203-206.

Charlesworth SM, Lees JA, 2001, The application of some mineral magnetic measurements and heavy metal analysis for characterizing fine sediments in an urban catchment, Coventry, UK, *J APPL GEOPHYS*, **48** (2), 113-125.

Charman DJ & Grattan JP, 1999, Multi-variate analyses of tephra geochemistry: a contribution to the correlation of distal tephra in the British Isles, *Geological Society Special Publication*, **161**, 147-160.

Chen FH, Li JJ, and Zhang WX, 1991, Loess stratigraphy of the Lanzhou profile and its comparison with deep-sea sediment and ice core record, *Geo. Journal*, **24**, 201–209.

Chen FH, Bloemendal J, Wang JM, et al, 1997, High-resolution multi-proxy climate records from Chinese loess, evidence for rapid climatic changes over the last 75 kyr, *Palaeogeogr Palaeocl.*, **30** (1-4): 323-335.

Chen FH, Feng ZD, Zhang JW, 2000, Loess particle size data indicative of stable winter monsoons during the last interglacial in the western part of the Chinese Loess Plateau, *Catena*, **39** (4): 233-244.

Cornie AB, Nelson DE and Huntley DJ, 1981, X-Ray fluorescence analysis as a rapid method of identifying tephras discovered in archaeological sites. In, Self, S. and Sparks, R.S.J. (eds) Tephra Studies, 103-107.

Dawson AG, *et al.*, 1997, A 200-year record of gale frequency, Edinburgh, Scotland: possible link with high-magnitude volcanic eruptions, *The Holocene*, 7(3), 337-341.

Day R, Fuller M and Schmidt, 1977, Hysteresis properties of titanomagnetites: Grain-size and compositional dependence, *Physics of theEearth and Planetary Interiors*, **13**, 260-267.

Dearing JA, Elner JK, Happey-Wood CM, 1981, Recent sediment flux and erosional processes in a Welsh Upland Lake Catchment based on magnetic susceptibility measurements, *Quat. Res.*, **16**, 356-372.

Dearing JA, 1983, Changing patterns of sediment accumulation in a small lake in Scnia, South Sweden, *Hydrobiologia* **103**,59-64.

Dearing JA, 1994, Environmental magnetic susceptibility, Department of Geography, University of Liverpool.

Dearing JA, Dann RJL, Hay K, Lees JA, Loveland PJ, 1996, Frequency-dependent susceptibility of environmental materials. *Geophysical Journal of International,* **124**, 228-240.

Dearing JA, Bird PM, Dann RJL, Benjamin SF, 1997, Secondary ferrimagnetic minerals in Welsh soils: a comparison of mineral magnetic detection methods and implications for mineral formation, *Geophysical Journal International*, **130**, 727-736.

Dearing JA, 1999, Magnetic susceptibility, In: Walden J, Oldfield F, Smith J (eds.), Environmental magnetism: a practical guide no. **6**, Quaternary Research Association, London, 35-62.

Dearing JA, Hannam JA, Anderson AS, et al. 2001, Magnetic, geochemical and DNA properties of highly magnetic soils in England, *Geophys. J Int.* **144** (1), 183-196.

deMenocal PB, Laine EP, and Ciesielski PF, 1988, A magnetic signature of bottom current erosion, *Physics of the Earth and Planetary Interiors*, **51**, 326–348.

deMenocal PB, Bloemendal J, and King JW, 1991, A rock-magnetic record of monsoonal dust deposition to the Arabian Sea: Evidence for a shift in the mode of deposition at 2.4 Ma, *Proceedings of the Ocean Drilling Program, Scientific Results*, **117**, 389-407.

Doh, SJ, King JW and Leinen M, 1988, A rock-magnetic study of giant piston core LL44-GPC3 from the central North Pacific and its paleooceanographic implications, *Paleoceanography*, **3**, 89–111.

Dugmore AJ, 1989, Icelandic volcanic ash in Scotland, *Scottish Geographical Magazine*, **105**,168-172.

Dugmore AJ, Buckland P, 1991, Tephrochronology and late Holocene soil erosion in south Iceland, in Maizels JK and caseldine (eds.), Environmental Change in Iceland: Past and present, 147-159.

Dugmore AJ, Newton AJ, Sugden DE, Larsen G, 1992, Geochemical stability of fine-grained silicic Holocene tephra isochrones in Scotland, *Journal of Quaternary Science*, **7**, 173-183.

Dugmore AJ, Larsen, G. and Newton, AJ, 1995, Seven tephra isochrones in Scotland, *The Holocene*, **5**, 257-266.

Dugmore AJ, Coles GM, Buckland PC, 1999, A Scottish speleothem record of the H-3 eruption or human impact? A comment on Baker, Smart, Barnes, Edwards and Farrant, *Holocene*. **9**(4): 501-503.

Dunlop DJ, 1973, Superparamagnetic and single-domain threshold size in magnetite, *Journal of Geophysical Research*, **78**(11), 1780-1793.

Dunlop, D.J., and Ö. Özdemir, 1997, Rock Magnetism: Fundamentals and Frontiers, Cambridge University Press.

Ebdon D. 1985, Statistics in Geography. Blackwell: Oxford.

Einasson T, 1961, Pollenanalytische Untersuchungen zur spat-und postglacialen kilmageschichte Islands, *Sonderoffentlichungen des Geologiches Institute der Universitat Koln*, *6*: 23-42.

Eiriksson J, Kunudsen KK, Haflidson H, Henriksen P, 2000, Late glacial Holocene palaeocenography of north Iceland shelf, *Journal of Quaternary Science*, 15, 23-42.

Fassbinder JWE, Stanjek H, and Vali H, 1990, Occurence of magnetic bacteria in soil, *Nature*, **343**, 161–163.

Forster IDL, Dearing JA, and Grew R, 1988, Lake-catchments: An evaluation of their contribution to studies of sediment yield and delivery processes, Sediment Budgets, *IAHS Publ.*, **174**, 413-423, Wallingford, Oxford.

Forster IDL, Grew R, and Dearing JA, 1990, Magnitude and frequency of sediment transport in angricultural catchments: A paired lake-catchnent study in Middle Land England. In Soil Erosion on Angtricultural Land, Eds, J.Boardman, IDL Forster and JA Dearing, Whiley, Chichester.

Frederichs T, Bleil U, Daumler K, Von Dobeneck T, Schmidt AM, 1999,The magnetic view on the marine paleoenvironment: parameters, techniques and potentials of rock magnetic studies as a key to paleoclimatic and paleoceanographic changes, In: Fischer G, Wefer G (eds.), Use of Proxies in Paleoceanography: Examples from the south Atlantic. Spring-Verilag Berlin Heidelberg, 575-599.

Frithriksson S, 1978, The degradation of Icelandic ecosystems, In: Holdgate MW and Woodman MJ (eds.), The Breakdown and Restoration of Ecosystems, 145-156. Plenum, London.

Gonzalez S, Jones JM, Williams DL, 1999, Characterization of tephras using magnetic properties: an example from SE Iceland, In: Firth C, McGuire WJ (eds.), *Volcanoes in the Quaternary*, Geological Society, London Special publications, 161, 125-145.

Grattan J and Sadler J, 1999, Regional warming of the lower atmosphere in the wake of volcanic eruptions: the role of the laki fissure eruption in the hot summer 1783, In: Firth C, McGuire WJ (eds.), *Volcanoes in the Quaternary*, Geological Society, London Special publications, 161, 161-171.

Grattan JP, Pyatt FB, 1999, Volcanic eruptions dry fogs and the European palaeoenvironmental record: localised phenomena or hemispheric impacts? *Global Planet Change*, **21** (1-3), 173-179.

Gronvold K, Oskarsson N, Johnsen SJ, et al., 1995, Ash layers from Iceland in the Greenland GRIP ice core correlated with oceanic and land sediments, *Earth Planet Sc. Lett.*, **135** (1-4): 149-155.

Giles TM, Newnham RM, Lower DJ and Munro A, 1999, Impact of tephra fall and environmental change: a 1000 year record from Matakana Island, Bay of Plenty, north Island, New Zealand, In: Firth C,

McGuire WJ (eds.), *Volcanoes in the Quaternary*, Geological Society, London Special Publications, **161**, 11-26.

Gudmundsson HJ, 1997, A review of the Holocene environmental history of Iceland, *Quaternary Science Review*, **16** (1), 81-92.

Haflidason H, Larsen G, Olafsson G, 1992, The recent sedimentation history of Thingvallavatn, Iceland. *Oikos*, **64**, 80-95.

Haflidason H, Eirisson J, Kreveld SV, 2000, The tephrochronlogy of Iceland and the north Atlantic region furing the middle and later quaternary: a review, *Journal of Quaternary science*, **15**(1), 3-22.

Hallsdóttir M, 1996, Sythesis of the Holocene history of vegetation in northern Iceland. *Palaoklimaforschung*, **20**, 203-214.

Hanesch M, Petersen N, 1999, Magnetic properties of a recent parabrown-earth from Southern Germany, *Earth Planet Sc. Lett*, **169** (1-2): 85-97.

Henshaw PC, & Merrill RT, 1980, Magnetic & chemical changes in marine sediments, Reviews of Geophysics & Space Physics, **18**, 483-504.

Hay KL, Dearing JA, Baban SMJ, Loveland PJ, 1997, A preliminary attempt to identify atmospherically-derived pollution particles in English topsoils form magnetic susceptibility measurements, *Physics and Chemistry of the Earth*, **22**, 207-210.

Heller F, and Liu TS, 1986, Palaeoclimatic and sedimentary history from magnetic susceptibility of loess in China, *Geophysical Research Letters*, **13**, 1169–1172.

Hesse PP, Evidence for bacterial paleoecological origin of mineral magnetic cycles in oxic and sub-oxic Tasman sea Sediments, *Mar. Geol.*, **117** (1-4): 1-17 MAR 1994

Hovan SA, Rea DK, Pisias NG, and Shackleton NJ, 1989, A direct link between the China loess and marine $\delta^{18}O$ records: aeolian flux to the north Pacific, *Nature*, ***340***, 296–298.

Hunt A, Jones J, and Oldfield F, 1984, magnetic measurements and heavy metals in atmospheric particulateres of anthropogenic origin, *Science Total Environment*, **33**, 129-139.

Hunt A, 1986, The application of mineral magnetic methods to atmospheric aerosol discrimination, *Physics of the Earth and Planetary Interiors*, **42**, 10–21.

Hunt J, and Hill PG, 1993, Tephra geochemistry: a discussion of some persistent analytical problems. *The Holocene*, **3**(3), 271-278.

Jakobsson S.V. 1979, Petrology of recent basalts of the Eastern Volcanic Zone, Iceland. *Acta Naturalia Islandica*, 26, 103.

Jakobsson S, and Moore JG, 1980, Through Surtsey, unique hole shows how volcano grew, *Geotimes V.*, **25**, 14-16.

Jones JM, 1985, Magnetic minerals and heavy metals in ombrotrophic peat PhD Thesis.

Kent DV, 1982, Apparent correlation of paleomagnetic intensity and climatic records in deep-sea sediments, *Nature*, **299**, 538-539.

Karlin R, and Levi S, 1983, Diagenesis of magnetic minerals in recent haemipelagic sediments, *Nature*, **303**, 327–330.

Karlin R, and Levi S, 1985, Geochemical and sedimentological control of the magnetic properties of hemipelagic sediments, *Journal of Geophysical Research B: Solid Earth*, **90**(10), 373–10,392.

Karlin R, Lyle M, and Heath GR, 1987, Authigenic magnetite formation in suboxic marine sediments, *Nature*, **326**, 490–493.

Karlin R, 1990, Magnetite diagenesis in marine sediments from the Oregon continental margin, *Journal of Geophysical Research B: Solid Earth*, *95*, 4405–4419.

King J, Banerjee SK, Marvin J, Ozdemir O, 1982, A comparison of different magnetic methods for determing the relative grain size of magnetite in natural materials: some results from sediments, *Earth and Planteary Science Letters*, **59**, 404-419.

King JW, and Channell GET, 1991, Sedimentary magnetism, environmental magnetism, and magnetostratigraphy, *Reviews of Geophysics*, *29, Suppl. (IUGG Report–Contributions in Geomagnetism and Paleomagnetism)*, 358–370.

Kukla, GJ, 1987, Loess stratigraphy in central China, *Quaternary Science Reviews*, *6*, 191–219.

Kukla G, Heller F, Liu XM, Xu TC, Liu TS, and An ZS, 1988, Pleistocene climates in China dated by magnetic susceptibility, *Geology*, **16**, 811-814.

Kukla GJ, and An ZS, 1989, Loess stratigraphy in central China, *Palaeogeography, Palaeoclimatology, Palaeoecology*, **72**, 203–225.

Kodama KP, Lyons JC, Siver PA, et al., A mineral magnetic and scaled-chrysophyte paleolimnological study of two northeastern Pennsylvania lakes: Records of fly ash deposition, land-use change, and paleorainfall variation, *J Paleolimnol.*, **7** (2): 173-189 FEB 1997

Kvamme T, Mangerud J, Furnes H, Ruddiman WF, 1989 Geochemistry of Pleistocene ash zones in cores from the North Atlantic. *Norsk Geoligosk Tidsskrift,* 69, 251-272.

Kovach WL, 1995, Mutilvariate data analysis, In Maddy D & Brew JS (eds.) Statistical modelling of quaternary science data, Technical Guild 5, Quaternary Research Association, Cambridge, Cambridge, 1-38.

Larsen G, 1984, Recent volcanic history of the Veidivion fissure swarn, Southern Iceland - An approach to volcanic risk assessment, *J Volcanol. Geoth. Res.*, **22** (1-2): 33-58.

Larsen G, Dugmore A, Neweton A, 1999, Geochemistry of historical-age silicic tephra in Iceland, *The Holocene*, **9**(4), 463-471.

Lees, 1994, Modelling the magnetic properties of natural and environmental material, Unpublish PhD thesis, Coventry University.

Lees JA, 1997, Mineral magnetic properties of mixtures of environmental and synthetic materials: linear additivity and interaction effects, Geophys J Int., 131 (2): 335-346.

Lees J, Dearing JA, 1999, Additional measurements using a vibrating magnetometer, In: Walden J, Oldfield F, Smith J (eds.), Environmental magnetism: a practical guide no. 6, Quaternary Research Association, London, 185-196.

Leslie BW, Lund SP, and Hammond DE, 1990, Rock magnetic evidence for the dissolution and authigenic growth of magnetic minerals within anoxic marine sediments of the California continental borderland, *Journal of Geophysical Research B: Solid Earth*, **95**, 4437–4452.

Li JJ, Feng ZD, Kang JC, Chen FH, *et al.*, 1992, The comparison of Lanzhou loess profile with Costok ice core in Antactic over the last glaciation cycle. Sci. Chian, B35, 476-487.

Lowe J *et al.*, 1996, Tephra, loess, and palaeosols - an integration. *Quaternary* Internationa,l **34-36**, 1-261

Lowe J, 1997, Vedde ash layer discovered in a small lake basin on the Scottish mainland, J GEOL SOC LONDON **154**: 605-612 Part 4.

Mackintosh AN, Dugmore AJ, Hubbard AL, 2002, Holocene climatic changes in Iceland: evidence from modelling glacier length fluctuations at Solheimajokull, *Quatern. Int.*, **91**, 39-52.

Maher BA, and Thompson R, 1991, Mineral magnetic record of the Chinese loess and paleosols, *Geology*, **19**, 3–6.

Maher BA, and Thompson R, 1992, Paleoclimatic significance of the mineral magnetic record of the Chinese loess and paleosols, *Quaternary Research*, **37**, 155–170.

Maher BA, 1988, Magnetic properties of sythetic sub-micron magnetites, *Geophysical Journal*, **94**, 83-96.

Maher BA and Thompson R, 1999, Quaternary climates, environments, and magnetism, Cambridge University Press.

Mauquoy D, Baraer K, 1999, A replicated 3000 yr. proxy-climate record from Coom Rigg Moss and Felecia Moss, the Border Mires, northern England, *Journal of Quaternary Science*, **14** (3), 263-275.

Mcdougall JM, Tarling DH, Warren SE, 1983, The magnetic sourcing of obsidian sample from Mediterranean and Near-east sources. *Journal Archaeology Science*, **10**, 441-452.

Mead GA, Tauxe L, and LaBrecque JL, 1986, Oligocene paleoceanography of the South Atlantic: Paleoclimatic implications of sediment accumulation rates and magnetic susceptibility measurements, *Paleoceanography*, **1**, 273-284.

Meynadier L, Valet JP, Hagee VL, Weeks R, *et al.*, 1991, Contribution of rock magnetic properties of the late Pleistocene paleoclimate record of the western equatorial Indian Ocean, *Terra Abstr.*, 3, 307-308, 1991.

Momose K, Kobayashi K, Minagawa K, Machid M, 1968, Identification of tephra by means of ferromagnetic miners in pimice. Bulletin Earth Research Institution, 46, 1275-1292.

Mulligan L, 2000, Late Holocene Environmental change in southeast Iceland. *Msc Dissertation*, the university of Liverpool.

Mullins CE, 1977, Magnetic susceptibility of the soil and its significance in soil science—a review, *Journal of Soil Science*, **28**, 223–246.

Qilliam M, 1992, Evidence for the dissolution of magnetic in recent Scottish peats, Quaternary Research, **37**, 171-182.

Ólafsdóttir *et al.*, 2002, Holocene land degradation and climatic change in northeastern Iceland, *The Holocene*, **12**, 159-167.

Oldfield F, Tolonen K, and Thompson R, 1981, History of particulate atmospheric pollution from magnetic measurements of dated Finnish peat Profiles. *Ambio,* **10**, 185-189.

Oldfield, F., A. Hunt, M.D.H. Jones, R. Chester, J.A. Dearing, L. Olsson, and J.M. Prospero, Magnetic differentiation of atmospheric dusts, *Nature*, **317**, 516–518, 1985.

Oldefield F, 1991, Environmental magnetism- a perspective, *Quaternary Science Reviews*, **10**, 73-85.

Oldfield F, Thompson R, Brown A, 1978, Changing atmospheric fallout of magnetic particles record in recent ombrotrophic peat section. *Science*, **199**, 679-690.

Oldfield F, 1994, Towards the discrimination of fine-grained ferrimagnets by magnetic measurements in lake and near-shore marine sediments, *Journal of Geophysical Research B: Solid Earth*, **99**, 9045–9050.

Oldfield F, Wu RJ, 2000, The magnetic properties of the recent sediments of Brothers Water, NW England

J Paleolimnol., **23** (2): 165-174.

Palsson H, 1999, Oral tradition and saga writing, *Fassbaender*. Wien.

Pawes A, Beske-Diehl S., Marshall SA, 1998, Use of magnetic hysterisis properties and electron spin resonance spectroscopy for the identification of volcanic ash: a preliminary study. *Geophys. J. Int.* **132**, 712-720.

Petermann H, and Bleil U, 1993, Detection of live magnetotactic bacteria in South Atlantic deep-sea sediments, *Earth and Planetary Science Letters*, **117**, 223-228.

Posner GH, Ploypradith P, Parker MH, et al., 1999, Antimalarial, antiproliferative, and antitumor activities of artemisinin-derived, chemically robust, trioxane dimmers, J Med Chem, **42** (21): 4275-4280.

Pouclet A, Horvath E, Gabris G, et al., 1999, The Bag Tephra, a widespread tephrochronological marker in Middle Europe: chemical and mineralogical investigations, *B Volcanol.*, **61** (4), 65-272

Rampino A R, 1991,Volcanism, Climate change, and the geology record, Sedimentation in Volcanic setting, SEPM special Pulication No. **45**, 9-18.

Richardson N. 1986, The mineral magnetic record in recent ombrotrophic peat sychronised by fine resolution pollen analysis, *Physics of the Earth and Planetary Interiors*, **42**, 48-56.

Robertson DJ, 1993, Discrimination of Tephra using Rockmagnetic Characteristics, *Journal Geomag. Geoelecter*, **45**, 167-178.

Robinson SG, 1986, The late Pleistocene paleoclimatic record of North Atlantic deep-sea sediments revealed by mineral-magnetic measurements, *Physics of the Earth and Planetary Interiors*, **42**, 22-47.

Robinson PT, Vonherzen RP, Cannat M, et al., 1989 Rmed and metamorphosed gabbros from the atlantis-II fracture-zone (Southwest Indian-Ocean), *Cr Acad Sci.*, II **308** (2): 215-220 JAN 13 1989

Robinson SG, 1997, Beginning Environmental Magnetism, School of Geography, University of Manchester.

Robock A, 2000, Volcanic eruptions and climate, *Reviews of Geophysics*, **38(2)**, 191-219.

Roberts AP, and Turner GM, 1993, Diagenetic formation of ferrimagnetic iron sulphide minerals in rapidly deposited marine sediments, South Island, New Zealand, *Earth and Planetary Science Letters*, **115**, 257–273.

Rose WI, Conway FM, Pullinger CR, et al., 1999, An improved age framework for late Quaternary silicic eruptions in northern Central America, *Bulletin of Volcanology*, **61** (1-2): 106-120.

Rummery TA, Bloemendal J, Dearing JA, Oldfield F, and Thompson R, 1979, The persistence of fire-induced magnetic oxides in soils and sediments, *Annales de Géophysique*, **35**, 103–107.

Runolfsson S, 1978, Soil conservation in Iceland, in Holdgate MW and Woodman MJ (eds.), The breakdown and restoration of ecosystems, 231-240. Plenum, London.

Sadler JP, Grattan JP, 1999, Volcanoes as agents of past environmental change, *Global Planet Change*, **21** (1-3), 181-196.

Sager WW, Hall SA, 1991, Magnetic-properties of black mud turbidities from ODP LEG 116, distal Bengal fan, *Aapg Bull.*, **75** (3): 665-665.

Shane P, 2000, Tephrochronology: a new Zealand case study, *EARTH-SCI RE*, **49** (1-4): 223-259.

Shu J, Dearing JA, Morse AP, et al., 2000, Magnetic properties of daily sampled total suspended particulates in Shanghai, *Environ Sci. Technol.*, **34** (12), 2393-2400.

Shu J, Dearing JA, Morse AP, et al., 2001, Determining the sources of atmospheric particles in Shanghai, China, from magnetic and geochemical properties, *Atmos. Environ*, **35** (15): 2615-2625.

Sigvaldason G, 1974, The petrology of Hekla and origin of silicic rocks in Iceland, In: Einarsson T, Kjartansson G, Thorarinsson S (eds.), *In the Eruption of Hekla* 1947-1948, 1, Societas Scientiarum Icelandic, Reykjavik, 1-44.

Simonarson LA, 1980, On climate in Iceland, In: Iceland, Icelandic Glaciological Society, 173-175.

Singer MJ, Verosub KL, TenPas J, and Fine P, 1992, Identification of pedogenic magnetic carriers in soils with citrate-bicarbonate-dithionite (abstract), *Eos, Transactions of the American Geophysical Union*, **73**(43), suppl., 137.

Smith GM, 1990, The magnetic structure of the marine basement, *CRC Critical Reviews in Aquatic Sciences*, **2**, 205–227.

Smith KP, 1995, Landnam: the settlement of Iceland in archaeological and historical perspective, *World Archaeology*, 26(3), 319-347.

Snowball I, Sandgren P, Petterson G, 1999, The mineral magnetic properties of an annually laminated Holocene lake-sediment sequence in northern Sweden, *The Holocene*, **9** (3), 353-362.

Snowball I, Zillen L, Gaillard MJ, 2002, Rapid early-Holocene environmental changes in northern Sweden based on studies of two varved lake-sediment sequences, *The Holocene*, **12** (1), 7-16.

Stockhausen H, 1998, Some new aspects for the modeling of isothermal remanent magnetization acquisition curves by cumulative log Gaussian functions, *Geophys. Res. Lett.*, **25** (12): 2217-2220.

Stoner JS, Channell JET, HillaireMarcel C, 1996, The magnetic signature of rapidly deposited detrital layers from the deep Labrador Sea: Relationship to North Atlantic Heinrich layers, *Paleochanography*, **11** (3): 309-325.

Stott Ap, 1986, Sediment tracing in a reservoir-catchments system using a magnetic mixing model, *Phys. Earth Planet. Interiors* **42**, 105-112.

Sweatman TR & Long JVP, 1969, Quantitative electron-probe microanalysis of rock-forming minerals, *Journal of Petrology*, **19** (2), 332.

Taxue L, 1993, Sedimentary records of relative paleointensity of the geomagnetic field: Teory and practice, *Review Geophysics*, 21, 319-354.

Thompson R, Batterbee RW, O'Sullivan PE, and Oldfield F, 1975, Magnetic susceptibility of lake sediments, *Limnology and Oceanography*, **20**, 687–698.

Thompson R, and Turner GM, 1979, British geomagnetic master curve 10,000-0 yr B.P. for dating European sediments, *Geophysical Research Letters*, **6**, 249–252.

Thompson R, Bloemendal J, Dearing JA, Oldfield F, 1980, Environmental applications of magnetic Measurements, *Science*, **4430**, 481-486.

Thompson R, Oldfield F, 1986, Environmental Magnetism, Allen and Unwin.

Thompson R, 1986, Modeling magnetization data using simples phys, *Earth planet In.*, **42** (1-2): 113-127.

Thorarionsson S, 1944, Tefrokronologiska studier pa Island, *Geografiska Annaler*, **26**, 1-217.

Thorarionsson S, 1958, The Oraefajokull eruption of 1362, Acta Naturlia Islandica, 2.

Thorarionsson S, 1961, Population change in Iceland, *Geographical Review*, **51**, 519-533.

Thorarinsson, 1967, The eruption of Hekla in historical times, In Einaarsson Th, Kjartansson G, and Thorarinsson S (eds), The eruption of Hekla 1947-1948, *Societas Scientatis Islandical*, **1**, 1-70.

Thorarionsson S, 1980, Tephrochrology and its application in Iceland, In: Iceland, Icelandic Glaciological society, 162-165.

Thorarionsson S, 1981a. Tephra study and Tephrocheronology: a historical review with special reference to Iceland. In: Self S and Sparks RS, Tephra studies, 1-12.

Thorarionsson S, 1981b. The application of Tephrochronology in Iceland. S.self and R.S. Sparks, Tephra studies, 109-134.

Thunell R, et al., 1979, The age, Origin, and Volcanologyical Significance of the Y-5 Ash layer in the Mediterranean, *Quaternary Research*, 12, 241-253.

Tite MS and Mullins C, 1971, Enhancemental of magnetic susceptibility of soil on archeological sites, *Archeometry*, **13**(2), 209-219.

Tric E, Laj C, Jehanno C, Valet JP, Kissel C, Mazaud A, and Iaccarino S, 1991, High-resolution record of the Upper Olduvai transition from Po Valley (Italy) sediments: support for dipolar transition geometry?, *Physics of the Earth and Planetary Interiors*, **65**, 319–336.

Turney CSM, 1988, Extraction of rhyolitic component of Vedde microtephra from minerogenic lake sediments, *J Paleplimnol*, (2), 199-206.

Vadyunina AF and Babania VF, 1972, Magnetic susceptibility of some soil in the USSR, *Soviet Soil Science*, 588-599.

Versub KL, Roberts AP, 1995, Environmental magnetism: past, present, and future. *Journal of Geophysical Research*, **100**, 2175-2192.

Von Dobeneck T, 1998, The concept of 'partial susceptibilities', *Geol. Carpathica.*, **49**, 228-229.

Wada K, Arnalds O, Kakuto Y, Wilding LP and Halmark CT, 1992, Clay minerals of four soil formed in eolian and tephra materials in Iceland, *Geoderma*, **52**, 351-365.

Walker GPL and Wilson CJN, 1983, lateral variations in the Taupo Ignimbrite. *Journal of Volcanology and Geothermal Research*, **18** (1-4): 117-133 1983

Walden J, 1999, Remanence measurements, In: Walden J, Oldfield F, Smith J (eds.), Environmental magnetism: a practical guide no. **6**, Quaternary Research Association, London, 63-88.

Walden J and Smith J, 1995, Factor analysis: a practical application In Maddy D & Brew JS (eds.) Statistical modelling of quaternary science data, Technical Guild 5, Quaternary Research Association, Cambridge, Cambridge, 39-106.

Wilcoxson K, 1967, Volcanoes, Cassell London.

Williams M, 1992, Evidence for the Dissolution of magnetite in recent Scottish peat, *Quaternary Research*, **37** 171-182..

Xie SJ, Dearing JA, Bloemendal J, et al., 1999, Association between the organic matter content and magnetic properties in street dust, Liverpool, UK, *Sci. Total. Environ.*, **241** (1-3): 205-214.

Xie SJ, Dearing JA, Bloemendal J, 2000, The organic matter content of street dust in Liverpool, UK, and its association with dust magnetic properties, *Atmos Environ*, **34** (2), 269-275.

Xie SJ, Dearing JA, Boyle JF, et al., 2001, Association between magnetic properties and element concentrations of Liverpool street dust and its implications, *J. Appl. Geophys.*, **48** (2), 83-92.

Yu, L., and Oldfield F, 1989, A multivariate mixing model for identifying sediment source from magnetic measurements, *Quaternary Research*, **32**, 168–181.

Zhou, LP, Oldfield F, Wintle AG, Robinson SG, and Wang JT, 1990, Partly pedogenic origin of magnetic variations in Chinese loess, *Nature*, **346**, 737–739.

Zoe G, 1999, Possible evidence for dissimilatory bacterial magnetite dominating the magnetic properties of recent lake sediments, *Earth and Planetary Science Letters,* **168**, 1-6.

Zolitschka B, A 14,000 year sediment yield record from western Germany based on annually laminated lake sediments, *Geomorphology*, **22** (1), 1-17.

Appendix 1 Hysteresis loops for the five studied profiles, Southeast Iceland.

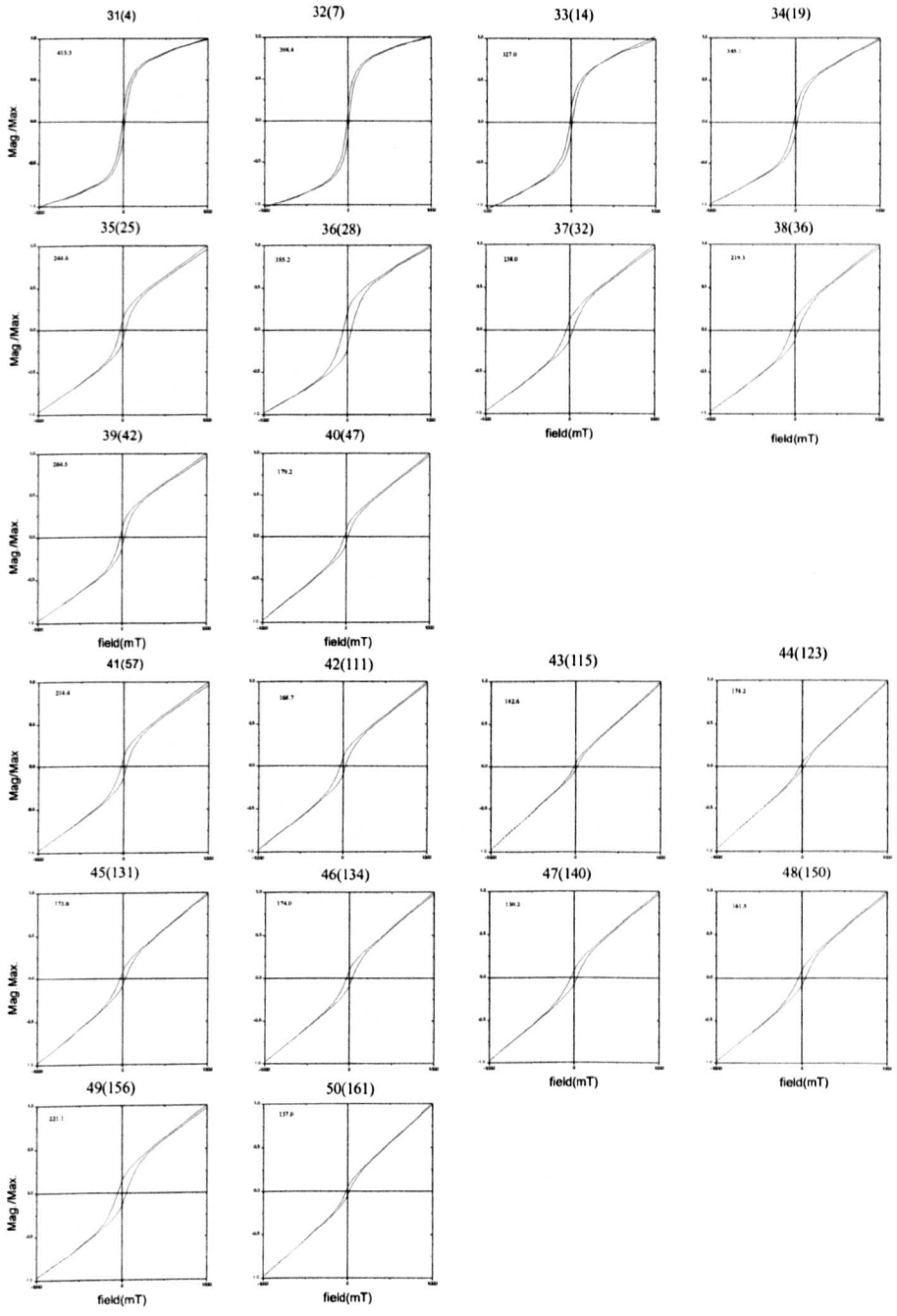

Hysteresis loops for Lax, SE Iceland ---Note: No. (Depth/cm)

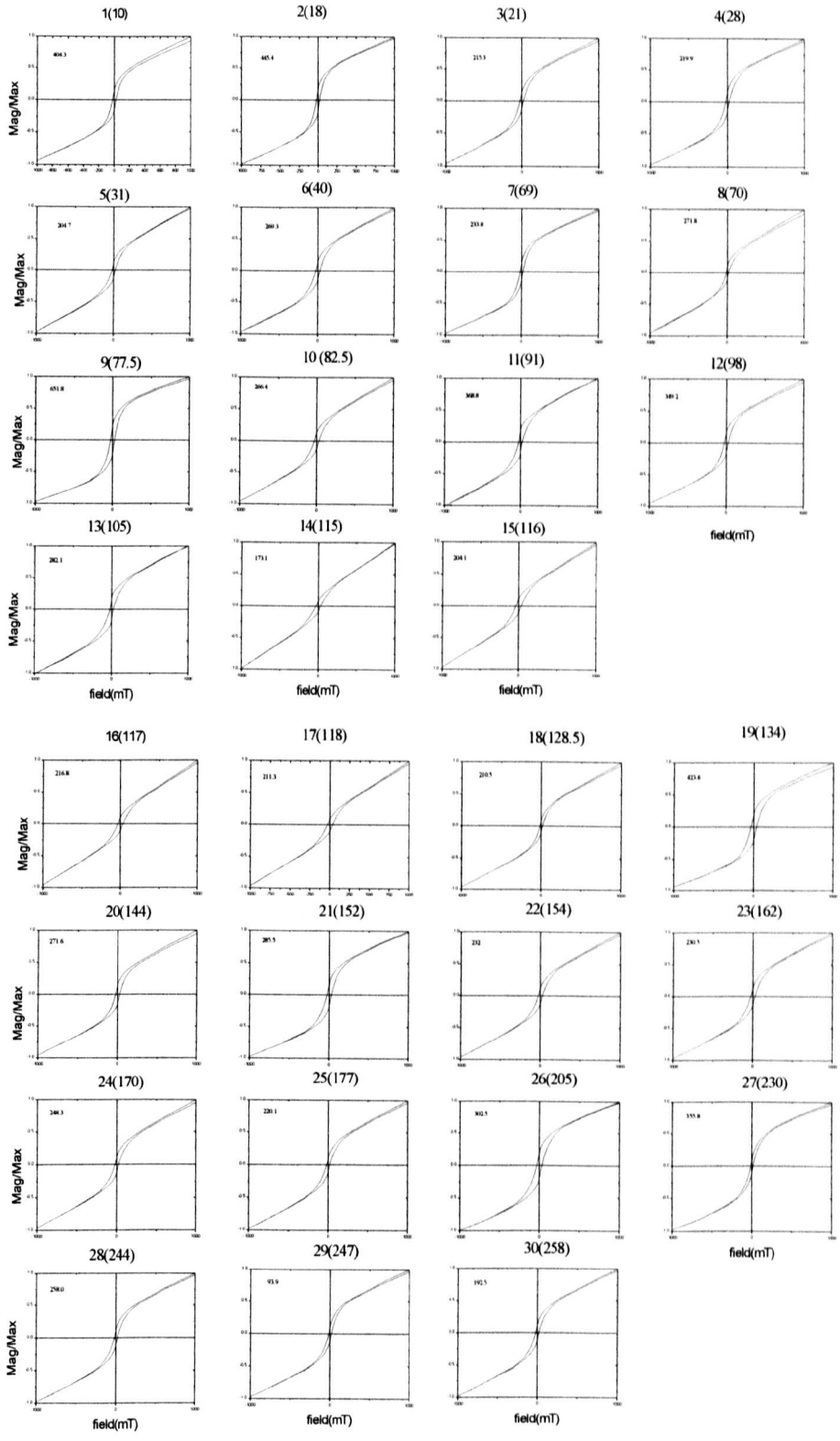

Hysteresis loops for Ska1, SE Iceland--- Note: No.(Depth/cm)

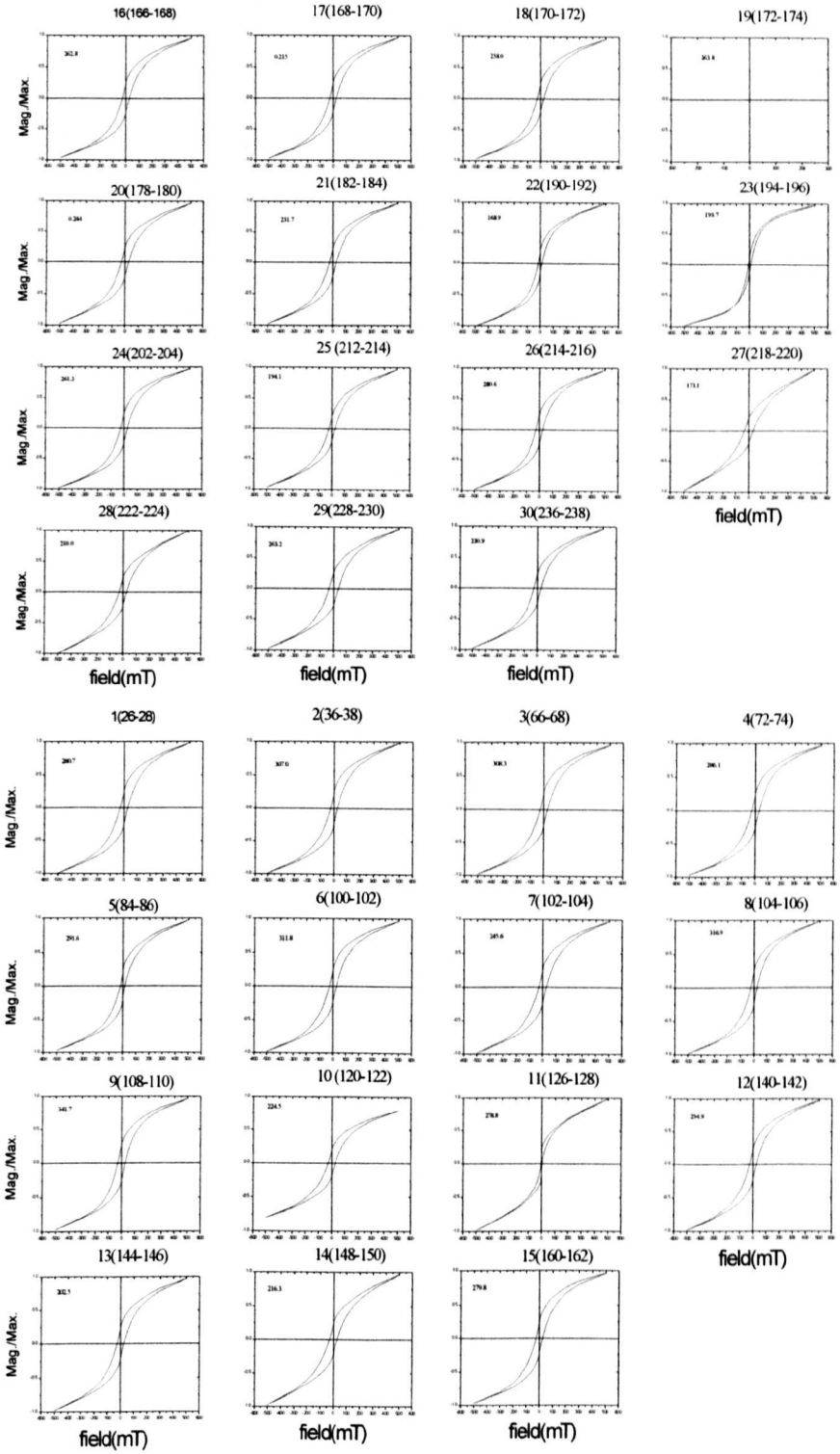

Hysteresis loops for Ska2, SE Iceland---No. (Depth/cm)

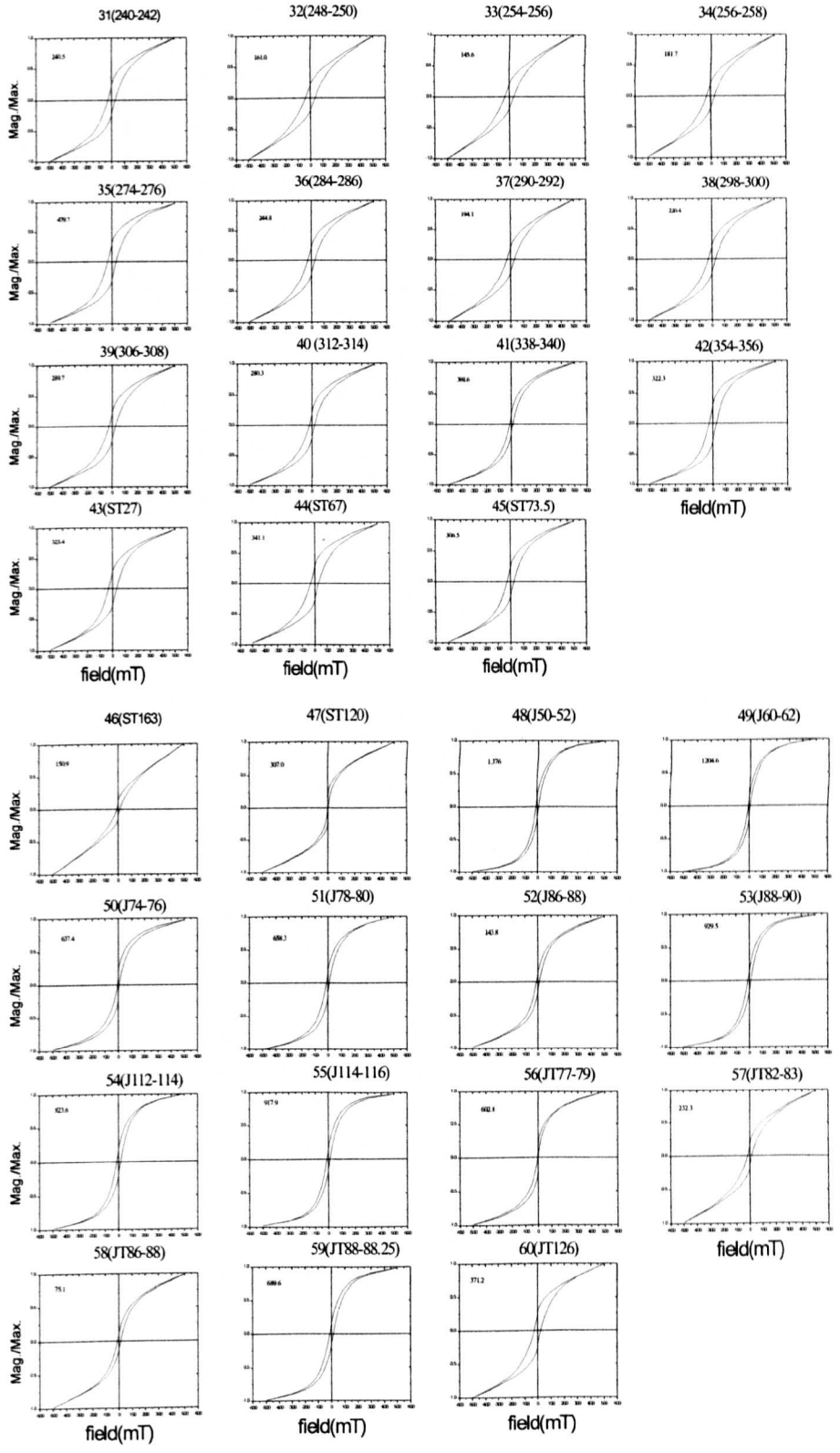

Hysteresis Loops for Ska2 (31- 47) and JL2 (48-60), SE Iceland---No. (Depth/cm)

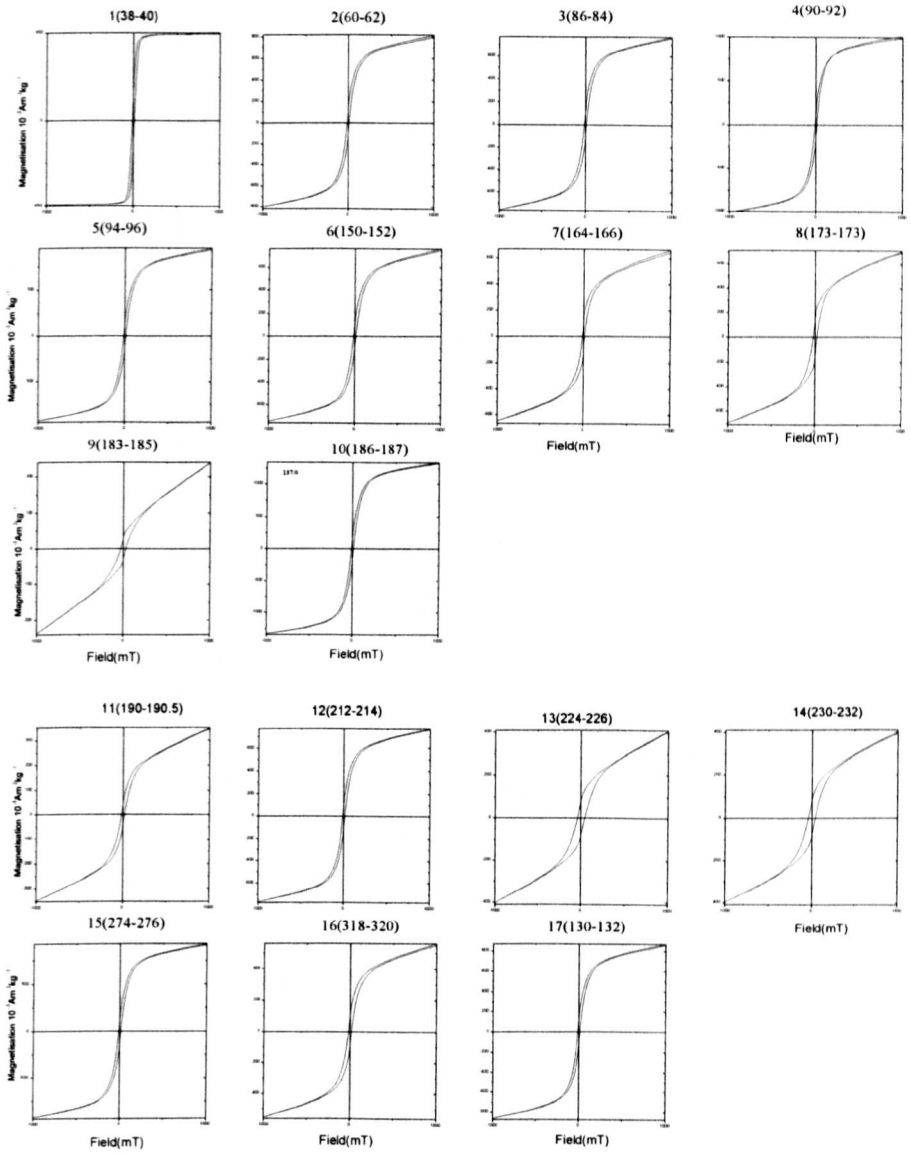

Hysteresis loops of JL1, Iceland ---Note: No. (Depth/cm)

Appendix 2 Strong field thermomagnetic curves of the five studied profiles, Lax, Ska1, Ska2, JL1 and JL2. Southeast Iceland. Measurement with VFTB.

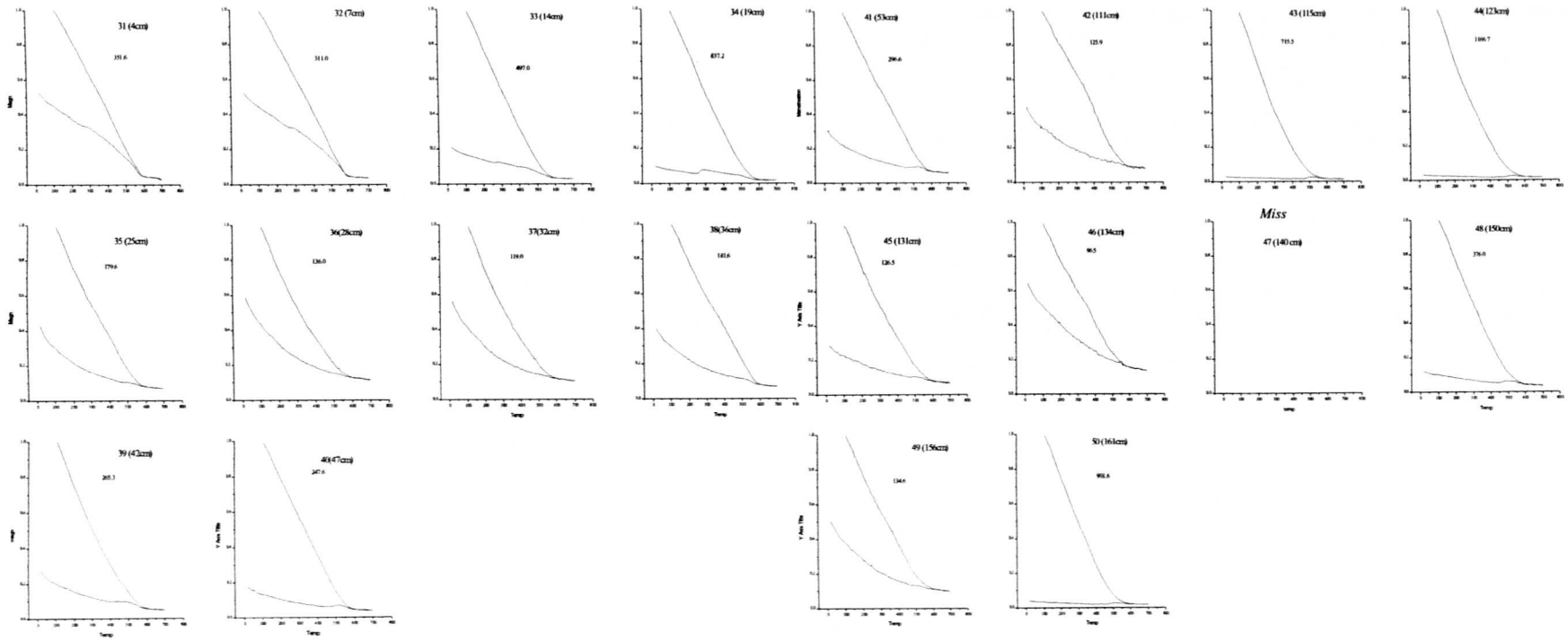

Strong field thermomagnetic curves of Lax, Iceland

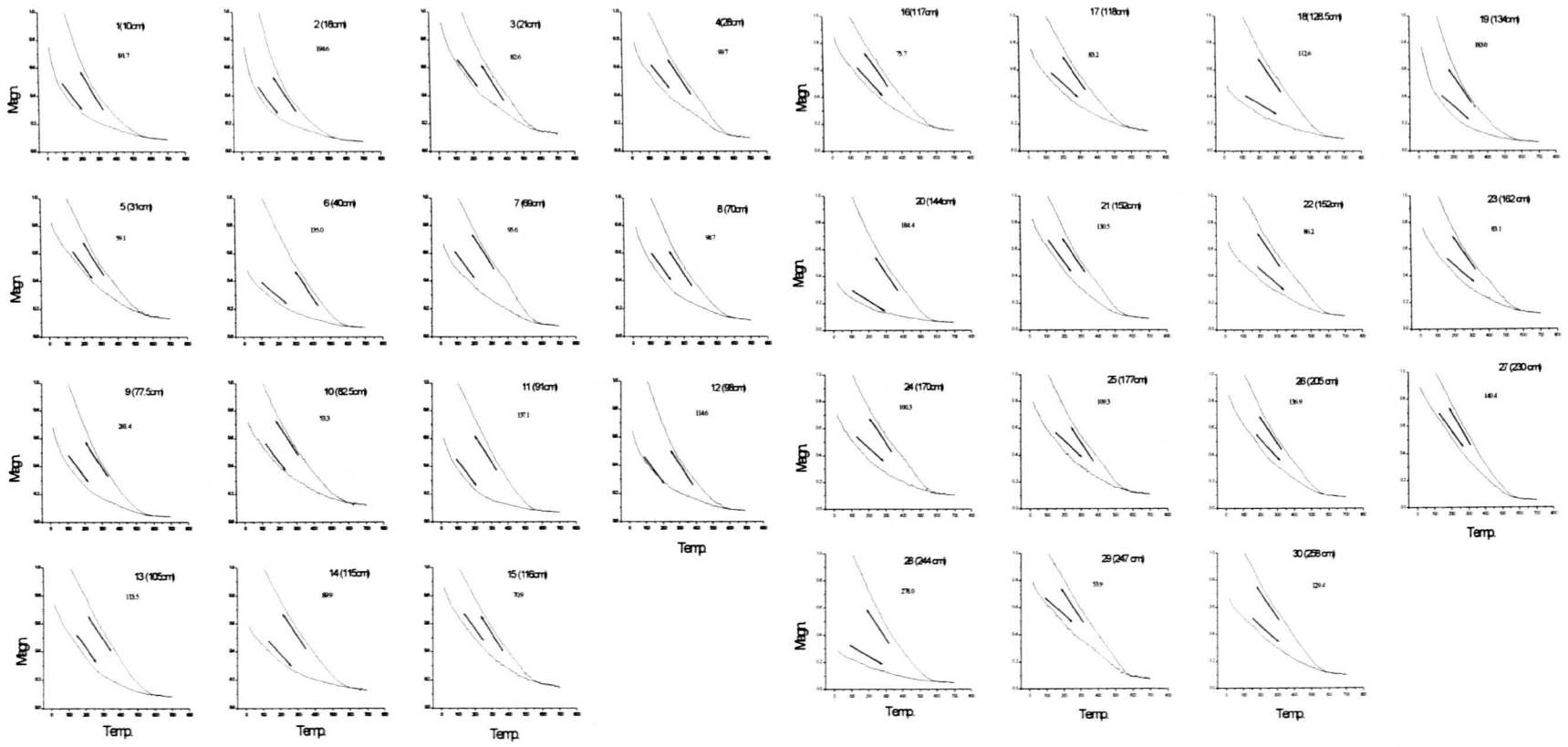

Strong field thermomagnetic curves for the samples from Ska1 SE Iceland.

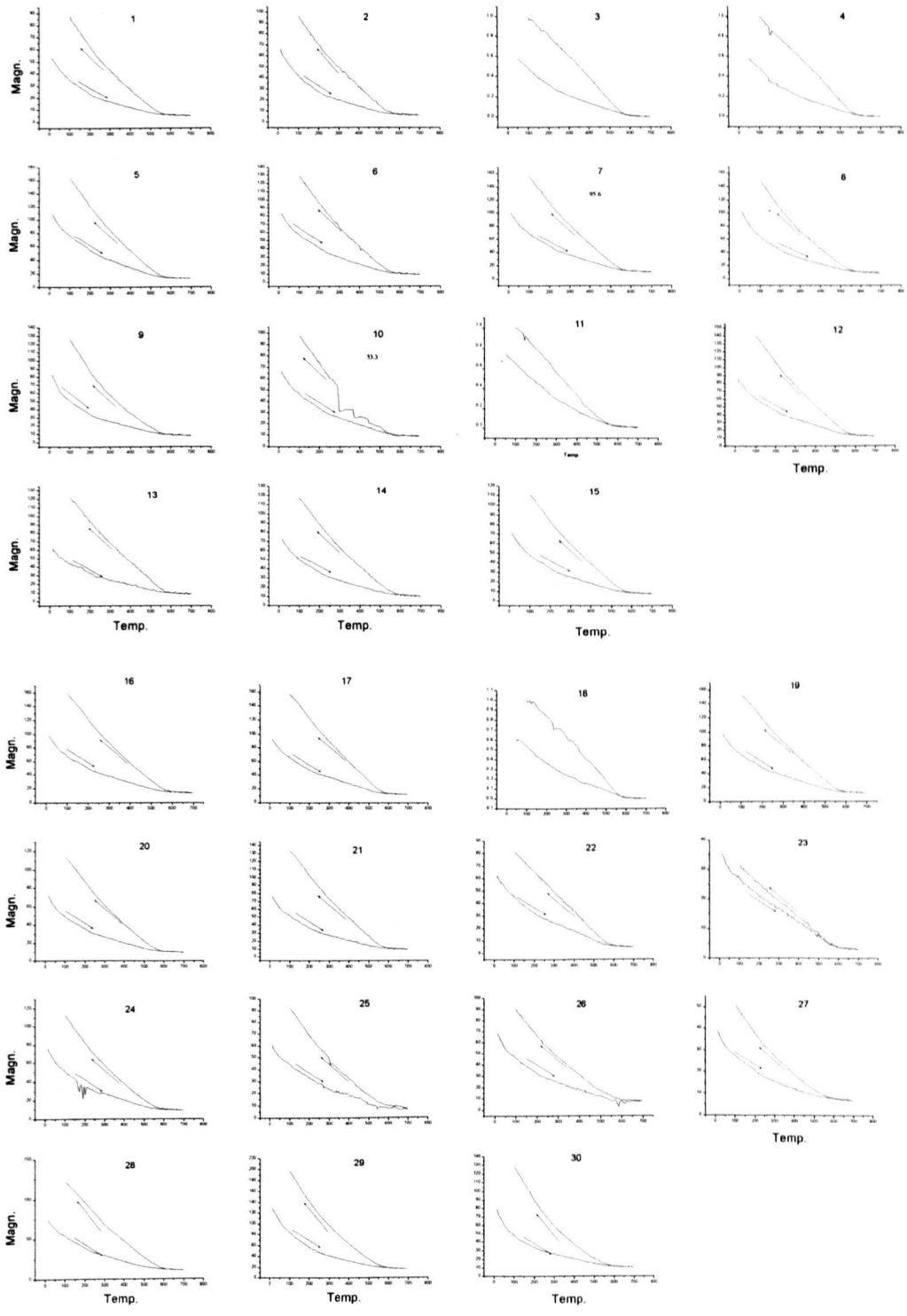

Strong field thermomagnetic curves for Ska2, SE Iceland

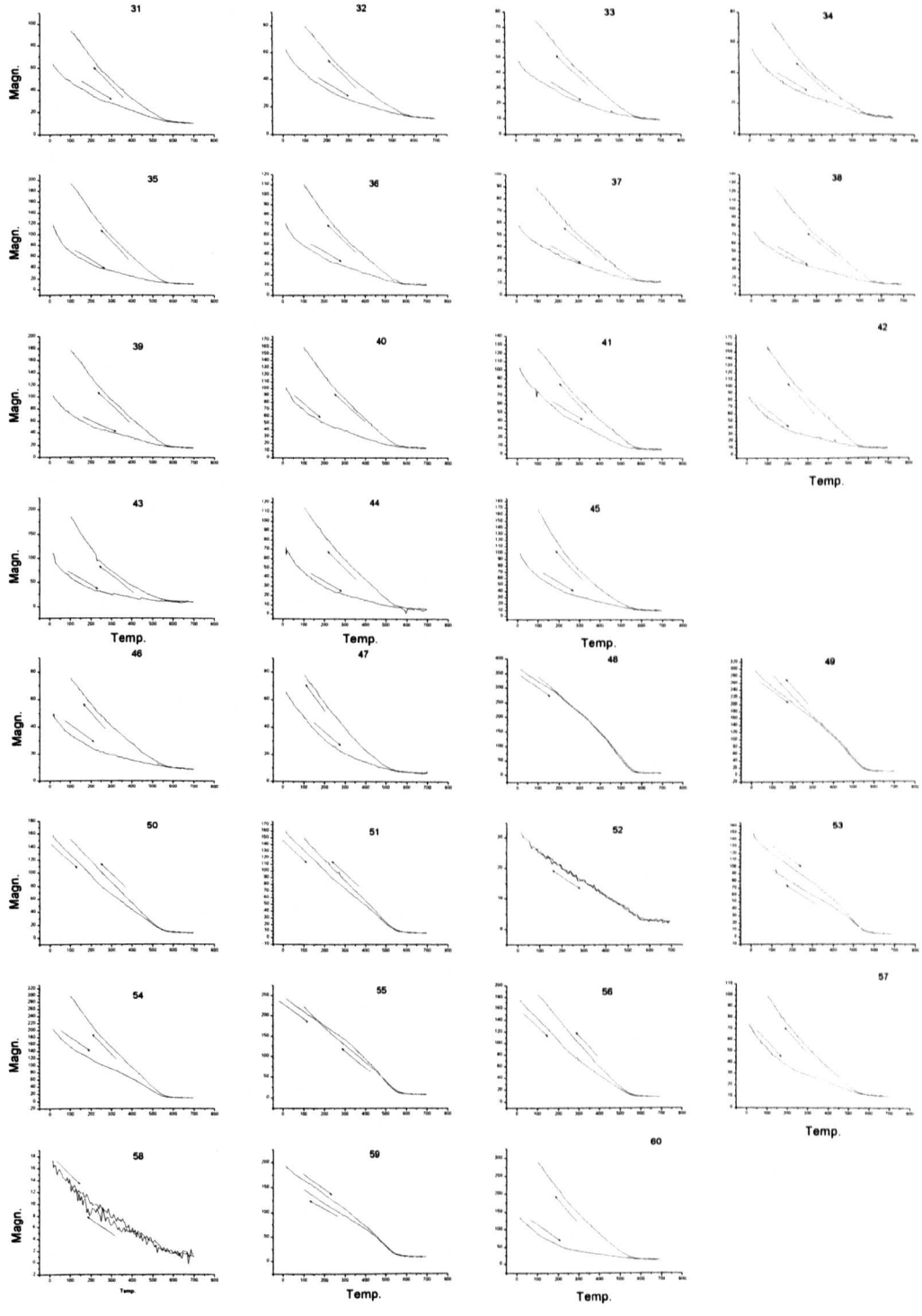

Strong field thermomagnetic curves for Ska2 (31 and 47) and JL2 (48-60), SE Iceland

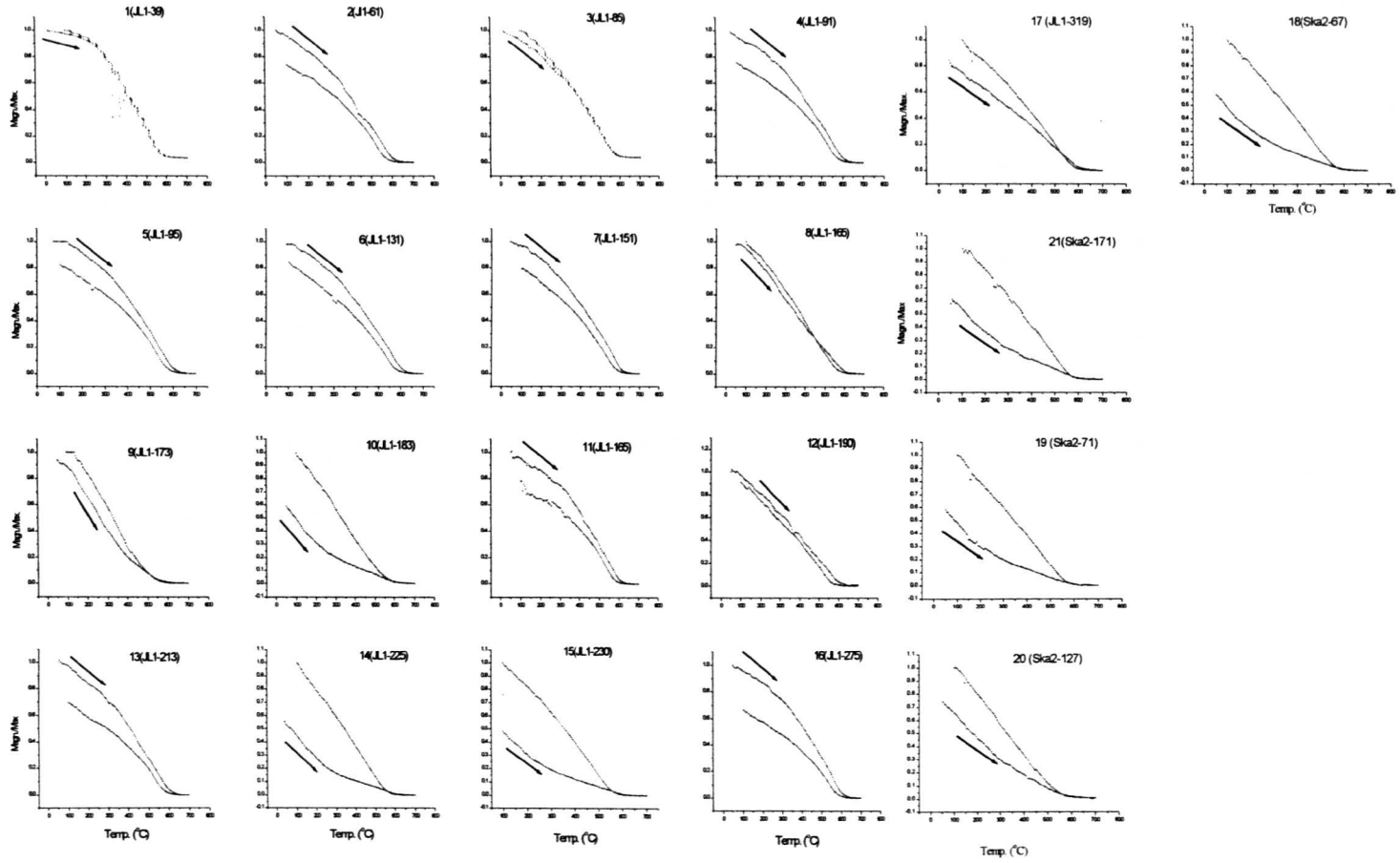

Strong field thermomagnetic curves of JL1, SE Iceland

Appendix 3: The results of LOI measurements.

Loss on ignition of selected samples of peat cores Lax, Iceland.

Cores	Lax	Lax	Lax	Lax	Lax	Lax	Lax	Lax	Lax	Lax	Lax	Lax	Lax	Lax	Lax	Lax	Lax	Lax	Lax	Lax
Depth	4	7	14	19	25	28	32	36	42	47	57	111	115	123	131	134	140	150	156	161
%loi	16.33	12.15	9.06	13.45	8.99	5.48	4.80	7.52	14.21	16.47	14.12	23.60	25.27	15.20	12.46	36.85	27.69	27.69	13.12	23.21

Loss on ignition of the selected samples from JL2 and Ska2, Iceland.

Depth	LOI	Profile	Depth	LOI	Profile
27.00	7.99	Ska2	241.00	11.61	Ska2
37.00	7.62	Ska2	249.00	5.79	Ska2
67.00	7.92	Ska2	255.00	5.33	Ska2
73.00	7.79	Ska2	257.00	13.73	Ska2
85.00	7.30	Ska2	275.00	9.49	Ska2
101.00	9.80	Ska2	285.00	12.80	Ska2
102.00	8.46	Ska2	291.00	9.30	Ska2
105.00	7.39	Ska2	299.00	11.78	Ska2
109.00	7.36	Ska2	307.00	13.97	Ska2
121.00	9.93	Ska2	313.00	12.57	Ska2
126.00	1.22	Ska2	339.00	6.04	Ska2
140.00	11.41	Ska2	355.00	17.97	Ska2
145.00	11.21	Ska2	27.00	4.52	Ska2
149.00	5.13	Ska2	67.00	4.75	Ska2
161.00	8.86	Ska2	73.50	4.23	Ska2
167.00	9.20	Ska2	103.00	3.02	Ska2
169.00	10.68	Ska2	120.00	0.95	Ska2
171.00	8.41	Ska2	51.00	3.66	JL2
173.00	8.29	Ska2	61.00	3.30	JL2
179.00	7.62	Ska2	75.00	2.08	JL2
183.00	6.41	Ska2	79.00	2.38	JL2
191.00	4.61	Ska2	87.00	2.47	JL2
195.00	2.33	Ska2	89.00	3.44	JL2
203.00	12.25	Ska2	113.00	5.00	JL2
213.00	14.98	Ska2	115.00	3.42	JL2
216.00	14.07	Ska2	78.00	1.75	JL2
219.00	7.47	Ska2	82.50	2.02	JL2
223.00	4.93	Ska2	87.00	2.11	JL2
229.00	5.12	Ska2	88.00	2.78	JL2
237.00	10.04	Ska2	126.00	4.29	JL2

Appendix 4: Overview of most of the known tephra-bearing eruptions in Iceland with their geochemical composition. The geochemical analyses were generally performed with a standard wavelength dispersive technique using an electron microprobe. All the analyses were performed on tephra particles, except a few from Hekla. (based on Haflidason et al, 2000)

Name	Age	SiO2	TiO2	Al2O3	FeO	MnO	MgO	CaO	Na2O	K2O	P2O5	Volcanic syster
G1983	*1983*	50.32	2.86	12.82	13.76	0.22	5.08	9.88	2.52	0.45	0.32	Grimsvotn
H1980	*1980*	50.4	1.84	14.33	11.23	0.27	2.92	7.23	4.17	1.3	1.12	Hekla
Ve1973	*1973*	47.7	3.2	16.3	13.72	0.23	4.5	8.3	4.5	1	0.53	Vestmannaeyja
H1970	*1970*	72.22	0.3	13.23	2.08	0.09	0.35	0.33	5.92	3.89	0.09	Hekla
H1970	*1970*	66.6	0.38	15.33	5.76	0.18	0.78	3.19	4.6	2.05	0.01	Hekla
Su1963	*1963*	46.7	2.1	15.5	12	0.18	9.2	10.5	3.1	0.47	0.32	Surty
A1961	*1961*	50.31	2.98	13.1	15.42	0.23	4.88	8.87	2.86	0.53	0.27	Askja
H1947	*1947*	62.15	0.98	15.13	8.01	0.22	1.28	4.46	4.38	1.73		Hekla
H1947	*1947*	69.93	0.35	13.43	4.77	0.11	0.16	1.19	5.18	3.35		Hekla
H1947	*1947*	69.61	0.38	13.51	5.67	0.11	0.14	1.1	5.46	3.46		Hekla
G1934	*1934*	50.3	3.08	12.8	14.4	0.26	5.14	9.92	2.56	0.52	0.38	Grimsvotn
G1922	*1922*	50.1	3.06	12.8	13.9	0.2	5.24	10.2	2.47	0.4	0.3	Grimsvotn
K1918	*1918*	47.46	4.23	12.42	14.45	0.26	4.79	9.69	2.8	0.69	0.79	Katla
K1918	*1918*	47.97	4.62	12.81	14.39	0.28	5	10.29	3.37	0.77		Katla
G/Th1903	*1903*	49.8	2.92	13.1	13.6	0.2	5.45	40.3	2.53	0.38	0.27	Thordarhvrna
G1892	*1892*	50.65	2.98	12.95	14.11	0.22	5.29	10.3	2.71	0.45	0.3	Grimsvotn
G1883	*1883*	49.8	2.78	13.7	13.64	0.24	5.32	10.6	2.8	0.55	0.32	Grimsvotn
A1875	*1875*	73.72	0.8	12.81	3.34	0.08	0.6	2.31	3.65	2.4	0.14	Askia
A1875	*1875*	72.21	0.79	12.42	3.28	0.11	0.64	2.3	3.38	2.43		Askia
V1862-64	*1862*	50.05	1.49	14.19	12.69	0.31	7.2	11.18	2.3	0.17	0.2	Veidivotn
K1860	*1860*	47.4	4.63	13.05	14.76	0.22	3.8	9.18	2.9	0.77	0.62	Katla
H1845	*1845*	56.89		14.18	13.35	0.54	4.05	6.23	2.35	2.64		Hekla
G1838	*1838*	50.47	3.01	12.44	13.46	0.25	5.08	10.46	2.36	0.43	0.34	Grimsvoth
E1821	*1821*	69.13	0.36	14.1	4.29	0.15	0.13	1.1	6.14	3.5		Eyjafjallajokull
G1823	*1823*	49.61	2.87	12.3	12.92	0.24	5.34	10.62	2.48	0.4	0.31	Grimsvotn
G1783-85	*1783*	49.27	3.1	12.56	14.22	0.25	5.28	10.57	2.14	0.46	0.33	Grimsvotn
Laki1783	*1783*	50.38	2.11	14.16	13	0.23	6.58	11.42	2.01	0.53		Lakagigar
Laki1783	*1783*	49.1	2.96	12.7	13.7	0.22	5.32	10.1	2.61	0.47	0.36	Lakagigar
G1774	*1774*	49.01	2.72	13.41	12.88	0.2	5.94	10.53	2.56	0.44	0.3	Grimsvotn
H1766	*1766*	60.24	1.09	15.38	9.21	0.23	1.53	5.33	2.95	1.6	47	Hekla
G1766	*1766*	49.33	1.74	13.4	11.66	0.2	6.76	11.72	2.3	0.22	0.16	Veidivotn
K1755	*1755*	47.02	4.77	13.59	15.14	0.24	5.38	8.88	2.37	1.12		Katla
K1755	*1755*	47.6	4.31	13.54	14.34	0.28	4.88	9.25	2.88	0.8	0.6	Katla
V1739	*1739*	49	1.75	13.79	12.44	0.2	6.52	12.18	2.51	0.26	0.18	Veidivotn
O1727	*1727*	57.92	1.62	13.65	12.71	0.37	1.37	5.21	2.42	1.63	0.61	Orefajokull
K1721	*1721*	49.1	4.41	13.06	14.28	0.23	5	9.86	3.01	0.73		Katla
H1721	*1721*	46.88	4.45	12.41	14.68	0.24	4.98	9.65	2.5	0.52	0.5	Katla
V1720	*1720*	49.86	1.52	13.53	11.41	0.2	4.46	12.16	2.56	0.24	0.18	Veidivotn
V1717	*1717*	50.39	1.78	14.05	12.15	0.24	6.61	12.01	2.36	0.2	0.17	Veidivotn
V1717	*1717*	49.57	1.78	13.5	12.12	0.23	6.85	12.29	2.52	0.2		Veidivotn
V1711	*1711*	49.23	1.71	13.56	12.04	0.22	6.67	12.04	2.4	0.25	0.17	Veidivotn
V1707	*1707*	49.5	1.69	13.56	12.07	0.24	6.37	11.65	2.34	0.24	0.16	Veidivotn
V1706	*1706*	48.95	1.69	13.58	12.31	0.26	6.71	12.04	2.36	0.26	0.18	Veidivotn
V1697	*1697*	50.61	1.79	13.76	12.66	0.21	7.29	11.42	2.58	0.22	0.17	Veidivotn
H1693	*1693*	55.23	1.64	15.31	10.96	0.4	2.59	5.66	2.97	2.19	0.8	Hekla
K1660	*1660*	46	4.72	13	15.2	0.27	4.45	9.55	3.4	0.86	0.72	Katla
G1659	*1659*	49.1	2.7	13.2	13.35	0.22	5.66	10.69	2.54	0.46	0.29	Grimsvotn
H1636	*1636*	61.49	1.25	15.02	10	0.35	1.6	5.85	2.7	1.61	0.55	Hekla
K1625	*1625*	46.6	4.54	13.05	14.88	0.22	4.13	9.47	3.4	0.78	0.73	Katla
G1619	*1619*	51.06	2.88	13.32	13.75	0.23	5.58	10.54	2.56	0.44	0.35	Grimsvotn
H1510	*1510*	58.37	2.26	12.91	12.45	0.31	2.23	5.62	3.36	1.94		Hekla
H1510	*1510*	62.69	0.95	15.17	7.82	0.23	1.31	4.5	4.42	1.74		Hekla

Table 9.1 Continue

Name	Age	SiO2	TiO2	Al2O3	FeO	MnO	MgO	CaO	Na2O	K2O	P2O5	Volcanic system
K1500	*1500*	46.55	4.52	12.31	14.97	0.23	5.06	10.41	2.71	0.63	0.62	Katla
K1500	*1500*	46.77	4.62	12.44	14.76	0.24	5.04	9.82	2.7	0.54	0.47	Katla
V1477	*1477*	50.65	1.96	12.6	12.86	0.25	9.34	12.14	2.12	0.22	0.2	Veidivotn
V1477	*1477*	49.89	1.9	13.02	12.45	0.23	6.66	12.05	0.23			Veidivotn
V1410	*1410*	19.98	1.86	13.11	12.35	0.21	6.79	12.64	2.28	0.18	0.19	Veidivotn
V1410	*1410*	49.18	1.81	13.43	11.94	0.23	6.96	12.08	2.35	25		Veidivotn
O1362	*1362*	71.46	0.22	13.13	3.16	0.05	0	0.99	5.45	3.535		Orefajokull
K1357	*1357*	47.65	4.46	13.72	14.54	0.28	3.76	8.96	2.45	0.78	0.65	Katla
G1354	*1354*	49.01	2.47	14.06	11.99	0.15	6.01	10.31	2.6	0.34	0.17	Grimsvotn
G1354	*1354*	49.9	2.83	13.11	13.22	0.22	5.48	10.5	2.94	0.46		Grimsvotn
H1341	*1341*	60.36	1.25	15.22	8.55	0.3	1.85	6.19	3.96	1.29		Hekla
H1341	*1341*	62.36	1.45	13.74	9.76	0.2	1.69	5.15	6.23	1.13		Hekla
V1340	*1340*	48.73	1.74	14.28	11.97	0.18	7.37	12.27	2.36	0.23		Veidivotn
H1300	*1300*	54.89	1.7	13.92	9.39	0.26	3.41	6.93	3.43	1.41	0.51	Hekla
H1300	*1300*	60.29	0.98	14.39	7.92	0.27	1.14	4.77	4.58	1.66		Hekla
H1300	*1300*	70.58	23	14.69	3.07	0.11	0.12	1.09	3.46	2.68	0.06	Hekla
K1262	*1300*	49.06	4.74	11.91	15.24	0.28	4.71	9.98	2.7	0.76	0.7	Katla
Re1226	*1226*	49.08	1.85	13.32	13.33	0.23	6.47	10.96	2.35	0.1	0.12	Reykjanes
Re1231	*1231*	46.4	1.68	13.89	12.24	0.18	6.91	12.47	2.41	0.05	0.08	Reykjanes
K1179	*1179*	48.26	4.6	12.58	13.62	0.26	4.85	10.04	3.42	0.82		Katla
V1159	*1159*	50.34	1.74	13.95	11.49	0.25	7.3	12.83	2.53	0.19		Veidivotn
V1159	*1159*	49.91	1.96	13.68	11.86	0.21	6.82	12.01	2.4	0.21	0.19	Veidivotn
H1158	*1158*	67.42	0.48	14.39	5.71	0.2	0.45	3.11	4.56	2.24		Hekla
H1158	*1158*	69.51	0.47	14.05	4.87	0.17	0.27	2.72	3.99	2.4	0.08	Hekla
H1158	*1158*	73.72	0.17	12.07	2.18	0.12	0.13	1.45	4.15	2.85	0.03	Hekla
H1104(H1)	*1104*	72.46	0.21	13.93	3.05	0.08	0.08	2.09	4.59	2.68		Hekla
Eld9334	*934*	46.52	4.37	12.72	15.08	0.21	5.41	11.15	2.8	0.57	0.44	Eldgja-katla
Katla-R	*920*	47.41	12.66	14.92	0.24	4.82	9.79	2.86	0.71	0.58		Katla
Settltment	*870*	49.76	1.8	13.25	12.85	0.23	6.47	11.68	2.45	0.16	0.19	Veidivotn
Settlement	*870*	70.41	0.3	14.34	2.29	0.24	0.23	1.2	4.69	4.73	0.06	Torfajokull
Twilling-b	*650*	50.43	3.57	12.48	14.39	0.23	4.39	9.43	3.03	0.64		Katla
Twilling-c	*550*	48.75	1.88	13.76	11.69	0.23	7.34	13.31	2.15	0.19		Veidivotn
Twilling-c	*550*	49.55	1.78	14.17	13.05	0.22	652	11.69	2.45	0.23	0.19	Veidivotn
Layer G	*150*	61.5	9	15.82	8.2	0.24	1.06	4.95	4.2	1.51		Torfajokull
G150	*150*	49.46	2.72	13.29	12.92	0.26	5.56	10.28	2.9	0.45		Grimsvotn
V150	*150*	50.13	1.94	13.34	14.43	0.3	5.79	11.03	2.68	0.33		Veidivotn
GG	*2100*	72.6	0.63	12.73	4.19	0.13	0.56	2.61	3.51	1.95		Glen Garry
SvV	*2500*	48.48	1.8	13.59	11.71	0.22	7.11	11.9	2.38	0.2		Veidivotn
H3	*2855*	72.49	0.2	14.13	2.88	0.13	0.1	1.97	5.48	2.56		Hekla
H-S	*3500*	72.3	0.2	13.75	2.72	0.09	0.13	1.83	4.03	2.52		Hekla
H-S	*3500*	66.71	0.47	14.72	5.49	0.13	0.53	3.17	4.66	2.04		Hekla
H4	*3830*	74.3	0.12	13.09	1.58	0.14	0	1.33	4.89	2.6		Hekla
QUB-141	*5811*	70.49	0.24	14.58	2.23		0.16	0.7	5.24	4.79		Snefellsjokull
Hoy Tephra	*5600*	71.19	0.19	14.02	221	0.06	0.16	0.69	4.68	4.72		Torfajokull
H5	*6100*	74.8	0.12	12.62	1.37	0.12	0	1.29	4.54	2.53		Hekla

Appendix 5: Principal coordinates analysis on chemical data (SPSS output)

	Spss Input Data									
The average of geochemistry of different tephra layers in tgis study.										
Samples were measured at Edinburgh										
	SiO2	TiO2	Al2O3	FeO	MnO	MgO	CaO	Na2O	K2O	Total
JL1(174)	49.388	1.972	13.162	12.654	0.237	6.444	11.375	2.542	0.231	98.005
JL1(186)	48.757	1.9767	13.427	12.103	0.2567	6.4567	11.13	2.54	0.25	96.897
JL1(186)	48.945	2.9225	12.943	13.36	0.2475	5.1	9.82	2.8	0.7875	96.925
JL1(186)	47.298	4.185	13.295	13.603	0.235	4.9175	10.118	2.8875	0.55	97.088
JL1(190)	71.728	0.2515	13.088	3.1646	0.1108	0.0338	1.0131	4.5362	3.3992	97.326
JL1(38)	64.24	0.04	17.07	2.26	0.03	0.03	0.62	6.94	4.84	96.07
JL1(38)	71.88	0.26	12.88	3.15	0.10	0.04	1.00	4.91	3.36	97.58
JL2 (74)	48.90	1.89	13.25	12.72	0.23	6.34	11.05	2.47	0.32	97.18
JL2 (86)	71.154	0.261	12.983	3.184	0.111	0.03	0.996	4.626	3.417	96.762
Lax(121)	48.92	1.47	13.52	10.71	0.20	8.08	12.71	2.14	0.14	97.90
Lax(154)	48.526	2.6378	12.824	12.762	0.2056	5.8956	10.658	2.7422	0.36	96.611
Lax(18)	47.24	4.79	12.35	14.81	0.25	4.97	9.73	3.18	0.76	98.07
Lax(38)	72.70	0.20	13.03	3.25	0.08	0.02	1.03	4.68	3.50	98.48
Ska1(136)	71.858	0.56	12.265	3.6775	0.17	0.3875	2.265	3.5	2.075	96.758
Ska1(175)	50.47	3.136	12.56	13.744	0.294	4.102	8.384	3.318	0.786	96.794
Ska1(237)	68.15	0.506	15.074	5.782	0.178	0.562	3.55	4.346	2.126	100.27
Ska1(75)	46.21	4.462	12.344	14.128	0.298	4.672	9.588	3.094	0.788	95.584
Ska2 H4	72.44	0.15	12.60	1.87	0.11	0.02	1.35	4.11	2.81	95.45
Ska2(256)	48.61	2.01	13.07	11.66	0.22	6.18	10.69	2.57	0.26	95.26
Ska2(89)	46.121	4.7056	12.378	14.328	0.2522	4.9033	9.6056	3.0989	0.7467	96.139
Samples were measure at Manchester.										
	SiO2	TiO2	Al2O3	FeO	MnO	MgO	CaO	Na2O	K2O	Total
b02	48.398	2.1153	13.169	12.371	0.203	6.5714	11.244	2.5202	0.2613	96.853
b03	56.583	1.5887	13.433	11.49	0.3297	1.381	5.3757	4.9697	1.4817	96.632
b03	49.123	2.0243	13.384	11.965	0.2023	6.881	11.446	2.5257	0.2677	97.819
b03	48.874	2.69	12.793	13.262	0.217	5.544	9.9275	2.8925	0.4283	96.628
b05	48.662	2.8751	12.66	13.596	0.2211	5.5864	9.9851	2.8566	0.403	96.846
b07	48.662	1.798	14.471	11.423	0.1778	6.2248	11.781	2.5703	0.2238	97.331
b07	48.799	2.8966	12.627	13.695	0.2296	5.5041	9.8717	2.8084	0.4233	96.855
b08	48.683	1.9538	12.971	12.917	0.2192	6.5041	11.131	2.494	0.2475	97.119
b11	48.442	2.6645	12.776	13.17	0.2077	5.9431	10.473	2.7735	0.3792	96.829
b14	48.878	1.8376	13.278	12.156	0.2036	6.9032	11.747	2.346	0.2254	97.574
b14	48.898	2.7123	12.7	13.274	0.2085	5.997	10.407	2.761	0.3913	97.35
b14	46.92	4.5785	12.381	14.455	0.2095	5.036	10.223	3.173	0.701	97.677
b12	47.966	1.8736	12.787	12.869	0.2137	6.4703	11.22	2.4748	0.2063	96.081
b18	48.557	1.8341	13.058	12.348	0.2164	6.9037	11.444	2.445	0.2144	97.02
b18	48.182	3.3346	12.033	14.796	0.2296	4.7889	8.9213	3.009	0.5156	95.809
b19	49.758	2.0793	13.148	12.782	0.2069	6.2541	10.758	2.6061	0.2974	97.891
b19	49.517	2.6225	12.885	13.243	0.2025	5.6683	10.071	2.87	0.3873	97.466
b20	48.878	2.9694	12.478	13.874	0.2308	5.1038	9.3041	3.039	0.4955	96.372
b33	49.183	2.7793	12.667	13.582	0.2265	5.5644	9.9754	2.8518	0.4053	97.235
b34	71.217	0.2415	13.192	3.23	0.096	0.0095	0.97	4.875	3.457	97.288
b34	48.442	3.0261	12.573	13.766	0.215	5.5979	10.061	2.8081	0.4549	96.944
b35	48.363	1.8589	13.042	12.554	0.2082	6.8506	11.663	2.4817	0.2	97.221
b15	48.92	1.9236	12.943	12.849	0.2152	6.5675	11.03	2.4613	0.2278	97.137
b21	52.643	0.107	27.877	0.7661	0.0055	0.1088	12.127	4.6693	0.1713	98.475
b23	48.534	2.5738	12.921	12.936	0.213	6.1323	10.507	2.7495	0.3605	96.927
b30	48.654	2.2356	12.816	13.353	0.2254	6.19	10.749	2.608	0.2804	97.112

SPSS input Data

The known tephra-bearing eruptions in Iceland with their geochemical composition (Based on Haflidason, et al, 2000)

Name	SiO2	TiO2	Al2O3	FeO	MnO	MgO	CaO	Na2O	K2O	
G1922	50.1	3.06	12.8	13.9	0.2	5.24	10.2	2.47	0.4	
K1918	47.97	4.62	12.81	14.39	0.28	5	10.29	3.37	0.77	
G/Th1903	49.8	2.92	13.1	13.6	0.2	5.45	40.3	2.53	0.38	
G1892	50.65	2.98	12.95	14.11	0.22	5.29	10.3	2.71	0.45	
G1883	49.8	2.78	13.7	13.64	0.24	5.32	10.6	2.8	0.55	
A1875	73.72	0.8	12.81	3.34	0.08	0.6	2.31	3.65	2.4	
A1875	72.21	0.79	12.42	3.28	0.11	0.64	2.3	3.38	2.43	
V1862-64	50.05	1.49	14.19	12.69	0.31	7.2	11.18	2.3	0.17	
K1860	47.4	4.63	13.05	14.76	0.22	3.8	9.18	2.9	0.77	
G1838	50.47	3.01	12.44	13.46	0.25	5.08	10.46	2.36	0.43	
E1821	69.13	0.36	14.1	4.29	0.15	0.13	1.1	6.14	3.5	
G1823	49.61	2.87	12.3	12.92	0.24	5.34	10.62	2.48	0.4	
G1783-85	49.27	3.1	12.56	14.22	0.25	5.28	10.57	2.14	0.46	
Laki1783	50.38	2.11	14.16	13	0.23	6.58	11.42	2.01	0.53	
Laki1783	49.1	2.96	12.7	13.7	0.22	5.32	10.1	2.61	0.47	
G1774	49.01	2.72	13.41	12.88	0.2	5.94	10.53	2.56	0.44	
H1766	60.24	1.09	15.38	9.21	0.23	1.53	5.33	2.95	1.6	
G1766	49.33	1.74	13.4	11.66	0.2	6.76	11.72	2.3	0.22	
K1755	47.02	4.77	13.59	15.14	0.24	5.38	8.88	2.37	1.12	
K1755	47.6	4.31	13.54	14.34	0.28	4.88	9.25	2.88	0.8	
V1739	49	1.75	13.79	12.44	0.2	6.52	12.18	2.51	0.26	
O1727	57.92	1.62	13.65	12.71	0.37	1.37	5.21	2.42	1.63	
K1721	49.1	4.41	13.06	14.28	0.23	5	9.86	3.01	0.73	
H1721	46.88	4.45	12.41	14.68	0.24	4.98	9.65	2.5	0.52	
V1720	49.86	1.52	13.53	11.41	0.2	4.46	12.16	2.56	0.24	
V1717	50.39	1.78	14.05	12.15	0.24	6.61	12.01	2.36	0.2	
V1717	49.57	1.78	13.5	12.12	0.23	6.85	12.29	2.52	0.2	
V1711	49.23	1.71	13.56	12.04	0.22	6.67	12.04	2.4	0.25	
V1707	49.5	1.69	13.56	12.07	0.24	6.37	11.65	2.34	0.24	
V1706	48.95	1.69	13.58	12.31	0.26	6.71	12.04	2.36	0.26	
V1697	50.61	1.79	13.76	12.66	0.21	7.29	11.42	2.58	0.22	
H1693	55.23	1.64	15.31	10.96	0.4	2.59	5.66	2.97	2.19	
K1660	46	4.72	13	15.2	0.27	4.45	9.55	3.4	0.86	
G1659	49.1	2.7	13.2	13.35	0.22	5.66	10.69	2.54	0.46	
H1636	61.49	1.25	15.02	10	0.35	1.6	5.85	2.7	1.61	
K1625	46.6	4.54	13.05	14.88	0.22	4.13	9.47	3.4	0.78	
G1619	51.06	2.88	13.32	13.75	0.23	5.58	10.54	2.56	0.44	
H1510	58.37	2.26	12.91	12.45	0.31	2.23	5.62	3.36	1.94	
H1510	62.69	0.95	15.17	7.82	0.23	1.31	4.5	4.42	1.74	
K1500	46.55	4.52	12.31	14.97	0.23	5.06	10.41	2.71	0.63	
K1500	46.77	4.62	12.44	14.76	0.24	5.04	9.82	2.7	0.54	
V1477	50.65	1.96	12.6	12.86	0.25	9.34	12.14	2.12	0.22	
V1477	49.89	1.9	13.02	12.45	0.23	6.66	12.05	2.54	0.23	
V1410	19.98	1.86	13.11	12.35	0.21	6.79	12.64	2.28	0.18	
V1410	49.18	1.81	13.43	11.94	0.23	6.96	12.08	2.35	25	
O1362	71.46	0.22	13.13	3.16	0.05	0	0.99	5.45	3.535	
K1357	47.65	4.46	13.72	14.54	0.28	3.76	8.96	2.45	0.78	
G1354	49.01	2.47	14.06	11.99	0.15	6.01	10.31	2.6	0.34	
G1354	49.9	2.83	13.11	13.22	0.22	5.48	10.5	2.94	0.46	
H1341	60.36	1.25	15.22	8.55	0.3	1.85	6.19	3.96	1.29	
H1341	62.36	1.45	13.74	9.76	0.2	1.69	5.15	6.23	1.13	
V1340	48.73	1.74	14.28	11.97	0.18	7.37	12.27	2.36	0.23	
H1300	54.89	1.7	13.92	9.39	0.26	3.41	6.93	3.43	1.41	
H1300	60.29	0.98	14.39	7.92	0.27	1.14	4.77	4.58	1.66	
H1300	70.58	23	14.69	3.07	0.11	0.12	1.09	3.46	2.68	
K1262	49.06	4.74	11.91	15.24	0.28	4.71	9.98	2.7	0.76	
Re1226	49.08	1.85	13.32	13.33	0.23	6.47	10.96	2.35	0.1	
Re1231	46.4	1.68	13.89	12.24	0.18	6.91	12.47	2.41	0.05	
K1179	48.26	4.6	12.58	13.62	0.26	4.85	10.04	3.42	0.82	
V1159	50.34	1.74	13.95	11.49	0.25	7.3	12.83	2.53	0.19	
V1159	49.91	1.96	13.68	11.86	0.21	6.82	12.01	2.4	0.21	
H1158	67.42	0.48	14.39	5.71	0.2	0.45	3.11	4.56	2.24	
H1158	69.51	0.47	14.05	4.87	0.17	0.27	2.72	3.99	2.4	
H1158	73.72	0.17	12.07	2.18	0.12	0.13	1.45	4.15	2.85	
H1104(H1)	72.46	0.21	13.93	3.05	0.08	0.08	2.09	4.59	2.68	
Eld9334	46.52	4.37	12.72	15.08	0.21	5.41	11.15	2.8	0.57	
Katla-R	47.41	12.66	14.92	0.24	4.82	9.79	2.86	0.71	0.58	
Settltment	49.76	1.8	13.25	12.85	0.23	6.47	11.68	2.45	0.16	
Settlement	70.41	0.3	14.34	2.29	0.24	0.23	1.2	4.69	4.73	
Twilling-b	50.43	3.57	12.48	14.39	0.23	4.39	9.43	3.03	0.64	
Twilling-c	48.75	1.88	13.76	11.69	0.23	7.34	13.31	2.15	0.19	
Twilling-c	49.55	1.78	14.17	13.05	0.22	6.52	11.69	2.45	0.23	
Layer G	61.5	9	15.82	8.2	0.24	1.06	4.95	4.2	1.51	
G150	49.46	2.72	13.29	12.92	0.26	5.56	10.28	2.9	0.45	
V150	50.13	1.94	13.34	14.43	0.3	5.79	11.03	2.68	0.33	
GG	72.6	0.63	12.73	4.19	0.13	0.56	2.61	3.51	1.95	
SvV	48.48	1.8	13.59	11.71	0.22	7.11	11.9	2.38	0.2	
H3	72.49	0.2	14.13	2.88	0.13	0.1	1.97	5.48	2.56	
H-S	72.3	0.2	13.75	2.72	0.09	0.13	1.83	4.03	2.52	
H-S	66.71	0.47	14.72	5.49	0.13	0.53	3.17	4.66	2.04	
H4	74.3	0.12	13.09	1.58	0.14	0	1.33	4.89	2.6	
Hoy Tephra	71.19	0.19	14.02	2.21	0.06	0.16	0.69	4.68	4.72	

This is a dissimilarity matrix of the samples which measured in Edinburgh
Rescaled Euclidean Distance

	JL1(38)	JL1(38)	JL1(174)	JL1(186)	JL1(186)	JL1(186)	JL1(190)	JL2 (74)	JL2 (86)	Lax(18)	Lax(38)	Lax(121)	Lax(154)	Ska1(75)	Ska1(136)	Ska1(175)	Ska1(237)	Ska2(89)	Ska2(256)	Ska2 H4
G1922	0.217	0.211	0.030	0.034	0.008	0.025	0.210	0.029	0.209	0.035	0.210	0.068	0.018	0.029	0.201	0.031	0.172	0.034	0.033	0.217
K1918	0.232	0.228	0.050	0.053	0.030	0.013	0.227	0.049	0.227	**0.010**	0.228	0.083	0.037	0.006	0.220	0.045	0.190	0.008	0.054	0.235
G/Th1903	0.541	0.537	0.372	0.374	0.391	0.383	0.537	0.375	0.537	0.389	0.537	0.356	0.378	0.388	0.526	0.414	0.506	0.388	0.379	0.537
G1892	0.217	0.210	0.030	0.034	0.007	0.025	0.209	0.028	0.209	0.035	0.209	0.069	0.018	0.029	0.201	0.030	0.172	0.035	0.033	0.217
G1883	0.217	0.214	0.024	0.026	0.010	0.022	0.213	0.021	0.213	0.039	0.214	0.062	0.013	0.033	0.206	0.038	0.175	0.037	0.027	0.221
A1875	0.076	0.019	0.207	0.205	0.198	0.216	0.018	0.208	0.019	0.224	0.018	0.218	0.205	0.219	0.005	0.180	0.040	0.225	0.196	0.016
A1875	0.078	0.020	0.208	0.206	0.199	0.217	0.019	0.208	0.020	0.225	0.019	0.219	0.205	0.220	0.005	0.180	0.042	0.225	0.197	0.016
V1862-64	0.223	0.220	0.015	0.012	0.040	0.050	0.219	0.014	0.219	0.067	0.220	0.034	0.025	0.062	0.211	0.065	0.182	0.065	0.018	0.226
K1860	0.228	0.225	0.065	0.068	0.038	0.025	0.225	0.063	0.224	0.019	0.225	0.101	0.052	0.016	0.218	0.042	0.187	0.018	0.067	0.233
G1838	0.213	0.204	0.030	0.034	0.014	0.032	0.203	0.030	0.203	0.042	0.203	0.067	0.020	0.037	0.194	0.031	0.166	0.042	0.031	0.210
E1821	0.047	0.021	0.208	0.206	0.197	0.214	0.022	0.208	0.021	0.222	0.022	0.221	0.205	0.217	0.037	0.177	0.035	0.222	0.197	0.034
G1823	0.214	0.205	0.024	0.028	0.016	0.033	0.205	0.024	0.205	0.045	0.205	0.059	0.014	0.040	0.196	0.037	0.168	0.045	0.024	0.211
G1783-85	0.227	0.219	0.031	0.037	0.017	0.025	0.219	0.030	0.218	0.033	0.219	0.069	0.021	0.028	0.210	0.039	0.181	0.033	0.037	0.226
Laki1783	0.222	0.219	0.012	0.010	0.031	0.041	0.218	0.009	0.218	0.059	0.218	0.040	0.018	0.053	0.210	0.058	0.180	0.057	0.016	0.224
Laki1783	0.219	0.212	0.028	0.032	0.007	0.023	0.212	0.026	0.211	0.034	0.212	0.067	0.016	0.028	0.203	0.033	0.174	0.033	0.031	0.219
G1774	0.217	0.214	0.016	0.017	0.017	0.028	0.213	0.013	0.213	0.045	0.213	0.051	0.006	0.040	0.205	0.045	0.175	0.043	0.017	0.220
H1766	0.103	0.097	0.131	0.128	0.118	0.135	0.095	0.130	0.095	0.146	0.096	0.149	0.128	0.140	0.091	0.100	0.054	0.146	0.121	0.104
G1766	0.219	0.215	0.014	0.010	0.043	0.054	0.214	0.017	0.214	0.071	0.215	0.025	0.026	0.066	0.206	0.067	0.177	0.069	0.013	0.220
K1755	0.239	0.237	0.066	0.068	0.045	0.030	0.236	0.063	0.236	0.024	0.236	0.098	0.054	0.025	0.230	0.055	0.199	0.022	0.070	0.245
K1755	0.225	0.224	0.053	0.055	0.028	0.015	0.223	0.050	0.223	0.019	0.223	0.087	0.040	0.014	0.216	0.040	0.185	0.016	0.055	0.231
V1739	0.229	0.227	0.015	0.014	0.042	0.049	0.226	0.016	0.226	0.067	0.226	0.031	0.025	0.061	0.218	0.070	0.188	0.064	0.022	0.232
O1727	0.139	0.126	0.119	0.119	0.100	0.117	0.124	0.118	0.124	0.122	0.125	0.147	0.113	0.117	0.118	0.076	0.089	0.123	0.112	0.134
K1721	0.223	0.219	0.047	0.050	0.022	0.012	0.218	0.045	0.218	0.016	0.218	0.082	0.033	**0.009**	0.211	0.036	0.181	0.014	0.049	0.226
H1721	0.238	0.232	0.054	0.058	0.033	0.020	0.232	0.052	0.231	0.009	0.232	0.089	0.042	0.010	0.224	0.047	0.195	**0.009**	0.059	0.239
V1720	0.209	0.205	0.032	0.031	0.044	0.056	0.204	0.033	0.204	0.075	0.204	0.050	0.036	0.068	0.195	0.063	0.165	0.073	0.029	0.209
V1717	0.220	0.217	0.013	0.008	0.040	0.050	0.216	0.014	0.216	0.069	0.217	0.029	0.024	0.064	0.208	0.066	0.178	0.067	0.014	0.222
V1717	0.227	0.223	0.014	0.013	0.044	0.053	0.222	0.017	0.222	0.070	0.222	0.025	0.027	0.065	0.214	0.071	0.185	0.068	0.019	0.228
V1711	0.224	0.221	0.013	0.011	0.043	0.052	0.220	0.015	0.220	0.070	0.220	0.026	0.025	0.064	0.212	0.069	0.182	0.067	0.017	0.226
V1707	0.219	0.215	**0.010**	0.006	0.037	0.049	0.214	0.012	0.214	0.067	0.214	0.032	0.022	0.062	0.205	0.062	0.176	0.065	0.011	0.220
V1706	0.228	0.224	0.012	0.011	0.042	0.051	0.223	0.014	0.223	0.068	0.224	0.028	0.025	0.063	0.215	0.069	0.185	0.066	0.019	0.229
V1697	0.221	0.217	0.010	0.008	0.037	0.049	0.216	**0.010**	0.216	0.065	0.217	0.032	0.021	0.060	0.208	0.062	0.179	0.063	0.013	0.222
H1693	0.127	0.127	0.109	0.106	0.092	0.109	0.126	0.107	0.126	0.119	0.127	0.131	0.104	0.113	0.123	0.074	0.086	0.118	0.099	0.136
K1660	0.243	0.242	0.069	0.072	0.047	0.029	0.241	0.066	0.241	0.017	0.242	0.102	0.057	0.019	0.235	0.057	0.204	0.016	0.074	0.250
G1659	0.221	0.216	0.018	0.021	0.014	0.025	0.215	0.016	0.215	0.041	0.216	0.056	0.007	0.035	0.207	0.043	0.178	0.040	0.023	0.222
H1636	0.111	0.100	0.127	0.125	0.114	0.132	0.098	0.127	0.098	0.141	0.099	0.147	0.124	0.136	0.092	0.095	0.058	0.142	0.117	0.106
K1625	0.236	0.234	0.065	0.068	0.041	0.025	0.233	0.063	0.233	0.016	0.234	0.099	0.052	0.015	0.227	0.049	0.196	0.014	0.069	0.242
G1619	0.215	0.209	0.024	0.027	**0.008**	0.027	0.208	0.022	0.208	0.040	0.208	0.062	0.012	0.034	0.200	0.034	0.170	0.040	0.025	0.215
H1510	0.137	0.123	0.113	0.113	0.093	0.111	0.122	0.112	0.122	0.115	0.122	0.140	0.106	0.110	0.116	0.068	0.088	0.116	0.105	0.132
H1510	0.081	0.074	0.151	0.148	0.139	0.156	0.072	0.150	0.072	0.166	0.073	0.157	0.147	0.160	0.070	0.120	0.031	0.166	0.140	0.082
K1500	0.248	0.243	0.057	0.061	0.041	0.025	0.242	0.055	0.242	0.013	0.242	0.089	0.046	0.016	0.235	0.057	0.205	0.013	0.064	0.250
K1500	0.241	0.236	0.056	0.060	0.037	0.021	0.235	0.054	0.235	0.007	0.235	0.090	0.044	0.010	0.227	0.050	0.198	0.007	0.061	0.243
V1477	0.241	0.233	0.036	0.038	0.061	0.070	0.232	0.038	0.232	0.079	0.232	0.033	0.045	0.078	0.223	0.085	0.198	0.078	0.041	0.238
V1477	0.225	0.219	0.008	0.011	0.038	0.049	0.218	0.013	0.218	0.065	0.218	0.032	0.020	0.060	0.209	0.064	0.181	0.063	0.015	0.224

This is a similarity matrix of the samples which measured in Edinburgh.
Rescaled Cosine of Vectors of Values

	JL1(38)	JL1(38)	JL1(174)	JL1(186)	JL1(186)	JL1(186)	JL1(190)	JL2 (74)	JL2 (86)	Lax(18)	Lax(38)	Lax(121)	Lax(154)	Ska1(75)	Ska1(136	Ska1(175	Ska1(237	Ska2(89)	Ska2(256)	Ska2 H4
G1922	0.948	0.951	0.999	0.999	1.000	0.999	0.952	0.999	0.952	0.999	0.952	0.995	1.000	0.999	0.956	0.999	0.968	0.999	0.999	0.948
K1918	0.942	0.944	0.997	0.997	0.999	1.000	0.944	0.997	0.944	1.000	0.944	0.993	0.999	1.000	0.948	0.998	0.961	1.000	0.997	0.940
G/Th1903	0.767	0.771	0.902	0.900	0.890	0.894	0.772	0.900	0.772	0.889	0.772	0.911	0.898	0.890	0.782	0.874	0.801	0.890	0.898	0.771
G1892	0.948	0.951	0.999	0.999	1.000	0.999	0.952	0.999	0.952	0.999	0.952	0.995	1.000	0.999	0.956	0.999	0.968	0.999	0.999	0.948
G1883	0.948	0.950	0.999	0.999	1.000	0.999	0.951	0.999	0.951	0.998	0.950	0.996	1.000	0.999	0.954	0.998	0.967	0.998	0.999	0.947
A1875	0.993	0.999	0.953	0.954	0.957	0.950	1.000	0.953	1.000	0.946	1.000	0.949	0.954	0.948	1.000	0.964	0.998	0.946	0.958	1.000
A1875	0.993	0.999	0.953	0.954	0.957	0.950	0.999	0.953	0.999	0.946	0.999	0.949	0.954	0.948	1.000	0.964	0.998	0.946	0.958	1.000
V1862-64	0.946	0.947	1.000	1.000	0.998	0.997	0.948	1.000	0.948	0.995	0.948	0.999	0.999	0.996	0.952	0.995	0.965	0.995	1.000	0.945
K1860	0.944	0.945	0.995	0.995	0.998	0.999	0.946	0.996	0.946	1.000	0.946	0.989	0.997	1.000	0.949	0.998	0.963	1.000	0.995	0.941
G1838	0.949	0.954	0.999	0.999	1.000	0.999	0.954	0.999	0.954	0.998	0.954	0.995	1.000	0.999	0.958	0.999	0.970	0.998	0.999	0.951
E1821	0.997	0.999	0.953	0.954	0.958	0.951	0.999	0.953	0.999	0.947	0.999	0.947	0.954	0.949	0.998	0.965	0.998	0.947	0.957	0.998
G1823	0.949	0.953	0.999	0.999	1.000	0.999	0.954	0.999	0.954	0.998	0.953	0.996	1.000	0.998	0.958	0.998	0.969	0.998	0.999	0.950
G1783-85	0.943	0.947	0.999	0.998	1.000	0.999	0.948	0.999	0.948	0.999	0.948	0.995	0.999	0.999	0.952	0.998	0.964	0.999	0.998	0.944
Laki1783	0.946	0.948	1.000	1.000	0.999	0.998	0.948	1.000	0.948	0.996	0.948	0.998	1.000	0.997	0.952	0.996	0.965	0.997	1.000	0.945
Laki1783	0.947	0.951	0.999	0.999	1.000	0.999	0.951	0.999	0.951	0.999	0.951	0.995	1.000	0.999	0.955	0.999	0.967	0.999	0.999	0.947
G1774	0.948	0.950	1.000	1.000	1.000	0.999	0.951	1.000	0.951	0.998	0.950	0.997	1.000	0.998	0.954	0.998	0.967	0.998	1.000	0.947
H1766	0.987	0.989	0.982	0.982	0.985	0.981	0.989	0.982	0.989	0.978	0.989	0.976	0.983	0.980	0.990	0.989	0.996	0.978	0.984	0.987
G1766	0.947	0.949	1.000	1.000	0.998	0.997	0.950	1.000	0.950	0.994	0.950	0.999	0.999	0.995	0.954	0.995	0.966	0.995	1.000	0.947
K1755	0.939	0.940	0.995	0.995	0.998	0.999	0.941	0.996	0.941	0.999	0.941	0.990	0.997	0.999	0.944	0.997	0.959	0.999	0.995	0.936
K1755	0.945	0.946	0.997	0.997	0.999	1.000	0.947	0.997	0.947	1.000	0.947	0.992	0.998	1.000	0.950	0.998	0.964	1.000	0.997	0.942
V1739	0.943	0.944	1.000	1.000	0.998	0.997	0.945	1.000	0.945	0.995	0.945	0.999	0.999	0.996	0.949	0.995	0.962	0.996	1.000	0.942
O1727	0.977	0.981	0.985	0.985	0.989	0.986	0.982	0.985	0.982	0.985	0.982	0.977	0.986	0.986	0.984	0.994	0.991	0.985	0.986	0.979
K1721	0.946	0.948	0.998	0.997	0.999	1.000	0.948	0.998	0.948	1.000	0.948	0.993	0.999	1.000	0.952	0.999	0.965	1.000	0.997	0.944
H1721	0.939	0.942	0.997	0.996	0.999	1.000	0.942	0.997	0.942	1.000	0.942	0.992	0.998	1.000	0.946	0.998	0.960	1.000	0.996	0.938
V1720	0.952	0.954	0.999	0.999	0.998	0.997	0.954	0.999	0.954	0.994	0.954	0.997	0.999	0.995	0.958	0.996	0.970	0.994	0.999	0.952
V1717	0.947	0.949	1.000	1.000	0.998	0.997	0.949	1.000	0.949	0.995	0.949	0.999	0.999	0.996	0.953	0.995	0.966	0.995	1.000	0.946
V1717	0.944	0.946	1.000	1.000	0.998	0.997	0.946	1.000	0.946	0.995	0.946	0.999	0.999	0.995	0.951	0.995	0.963	0.995	1.000	0.944
V1711	0.945	0.947	1.000	1.000	0.998	0.997	0.947	1.000	0.947	0.995	0.947	0.999	0.999	0.995	0.952	0.995	0.964	0.995	1.000	0.945
V1707	0.947	0.950	1.000	1.000	0.998	0.997	0.950	1.000	0.950	0.995	0.950	0.999	0.999	0.996	0.954	0.996	0.967	0.995	1.000	0.947
V1706	0.944	0.946	1.000	1.000	0.998	0.997	0.946	1.000	0.946	0.995	0.946	0.999	0.999	0.996	0.950	0.995	0.963	0.995	1.000	0.943
V1697	0.946	0.949	1.000	1.000	0.998	0.997	0.949	1.000	0.949	0.995	0.949	0.999	0.999	0.996	0.953	0.996	0.965	0.996	1.000	0.946
H1693	0.981	0.981	0.987	0.988	0.991	0.988	0.982	0.988	0.982	0.985	0.982	0.982	0.988	0.987	0.983	0.994	0.991	0.986	0.989	0.979
K1660	0.937	0.938	0.995	0.995	0.998	0.999	0.938	0.995	0.939	1.000	0.938	0.989	0.997	1.000	0.942	0.997	0.957	1.000	0.994	0.934
G1659	0.947	0.949	1.000	0.999	1.000	0.999	0.949	1.000	0.950	0.998	0.949	0.997	1.000	0.999	0.953	0.998	0.966	0.998	0.999	0.946
H1636	0.985	0.988	0.983	0.983	0.986	0.982	0.989	0.983	0.989	0.979	0.988	0.977	0.984	0.981	0.990	0.990	0.996	0.979	0.985	0.987
K1625	0.941	0.942	0.996	0.995	0.998	0.999	0.942	0.996	0.942	1.000	0.942	0.990	0.997	1.000	0.945	0.998	0.960	1.000	0.995	0.938
G1619	0.949	0.952	0.999	0.999	1.000	0.999	0.953	0.999	0.953	0.998	0.952	0.996	1.000	0.999	0.956	0.999	0.969	0.998	0.999	0.949
H1510	0.978	0.982	0.987	0.987	0.991	0.987	0.982	0.987	0.982	0.987	0.982	0.979	0.988	0.988	0.984	0.995	0.991	0.986	0.988	0.979
H1510	0.992	0.993	0.976	0.977	0.979	0.974	0.994	0.976	0.994	0.971	0.994	0.970	0.977	0.973	0.994	0.984	0.999	0.971	0.979	0.992
K1500	0.934	0.937	0.997	0.996	0.998	0.999	0.938	0.997	0.938	1.000	0.937	0.992	0.998	1.000	0.942	0.997	0.956	1.000	0.996	0.933
K1500	0.937	0.940	0.997	0.996	0.999	1.000	0.941	0.997	0.941	1.000	0.941	0.991	0.998	1.000	0.945	0.998	0.958	1.000	0.996	0.937

	Rescaled Euclidean Distance																					
	b02	b03	b03	b03	b05	b07	b07	b08	b11	b14	b14	b14	b33	b12	b18	b18	b19	b19	b20	b34	b34	b35
	27cm	85cm	85cm	85cm	105cm	121cm	121cm	127cm	149cm	169cm	169cm	169cm	195cm	223cm	229cm	229cm	257cm	257cm	275cm	293cm	293cm	299cm
G1922	0.032	0.105	0.038	0.008	0.007	0.048	0.005	0.027	0.014	0.040	0.012	0.032	0.006	0.030	0.037	0.022	0.022	0.010	0.010	0.208	0.008	0.037
K1918	0.049	0.120	0.056	0.031	0.027	0.063	0.027	0.046	0.032	0.057	0.032	0.005	0.030	0.047	0.054	0.026	0.045	0.034	0.027	0.226	0.024	0.053
G/Th1903	0.370	0.466	0.370	0.388	0.387	0.365	0.389	0.372	0.380	0.365	0.382	0.380	0.388	0.369	0.368	0.401	0.380	0.388	0.397	0.536	0.385	0.364
G1892	0.032	0.104	0.038	0.007	0.005	0.048	0.004	0.027	0.014	0.040	0.012	0.032	0.004	0.030	0.037	0.021	0.022	0.009	0.008	0.208	0.007	0.037
G1883	**0.025**	0.108	0.031	0.009	0.010	0.037	0.012	0.022	0.011	0.033	0.012	0.034	0.011	0.024	0.030	0.032	0.018	0.010	0.019	0.211	0.012	0.031
A1875	0.210	0.113	0.206	0.199	0.204	0.209	0.203	0.210	0.207	0.211	0.205	0.226	0.201	0.214	0.211	0.207	0.200	0.198	0.198	0.020	0.208	0.216
A1875	0.210	0.114	0.207	0.200	0.205	0.210	0.203	0.211	0.207	0.212	0.205	0.226	0.201	0.215	0.212	0.208	0.201	0.198	0.199	0.021	0.208	0.216
V1862-64	0.012	0.125	0.012	0.033	0.035	0.020	0.037	0.015	0.026	0.012	0.028	0.061	0.035	0.016	0.011	0.060	0.018	0.031	0.046	0.218	0.037	0.014
K1860	0.064	0.113	0.071	0.042	0.039	0.076	0.038	0.061	0.047	0.073	0.047	0.023	0.041	0.063	0.070	0.026	0.058	0.045	0.034	0.223	0.037	0.069
G1838	0.033	0.101	0.038	0.014	0.015	0.048	0.014	0.029	0.019	0.040	0.017	0.039	0.013	0.032	0.037	0.030	0.023	0.013	0.017	0.202	0.017	0.038
E1821	0.210	0.103	0.207	0.198	0.203	0.209	0.202	0.211	0.206	0.213	0.204	0.224	0.200	0.215	0.212	0.205	0.201	0.197	0.196	0.017	0.207	0.217
G1823	0.026	0.105	0.031	0.013	0.015	0.042	0.015	0.023	0.015	0.033	0.013	0.041	0.013	0.026	0.030	0.035	0.017	0.012	0.021	0.203	0.017	0.032
G1783-85	0.033	0.114	0.040	0.016	0.012	0.050	0.012	0.028	0.017	0.040	0.016	0.029	0.013	0.029	0.037	0.024	0.026	0.017	0.018	0.217	0.010	0.037
Laki1783	0.009	0.121	0.013	0.026	0.028	0.021	0.030	0.011	0.019	0.013	0.021	0.053	0.028	0.013	0.013	0.053	0.013	0.025	0.039	0.216	0.030	0.014
Laki1783	0.030	0.107	0.036	**0.006**	0.003	0.046	0.002	0.025	0.011	0.038	0.010	0.031	0.003	0.027	0.035	0.023	0.021	0.008	0.010	0.210	0.004	0.035
G1774	0.015	0.112	0.021	0.011	0.014	0.030	0.016	0.014	0.007	0.023	0.009	0.040	0.015	0.017	0.021	0.039	0.009	0.011	0.025	0.211	0.016	0.022
H1766	0.133	0.039	0.132	0.120	0.125	0.132	0.124	0.134	0.129	0.136	0.127	0.147	0.122	0.137	0.136	0.128	0.123	0.119	0.119	0.093	0.129	0.140
G1766	0.012	0.124	0.005	0.036	0.039	0.016	0.042	0.018	0.030	0.006	0.031	0.065	0.039	0.019	0.010	0.065	0.019	0.034	0.050	0.213	0.041	0.013
K1755	0.064	0.128	0.071	0.047	0.043	0.076	0.042	0.061	0.049	0.072	0.049	0.027	0.045	0.062	0.069	0.035	0.060	0.049	0.041	0.234	0.040	0.068
K1755	0.052	0.114	0.058	0.031	0.028	0.063	0.028	0.049	0.035	0.060	0.035	0.020	0.031	0.051	0.057	0.024	0.046	0.034	0.026	0.221	0.026	0.057
V1739	0.011	0.131	**0.012**	0.036	0.038	0.014	0.040	0.016	0.028	0.008	0.030	0.059	0.039	0.014	0.011	0.063	0.022	0.035	0.050	0.224	0.039	0.009
O1727	0.123	**0.030**	0.123	0.103	0.106	0.127	0.104	0.120	0.113	0.127	0.111	0.125	0.103	0.124	0.126	0.102	0.110	0.103	0.097	0.123	0.109	0.129
K1721	0.046	0.111	0.053	0.025	0.021	0.060	0.020	0.043	0.028	0.055	0.028	0.015	0.023	0.045	0.052	0.020	0.040	0.027	0.019	0.216	0.019	0.052
H1721	0.053	0.123	0.061	0.035	0.030	0.069	0.029	0.050	0.036	0.062	0.036	0.011	0.032	0.050	0.058	0.022	0.049	0.037	0.029	0.230	0.026	0.057
V1720	0.034	0.110	0.033	0.042	0.046	0.028	0.047	0.036	0.040	0.034	0.041	0.068	0.045	0.037	0.036	0.067	0.033	0.040	0.053	0.202	0.048	0.037
V1717	0.010	0.123	0.007	0.035	0.038	0.011	0.040	0.017	0.028	0.007	0.030	0.062	0.038	0.017	0.010	0.063	0.018	0.033	0.049	0.215	0.040	0.013
V1717	0.011	0.130	0.008	0.038	0.040	0.016	0.042	0.017	0.030	0.004	0.032	0.062	0.040	0.016	0.008	0.066	0.022	0.036	0.052	0.221	0.041	0.009
V1711	0.010	0.127	0.007	0.036	0.039	0.014	0.041	0.016	0.029	0.004	0.031	0.062	0.039	0.016	0.008	0.065	0.020	0.035	0.050	0.219	0.041	0.009
V1707	0.010	0.120	0.007	0.031	0.035	0.015	0.037	0.014	0.025	0.008	0.027	0.061	0.034	0.015	0.010	0.060	0.015	0.029	0.045	0.212	0.037	0.013
V1706	0.009	0.129	0.009	0.036	0.038	0.016	0.040	0.014	0.028	0.004	0.030	0.061	0.038	0.013	0.007	0.063	0.020	0.034	0.050	0.222	0.039	0.007
V1697	0.007	0.122	0.005	0.030	0.032	0.022	0.034	0.010	0.023	0.007	0.024	0.059	0.032	0.012	0.005	0.058	0.013	0.028	0.043	0.215	0.034	0.010
H1693	0.111	0.035	0.110	0.095	0.100	0.110	0.098	0.110	0.104	0.115	0.102	0.120	0.097	0.114	0.114	0.101	0.100	0.094	0.093	0.124	0.103	0.118
K1660	0.067	0.130	0.075	0.049	0.045	0.079	0.045	0.064	0.051	0.075	0.052	0.019	0.048	0.064	0.072	0.034	0.064	0.052	0.043	0.239	0.042	0.071
G1659	0.018	0.113	0.025	0.009	**0.010**	0.035	0.012	0.015	0.005	0.027	0.006	0.036	0.011	0.017	0.024	0.034	0.012	0.009	0.021	0.214	0.011	0.024
H1636	0.130	0.037	0.128	0.116	0.121	0.130	0.119	0.130	0.125	0.133	0.123	0.143	0.118	0.134	0.133	0.123	0.119	0.115	0.114	0.096	0.124	0.137
K1625	0.064	0.122	0.071	0.044	0.040	0.075	0.040	0.061	0.047	0.072	0.047	0.018	0.043	0.061	0.069	0.029	0.059	0.047	0.037	0.231	0.038	0.068
G1619	0.025	0.105	0.031	0.005	0.007	0.041	**0.007**	0.022	0.010	0.033	0.008	0.037	0.005	0.025	0.030	0.029	0.015	0.004	0.014	0.206	0.010	0.032
H1510	0.116	0.024	0.116	0.096	0.099	0.122	0.098	0.114	0.106	0.121	0.103	0.118	0.096	0.118	0.119	0.095	0.104	0.096	0.090	0.120	0.102	0.123
H1510	0.153	0.050	0.151	0.140	0.145	0.151	0.144	0.153	0.149	0.156	0.147	0.167	0.142	0.157	0.155	0.148	0.143	0.139	0.139	0.070	0.149	0.160
K1500	0.055	0.134	0.063	0.042	0.036	0.071	0.036	0.052	0.040	0.063	0.041	0.009	0.039	0.052	0.060	0.031	0.053	0.044	0.038	0.240	0.032	0.058
K1500	0.055	0.127	0.062	0.038	0.032	0.070	0.032	0.051	0.038	0.063	0.038	**0.008**	0.035	0.052	0.060	0.025	0.051	0.040	0.032	0.233	0.029	0.058

This is a similarity matrix for the samples which measured in Manchester.
Rescaled Cosine of Vectors of Values

Ska2	b02 27cm	b03 85cm	b03 85cm	b03 85cm	b05 105cm	b07 121cm	b07 121cm	b08 127cm	b11 149cm	b14 169cm	b14 169cm	b14 169cm	b33 195cm	b12 223cm	b18 229cm	b18 229cm	b19 257cm	b19 257cm	b20 275cm	b34 293cm	b34 293cm	b35 299cm
G1922	0.999	0.988	0.998	1	1	0.997	1	0.999	1	0.998	1	0.999	1	0.999	0.998	0.999	0.999	1	1	0.952	1	0.998
K1918	0.997	0.985	0.997	0.999	0.999	0.996	0.999	0.998	0.999	0.996	0.999	1	0.999	0.997	0.997	0.999	0.998	0.999	0.999	0.945	0.999	0.997
G/Th1903	0.902	0.835	0.902	0.891	0.891	0.905	0.89	0.901	0.896	0.905	0.895	0.895	0.891	0.903	0.903	0.882	0.896	0.891	0.885	0.772	0.892	0.906
G1892	0.999	0.988	0.998	1	1	0.997	1	0.999	1	0.998	1	0.999	1	0.999	0.998	0.999	0.999	1	1	0.952	1	0.998
G1883	0.999	0.987	0.999	1	1	0.998	1	0.999	1	0.999	1	0.999	1	0.999	0.999	0.999	1	1	1	0.951	1	0.999
A1875	0.952	0.985	0.953	0.956	0.954	0.953	0.955	0.952	0.953	0.951	0.954	0.945	0.956	0.95	0.951	0.953	0.956	0.957	0.957	0.999	0.953	0.949
A1875	0.952	0.985	0.953	0.956	0.954	0.952	0.954	0.951	0.953	0.951	0.954	0.945	0.955	0.95	0.951	0.953	0.956	0.957	0.956	0.999	0.953	0.949
V1862-64	1	0.983	1	0.999	0.999	0.999	0.998	1	0.999	1	0.999	0.996	0.999	1	1	0.996	1	0.999	0.998	0.948	0.998	1
K1860	0.995	0.987	0.994	0.998	0.998	0.994	0.998	0.996	0.997	0.994	0.998	0.999	0.998	0.996	0.994	0.999	0.996	0.998	0.999	0.946	0.998	0.995
G1838	0.999	0.989	0.998	1	1	0.997	1	0.999	1	0.998	1	0.998	1	0.999	0.998	0.999	0.999	1	1	0.954	1	0.998
E1821	0.951	0.987	0.953	0.956	0.955	0.952	0.955	0.951	0.953	0.95	0.954	0.946	0.956	0.95	0.951	0.954	0.955	0.957	0.957	1	0.953	0.949
G1823	0.999	0.988	0.999	1	1	0.998	1	0.999	1	0.999	1	0.998	1	0.999	0.999	0.999	1	1	0.999	0.954	1	0.999
G1783-85	0.999	0.986	0.998	1	1	0.997	1	0.999	1	0.998	1	0.999	1	0.999	0.998	0.999	0.999	1	1	0.948	1	0.998
Laki1783	1	0.984	1	0.999	0.999	0.999	0.999	1	1	1	0.999	0.997	0.999	1	1	0.997	1	0.999	0.998	0.949	0.999	1
Laki1783	0.999	0.988	0.998	1	1	0.998	1	0.999	1	0.998	1	0.999	1	0.999	0.999	0.999	0.999	1	1	0.951	1	0.999
G1774	1	0.986	0.999	1	1	0.999	1	1	1	0.999	1	0.998	1	1	0.999	0.998	1	1	0.999	0.951	1	0.999
H1766	0.981	0.998	0.981	0.984	0.983	0.982	0.983	0.981	0.982	0.98	0.982	0.977	0.984	0.98	0.98	0.982	0.983	0.984	0.985	0.989	0.982	0.979
G1766	1	0.983	1	0.998	0.998	1	0.998	1	0.999	1	0.999	0.995	0.998	1	1	0.995	1	0.999	0.997	0.95	0.998	1
K1755	0.996	0.983	0.995	0.998	0.998	0.994	0.998	0.996	0.997	0.994	0.997	0.999	0.998	0.996	0.995	0.999	0.996	0.997	0.998	0.941	0.998	0.995
K1755	0.997	0.986	0.996	0.999	0.999	0.996	0.999	0.997	0.999	0.996	0.999	0.999	0.999	0.997	0.996	0.999	0.998	0.999	0.999	0.947	0.999	0.996
V1739	1	0.982	1	0.998	0.998	1	0.998	1	0.999	1	0.999	0.996	0.998	1	1	0.996	0.999	0.999	0.997	0.945	0.998	1
O1727	0.984	0.999	0.984	0.989	0.988	0.983	0.988	0.984	0.986	0.983	0.987	0.984	0.988	0.984	0.983	0.989	0.987	0.989	0.99	0.982	0.987	0.982
K1721	0.998	0.987	0.997	0.999	0.999	0.996	0.999	0.998	0.999	0.997	0.999	1	0.999	0.998	0.997	0.999	0.998	0.999	1	0.949	1	0.997
H1721	0.997	0.984	0.996	0.999	0.999	0.995	0.999	0.997	0.998	0.996	0.999	1	0.999	0.997	0.996	0.999	0.997	0.998	0.999	0.943	0.999	0.996
V1720	0.999	0.987	0.999	0.998	0.998	0.999	0.997	0.998	0.998	0.999	0.998	0.995	0.998	0.998	0.998	0.995	0.999	0.998	0.997	0.955	0.997	0.998
V1717	1	0.984	1	0.999	0.998	1	0.998	1	0.999	1	0.999	0.996	0.998	1	1	0.995	1	0.999	0.997	0.949	0.998	1
V1717	1	0.982	1	0.998	0.998	1	0.998	1	0.999	1	0.999	0.996	0.998	1	1	0.995	0.999	0.998	0.997	0.947	0.998	1
V1711	1	0.983	1	0.998	0.998	1	0.998	1	0.999	1	0.999	0.996	0.998	1	1	0.995	0.999	0.999	0.997	0.948	0.998	1
V1707	1	0.984	1	0.999	0.999	1	0.998	1	0.999	1	0.999	0.996	0.999	1	1	0.996	1	0.999	0.998	0.95	0.998	1
V1706	1	0.982	1	0.998	0.998	1	0.998	1	0.999	1	0.999	0.996	0.998	1	1	0.995	0.999	0.999	0.997	0.946	0.998	1
V1697	1	0.984	1	0.999	0.999	0.999	0.999	1	0.999	1	0.999	0.996	0.999	1	1	0.996	1	0.999	0.998	0.949	0.999	1
H1693	0.987	0.998	0.987	0.99	0.989	0.987	0.989	0.987	0.988	0.986	0.989	0.985	0.99	0.986	0.986	0.989	0.989	0.99	0.991	0.982	0.988	0.985
K1660	0.995	0.983	0.994	0.997	0.998	0.993	0.998	0.996	0.997	0.994	0.997	1	0.998	0.996	0.994	0.999	0.996	0.997	0.998	0.939	0.998	0.995
G1659	1	0.986	0.999	1	1	0.999	1	1	1	0.999	1	0.999	1	1	0.999	0.999	1	1	0.999	0.95	1	0.999
H1636	0.982	0.998	0.982	0.985	0.984	0.982	0.985	0.982	0.983	0.981	0.984	0.979	0.985	0.981	0.981	0.984	0.985	0.986	0.986	0.989	0.983	0.98
K1625	0.996	0.985	0.994	0.998	0.998	0.994	0.998	0.996	0.998	0.994	0.998	1	0.998	0.996	0.995	0.999	0.996	0.998	0.999	0.943	0.998	0.995
G1619	0.999	0.988	0.999	1	1	0.998	1	0.999	1	0.999	1	0.999	1	0.999	0.999	0.999	1	1	1	0.953	1	0.999
H1510	0.986	0.999	0.985	0.99	0.989	0.984	0.99	0.986	0.988	0.984	0.989	0.986	0.99	0.985	0.985	0.99	0.988	0.99	0.991	0.983	0.989	0.984
H1510	0.975	0.997	0.975	0.979	0.977	0.976	0.977	0.975	0.976	0.974	0.977	0.971	0.978	0.973	0.974	0.976	0.978	0.979	0.979	0.994	0.976	0.973
K1500	0.997	0.981	0.996	0.998	0.999	0.995	0.999	0.997	0.998	0.996	0.998	1	0.998	0.997	0.996	0.999	0.997	0.998	0.998	0.938	0.999	0.996
K1500	0.997	0.983	0.996	0.998	0.999	0.995	0.999	0.997	0.998	0.996	0.998	1	0.999	0.997	0.996	0.999	0.997	0.998	0.999	0.941	0.999	0.996

Appendix 6: The results of factor analysis on magnetic data (SPSS output)

Factor analysis on mass specific magnetic parameters of Lax, total variance explained.

Total Variance Explained-Lax

Component	Initial Eigenvalues			Extraction Sums of Squared Loadings			Rotation Sums of Squared Loadings		
	Total	% of Variance	Cumulative %	Total	% of Variance	Cumulative %	Total	% of Variance	Cumulative %
1	4.835	80.582	80.582	4.835	80.582	80.582	3.921	65.348	65.348
2	.742	12.370	92.952	.742	12.370	92.952	1.656	27.605	92.952
3	.308	5.128	98.080						
4	7.728E-02	1.288	99.368						
5	2.956E-02	.493	99.860						
6	8.372E-03	.140	100.000						

Extraction Method: Principal Component Analysis.

Factor analysis on mass specific magnetic parameters of Lax, component matrix.

Component Matrix--Lax[a]

	Component	
	1	2
XLF	**.960**	-.211
SOFT	.953	-.199
XFD	.838	-.242
XARM	**.964**	-8.44E-02
SIRM	**.969**	.192
HIRM	.658	**.746**

Extraction Method: Principal Component Analysis.

a. 2 components extracted.

Factor analysis on ratios of Lax, total variance explained.

Total Variance Explained--Lax

Component	Initial Eigenvalues			Extraction Sums of Squared Loadings		
	Total	% of Variance	Cumulative %	Total	% of Variance	Cumulative %
1	3.123	39.038	39.038	3.123	39.038	39.038
2	1.505	18.818	57.856	1.505	18.818	57.856
3	1.470	18.381	76.237	1.470	18.381	76.237
4	.896	11.202	87.439			
5	.409	5.110	92.549			
6	.380	4.746	97.295			
7	.146	1.825	99.120			
8	7.043E-02	.880	100.000			

Extraction Method: Principal Component Analysis.

Factor analysis ratios of Lax, component matrix.

Component Matrix--Lax[a]

	Component		
	1	2	3
XFD100	-4.20E-02	.516	-.130
XARMSIRM	.268	.340	**-.794**
XARMXLF	-.237	**.793**	-8.56E-02
SIRMXLF	-.534	.108	.699
S20	.883	-.273	6.151E-02
S40	**.943**	-6.33E-02	.119
S100	.902	.213	.155
S300	.475	.600	.534

Extraction Method: Principal Component Analysis.

a. 3 components extracted.

Factor analysis on mass specific magnetic parameters of Ska1, total variance explained

Total Variance Explained--Ska1

Component	Initial Eigenvalues			Extraction Sums of Squared Loadings		
	Total	% of Variance	Cumulative %	Total	% of Variance	Cumulative %
1	4.410	73.508	73.508	4.410	73.508	73.508
2	.802	13.374	86.882	.802	13.374	86.882
3	.462	7.703	94.585			
4	.270	4.494	99.078			
5	3.879E-02	.647	99.725			
6	1.652E-02	.275	100.000			

Extraction Method: Principal Component Analysis.

Factor analysis on mass specific magnetic parameters of Ska1, component matrix.

Component Matrix--Ska1[a]

	Component	
	1	2
XLF	**.901**	-.282
SOFT	.910	-.206
XFD	.828	-4.93E-02
XARM	**.937**	-6.18E-02
SIRM	**.951**	9.578E-02
HIRM	.551	**.815**

Extraction Method: Principal Component Analysis.

a. 2 components extracted.

Factor analysis on magnetic parameter ratios of Ska1, total variance explained.

Total Variance Explained--Ska1

Component	Initial Eigenvalues			Extraction Sums of Squared Loadings		
	Total	% of Variance	Cumulative %	Total	% of Variance	Cumulative %
1	3.786	47.323	47.323	3.786	47.323	47.323
2	1.997	24.963	72.286	1.997	24.963	72.286
3	.989	12.364	84.650			
4	.638	7.969	92.619			
5	.408	5.104	97.723			
6	.133	1.667	99.390			
7	3.052E-02	.382	99.772			
8	1.825E-02	.228	100.000			

Extraction Method: Principal Component Analysis.

Factor analysis on magnetic parameter ratios of Ska1, component matrix.

Component Matrix--Ska2[a]

	Component	
	1	2
XFD100	-.191	.560
XARMSIRM	.668	.532
XARMXLF	-.282	**.880**
SIRMXLF	-.636	.557
S20	.876	-.172
S40	**.935**	-3.67E-02
S100	.888	.294
S300	.624	.445

Extraction Method: Principal Component Analysis.

a. 2 components extracted.

Factor analysis on mass specific magnetic parameters of Ska2, total variance explained.

Total Variance Explained--Ska2

	Initial Eigenvalues			Extraction Sums of Squared Loadings			Rotation Sums of Squared Loadings		
Component	Total	% of Variance	Cumulative %	Total	% of Variance	Cumulative %	Total	% of Variance	Cumulative %
1	4.578	76.294	76.294	4.578	76.294	76.294	3.904	65.058	65.058
2	.940	15.662	91.956	.940	15.662	91.956	1.614	26.897	91.956
3	.342	5.694	97.650						
4	8.324E-02	1.387	99.037						
5	3.712E-02	.619	99.656						
6	2.065E-02	.344	100.000						

Extraction Method: Principal Component Analysis.

Factor analysis on mass specific magnetic parameters of Ska2

Rotated Component Matrix--Ska2[a]

	Component	
	1	2
XLF	**.963**	.101
SOFT	.904	.335
XFD	.943	6.418E-02
XARM	.811	.483
SIRM	.774	.584
HIRM	.115	**.956**

Extraction Method: Principal Component Analysis.
Rotation Method: Varimax with Kaiser Normalization.

a. Rotation converged in 3 iterations.

Factor analysis on magnetic parameter ratios of Ska2, total variance explained.

Total Variance Explained--Ska2

	Initial Eigenvalues			Extraction Sums of Squared Loadings		
Component	Total	% of Variance	Cumulative %	Total	% of Variance	Cumulative %
1	4.118	51.471	51.471	4.118	51.471	51.471
2	1.575	19.691	71.162	1.575	19.691	71.162
3	1.069	13.367	84.529	1.069	13.367	84.529
4	.670	8.373	92.901			
5	.318	3.969	96.870			
6	.137	1.715	98.585			
7	9.817E-02	1.227	99.812			
8	1.501E-02	.188	100.000			

Extraction Method: Principal Component Analysis.

Factor analysis on magnetic parameter ratios of Ska2

Component Matrix--Ska[a]

	Component		
	1	2	3
XFD100	.115	.288	**.882**
XARMSIRM	.780	.394	.166
XARMXLF	-.359	**.906**	-7.86E-02
SIRMXLF	-.786	.534	-.197
S20	**.925**	-.137	-.115
S40	.918	8.593E-02	-3.27E-02
S100	.888	.333	-5.33E-02
S300	.512	.306	-.449

Extraction Method: Principal Component Analysis.

a. 3 components extracted.

Factor analysis on mass specific magnetic parameters of JL1, total variance explained.

Total Variance Explained--JL1

	Initial Eigenvalues			Extraction Sums of Squared Loadings		
Component	Total	% of Variance	Cumulative %	Total	% of Variance	Cumulative %
1	4.132	68.865	68.865	4.132	68.865	68.865
2	1.185	19.747	88.612	1.185	19.747	88.612
3	.337	5.620	94.232			
4	.171	2.857	97.089			
5	.118	1.960	99.049			
6	5.706E-02	.951	100.000			

Extraction Method: Principal Component Analysis.

Factor analysis on mass specific magnetic parameters of JL1.

Component Matrix--JL1[a]

	Component	
	1	2
XLF	**.947**	-.165
SOFT	**.959**	-7.22E-02
XFD	.846	.107
XARM	.919	-7.55E-02
SIRM	.850	.436
HIRM	-.171	**.972**

Extraction Method: Principal Component Analysis.

a. 2 components extracted.

Factor analysis on magnetic parameter ratios of JL1, total variance explained.

Total Variance Explained--JL1

Component	Initial Eigenvalues			Extraction Sums of Squared Loadings		
	Total	% of Variance	Cumulative %	Total	% of Variance	Cumulative %
1	5.943	66.031	66.031	5.943	66.031	66.031
2	1.780	19.774	85.805	1.780	19.774	85.805
3	.603	6.702	92.507			
4	.292	3.241	95.749			
5	.204	2.268	98.016			
6	.102	1.136	99.153			
7	4.707E-02	.523	99.676			
8	2.343E-02	.260	99.936			
9	5.742E-03	6.380E-02	100.000			

Extraction Method: Principal Component Analysis.

Factor analysis on magnetic parameter ratios of JL1

Component Matrix--JL1[a]

	Component	
	1	2
XFD100	-.814	.125
SIRMARM	-.617	-.778
XARMSIRM	.429	**.896**
XARMXLF	-.790	.483
SIRMXLF	-.938	-.127
S20	.936	-.128
S40	**.957**	-7.90E-02
S100	.917	-.113
S300	.759	-.266

Extraction Method: Principal Component Analysis.
a. 2 components extracted.

Factor analysis on mass specific magnetic parameters of JL2, total variance explained.

Total Variance Explained--JL2

Component	Initial Eigenvalues			Extraction Sums of Squared Loadings		
	Total	% of Variance	Cumulative %	Total	% of Variance	Cumulative %
1	4.248	70.793	70.793	4.248	70.793	70.793
2	1.043	17.377	88.169	1.043	17.377	88.169
3	.433	7.215	95.384			
4	.178	2.965	98.349			
5	8.695E-02	1.449	99.798			
6	1.210E-02	.202	100.000			

Extraction Method: Principal Component Analysis.

Factor analysis on mass specific magnetic parameters of JL2.

Component Matrix--JL2[a]

	Component	
	1	2
XLF	.966	-.147
SOFT	.947	-.107
XFD	.822	8.363E-02
XARM	.922	2.860E-03
SIRM	.942	.120
HIRM	5.952E-02	.994

Extraction Method: Principal Component Analysis.

a. 2 components extracted.

Factor analysis on magnetic parameter ratios of JL2, total variance explained.

Total Variance Explained--JL2

Component	Initial Eigenvalues			Extraction Sums of Squared Loadings		
	Total	% of Variance	Cumulative %	Total	% of Variance	Cumulative %
1	5.695	71.182	71.182	5.695	71.182	71.182
2	1.316	16.448	87.631	1.316	16.448	87.631
3	.630	7.871	95.501			
4	.185	2.310	97.811			
5	.110	1.374	99.186			
6	3.881E-02	.485	99.671			
7	1.637E-02	.205	99.876			
8	9.976E-03	.125	100.000			

Extraction Method: Principal Component Analysis.

Factor analysis on magnetic parameter ratios of JL2

Component Matrix--JL2[a]

	Component	
	1	2
XFD100	-.016	.246
XARMSIRM	.104	.990
XARMXLF	-.861	.419
SIRMXLF	-.912	-.284
S20	.951	3.196E-02
S40	.975	9.230E-02
S100	.982	.101
S300	.676	5.178E-03

Extraction Method: Principal Component Analysis.

a. 2 components extracted.

Appendix 7: Principal coordinates analysis on magnetic data (SPSS output)

Similarity coefficient (SC) and Euclidean distance (ED) between tephra layers from JL1-JL2, SE Iceland.

JL2 / JL1		51 cm	61 cm	75 cm	79 cm	87 cm	89 cm	113 cm	115 cm
39	ED	0.06	0.0924	0.1178	0.0765	0.095	0.0301	0.0475	0.044
cm	SC	0.9985	0.9962	0.9938	0.9974	0.9959	0.9996	0.999	0.9992
85	ED	0.0793	0.0986	0.1056	0.0643	0.083	0.0496	0.028	0.059
cm	SC	0.9973	0.9957	0.995	0.9982	0.9968	0.9989	0.9997	0.9986
91	ED	0.0445	0.0923	0.1296	0.0894	0.1071	0.0165	0.0646	0.0371
cm	SC	0.9992	0.9962	0.9925	0.9965	0.9948	0.9999	0.9982	0.9994
93	ED	**0.02**	0.1043	0.1544	0.1142	0.1262	0.0134	0.0866	0.0269
cm	SC	**1**	0.9951	0.9895	0.9943	0.9929	0.9999	0.9968	0.9997
131	ED	0.0738	0.0979	0.1102	0.0688	0.0861	0.0442	0.0336	0.0538
cm	SC	0.9977	0.9957	0.9945	0.9979	0.9966	0.9992	0.9995	0.9988
149	ED	0.0718	0.0974	0.1074	0.0665	0.089	0.0426	0.0363	0.0562
cm	SC	0.9978	0.9958	0.9948	0.998	0.9964	0.9992	0.9994	0.9987
151	ED	0.0658	**0.08**	0.1086	0.0681	0.0922	0.0364	0.0505	0.0532
cm	SC	0.9982	**1**	0.9947	0.9979	0.9961	0.9994	0.9989	0.9988
171	ED	0.2065	0.1672	**0.04**	0.0751	0.1203	0.1777	0.1115	0.1917
cm	SC	0.9812	0.9877	**1**	0.9974	0.9934	0.9859	0.9943	0.9838
181	ED	0.2288	0.1841	0.0617	0.0964	0.1299	0.1991	0.1295	0.2113
cm	SC	0.9768	0.9849	0.9982	0.9957	0.9922	0.9822	0.9922	0.9802
185	ED	0.0586	0.0856	0.1244	0.0826	0.0928	0.0283	0.0527	0.0357
cm	SC	0.9985	0.9967	0.9931	0.997	0.9961	0.9996	0.9988	0.9995
189	ED	0.081	0.0995	0.1369	0.0961	**0.09**	0.0568	0.0575	0.0483
cm	SC	0.9971	0.9955	0.9917	0.996	**1**	0.9985	0.9986	0.999
191	ED	0.0386	0.095	0.141	0.0997	0.1081	**0.01**	0.0697	0.0219
cm	SC	0.9994	0.9959	0.9912	0.9957	0.9948	**1**	0.9979	0.9998
215	ED	0.0606	0.0943	0.124	0.0823	0.0937	0.0312	**0.05**	0.0382
cm	SC	0.9984	0.996	0.9931	0.997	0.996	0.9996	**1**	0.9994
219	ED	0.0452	0.0929	0.145	0.1031	0.1086	0.0217	0.0703	**0.02**
cm	SC	0.9991	0.9961	0.9908	0.9954	0.9948	0.9998	0.9979	**1**
227	ED	0.1446	0.1269	0.0611	0.0389	0.0735	0.1145	0.0388	0.1234
cm	SC	0.9909	0.9929	0.9982	0.9993	0.9975	0.9942	0.9993	0.9935
275	ED	0.0396	0.0937	0.1377	0.0967	0.1097	0.01	0.0678	0.0256
cm	SC	0.9993	0.996	0.9916	0.9959	0.9946	1	0.998	0.9997
319	ED	0.1246	0.1051	0.0937	0.06	0.0719	0.0947	0.0352	0.0966
cm	SC	0.9932	0.9951	0.996	0.9984	0.9976	0.996	0.9994	0.9959

Similarity coefficient (SC) and Euclidean distance (ED) between tephra layers from Ska2-JL1, SE Iceland.

JL1 / Ska2		39 cm	85 cm	91 cm	93 cm	131 cm	149 cm	151 cm	171 cm	181 cm	185 cm	189 cm	191 cm	215 cm	219 cm	227 cm	275 cm	319 cm
27.0	ED	0.45	0.45	0.45	0.47	0.45	0.45	0.44	0.41	0.40	0.44	0.45	0.46	0.45	0.45	0.43	0.46	0.42
cm	SC	0.92	0.92	0.91	0.91	0.92	0.92	0.92	0.93	0.93	0.92	0.92	0.91	0.92	0.91	0.92	0.91	0.93
35.0	ED	0.54	0.54	0.55	0.56	0.54	0.54	0.53	0.50	0.50	0.54	0.54	0.55	0.55	0.55	0.53	0.55	0.52
cm	SC	0.88	0.88	0.88	0.88	0.88	0.88	0.89	0.90	0.91	0.89	0.89	0.88	0.88	0.88	0.89	0.88	0.90
67.0	ED	0.49	0.48	0.49	0.50	0.49	0.49	0.47	0.44	0.43	0.48	0.48	0.49	0.49	0.49	0.46	0.49	0.46
cm	SC	0.90	0.91	0.90	0.90	0.90	0.90	0.91	0.92	0.92	0.91	0.91	0.90	0.90	0.90	0.91	0.90	0.92
73.0	ED	0.47	**0.47**	0.47	0.49	0.47	0.47	0.46	0.42	0.42	0.46	0.47	0.48	0.47	0.47	0.45	0.48	0.44
cm	SC	0.91	**0.91**	0.91	0.90	0.91	0.91	0.92	0.93	0.93	0.91	0.91	0.91	0.91	0.91	0.92	0.91	0.92
85.0	ED	0.49	0.49	**0.49**	0.51	0.49	0.49	0.47	0.44	0.44	0.48	0.49	0.50	0.49	0.49	0.47	0.49	0.46
cm	SC	0.90	0.90	**0.90**	0.90	0.90	0.90	0.91	0.92	0.92	0.91	0.90	0.90	0.90	0.90	0.91	0.90	0.91
101.0	ED	0.51	0.51	0.51	0.53	0.51	0.51	0.49	0.46	0.46	0.50	0.50	0.52	0.51	0.51	0.49	0.51	0.48
cm	SC	0.90	0.90	0.89	0.89	0.90	0.90	0.90	0.92	0.92	0.90	0.90	0.89	0.90	0.89	0.91	0.89	0.91
105.0	ED	0.38	0.38	0.39	0.40	0.38	0.38	0.37	0.34	0.33	0.38	0.38	0.39	0.38	0.39	0.36	0.39	0.35
cm	SC	0.94	0.94	0.94	0.93	0.94	0.94	0.94	0.95	0.95	0.94	0.94	0.93	0.94	0.94	0.95	0.94	0.95
109.0	ED	0.28	0.27	0.29	**0.31**	0.28	0.28	0.27	0.23	0.23	0.27	0.27	0.29	0.28	0.29	0.25	0.29	0.24
cm	SC	0.97	0.97	0.96	**0.96**	0.97	0.97	0.97	0.98	0.98	0.97	0.97	0.96	0.97	0.96	0.97	0.96	0.97
121.0	ED	0.56	0.56	0.57	0.58	0.56	0.56	0.55	0.51	0.51	0.56	0.56	0.57	0.56	0.57	0.54	0.57	0.53
cm	SC	0.88	0.88	0.88	0.87	0.88	0.88	0.88	0.90	0.90	0.88	0.88	0.87	0.88	0.88	0.89	0.87	0.89
141.0	ED	0.36	0.36	0.37	0.38	**0.36**	0.36	0.35	0.31	0.31	0.36	0.36	0.37	0.36	0.37	0.34	0.37	0.33
cm	SC	0.94	0.94	0.94	0.94	**0.94**	0.94	0.95	0.96	0.96	0.94	0.94	0.94	0.94	0.94	0.95	0.94	0.95
145.0	ED	0.47	0.46	0.47	0.49	0.46	0.47	0.45	0.42	0.41	0.46	0.46	0.47	0.47	0.47	0.44	0.47	0.44
cm	SC	0.91	0.91	0.91	0.90	0.91	0.91	0.92	0.93	0.93	0.91	0.91	0.91	0.91	0.91	0.92	0.91	0.92
149.0	ED	0.78	0.78	0.79	0.80	0.78	0.78	0.77	0.74	0.73	0.78	0.78	0.79	0.78	0.79	0.76	0.79	0.76
cm	SC	0.80	0.80	0.79	0.79	0.80	0.80	0.80	0.82	0.83	0.80	0.80	0.79	0.80	0.79	0.81	0.79	0.81
161.0	ED	0.37	0.37	0.38	0.39	0.37	0.37	**0.36**	0.33	0.33	0.37	0.37	0.38	0.37	0.38	0.35	0.38	0.35
cm	SC	0.94	0.94	0.94	0.93	0.94	0.94	**0.95**	0.95	0.95	0.94	0.94	0.94	0.94	0.94	0.95	0.94	0.95
167.0	ED	0.37	0.36	0.37	0.39	0.36	0.36	0.35	0.31	0.30	0.36	0.36	0.38	0.37	0.37	0.33	0.38	0.33
cm	SC	0.94	0.94	0.94	0.93	0.94	0.94	0.95	0.96	0.96	0.94	0.94	0.94	0.94	0.94	0.95	0.94	0.95
169.0	ED	0.37	0.37	0.38	0.40	0.37	0.37	0.36	0.33	0.32	0.37	0.37	0.38	0.38	0.38	0.35	0.38	0.34
cm	SC	0.94	0.94	0.94	0.93	0.94	0.94	0.94	0.95	0.96	0.94	0.94	0.94	0.94	0.94	0.95	0.94	0.95
171.0	ED	0.56	0.56	0.57	0.58	0.56	0.56	0.55	0.51	0.51	0.56	0.56	0.57	0.56	0.57	0.54	0.57	0.53
cm	SC	0.88	0.88	0.88	0.87	0.88	0.88	0.88	0.90	0.90	0.88	0.88	0.87	0.88	0.88	0.89	0.87	0.89
173.0	ED	0.40	0.40	0.41	0.43	0.40	0.40	0.39	**0.36**	**0.35**	**0.40**	0.40	0.41	0.41	0.41	0.38	0.41	0.37
cm	SC	0.93	0.93	0.93	0.92	0.93	0.93	0.94	**0.95**	**0.95**	**0.93**	0.93	0.93	0.93	0.93	0.94	0.93	0.94
180.6	ED	0.52	0.52	0.53	0.54	0.52	0.52	0.51	**0.48**	**0.47**	**0.52**	0.52	0.53	0.52	0.53	0.50	0.53	0.49
cm	SC	0.89	0.89	0.89	0.88	0.89	0.89	0.90	**0.91**	**0.91**	**0.89**	0.89	0.89	0.89	0.89	0.90	0.89	0.90
190.6	ED	0.36	0.36	0.36	0.38	0.36	0.36	0.35	**0.33**	**0.33**	**0.35**	**0.35**	0.36	0.36	0.36	0.34	0.36	0.33
cm	SC	0.95	0.95	0.94	0.94	0.95	0.95	0.95	**0.95**	**0.96**	**0.95**	**0.95**	0.94	0.95	0.94	0.95	0.94	0.95
201.0	ED	0.39	0.38	0.39	0.41	0.39	0.39	0.37	**0.34**	**0.34**	**0.38**	0.38	**0.40**	0.39	0.39	0.36	0.39	0.36
cm	SC	0.94	0.94	0.93	0.93	0.94	0.94	0.94	**0.95**	**0.95**	**0.94**	0.94	**0.93**	0.94	0.93	0.94	0.93	0.95
213.0	ED	0.40	0.40	0.41	0.42	0.40	0.40	0.39	0.36	0.36	0.40	0.40	0.41	**0.40**	0.41	0.38	0.41	0.38
cm	SC	0.93	0.93	0.93	0.92	0.93	0.93	0.94	0.95	0.95	0.93	0.93	0.93	**0.93**	0.93	0.94	0.93	0.94
215.0	ED	0.38	0.38	0.38	0.40	0.38	0.38	0.37	0.34	0.33	0.37	0.38	0.39	0.38	**0.38**	0.36	0.39	0.35
cm	SC	0.94	0.94	0.94	0.93	0.94	0.94	0.94	0.95	0.95	0.94	0.94	0.94	0.94	**0.94**	0.95	0.94	0.95
219.0	ED	0.49	0.49	0.50	0.51	0.49	0.49	0.48	0.43	0.43	0.49	0.49	0.50	0.49	0.50	0.46	0.50	0.46
cm	SC	0.90	0.90	0.90	0.89	0.90	0.90	0.91	0.92	0.93	0.90	0.90	0.90	0.90	0.90	0.91	0.90	0.91
223.0	ED	0.43	0.42	0.43	0.45	0.43	0.43	0.41	0.38	0.38	0.42	0.42	0.43	0.43	0.43	**0.40**	0.43	0.40
cm	SC	0.92	0.93	0.92	0.92	0.92	0.92	0.93	0.94	0.94	0.93	0.93	0.92	0.92	0.92	**0.93**	0.92	0.93
229.0	ED	0.56	0.55	0.56	0.58	0.55	0.55	0.54	0.50	0.49	0.55	0.55	0.56	0.56	0.56	0.53	0.56	0.52
cm	SC	0.88	0.88	0.88	0.87	0.88	0.88	0.88	0.90	0.91	0.88	0.88	0.87	0.88	0.88	0.89	0.88	0.89
237.6	ED	0.31	0.31	0.32	0.34	0.31	0.31	0.30	0.27	0.26	0.31	0.31	0.33	0.32	0.32	0.28	0.32	0.28
cm	SC	0.96	0.96	0.95	0.95	0.96	0.96	0.96	0.97	0.97	0.96	0.96	0.95	0.96	0.95	0.96	0.95	0.97
241.0	ED	0.50	0.50	0.50	0.52	0.50	0.50	0.49	0.46	0.45	0.49	0.50	0.51	0.50	0.50	0.48	0.51	0.47
cm	SC	0.90	0.90	0.90	0.89	0.90	0.90	0.91	0.92	0.92	0.90	0.90	0.90	0.90	0.90	0.91	0.90	0.91
247.0	ED	0.99	0.99	1.00	1.01	0.99	0.99	0.98	0.94	0.93	0.99	0.99	1.00	0.99	1.00	0.97	1.00	0.97
cm	SC	0.71	0.72	0.71	0.70	0.71	0.71	0.72	0.75	0.75	0.72	0.72	0.71	0.71	0.71	0.73	0.71	0.73
249.0	ED	0.78	0.78	0.79	0.80	0.78	0.78	0.77	0.73	0.72	0.78	0.78	0.79	0.78	0.79	0.76	0.79	0.76
cm	SC	0.79	0.79	0.79	0.78	0.79	0.79	0.80	0.82	0.83	0.80	0.80	0.79	0.79	0.79	0.81	0.79	0.81
251.0	ED	0.88	0.88	0.88	0.90	0.88	0.88	0.86	0.83	0.82	0.87	0.88	0.89	0.88	0.88	0.86	0.88	0.85
cm	SC	0.76	0.76	0.76	0.75	0.76	0.76	0.77	0.79	0.79	0.76	0.76	0.75	0.76	0.75	0.77	0.75	0.77
255.0	ED	0.71	0.71	0.71	0.73	0.71	0.71	0.70	0.66	0.65	0.70	0.71	0.72	0.71	0.71	0.69	0.72	0.68
cm	SC	0.82	0.82	0.82	0.81	0.82	0.82	0.83	0.85	0.85	0.82	0.82	0.82	0.82	0.82	0.83	0.82	0.84
257.0	ED	0.39	0.38	0.39	0.41	0.38	0.39	0.37	0.34	0.33	0.38	0.38	0.40	0.39	0.39	0.36	0.39	0.36
cm	SC	0.94	0.94	0.93	0.93	0.94	0.94	0.94	0.95	0.95	0.94	0.94	0.93	0.94	0.93	0.94	0.93	0.95
275.0	ED	0.41	0.41	0.42	0.43	0.41	0.41	0.40	0.36	0.35	0.41	0.41	0.42	0.41	0.42	0.38	0.42	0.38
cm	SC	0.93	0.93	0.93	0.92	0.93	0.93	0.93	0.95	0.95	0.93	0.93	0.92	0.93	0.93	0.94	0.92	0.94
285.0	ED	0.22	0.21	0.23	0.25	0.22	0.22	0.21	0.16	0.16	0.22	0.22	0.24	0.22	0.23	0.18	0.23	0.18
cm	SC	0.98	0.98	0.98	0.97	0.98	0.98	0.98	0.99	0.99	0.98	0.98	0.97	0.98	0.98	0.98	0.97	0.98
291.0	ED	0.37	0.37	0.38	0.39	0.37	0.37	0.36	0.32	0.31	0.37	0.37	0.38	0.37	0.38	0.35	0.38	0.34
cm	SC	0.94	0.94	0.94	0.93	0.94	0.94	0.94	0.96	0.96	0.94	0.94	0.94	0.94	0.94	0.95	0.94	0.95
299.0	ED	0.40	0.40	0.40	0.42	0.40	0.40	0.39	0.35	0.35	0.39	0.40	0.41	0.40	0.41	0.37	0.41	0.37
cm	SC	0.93	0.93	0.93	0.92	0.93	0.93	0.94	0.95	0.95	0.93	0.93	0.93	0.93	0.93	0.94	0.93	0.94
309.0	ED	0.25	0.25	0.26	0.28	0.25	0.25	0.24	0.21	0.21	0.25	0.25	0.26	0.25	0.26	0.23	**0.26**	0.22
cm	SC	0.97	0.97	0.97	0.97	0.97	0.97	0.97	0.98	0.98	0.97	0.97	0.97	0.97	0.97	0.98	**0.97**	0.98
313.0	ED	0.40	0.40	0.41	0.43	0.40	0.40	0.39	0.35	0.34	0.40	0.40	0.41	0.40	0.41	0.38	0.41	0.37
cm	SC	0.93	0.93	0.93	0.92	0.93	0.93	0.94	0.95	0.95	0.93	0.93	0.93	0.93	0.93	0.94	0.93	0.94
339.0	ED	0.27	0.27	0.28	0.29	0.27	0.27	0.26	0.27	0.26	0.26	0.26	0.28	0.27	0.27	0.26	0.28	**0.24**
cm	SC	0.97	0.97	0.97	0.96	0.97	0.97	0.97	0.97	0.97	0.97	0.97	0.97	0.97	0.97	0.97	0.97	**0.97**
355.0	ED	0.23	0.22	0.24	0.26	0.23	0.23	0.22	0.17	0.16	0.23	0.23	0.25	0.23	0.24	0.19	0.24	0.20
cm	SC	0.98	0.98	0.97	0.97	0.98	0.98	0.98	0.99	0.99	0.98	0.98	0.97	0.97	0.97	0.98	0.97	0.98

Similarity coefficient (SC) and Euclidean distance (ED) between tephra layers from Ska2-JL2, SE Iceland.

JL1 / SKA2		51 cm	61 cm	75 cm	79 cm	87 cm	89 cm	113 cm	115 cm
85	ED	0.51	0.40	0.43	0.45	0.46	0.50	0.48	0.50
cm	SC	0.89	0.94	0.92	0.92	0.91	0.90	0.91	0.90
101	ED	0.53	0.42	0.45	0.47	0.48	0.52	0.50	0.52
cm	SC	0.89	0.93	0.92	0.91	0.91	0.89	0.90	0.89
105	ED	0.41	0.30	0.33	0.34	0.35	0.39	0.37	0.39
cm	SC	0.93	0.96	0.95	0.95	0.95	0.93	0.94	0.93
109	ED	**0.32**	0.21	0.22	0.23	0.25	0.29	0.26	0.30
cm	SC	**0.96**	0.98	0.98	0.98	0.97	0.96	0.97	0.96
121	ED	0.59	0.48	0.51	0.52	0.53	0.57	0.55	0.57
cm	SC	0.87	0.91	0.90	0.90	0.89	0.87	0.88	0.87
141	ED	0.39	0.28	0.30	0.32	0.33	0.37	0.35	0.38
cm	SC	0.93	0.97	0.96	0.96	0.95	0.94	0.95	0.94
145	ED	0.49	0.38	0.41	0.42	0.44	0.48	0.46	0.48
cm	SC	0.90	0.94	0.93	0.93	0.92	0.91	0.91	0.91
149	ED	0.80	0.69	0.73	0.74	0.76	0.79	0.78	0.79
cm	SC	0.78	0.84	0.83	0.82	0.81	0.79	0.80	0.79
161	ED	0.40	**0.29**	0.32	0.33	0.35	0.38	0.36	0.38
cm	SC	0.93	**0.97**	0.96	0.95	0.95	0.94	0.94	0.94
167	ED	0.40	0.29	0.30	0.32	0.33	0.38	0.35	0.38
cm	SC	0.93	0.96	0.96	0.96	0.95	0.94	0.95	0.94
169	ED	0.41	0.29	**0.32**	0.33	0.35	0.39	0.36	0.39
cm	SC	0.93	0.96	**0.96**	0.95	0.95	0.94	0.94	0.94
171	ED	0.59	0.48	0.51	0.52	0.53	0.57	0.55	0.57
cm	SC	0.87	0.91	0.90	0.90	0.89	0.87	0.88	0.87
173	ED	0.43	0.32	0.35	0.36	0.38	0.41	0.39	0.42
cm	SC	0.92	0.96	0.95	0.94	0.94	0.93	0.93	0.93
181	ED	0.55	0.44	0.47	0.48	0.50	0.53	0.51	0.53
cm	SC	0.88	0.93	0.91	0.91	0.90	0.89	0.90	0.89
191	ED	0.38	0.27	0.32	0.32	**0.33**	0.36	0.35	0.37
cm	SC	0.94	0.97	0.96	0.96	**0.95**	0.94	0.95	0.94
201	ED	0.42	0.30	0.33	0.34	0.36	**0.40**	0.38	0.40
cm	SC	0.93	0.96	0.95	0.95	0.94	**0.93**	0.94	0.93
213	ED	0.43	0.32	0.35	0.36	0.38	0.41	**0.39**	0.42
cm	SC	0.92	0.96	0.95	0.94	0.94	0.93	**0.93**	0.93
215	ED	0.41	0.30	0.33	0.34	0.35	0.39	0.37	**0.39**
cm	SC	0.93	0.96	0.95	0.95	0.95	0.94	0.94	**0.93**
219	ED	0.52	0.41	0.43	0.44	0.46	0.50	0.48	0.51
cm	SC	0.89	0.93	0.93	0.92	0.91	0.90	0.91	0.90
223	ED	0.45	0.34	0.37	0.38	0.40	0.43	0.42	0.44
cm	SC	0.91	0.95	0.94	0.94	0.93	0.92	0.93	0.92
229	ED	0.58	0.47	0.50	0.51	0.53	0.57	0.54	0.57
cm	SC	0.87	0.91	0.90	0.90	0.89	0.87	0.88	0.87

Rescaled Euclidean distance of magnetic data of tephra layers between Ska1 and JL2, SE Iceland.

JL2 / Ska1	*51*	*61*	*75*	*79*	*87*	*89*	*113*	*115*
7.55	0.78	0.726	0.428	0.41	0.471	0.599	0.449	0.615
18	0.679	0.677	0.454	0.41	0.497	0.516	0.367	0.52
22	0.316	0.484	0.522	0.406	0.49	0.149	0.313	0.182
28	0.766	0.679	0.361	0.334	0.169	0.547	0.455	0.591
32	0.865	0.753	0.364	0.404	0.385	0.67	0.541	0.715
35	0.807	0.68	0.287	0.348	0.461	0.627	0.481	0.666
37	0.813	0.675	0.283	0.345	0.446	0.629	0.49	0.67
38	0.819	0.715	0.322	0.356	0.37	0.621	0.494	0.666
40	0.816	0.719	0.355	0.363	0.286	0.607	0.496	0.652
46	0.608	0.568	0.333	0.25	0.221	0.381	0.313	0.418
65.5	0.799	0.714	0.372	0.357	0.209	0.583	0.481	0.627
67.5	0.788	0.701	0.362	0.348	0.224	0.573	0.467	0.616
69	0.761	0.718	0.403	0.365	0.163	0.541	0.449	0.585
70	0.928	0.822	0.438	0.468	0.383	0.728	0.6	0.771
71	0.873	0.781	0.409	0.419	0.289	0.664	0.548	0.709
77.5	**0.565**	0.629	0.441	0.4	0.655	0.46	0.291	0.451
82.5	0.889	0.794	0.418	0.44	0.317	0.681	0.589	0.736
88.55	0.912	0.806	0.421	0.464	0.496	0.729	0.576	0.763
95	0.821	0.773	0.457	0.461	0.506	0.65	0.492	0.671
98	0.818	0.824	0.51	0.476	0.361	0.624	0.499	0.653
108.55	0.98	0.851	0.462	0.512	0.462	0.787	0.66	0.831
114	1	0.866	**0.496**	0.527	0.398	0.797	0.694	0.844
115	0.991	0.861	0.497	0.525	0.378	0.788	0.692	0.837
116	0.947	0.833	0.461	0.484	0.333	**0.74**	0.633	0.788
117	0.956	0.837	0.468	0.492	0.345	0.75	0.644	0.798
118	0.922	0.812	0.448	0.466	0.295	0.712	0.617	0.763
124	0.881	0.784	0.439	0.438	0.222	0.666	0.577	0.717
128.5	0.893	0.86	0.55	0.553	0.429	0.703	0.67	0.767
131	0.792	0.756	0.455	0.428	0.299	0.587	0.474	0.622
134	0.836	0.651	0.401	0.438	0.594	0.672	0.526	0.69
136	0.722	0.665	0.444	0.45	0.718	0.608	0.427	0.603
138	0.755	0.684	0.41	0.414	0.593	0.604	0.429	0.612
144	0.798	0.729	0.412	0.384	0.24	0.584	0.474	0.621
149	0.834	0.749	0.455	0.436	0.191	0.621	0.556	0.672
152	0.809	0.718	0.342	0.344	0.329	0.604	0.487	0.645
155	0.933	0.819	0.436	0.462	0.348	0.728	0.62	0.776
158.55	0.951	0.825	0.449	0.485	0.386	0.751	0.64	0.799
170	0.869	0.774	0.423	0.416	0.249	0.655	0.563	0.701
177.55	0.858	0.77	0.443	0.421	0.246	0.642	0.564	0.688
225.55	0.769	0.679	0.304	0.307	0.278	0.56	0.447	0.606
231	0.759	0.702	0.436	0.376	0.291	0.547	**0.466**	0.576
232	0.725	0.646	0.316	0.288	0.251	0.511	0.394	0.549
245.55	0.784	0.772	0.477	0.427	0.113	0.564	0.504	0.612
258	0.83	0.799	0.47	0.433	0.182	0.612	0.531	0.657
263	0.852	0.793	0.426	0.415	0.248	0.641	0.535	0.685

Similarity matrix (Rescaled cosine) of magnetic data of tephra layers between Ska1 and JL2, SE Iceland.

Ska1 \ JL2	*51*	*61*	*75*	*79*	*87*	*89*	*113*	*115*
7.55	0.530	0.501	0.745	0.766	0.704	0.615	0.758	0.630
18	0.658	0.592	0.776	0.822	0.775	0.733	0.851	0.747
22	0.936	0.787	0.702	0.835	0.802	0.972	0.893	0.964
28	0.602	0.566	0.726	0.778	0.884	0.703	0.786	0.709
32	0.372	0.399	0.722	0.664	0.578	0.450	0.612	0.447
35	0.476	0.536	0.834	0.768	0.528	0.539	0.699	0.537
37	0.467	0.543	0.833	0.764	0.526	0.531	0.688	0.529
38	0.461	0.473	0.782	0.740	0.629	0.541	0.686	0.537
40	0.474	0.468	0.733	0.726	0.745	0.570	0.690	0.568
46	0.777	0.703	0.777	0.869	0.889	0.863	0.891	0.869
65.5	0.524	0.486	0.706	0.738	0.837	0.627	0.733	0.632
67.5	0.535	0.506	0.722	0.749	0.828	0.635	0.742	0.639
69	0.576	0.468	0.658	0.724	0.908	0.681	0.759	0.683
70	0.234	0.246	0.594	0.545	0.563	0.324	0.506	0.328
71	0.360	0.333	0.639	0.629	0.715	0.461	0.609	0.463
77.5	**0.773**	0.681	0.873	0.909	0.656	0.817	0.932	0.828
82.5	0.324	0.303	0.622	0.585	0.653	0.423	0.530	0.404
88.55	0.304	0.333	0.684	0.624	0.501	0.380	0.573	0.386
95	0.479	0.443	0.723	0.718	0.670	0.558	0.718	0.567
98	0.464	0.317	0.573	0.627	0.784	0.557	0.684	0.566
108.6	0.121	0.189	0.558	0.467	0.405	0.201	0.388	0.200
114	0.000	0.084	**0.435**	0.360	0.403	0.095	0.269	0.100
115	0.012	0.085	0.434	0.361	0.428	0.106	0.276	0.111
116	0.172	0.193	0.528	0.484	0.595	**0.275**	0.435	0.275
117	0.144	0.178	0.511	0.461	0.557	0.243	0.408	0.246
118	0.244	0.252	0.559	0.526	0.672	0.351	0.483	0.345
124	0.378	0.339	0.587	0.603	0.818	0.490	0.602	0.490
128.5	0.320	0.195	0.419	0.421	0.544	0.397	0.388	0.354
131	0.501	0.421	0.640	0.680	0.846	0.605	0.711	0.606
134	0.463	0.606	0.797	0.755	0.520	0.534	0.686	0.547
136	0.637	0.648	0.876	0.866	0.544	0.687	0.845	0.703
138	0.575	0.585	0.826	0.820	0.609	0.642	0.802	0.657
144	0.502	0.447	0.649	0.698	0.828	0.607	0.718	0.617
149	0.491	0.430	0.542	0.599	0.859	0.589	0.632	0.587
152	0.490	0.470	0.752	0.754	0.664	0.578	0.707	0.584
155	0.212	0.232	0.585	0.535	0.563	0.307	0.468	0.307
158.6	0.161	0.218	0.556	0.484	0.480	0.246	0.416	0.247
170	0.389	0.355	0.614	0.641	0.764	0.498	0.608	0.505
177.6	0.419	0.366	0.570	0.629	0.769	0.530	0.607	0.539
225.6	0.570	0.547	0.806	0.806	0.750	0.656	0.772	0.655
231	0.570	0.497	0.612	0.711	0.763	0.665	**0.727**	0.687
232	0.632	0.599	0.788	0.827	0.813	0.722	0.827	0.732
245.6	0.540	0.358	0.516	0.618	0.946	0.649	0.680	0.644
258	0.455	0.293	0.521	0.604	0.874	0.567	0.640	0.569
263	0.411	0.304	0.605	0.636	0.777	0.514	0.642	0.519

Rescaled Euclidean Distance of magnetic data of tephra layers between Ska1 and JL1, SE Iceland.

Ska1 \ JL1	39	85	91	93	131	149	151	167	181	185	189	191	215	219	227	275	319
7.55	0.592	0.528	0.65	0.758	0.55	0.546	0.519	0.435	0.293	0.472	0.492	0.529	0.531	0.545	0.358	0.661	0.368
18	0.505	0.444	0.572	0.661	0.465	0.467	0.464	0.481	0.414	0.411	0.402	0.45	0.45	0.456	0.311	0.567	0.314
22	0.26	0.222	0.314	0.363	0.226	0.273	0.228	0.63	0.641	0.183	0.199	0.118	0.196	0.152	0.364	0.271	0.334
28	0.582	0.479	0.661	0.775	0.536	0.547	0.455	0.433	0.252	0.379	0.462	0.448	0.505	0.488	0.341	0.653	0.364
32	0.663	0.573	0.739	0.849	0.629	0.625	0.551	0.372	0.203	0.508	0.587	0.572	0.61	0.602	0.409	0.736	0.461
35	0.604	0.531	0.67	0.781	0.575	0.563	0.502	0.256	0.132	0.486	0.551	0.548	0.563	0.567	0.353	0.675	0.409
37	0.612	0.539	0.678	0.791	0.584	0.572	0.505	0.262	0.125	0.487	0.558	0.552	0.57	0.573	0.365	0.684	0.416
38	0.619	0.539	0.686	0.803	0.583	0.577	0.506	0.336	0.131	0.468	0.547	0.532	0.563	0.566	0.367	0.694	0.419
40	0.623	0.533	0.695	0.811	0.582	0.583	0.502	0.399	0.191	0.444	0.528	0.51	0.556	0.549	0.374	0.696	0.412
46	0.429	**0.342**	0.496	0.617	0.374	0.392	0.307	0.42	0.287	0.222	0.292	0.289	0.338	0.334	0.225	0.499	0.216
65.5	0.612	0.512	0.689	0.804	0.566	0.575	0.489	0.433	0.234	0.417	0.499	0.485	0.538	0.525	0.364	0.684	0.393
67.5	0.599	0.5	0.676	0.79	0.554	0.561	0.478	0.421	0.228	0.407	0.486	0.475	0.526	0.512	0.349	0.671	0.378
69	0.579	0.478	**0.657**	0.77	0.528	0.543	0.464	0.476	0.293	0.377	0.454	0.438	0.498	0.486	0.344	0.651	0.372
70	0.73	0.637	0.805	0.917	0.692	0.691	0.618	0.454	0.256	0.564	0.64	0.63	0.67	0.663	0.472	0.803	0.517
71	0.681	0.586	0.756	0.871	0.639	0.642	0.563	0.451	0.236	0.5	0.581	0.566	0.614	0.606	0.427	0.755	0.469
77.5	0.4	0.391	0.44	**0.517**	0.378	0.358	0.417	0.445	0.465	0.419	0.379	0.436	0.384	0.425	0.29	0.456	0.311
82.5	0.703	0.617	0.769	0.887	0.664	0.665	0.577	0.465	0.251	0.526	0.624	0.587	0.639	0.636	0.474	0.776	0.522
88.6	0.706	0.63	0.772	0.883	0.672	0.663	0.612	0.392	0.22	0.577	0.633	0.64	0.657	0.662	0.447	0.779	0.495
95	0.626	0.554	0.696	0.793	0.589	0.585	0.561	0.45	0.341	0.514	0.54	0.563	0.575	0.58	0.388	0.694	0.423
98	0.643	0.549	0.722	0.821	0.594	**0.606**	0.567	0.555	0.412	0.488	0.525	0.535	0.573	0.568	0.414	0.712	0.447
109	0.779	0.69	0.849	0.96	0.744	0.739	0.664	**0.456**	0.272	0.622	0.701	0.688	0.724	0.718	0.526	0.849	0.573
114	0.816	0.724	0.885	1	0.779	0.779	0.69	0.533	0.325	0.639	0.728	0.708	0.753	0.743	0.576	0.886	0.612
115	0.811	0.713	0.885	0.996	0.774	0.777	0.683	0.544	**0.357**	0.63	0.722	0.697	0.749	0.733	0.576	0.88	0.614
116	0.758	0.661	0.832	0.946	0.718	0.721	0.634	0.501	0.293	0.575	0.663	**0.641**	0.693	0.68	0.511	0.829	0.552
117	0.768	0.668	0.845	0.956	0.729	0.733	0.644	0.508	0.313	0.585	0.673	0.652	0.704	0.688	0.522	0.838	0.562
118	0.736	0.637	0.812	0.925	0.696	0.701	0.608	0.5	0.302	0.546	0.641	0.611	0.669	0.653	0.496	0.807	0.537
124	0.698	0.594	0.778	0.89	0.656	0.666	0.571	0.504	0.312	0.501	0.592	0.566	0.628	0.609	0.461	0.769	0.497
129	0.748	0.68	0.799	0.908	0.714	0.717	0.633	0.621	0.481	0.593	0.698	0.628	0.692	0.692	0.598	0.811	0.648
131	0.607	0.516	0.684	0.79	0.558	0.57	0.513	0.504	0.341	0.432	0.486	0.484	**0.533**	0.524	0.373	0.678	0.399
134	0.659	0.62	0.705	0.816	0.636	0.623	0.581	0.371	0.304	0.578	0.6	0.638	0.626	0.641	0.451	0.723	0.456
136	0.54	0.526	0.575	0.665	0.521	0.497	0.527	0.377	0.401	0.542	0.515	0.581	0.526	0.565	0.372	0.598	0.388
138	0.563	0.521	0.614	0.716	0.532	0.519	0.516	0.372	0.314	0.502	0.5	0.552	0.526	0.552	0.344	0.63	0.363
144	0.611	0.52	0.683	0.801	0.562	0.573	0.5	0.467	0.26	0.426	0.488	0.491	0.535	0.531	0.366	0.685	0.387
149	0.663	0.547	0.751	0.852	0.62	0.637	0.536	0.535	0.399	0.455	0.549	0.513	0.591	0.554	0.449	0.726	0.478
152	0.621	0.543	0.68	0.804	0.58	0.577	0.503	0.382	0.14	0.458	0.534	0.527	0.555	0.563	0.378	0.696	0.411
155	0.744	0.649	0.816	0.93	0.706	0.706	0.62	0.472	0.265	0.567	0.656	0.634	0.681	0.671	**0.498**	0.815	0.54
159	0.76	0.662	0.837	0.946	0.724	0.725	0.638	0.476	0.302	0.587	0.674	0.654	0.701	0.685	0.513	0.829	0.557
170	0.689	0.594	0.758	0.876	0.645	0.65	0.56	0.483	0.261	0.495	0.583	0.564	0.615	0.606	0.452	0.76	0.48
178	0.683	0.594	0.746	0.868	0.638	0.645	0.554	0.509	0.284	0.489	0.575	0.557	0.606	0.602	0.461	0.754	0.481
226	0.577	0.486	0.648	0.765	0.536	0.536	0.455	0.354	0.154	0.402	0.487	0.47	0.511	0.506	0.326	0.65	0.368
231	0.583	0.507	0.637	0.763	0.532	0.544	0.47	0.496	0.298	0.401	0.453	0.47	0.499	0.507	0.376	0.654	0.368
232	0.533	0.443	0.606	0.725	0.486	0.493	0.419	0.375	0.184	0.355	0.42	0.425	0.46	0.458	0.279	0.608	**0.303**
246	0.617	0.508	0.699	0.804	0.566	0.586	0.5	0.561	0.399	0.401	0.489	0.453	0.533	0.508	0.411	0.684	0.438
258	0.656	0.556	0.73	0.843	0.606	0.619	0.539	0.54	0.341	0.454	0.536	0.513	0.574	0.564	0.433	0.727	0.461
263	0.669	0.57	0.744	0.858	0.623	0.63	0.552	0.482	0.276	0.481	0.562	0.546	0.596	0.588	0.424	0.742	0.463

Similarity matrix (Rescaled cosine) of magnetic data of tephra layers between Ska1 and JL1, SE Iceland.

Ska1 \ JL1	39	85	91	93	131	149	151	167	181	185	189	191	215	219	227	275	319
7.55	0.626	0.649	0.605	0.553	0.658	0.666	0.646	0.725	0.893	0.687	0.705	0.640	0.667	0.639	0.811	0.583	0.808
18	0.742	0.774	0.706	0.673	0.769	0.769	0.749	0.722	0.831	0.799	0.817	0.765	0.776	0.766	0.888	0.706	0.882
22	0.926	0.943	0.909	0.912	0.940	0.917	0.944	0.547	0.510	0.975	0.953	0.987	0.953	0.972	0.858	0.930	0.878
28	0.681	0.723	0.645	0.598	0.717	0.705	0.722	0.662	0.815	0.792	0.791	0.753	0.736	0.739	0.831	0.645	0.846
32	0.495	0.525	0.459	0.412	0.512	0.531	0.526	0.757	0.875	0.547	0.537	0.502	0.514	0.500	0.705	0.449	0.663
35	0.594	0.605	0.572	0.524	0.603	0.629	0.621	0.881	0.950	0.605	0.600	0.560	0.597	0.569	0.779	0.552	0.736
37	0.582	0.590	0.562	0.511	0.589	0.616	0.614	0.878	0.950	0.597	0.588	0.549	0.585	0.557	0.765	0.540	0.726
38	0.576	0.590	0.557	0.500	0.596	0.615	0.610	0.801	0.942	0.622	0.609	0.579	0.599	0.567	0.764	0.529	0.727
40	0.577	0.605	0.552	0.496	0.606	0.614	0.621	0.715	0.888	0.666	0.650	0.622	0.620	0.604	0.760	0.533	0.746
46	0.835	**0.854**	0.821	0.776	0.868	0.854	0.869	0.686	0.801	0.921	0.920	0.894	0.886	0.876	0.910	0.807	0.936
65.5	0.613	0.655	0.580	0.529	0.651	0.645	0.653	0.660	0.840	0.722	0.719	0.680	0.669	0.663	0.790	0.572	0.792
67.5	0.627	0.667	0.592	0.543	0.662	0.658	0.666	0.679	0.845	0.731	0.726	0.689	0.678	0.674	0.801	0.586	0.802
69	0.650	0.696	**0.614**	0.568	0.694	0.678	0.683	0.580	0.762	0.768	0.763	0.739	0.712	0.708	0.799	0.611	0.798
70	0.350	0.388	0.312	0.258	0.377	0.392	0.379	0.619	0.808	0.426	0.426	0.373	0.384	0.366	0.593	0.298	0.560
71	0.466	0.503	0.432	0.374	0.501	0.505	0.501	0.627	0.837	0.562	0.558	0.515	0.513	0.495	0.682	0.415	0.661
77.5	0.850	0.855	0.832	**0.805**	0.864	0.877	0.837	0.823	0.864	0.843	0.863	0.820	0.859	0.828	0.949	0.818	0.922
82.5	0.417	0.431	0.405	0.338	0.446	0.458	0.470	0.602	0.819	0.506	0.466	0.471	0.458	0.427	0.594	0.367	0.555
88.6	0.425	0.446	0.398	0.343	0.445	0.469	0.445	0.731	0.887	0.461	0.469	0.408	0.444	0.411	0.658	0.374	0.618
95	0.585	0.621	0.547	0.507	0.612	0.622	0.596	0.713	0.849	0.639	0.651	0.599	0.615	0.598	0.784	0.541	0.755
98	0.541	0.598	0.493	0.457	0.585	**0.572**	0.548	0.517	0.686	0.634	0.650	0.605	0.594	0.586	0.723	0.498	0.701
109	0.235	0.264	0.206	0.152	0.256	0.280	0.272	**0.615**	0.786	0.293	0.285	0.238	0.259	0.237	0.484	0.186	0.443
114	0.084	0.111	0.067	0.000	0.114	0.134	0.137	0.450	0.706	0.177	0.172	0.113	0.129	0.104	0.337	0.035	0.328
115	0.092	0.135	0.062	0.004	0.122	0.136	0.144	0.440	**0.663**	0.196	0.189	0.133	0.138	0.129	0.345	0.046	0.335
116	0.276	0.316	0.241	0.181	0.309	0.318	0.321	0.529	0.760	0.383	0.373	**0.330**	0.323	0.311	0.517	0.224	0.496
117	0.244	0.294	0.205	0.151	0.277	0.286	0.289	0.517	0.725	0.352	0.346	0.296	0.291	0.287	0.492	0.197	0.475
118	0.344	0.390	0.307	0.252	0.379	0.382	0.397	0.540	0.752	0.466	0.443	0.420	0.396	0.395	0.563	0.298	0.545
124	0.466	0.523	0.420	0.369	0.508	0.496	0.511	0.535	0.738	0.600	0.591	0.559	0.527	0.533	0.666	0.422	0.660
129	0.334	0.332	0.339	0.288	0.355	0.357	0.387	0.322	0.468	0.408	0.331	0.411	0.365	0.336	0.378	0.300	0.325
131	0.590	0.637	0.548	0.503	0.630	0.619	0.617	0.580	0.763	0.699	0.697	0.668	**0.645**	0.641	0.764	0.547	0.753
134	0.557	0.552	0.546	0.483	0.567	0.588	0.592	0.819	0.922	0.577	0.592	0.518	0.567	0.535	0.736	0.515	0.736
136	0.738	0.737	0.724	0.681	0.750	0.772	0.736	0.888	0.944	0.720	0.751	0.678	0.741	0.700	0.891	0.699	0.867
138	0.681	0.692	0.660	0.612	0.701	0.717	0.689	0.834	0.938	0.696	0.722	0.650	0.698	0.663	0.858	0.638	0.840
144	0.589	0.622	0.561	0.501	0.631	0.621	0.620	0.599	0.812	0.693	0.705	0.650	0.647	0.629	0.766	0.543	0.772
149	0.544	0.625	0.478	0.462	0.581	0.552	0.588	0.441	0.521	0.691	0.673	0.669	0.603	0.651	0.671	0.522	0.681
152	0.582	0.586	0.582	0.512	0.612	0.628	0.619	0.743	0.937	0.641	0.641	0.591	0.623	0.578	**0.756**	0.535	0.749
155	0.314	0.349	0.288	0.229	0.344	0.361	0.361	0.601	0.810	0.406	0.393	0.351	0.358	0.339	0.549	0.266	0.526
159	0.268	0.315	0.227	0.182	0.292	0.307	0.309	0.589	0.739	0.349	0.341	0.295	0.300	0.298	0.509	0.225	0.481
170	0.467	0.498	0.451	0.385	0.508	0.510	0.519	0.572	0.814	0.588	0.579	0.536	0.533	0.513	0.655	0.422	0.667
178	0.480	0.496	0.480	0.405	0.525	0.521	0.534	0.507	0.774	0.603	0.598	0.553	0.553	0.522	0.634	0.437	0.664
226	0.668	0.692	0.647	0.595	0.695	0.704	0.706	0.788	0.925	0.738	0.726	0.697	0.705	0.686	0.834	0.628	0.817
231	0.637	0.644	0.641	0.571	0.680	0.669	0.669	0.549	0.762	0.730	0.756	0.684	0.704	0.668	0.750	0.598	**0.797**
232	0.720	0.746	0.697	0.645	0.754	0.751	0.750	0.747	0.896	0.796	0.806	0.755	0.765	0.746	0.875	0.681	0.879
246	0.585	0.649	0.540	0.506	0.633	0.605	0.622	0.405	0.572	0.735	0.714	0.718	0.659	0.675	0.700	0.553	0.702
258	0.514	0.563	0.485	0.432	0.564	0.548	0.550	0.440	0.670	0.652	0.641	0.621	0.589	0.580	0.668	0.472	0.669
263	0.494	0.540	0.463	0.409	0.538	0.535	0.525	0.563	0.779	0.603	0.601	0.562	0.554	0.538	0.691	0.448	0.675

Rescaled cosine of magnetic data of tephra layers between Lax and Ska1, SE Iceland.

Ska1 \ Lax	4	7	13.6	18.6	24.6	28.6	32	33.6	36.6	41.6	47	53	55	112	115	123	133	141	150	154	156	160
7.55	0.83	0.81	0.91	0.91	0.96	0.82	0.85	0.91	0.93	0.93	0.74	0.89	0.86	0.84	0.67	0.66	0.78	0.72	0.32	0.79	0.49	0.76
18	0.89	0.79	0.93	0.93	0.93	0.74	0.75	0.85	0.87	0.86	0.64	0.82	0.78	0.76	0.62	0.65	0.70	0.61	0.25	0.68	0.40	0.72
22	**0.96**	0.76	0.89	0.88	0.65	0.42	0.35	0.54	0.53	0.50	0.40	0.52	0.51	0.44	0.43	0.42	0.42	0.30	0.00	0.24	0.09	0.60
28	0.91	**0.80**	0.96	0.97	0.93	0.73	0.74	0.87	0.87	0.86	0.69	0.84	0.81	0.79	0.70	0.69	0.76	0.67	0.27	0.67	0.41	0.82
32	0.77	0.69	0.86	0.86	0.92	0.87	0.86	0.88	0.90	0.91	0.65	0.86	0.80	0.78	0.59	0.58	0.78	0.79	0.47	0.79	0.61	0.69
35	0.78	0.72	0.86	0.85	0.88	0.91	0.83	0.82	0.84	0.86	0.61	0.82	0.78	0.73	0.52	0.49	0.71	0.75	0.43	0.72	0.57	0.62
37	0.76	0.72	0.85	0.84	0.87	0.91	0.83	0.81	0.83	0.85	0.62	0.81	0.77	0.73	0.53	0.48	0.70	0.76	0.43	0.72	0.57	0.62
38	0.82	0.78	0.90	0.90	0.92	0.86	0.83	0.87	0.89	0.89	0.70	0.87	0.83	0.78	0.61	0.58	0.79	0.77	0.41	0.75	0.57	0.73
40	0.85	0.79	0.92	0.93	0.94	0.81	0.82	0.91	0.91	0.90	0.74	0.88	0.84	0.82	0.69	0.65	0.82	0.77	0.38	0.76	0.53	0.81
46	0.97	0.87	0.98	**0.98**	0.86	0.65	0.63	0.78	0.77	0.75	0.65	0.77	0.76	0.70	0.65	0.62	0.66	0.55	0.15	0.53	0.29	0.78
65.5	0.88	0.79	0.94	0.95	**0.95**	0.75	0.79	0.90	0.91	0.89	0.72	0.87	0.83	0.82	0.71	0.70	0.80	0.72	0.32	0.73	0.47	0.83
67.5	0.88	0.78	0.94	0.95	0.95	0.77	0.80	0.91	0.91	0.90	0.72	0.87	0.83	0.82	0.70	0.69	0.80	0.72	0.33	0.74	0.48	0.82
69	0.91	0.79	0.94	0.95	0.91	0.64	0.68	0.85	0.86	0.83	0.69	0.84	0.78	0.76	0.68	0.72	0.77	0.61	0.22	0.64	0.38	0.83
70	0.69	0.65	0.80	0.81	0.94	0.84	0.89	0.91	0.94	0.94	0.70	0.89	0.82	0.84	0.64	0.65	0.83	0.81	0.48	0.87	0.63	0.72
71	0.79	0.73	0.87	0.88	0.95	0.78	0.83	0.92	0.93	0.92	0.74	0.90	0.85	0.84	0.69	0.71	0.85	0.76	0.39	0.80	0.55	0.80
77.5	0.89	0.81	0.91	0.88	0.83	0.69	0.65	0.72	0.76	0.75	0.55	0.73	0.69	0.63	0.48	0.52	0.59	0.50	0.19	0.55	0.33	0.59
82.5	0.77	0.74	0.82	0.83	0.84	0.69	0.71	0.82	0.81	0.79	0.73	0.83	0.78	0.73	0.65	0.60	0.83	0.73	0.37	0.66	0.52	0.80
88.55	0.70	0.69	0.81	0.81	0.93	**0.91**	0.91	0.90	0.93	0.95	0.70	0.89	0.84	0.83	0.59	0.59	0.80	0.81	0.47	0.86	0.63	0.67
95	0.80	0.72	0.88	0.88	0.96	0.81	**0.84**	0.89	0.93	0.93	0.67	0.86	0.80	0.80	0.62	0.65	0.77	0.71	0.37	0.79	0.51	0.71
98	0.80	0.68	0.85	0.85	0.87	0.61	0.66	0.81	0.86	0.83	0.61	0.81	0.72	0.71	0.57	0.70	0.72	0.54	0.21	0.67	0.37	0.70
108.6	0.60	0.58	0.72	0.73	0.89	0.88	0.91	**0.88**	0.90	0.92	0.68	0.86	0.80	0.81	0.59	0.55	0.82	0.87	0.58	0.88	0.70	0.66
114	0.48	0.54	0.61	0.63	0.79	0.76	0.85	0.84	0.82	0.83	0.72	0.81	0.79	0.81	0.66	0.56	0.80	0.85	0.53	0.84	0.65	0.69
115	0.50	0.49	0.61	0.63	0.77	0.72	0.79	0.80	0.79	0.80	0.63	0.75	0.71	0.75	0.60	0.54	0.75	0.81	0.53	0.80	0.62	0.65
116	0.66	0.63	0.77	0.79	0.90	0.77	0.85	0.90	**0.90**	0.90	0.73	0.87	0.81	0.83	0.69	0.67	0.85	0.82	0.48	0.84	0.61	0.78
117	0.63	0.58	0.74	0.76	0.89	0.78	0.86	0.89	0.90	0.90	0.68	0.84	0.78	0.82	0.66	0.64	0.82	0.83	0.52	0.85	0.63	0.74
118	0.72	0.64	0.80	0.82	0.89	0.72	0.79	0.88	0.87	0.87	0.70	0.83	0.78	0.79	0.69	0.66	0.83	0.79	0.46	0.77	0.57	0.80
124	0.80	0.68	0.86	0.88	0.90	0.68	0.73	0.86	0.87	0.85	0.68	0.83	0.77	0.78	0.69	0.72	0.80	0.70	0.35	0.71	0.47	0.81
128.5	0.64	0.59	0.63	0.64	0.52	0.31	0.30	0.48	0.47	0.43	0.47	0.52	0.48	0.39	0.40	0.40	0.55	0.37	0.10	0.26	0.22	0.60
131	0.86	0.75	0.91	0.93	0.95	0.68	0.75	0.89	0.91	0.89	0.70	0.86	0.80	0.80	0.70	0.74	0.80	0.66	0.29	0.72	0.43	0.83
134	0.68	0.69	0.79	0.78	0.85	0.92	0.85	0.80	0.79	0.83	0.64	0.78	0.79	0.76	0.58	0.49	0.66	0.75	0.38	0.72	0.51	0.61
136	0.80	0.77	0.87	0.85	0.87	0.86	0.78	0.78	0.81	**0.83**	0.59	0.78	0.76	0.71	0.51	0.50	0.63	0.63	0.29	0.67	0.45	0.57
138	0.81	0.78	0.89	0.88	0.92	0.87	0.84	0.85	0.88	0.89	0.66	0.84	0.81	0.78	0.58	0.57	0.70	0.69	0.33	0.74	0.49	0.65
144	0.87	0.81	0.93	0.94	0.95	0.73	0.77	0.90	0.91	0.89	**0.76**	0.90	0.86	0.84	0.74	0.77	0.81	0.68	0.25	0.72	0.42	0.84
149	0.85	0.62	0.88	0.90	0.84	0.57	0.61	0.78	0.77	0.75	0.52	0.70	0.63	0.66	0.61	0.64	0.67	0.59	0.29	0.58	0.36	0.76
152	0.83	0.85	0.90	0.90	0.90	0.82	0.81	0.88	0.89	0.88	0.77	**0.89**	0.88	0.81	0.65	0.61	0.79	0.73	0.31	0.73	0.50	0.76
155	0.68	0.66	0.78	0.80	0.89	0.81	0.86	0.89	0.90	0.90	0.72	0.87	0.82	0.82	0.64	0.61	0.83	0.82	0.48	0.84	0.63	0.75
158.6	0.63	0.56	0.74	0.76	0.88	0.83	0.87	0.87	0.88	0.89	0.62	0.81	0.75	0.78	0.59	0.56	0.78	0.84	0.55	0.84	0.66	0.67
170	0.81	0.79	0.87	0.89	0.90	0.73	0.79	0.90	0.90	0.87	0.79	0.89	**0.86**	0.83	0.73	0.69	0.83	0.73	0.31	0.75	0.48	0.85
177.6	0.82	0.85	0.86	0.88	0.85	0.65	0.70	0.85	0.83	0.80	0.81	0.86	0.86	0.80	0.75	0.69	0.80	0.66	0.20	0.66	0.39	0.87
225.6	0.88	0.81	0.94	0.94	0.92	0.80	0.79	0.87	0.88	0.87	0.69	0.86	0.82	0.77	0.63	0.60	0.77	0.72	0.34	0.71	0.50	0.77
231	0.90	0.92	0.93	0.93	0.86	0.65	0.66	0.82	0.81	0.78	0.77	0.84	0.85	0.78	0.72	**0.72**	0.71	0.56	0.10	0.59	0.28	0.81
232	0.91	0.84	0.96	0.96	0.94	0.78	0.77	0.87	0.88	0.87	0.71	0.86	0.83	0.80	0.67	0.67	0.75	0.68	0.27	0.69	0.43	0.78
245.6	0.87	0.70	0.87	0.89	0.81	0.47	0.52	0.75	0.77	0.72	0.59	0.73	0.66	0.64	0.60	0.68	0.69	0.48	0.13	0.52	0.27	0.79
258	0.83	0.75	0.86	0.87	0.83	0.53	0.60	0.80	0.83	0.77	0.69	0.81	0.75	0.71	0.63	0.71	0.76	0.53	0.15	0.61	0.33	0.81
263	0.81	0.74	0.87	0.87	0.89	0.68	0.73	0.87	0.90	0.87	0.70	0.87	0.80	0.77	0.63	0.69	**0.80**	0.65	0.28	0.73	0.46	0.78

Rescaled Euclidean distance of magnetic data of tephra layers between Lax and Ska1, SE Iceland.

Ska1 \ Lax	4	7	14	19	25	29	32	34	37	42	47	53	55	112	115	123	133	141	150	154	156	160
7.55	0.32	0.44	0.28	0.28	0.25	0.35	0.38	0.38	0.34	0.32	0.42	0.38	0.39	0.43	0.45	0.46	0.43	0.52	0.60	0.46	0.54	0.43
18	0.33	0.47	0.37	0.38	0.40	0.52	0.55	0.53	0.50	0.48	0.58	0.53	0.54	0.58	0.59	0.55	0.58	0.67	0.73	0.61	0.68	0.56
22	**0.42**	0.58	0.58	0.60	0.74	0.84	0.87	0.82	0.81	0.82	0.85	0.83	0.83	0.86	0.85	0.85	0.86	0.91	100	0.91	0.98	0.80
28	0.23	**0.50**	0.09	0.08	0.12	0.27	0.25	0.19	0.18	0.19	0.28	0.21	0.22	0.25	0.27	0.36	0.25	0.31	0.45	0.29	0.43	0.21
32	0.33	0.55	0.20	0.20	0.14	0.19	0.22	0.22	0.19	0.17	0.31	0.23	0.25	0.28	0.34	0.43	0.26	0.32	0.40	0.28	0.36	0.30
35	0.35	0.52	0.26	0.27	0.26	0.23	0.32	0.35	0.32	0.30	0.41	0.34	0.36	0.40	0.45	0.52	0.39	0.44	0.49	0.40	0.44	0.42
37	0.35	0.52	0.25	0.27	0.25	0.22	0.31	0.33	0.31	0.29	0.40	0.33	0.34	0.38	0.43	0.52	0.37	0.42	0.48	0.39	0.43	0.40
38	0.29	0.49	0.18	0.18	0.16	0.21	0.25	0.25	0.22	0.21	0.31	0.24	0.26	0.30	0.35	0.43	0.28	0.36	0.44	0.32	0.40	0.30
40	0.27	0.49	0.15	0.13	0.12	0.23	0.23	0.20	0.18	0.17	0.27	0.21	0.23	0.26	0.29	0.39	0.24	0.32	0.43	0.29	0.40	0.24
46	0.10	0.38	0.14	**0.15**	0.27	0.40	0.42	0.37	0.35	0.36	0.40	0.37	0.37	0.41	0.41	0.45	0.41	0.48	0.60	0.46	0.58	0.35
65.5	0.26	0.51	0.12	0.10	**0.10**	0.25	0.23	0.18	0.16	0.16	0.26	0.19	0.21	0.23	0.27	0.35	0.23	0.30	0.43	0.27	0.41	0.21
67.5	0.25	0.50	0.12	0.11	0.10	0.26	0.24	0.20	0.18	0.17	0.28	0.21	0.23	0.26	0.28	0.36	0.25	0.33	0.45	0.29	0.42	0.23
69	0.21	0.48	0.13	0.12	0.17	0.34	0.32	0.25	0.23	0.24	0.31	0.25	0.28	0.30	0.32	0.35	0.29	0.38	0.51	0.35	0.48	0.25
70	0.38	0.59	0.23	0.22	0.11	0.19	0.16	0.16	0.13	0.11	0.26	0.17	0.20	0.22	0.29	0.38	0.20	0.27	0.37	0.21	0.33	0.25
71	0.33	0.55	0.18	0.16	0.10	0.23	0.19	0.15	0.12	0.13	0.24	0.15	0.18	0.21	0.26	0.35	0.19	0.27	0.40	0.23	0.37	0.21
77.5	0.45	0.51	0.53	0.56	0.61	0.68	0.73	0.72	0.69	0.68	0.76	0.72	0.72	0.77	0.79	0.75	0.77	0.84	0.90	0.80	0.84	0.76
82.5	0.34	0.54	0.21	0.20	0.19	0.28	0.24	0.20	0.20	0.21	0.24	0.19	0.21	0.24	0.27	0.40	0.20	0.27	0.40	0.27	0.38	0.20
88.55	0.39	0.55	0.27	0.27	0.18	**0.20**	0.24	0.27	0.23	0.20	0.34	0.27	0.29	0.32	0.39	0.44	0.32	0.39	0.45	0.32	0.38	0.36
95	0.37	0.52	0.33	0.34	0.29	0.40	**0.42**	0.42	0.38	0.36	0.48	0.43	0.45	0.48	0.51	0.49	0.47	0.56	0.61	0.49	0.55	0.48
98	0.34	0.56	0.30	0.31	0.30	0.45	0.44	0.39	0.35	0.35	0.46	0.39	0.42	0.45	0.47	0.41	0.43	0.52	0.62	0.46	0.57	0.43
108.6	0.43	0.62	0.28	0.26	0.16	0.16	0.14	**0.17**	0.15	0.13	0.27	0.18	0.21	0.22	0.30	0.43	0.21	0.25	0.32	0.20	0.29	0.27
114	0.47	0.66	0.31	0.29	0.21	0.22	0.13	0.13	0.15	0.15	0.21	0.14	0.16	0.13	0.22	0.42	0.14	0.14	0.30	0.12	0.31	0.19
115	0.47	0.69	0.31	0.29	0.23	0.25	0.16	0.14	0.16	0.17	0.24	0.16	0.18	0.14	0.23	0.43	0.15	0.13	0.30	0.12	0.32	0.20
116	0.40	0.62	0.25	0.22	0.14	0.22	0.14	0.11	**0.11**	0.11	0.21	0.13	0.16	0.15	0.22	0.37	0.14	0.19	0.33	0.15	0.32	0.18
117	0.42	0.64	0.26	0.24	0.15	0.22	0.13	0.11	0.11	0.11	0.23	0.14	0.17	0.15	0.23	0.38	0.15	0.18	0.31	0.14	0.31	0.19
118	0.38	0.61	0.23	0.20	0.15	0.25	0.17	0.12	0.13	0.14	0.23	0.15	0.18	0.17	0.23	0.38	0.15	0.20	0.34	0.18	0.34	0.17
124	0.34	0.60	0.19	0.17	0.14	0.27	0.20	0.13	0.13	0.15	0.24	0.15	0.18	0.17	0.22	0.35	0.16	0.22	0.37	0.20	0.37	0.16
128.5	0.45	0.62	0.41	0.41	0.47	0.55	0.53	0.47	0.47	0.49	0.48	0.46	0.47	0.50	0.50	0.57	0.45	0.51	0.62	0.53	0.61	0.43
131	0.27	0.49	0.22	0.22	0.21	0.39	0.37	0.33	0.30	0.29	0.38	0.33	0.36	0.39	0.39	0.37	0.37	0.47	0.56	0.42	0.52	0.34
134	0.51	0.57	0.45	0.46	0.43	0.38	0.48	0.52	0.50	0.47	0.55	0.52	0.51	0.55	0.58	0.63	0.57	0.62	0.66	0.57	0.60	0.58
136	0.51	0.53	0.52	0.54	0.54	0.55	0.64	0.66	0.63	**0.61**	0.70	0.66	0.66	0.71	0.74	0.73	0.72	0.78	0.82	0.73	0.75	0.72
138	0.41	0.48	0.39	0.41	0.39	0.42	0.50	0.51	0.48	0.45	0.56	0.51	0.51	0.56	0.59	0.59	0.57	0.64	0.69	0.58	0.63	0.57
144	0.26	0.47	0.13	0.13	0.11	0.29	0.26	0.21	0.19	0.19	**0.26**	0.21	0.22	0.26	0.28	0.31	0.25	0.35	0.48	0.30	0.45	0.23
149	0.29	0.61	0.18	0.15	0.18	0.32	0.27	0.20	0.20	0.22	0.32	0.24	0.26	0.25	0.28	0.38	0.25	0.28	0.42	0.27	0.43	0.21
152	0.29	0.46	0.16	0.16	0.15	0.21	0.22	0.20	0.18	0.18	0.24	**0.18**	0.19	0.24	0.30	0.40	0.24	0.31	0.44	0.28	0.40	0.25
155	0.39	0.60	0.24	0.22	0.15	0.20	0.14	0.12	0.11	0.11	0.22	0.13	0.16	0.16	0.25	0.40	0.15	0.20	0.33	0.16	0.32	0.19
158.6	0.41	0.64	0.26	0.24	0.16	0.19	0.14	0.14	0.13	0.12	0.27	0.17	0.20	0.18	0.27	0.42	0.18	0.20	0.31	0.16	0.31	0.23
170	0.33	0.54	0.18	0.16	0.14	0.24	0.18	0.12	0.12	0.14	0.19	0.12	**0.14**	0.16	0.21	0.36	0.16	0.22	0.39	0.19	0.37	0.15
177.6	0.33	0.52	0.19	0.17	0.18	0.28	0.21	0.14	0.15	0.18	0.17	0.14	0.14	0.17	0.20	0.36	0.17	0.23	0.42	0.22	0.41	0.13
225.6	0.24	0.47	0.13	0.13	0.15	0.24	0.26	0.23	0.21	0.20	0.30	0.23	0.25	0.29	0.33	0.42	0.28	0.34	0.45	0.31	0.42	0.27
231	0.23	0.41	0.13	0.13	0.19	0.31	0.29	0.23	0.22	0.24	0.24	0.22	0.21	0.26	0.27	**0.34**	0.27	0.34	0.51	0.32	0.49	0.23
232	0.21	0.44	0.10	0.11	0.15	0.27	0.29	0.25	0.23	0.23	0.31	0.25	0.26	0.30	0.33	0.39	0.31	0.38	0.50	0.34	0.46	0.29
245.6	0.25	0.54	0.20	0.19	0.25	0.42	0.38	0.30	0.28	0.30	0.36	0.30	0.33	0.35	0.36	0.37	0.32	0.41	0.54	0.38	0.52	0.28
258	0.29	0.53	0.19	0.18	0.21	0.36	0.31	0.23	0.21	0.24	0.28	0.23	0.25	0.28	0.30	0.35	0.25	0.34	0.49	0.31	0.47	0.22
263	0.31	0.54	0.18	0.17	0.15	0.29	0.24	0.18	0.15	0.17	0.26	0.18	0.21	0.23	0.28	0.36	**0.21**	0.30	0.43	0.25	0.41	0.22